AN AIRBORNE WINDSHEAR DETECTION SYSTEM FOR GENERAL AVIATION AIRCRAFT

by

Helen Katherine Dyne

Department of Aeronautics and Astronautics

Faculty of Engineering and Applied Science

University of Southampton

Thesis submitted for the degree of Doctor of Philosophy

August 1995

UNIVERSITY OF SOUTHAMPTON

ABSTRACT

FACULTY OF ENGINEERING AND APPLIED SCIENCE
AERONAUTICS AND ASTRONAUTICS

Doctor of Philosophy

AN AIRBORNE WINDSHEAR DETECTION SYSTEM FOR GENERAL AVIATION AIRCRAFT

by Helen Katherine Dyne

This work considers the requirements for a windshear detection system suitable for general aviation aircraft and evaluates a possible method for detecting windshear.

Initially, the phenomenon of windshear is introduced, and the hazard presented to aircraft by low-altitude windshear, and particularly by microbursts, is discussed. The work examines models for describing the various forms of atmospheric disturbances.

The existing ground-based and airborne techniques for detecting windshear are examined. General aviation aircraft differ from transport aircraft in the cost and sophistication of their on-board systems: the instrumentation commonly available on this class of aircraft and the sensors which could be used to measure the required aircraft parameters are discussed.

A method for estimating the wind acting on the aircraft using a minimum number of measurements of control inputs and aircraft parameters is presented. The technique is derived from the theory of observers and uses a linear, time-invariant model of the aircraft. The effect of model and sensor inaccuracies is considered.

The forms of wind which constitute a hazard are examined and used to derive algorithms to determine when the wind conditions constitute a dangerous windshear. The windshear detection system comprises the wind estimation and hazard evaluation stages, and the performance of this under various wind conditions is assessed. The operational requirements of the system are also addressed.

To my Parents

CONTENTS

Page

CHAPTER 6: Hazard Evaluation and Warning Methods

CHAPTER 7: The Windshear Detection System

LIST OF FIGURES

ACKNOWLEDGEMENTS

Over the years that this research has been in progress there are many people who have helped and supported the effort. In particular, I would like to thank Professor D. McLean for his guidance and encouragement.

I am grateful to friends and colleagues of the Department of Aeronautics and Astronautics for their continued support and interest; also to the members of ISVR, especially for their computing assistance, and to academic staff of ECS for their help with the work on the Aerosoft simulator.

I derived great benefit from the award of the Amelia Earhart Fellowship by Zonta International. This enabled me to visit organisations in the USA involved with the windshear problem and to gain a perspective on the aeronautical community.

My colleagues at Meggit Avionics also deserve a mention, their interest in my research was a source of encouragement.

Finally, I would like to thank my husband, Stuart, for his assistance and support - and for his flexible approach to our lifestyle!

1 THE WINDSHEAR PHENOMENON

1.1 Introduction

Windshear is a phenomenon which is of great interest and concern to the aviation community: it is a significant weather hazard to aircraft. There has been considerable research into the design of windshear detection and warning systems for larger, transport aircraft, but a low-cost system suitable for general aviation aircraft has not yet been developed. This thesis describes a technique for estimating the wind components acting on an aircraft and indicating the extent of the windshear hazard to the pilot. The method is applied to the design of an airborne detection system for general aviation aircraft.

Although the SI system of units is now recognised as standard, it has not been generally accepted within the international aeronautical industry. International conventions and air traffic procedures require that an aircraft's altitude is measured in feet, while horizontal distances are described in kilometres. An aircraft's airspeed is calibrated in knots, but the vertical speed is measured in feet per minute. Wind components are usually described in knots. The units used in this work are those which are conventionally used by authorities in the field of aeronautics but, where appropriate, the SI equivalent has been included. Table 1.1 provides a comparison of these units.

Table 1.1: Conversion Factors

Conventional Unit	SI Unit	Alternatives
1 foot (ft)	0.3048 m	-
1 knot (kt)	0.5148 m/s	1.6890 ft/s, 101.34 ft/min

1.1.1 Outline of Thesis

The phenomenon of windshear, and the hazard it presents to aircraft, is introduced in this chapter.

The response of an aircraft to changing winds is examined in Chapter 2 together with the analysis of the effect of wind on the aircraft's energy. Mathematical models of atmospheric disturbances are described. These can

be used in the analysis of an aircraft encounter with various wind phenomena.

Chapter 3 examines both ground-based and airborne methods of detecting windshear and considers the relative merits of the different technologies. The systems and instrumentation generally found on typical general aviation aircraft are described. Sensors which could be used in an airborne detection system to measure the various parameters associated with aircraft motion are also considered.

Chapter 4 describes how a technique for estimating the longitudinal components of the wind acting on an aircraft can be developed, using observer theory as its basis. The method is evaluated using computer-based design and simulation tools.

The performance of the estimation algorithm is affected by changes in the aircraft dynamics at different phases of flight, as well as by limitations in the sensing of required parameters. Chapter 5 examines how these factors affect the estimation of the wind components.

The form of the estimated wind components requires evaluation to determine whether they constitute a windshear condition. Chapter 6 considers the properties of an hazardous windshear and examines the effectiveness of criteria which are designed to assess the wind hazard. Finally, an optimum method of providing a warning to a pilot is considered.

In Chapter 7 the performance of the combined wind estimation and evaluation algorithm is assessed. The requirements for the system as a whole are discussed, and the suitability of the system for use as an airborne windshear detection system on general aviation aircraft is considered.

1.2 Windshear

Windshear is a phenomenon which relates to changes in the wind conditions and is defined as: "A change in the wind speed and/or direction in a very short distance in the atmosphere". [1] When considering the effect on an aircraft of a change in wind, an airspeed change in excess of 15 knots (~7.5 ms^{-1}) or a vertical speed change in excess of 500 feet per minute (~2.5 ms^{-1}, 5 kts) over a short period of time is classed as a windshear because

at these values a significant effect on the aircraft flight path can result. This feature distinguishes windshear from gusts, which are sudden wind changes of smaller magnitude, and turbulence which comprises higher frequency atmospheric disturbances. Turbulence may affect the aircraft control and ride quality but, in general, it does not produce a significant effect on the flight trajectory. The characteristics of these phenomena are discussed further in Chapter 2. Windshear can be described as a rate of change of wind; however, in aircraft analysis, it is frequently described in terms of the maximum wind change which is measured over a short, but unspecified, time or distance.

Although the effect of wind on aircraft dynamics is well known, it is only relatively recently, as a result of several major accidents, that the hazard of windshear to aircraft during low-altitude phases of flight viz. take-off, approach and landing has been fully recognised. Five of the major accidents which prompted windshear investigations are shown in Table 1.2. [2, 3, 4]

Table 1.2: Windshear Accidents

Date	Location	Casualties
June 1975	JFK Airport, New York	112 fatalities
		12 injuries
June 1976	Philadelphia, PA	0 fatalities
		87 injuries
July 1982	New Orleans, LA	153 fatalities
		9 injuries
August 1985	Dallas/Ft Worth, TX	135 fatalities
		25 injuries
July 1994	Charlotte, NC	37 fatalities
		21 injuries

In total, between 1964 and 1985, windshear was a contributing factor in incidents involving 619 fatalities and 231 injuries. In the USA approximately 50% of all fatal accidents are weather related - a statistic which has remained constant for 30 years. [5]

1.3 Forms of Windshear

Windshear can arise from a variety of meteorological conditions where air masses of differing properties, such as temperature or humidity, interact, or where windshear is induced by the local terrain. The principal causes are summarised in this section. [1, 2, 6, 7, 8]

1.3.1 Air Mass Fronts

An 'air mass' front arises when masses of air of different temperature or humidity come into contact with each other. Their differing properties mean that they do not mix readily and the boundary between the two bodies of air can exhibit temperature gradients and large changes in airflow. Frontal systems commonly occur as a result of air circulation around regions of low pressure in the form of warm or cold fronts. A vertical cross-section of a frontal system is shown in Figure 1.1. [1]

A cold front forms when colder air, which is more dense, moves towards a body of warm, less dense air. The cooler air pushes below the warm air and a transition zone or 'front' develops along the boundary between the two air masses. The severity of a windshear is determined by the temperature differences between the two bodies of air, and strong shears may occur when that difference exceeds 6°C. The thickness and temperature gradient of the transition zone are also indicative of the windshear hazard: a narrower zone causes a stronger shear and it has a larger temperature gradient across it.

A warm front occurs when the warm air advances towards cooler air and rises above the denser air mass. The velocity of the advancing air is greater at higher altitudes than close to the ground and so a vertical wind gradient develops.

Frontal systems may give rise to thunderstorm conditions. These are discussed separately in Section 1.3.3.

1.3.2 Sea Breeze Front

A sea breeze front, a form of frontal system which occurs in coastal regions, is produced by the diurnal temperature differences between the land and the sea. Since the sea has a much higher specific heat capacity it changes

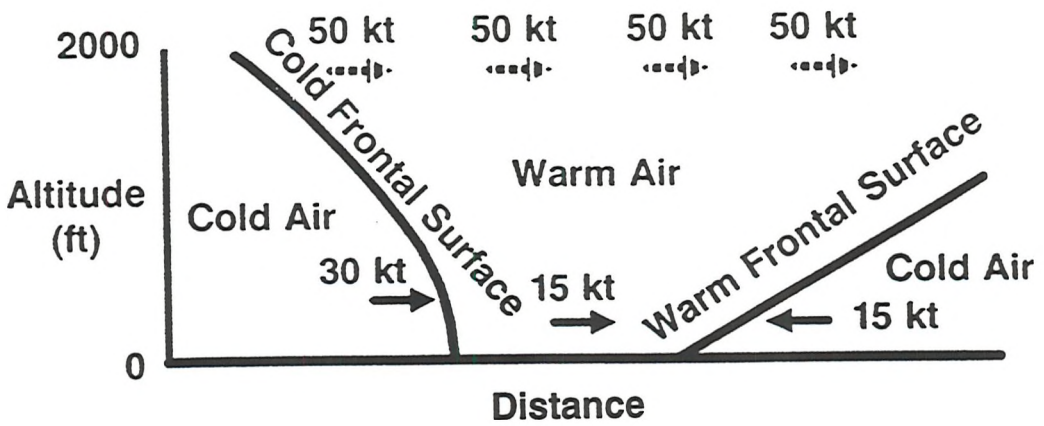

Figure 1.1: Cross-Section of a Frontal System

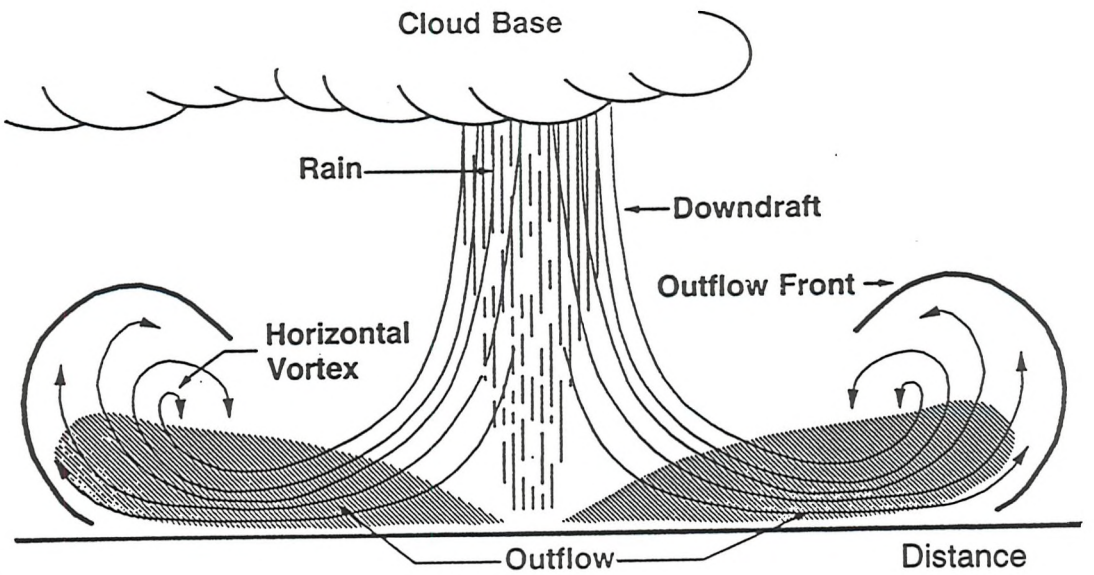

Figure 1.2: Formation of a Downburst

temperature much more slowly than the land. During the day the air over the land is warmer than that over the sea, causing a circulation of the air to develop. Usually, the circulation intensifies from a light sea breeze in mid-morning to a stronger wind during the afternoon when the resulting sea breeze front may move inland. At night the temperature difference is reversed and so the wind blows from land to sea. Sea breezes occur regularly during summer months. In areas with temperature climates, such as the British Isles, they generally only produce moderate windshear of less than 10 knots, but in warmer, tropical climates sea breezes are usually in excess of 20 knots. [8]

1.3.3 Thunderstorms

Thunderstorms are generated by both frontal systems and 'air mass' weather conditions. An air mass thunderstorm is generated by local heating of the air at the earth's surface. The warm, moist air begins to rise and cool to form droplets as cumulus clouds. As this continues the droplets become too large to be supported by the updraft and begin to fall. The descending downdraft cools the surrounding air and drags that air with it, increasing the intensity of the flow. This usually results in intense precipitation at ground level. On reaching the ground the downdraft spreads in all directions and, in some cases, it may curl to form a horizontal vortex ring. A diagram of a typical downburst is shown in Figure 1.2. [1] The precipitation continues until the extent of the downdraft cuts off the heated updraft and inhibits circulation; the thunderstorm then begins to die and the downdraft to weaken. The principal difference between an air-mass thunderstorm and a frontal thunderstorm is that the frontal storm is often tilted, allowing the precipitation to fall at a distance from the updraft, and so the downflow may be intensified and sustained for longer.

1.3.4 Microbursts

The level of hazard associated with a downdraft is related to its size. It is only relatively recently that a small-scale, intense downdraft known as a 'microburst' has been identified. [9] These microbursts have downdrafts up to 3 km in diameter which may spread horizontally on reaching the ground to a diameter of up to 5 km. Their small size means that the wind speeds change rapidly over a relatively short distance, which makes them especially hazardous to aircraft. Microbursts are not always associated with heavy rain

and thunderstorms; some occur in high-altitude clouds in which the precipitation has evaporated at a considerable height above ground level. These 'dry' microbursts are particularly difficult to identify since the weather conditions and cloud formations appear benign, but the windshear produced may be as severe as a wet microburst.

Both wet and dry forms of microburst are similar in their intensity, size and duration. The microburst is short-lived, developing to maximum intensity in an average of six to seven minutes. After the initial stages of formation, when the downdraft has reached the ground, the microburst expands horizontally and increases in intensity for approximately five minutes. The intensity doubles to a maximum during this period. The intensity of a microburst reaches 50 knots (~25 ms^{-1}) on average, but microbursts with wind changes of nearly 100 knots have been recorded. [1] In general the microburst dissipates approximately ten to twenty minutes after ground contact. Figure 1.3 shows the intensity distribution of microbursts at ground level measured during the 'JAWS' study in the USA, the study is described in Section 1.5. [1]

1.3.5 Gust Fronts

A gust front is produced as the horizontal outflow of a downburst moves outwards from the location of the downburst. The outflow meets with warmer air and evolves into a front. Behind the front there is a region of unsteady air which gives rise to windshear and turbulence. The gust front may extend up to tens of kilometres from the location of the downdraft, by which time it is considerably weakened, or it may remain close to the downdraft which produced it, depending on the nature of the downdraft and the surrounding air conditions.

1.3.6 Terrain-Induced Windshear and Mountain Waves

Natural features of the terrain can affect the flow of air in such a way that an aircraft flying in the vicinity may experience sudden changes in conditions. Airports situated near breaks in mountain ranges or abrupt changes in terrain are prone to gusting winds, which may be severe.

Variations in the direction of the wind as it passes over the contours of the terrain are often produced. Mountain waves occur when wind at high

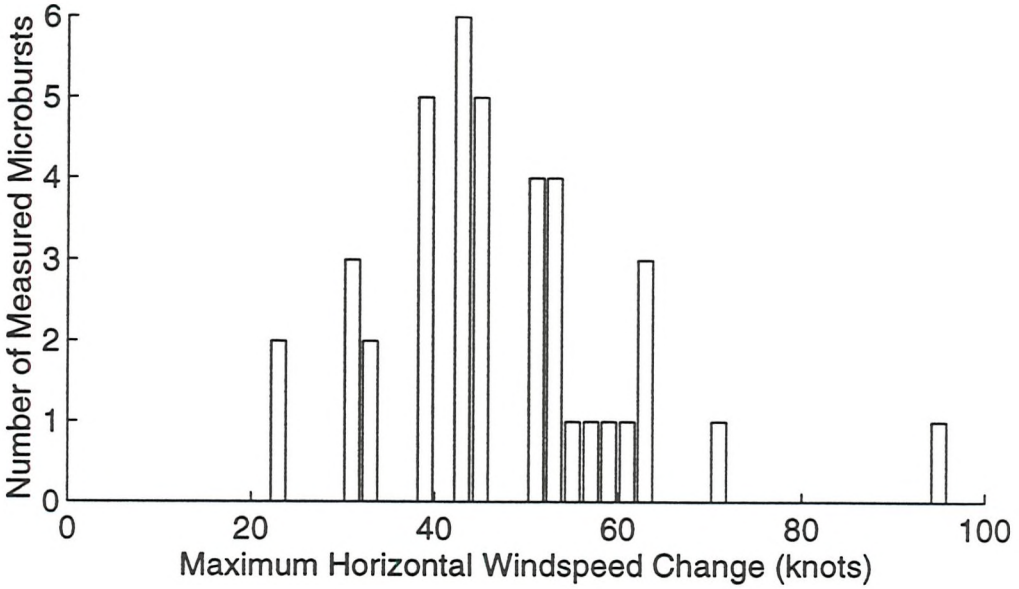

Figure 1.3: Microburst Intensity Distribution

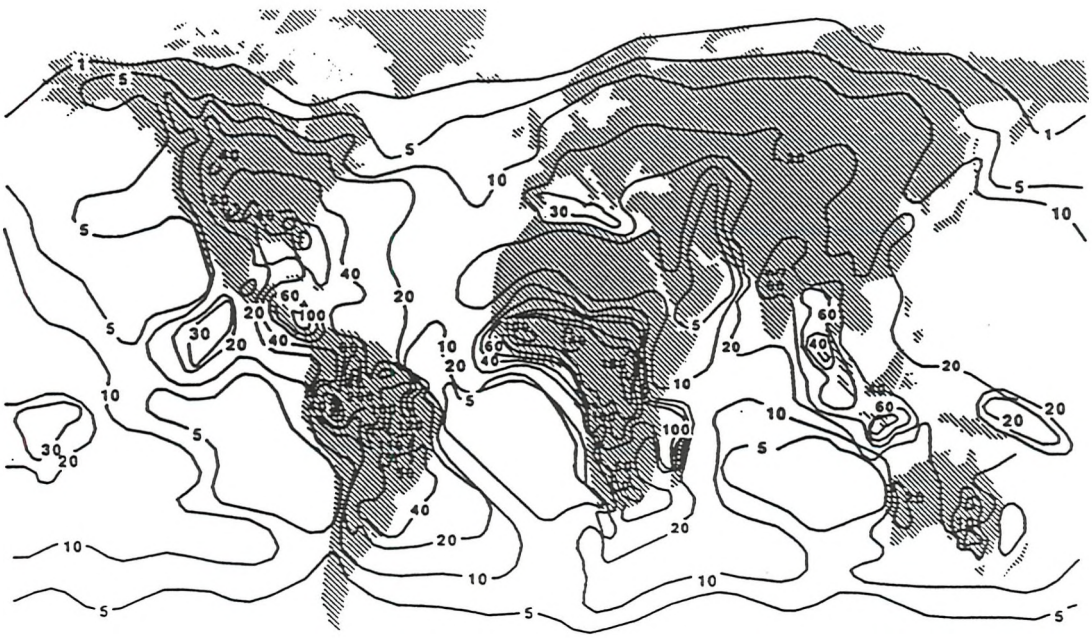

Figure 1.4: Annual Occurrences of Thunderstorms Worldwide

altitude crosses a mountain range. On the lee side there is a region of lower pressure which creates a strong airflow down the contours of the slope, producing waves in the air currents, and these may result in strong windshear and turbulence. Mountain waves are a frequent occurrence in the Rocky Mountain region of the USA. The phenomenon is being investigated further following an aircraft accident at Colorado Springs, in March 1991, when it was considered as a possible cause. [10]

1.3.7 Solitary Waves

A solitary wave is an isolated circulation in the air which may be produced either where a gust front or sea breeze front decays, or by wind flowing down slopes. [11, 12] These waves have an updraft at the leading edge and a downdraft of similar strength at the trailing edge, and the circulation may extend horizontally for distances ranging from a few hundred metres up to ten kilometres. The waves move slowly and are relatively long-lasting. They are observed frequently in some areas of Australia.

1.3.8 Low-Level Jet Stream

Frictional effects of the earth's surface produce a boundary layer which typically extends to a height of five hundred feet and, as a consequence, aircraft often experience an increase in the magnitude of the wind immediately above the ground. Larger wind changes are sometimes produced when there is a strong temperature inversion at low altitudes, i.e. where air temperatures close to the ground are cooler than those above. This can cause a strong current of air near the ground. Such conditions are typically generated by diurnal processes during the night, as a result of radiant cooling of the air, or by frontal activity where a cold front advances on warmer air to produce a temperature inversion. The low-level 'jet streams' produce rapid changes in the wind velocity with altitude and are a hazard to aircraft during low-altitude operations. [1, 2, 13]

1.3.9 Tornadoes

Tornadoes and other high speed atmospheric vortices such as water spouts and dust devils form under thunderstorm conditions and have extremely strong windshear associated with them. The development of conditions resulting in tornadoes can be identified, and they can be detected and

tracked by weather radar during their formation and development to enable the region surrounding them to be avoided by aviation.

1.4 Windshear Hazard

The degree of hazard of a windshear condition to aircraft is related not only to the magnitude of the shear at low altitude but also to the ability to predict and forecast the event. Conditions which are large in scale, slow to develop and slow-moving are more easily predicted and therefore pose much less of a threat than smaller, faster developing events which generate windshear of a similar severity. An examination of aircraft accident statistics shows that, of fifty-one windshear-related accidents, sixty-five percent were associated with thunderstorm conditions, usually containing microbursts, and another fourteen percent were related to frontal systems; the other windshear generating conditions made a smaller contribution. Table 1.3 shows the number of accidents and incidents in which the weather system listed was the primary cause.

Table 1.3: Windshear Hazard [1]

Weather System	Number of Accidents/Incidents
Storms	33
Front	7
Strong Surface Winds	2
Unstable (Turbulent) Air	2
Temperature Inversion	1
Sea Breeze Front	0
Mountain Wave	0
Unknown	6
Total	51

The microburst is the most severe windshear threat to aircraft and its small size makes it very difficult to detect using standard aviation weather detection systems. Thunderstorms are most prevalent in tropical regions, as can be seen in Figure 1.4 [1], and so these areas are likely to be susceptible to microburst formation. However, because of the low density of air traffic in these regions only a few windshear accidents have been recorded. An area which has a much higher volume of air traffic is North America, and research in the USA has revealed that there are two main areas which are

particularly susceptible to microbursts: in the southern states around the Gulf of Mexico thunderstorms are prevalent and, on average, occur on more than sixty days per year. From statistics collected it is suggested that approximately five percent of thunderstorms in that region produce microbursts. [1] In the high plains and mountainous regions of Central USA, e.g. near Denver, conditions are dryer and dry microbursts are relatively common. As a consequence, the majority of windshear-related accidents have occurred in the USA. Some regions of Australia have also been found to be prone to dry microbursts.

1.5 Windshear Investigations

The first aircraft accident attributed to windshear was in 1974 in Sydney, Australia, when a downdraft and outflow were recognised to have caused rapidly varying winds close to the ground. During the investigations into the accident at John F. Kennedy Airport in New York in the following year, Professor Theodore Fujita of the University of Chicago first hypothesised the existence of a phenomenon which he called the downburst. This was authenticated during the Northern Illinois Meteorological Research On Downbursts (NIMROD) project in 1978 using Doppler radar techniques.

In 1982 the Joint Airport Weather Study (JAWS) was carried out by the National Center for Atmospheric Research (NCAR) and the University of Chicago. [1, 2, 5] Over one hundred microbursts were observed and information on their frequency, characteristics and detectability was collected. The study enabled the characteristics of microbursts to be quantified.

In 1983, following the accident at New Orleans International Airport, the American National Academy of Sciences (NAS) was contracted by the Federal Aviation Authority (FAA) to study the hazard to aircraft posed by windshear. The study was broad and included an investigation into the knowledge of windshear phenomena, the effectiveness of detection and measurement systems, the communication of warnings, the adequacy of pilot training and the effects of windshear on aircraft performance. The committee was also asked to recommend any research and development needed to combat the risks. [2]

The recommendations presented by the committee were for a short-term programme of information, education and pilot training and an improvement and extended use of the 'Low-Level Wind Shear Alert System' (LLWAS) which was already in use at some airports. In the medium term it was recommended that airborne windshear detection systems should be developed further. The longer-term plan was to research and develop enhanced ground-based and airborne detection systems using technologies which were still in the early stages of development.

1.6 General Aviation and Windshear

1.6.1 Aircraft Accidents and Incidents

The windshear accident statistics have yielded useful information on the meteorological and geographical effects which produce hazardous windshear. Nearly all these data relate to transport aircraft and there is relatively little information about general aviation aircraft accidents or incidents which have been caused by windshear.

In the United States general aviation aircraft outnumber carrier aircraft by a factor of fifty and the total general aviation flying hours are five times those of air carriers. The National Transportation Safety Board (NTSB) have indicated that approximately 40% of general aviation aircraft accidents are weather-related, but relatively few have been attributed to windshear. [2] Although general aviation aircraft may have more flexibility in their scheduling of flights, it has been shown that the possibility of predicting and therefore avoiding the most threatening windshear events is poor, and so general aviation aircraft are not significantly less susceptible to windshear than transport aircraft. [2] A more feasible reason is that such general aviation accidents and incidents are only investigated if there are fatalities and these investigations need not include trained meteorologists. Furthermore, these aircraft are not equipped with flight data recorders and so the ability to positively identify a windshear related accident is much reduced.

1.6.2 General Aviation Pilots

A general aviation pilot is not, in general, professional and so he has much greater difficulty in achieving and maintaining flying skills. [2, 14, 15] After

a pilot's basic flying skills have levelled-off, human factors research has shown that the ability to recognise situations and interpret alternative courses of action continues to increase. As a consequence an 'expert' pilot shows a greater integration of skill when exposed to a stressful situation, whereas such integration breaks down for a less-experienced pilot, even though he may be equally competent at each of the tasks individually.

The task of flying a general aviation aircraft is significantly different from that for a transport aircraft. The operating procedures for air traffic control are geared to the requirements of airline operations, and, as a consequence, they are less suited to general aviation, with their single pilot and more limited on-board systems. In addition, general aviation pilots may receive less instruction and information about the routes and airports being used than commercial pilots. Instrument flying of general aviation aircraft is particularly prone to errors, and accidents during instrument approaches have been shown to be seventeen times more likely for general aviation aircraft accident compared to transport aircraft. [14]

The differences between professional and private pilots have been emphasised by a comparison of the causes of accidents involving general aviation aircraft being flown by both private pilots and airline pilots. [14] This showed that the major causes for the private pilot accidents were weather related and were caused in part by pilot inexperience and misjudgement. In contrast, overconfidence and the taking of excessive risks were the principal causes of accidents among the airline pilots.

A general aviation pilot is likely to be less able to recognise and respond to a windshear situation than a professional pilot since a windshear is an abnormal event with which the general aviation pilot will be unfamiliar. An on-board windshear detection system could both identify and provide an alert for the hazard before the pilot has assessed the situation, and could, thereby, assist the pilot to take avoiding action.

2 THE EFFECT OF WIND ON AIRCRAFT

2.1 Aircraft Dynamics

2.1.1 Aircraft Equations of Motion

The derivation of the linearised equations of motion of an aircraft, and the notation used in these equations, are summarised in Appendix A. The longitudinal motion of an aircraft flying straight with wings level is described by equations 2.1 to 2.4

$$\dot{u} = X_u(u+u_g) + X_w(w+w_g) - g\cos\Theta_0\theta + \sum X_\delta\delta \tag{2.1}$$

$$\dot{w} = Z_u(u+u_g) + Z_w(w+w_g) + U_0 q + g\sin\Theta_0\theta + \sum Z_\delta\delta \tag{2.2}$$

$$\dot{q} = \tilde{M}_u(u+u_g) + \tilde{M}_w(w+w_g) + \tilde{M}_q(q+q_g) + \sum M_\delta\delta \tag{2.3}$$

$$\dot{\theta} = q \tag{2.4}$$

The combined inertial and wind velocities are equivalent to the air-relative velocity because the air relative velocity is defined as:

$$u_a = u + u_g \tag{2.5}$$

$$w_a = w + w_g \tag{2.6}$$

The wind velocity will, therefore, directly affect the motion of the aircraft.

2.1.2 Aircraft Flight Characteristics

The state equation, equation A23, representing the longitudinal flight dynamics of an aircraft for small perturbations is in standard form for analysis of a linear system. The aircraft's flight characteristics can be deduced by examination of these equations. [6, 16]

Both the pilot's control inputs and the gust variables are considered to be inputs to the dynamic system. Transfer functions which relate the effect of each input on each state can be derived and in every case the denominator of this function is identically the characteristic polynomial of the system which can be found by evaluating the relationship in equation 2.7, i.e.

$$\det|\lambda I - A| = 0 \tag{2.7}$$

This yields a quartic polynomial in lambda and, often, this can be factorised into two quadratic factors where each factor represents an oscillatory mode of the aircraft; they are classically known as 'phugoid' and 'short period' modes.

$$(\lambda^2 + 2\zeta_{ph}\omega_{ph}\lambda + \omega_{ph}^2)(\lambda^2 + 2\zeta_{sp}\omega_{sp}\lambda + \omega_{sp}^2) = 0 \qquad (2.8)$$

Here ζ represents the damping factor and ω the natural frequency of the mode and the subscripts *ph* and *sp* refer to the phugoid and short period modes respectively.

The phugoid is a lightly-damped, long period oscillation in which there is an exchange of potential and kinetic energy causing both speed and height to oscillate: It principally affects the aircraft forward speed, u, and pitch attitude, θ. The short period mode is a high frequency, relatively highly-damped mode and can be most clearly seen in its effect on the aircraft heave motion, w, and the pitch rate, q. In some aircraft the short period mode is not oscillatory but is instead simply composed of two decaying transients; this is the case for the dynamics of Cessna 402B aircraft which is used in subsequent chapters.

For an aircraft to be dynamically stable the roots of the characteristic equation must have negative real parts. The static stability of an aircraft is also significant when considering the response of an aircraft to an input. An aircraft is statically stable if, in response to an input, it produces forces and moments which tend to oppose the effect of the input and return the aircraft to an equilibrium. An input to the longitudinal mode of the aircraft will directly or indirectly cause a pitching moment about the centre of gravity and so it is the M_w stability derivative which determines whether the aircraft is statically stable.

$$M_w \propto \frac{\partial M}{\partial w} \qquad (2.9)$$

An input which produces a 'pitch up' motion produces a corresponding increase in angle of attack and hence in heave velocity, w. If M_w is negative then a pitch down moment will result which reduces the effect; the aircraft is statically stable. The sign of M_w depends on the relative positions of the aircraft's centre of gravity and the point through which the total lift vector

acts, the neutral point; for positive static stability the centre of gravity should be forward of the neutral point.

2.2 Aircraft in Wind

2.2.1 Aircraft Response to Windshear

Figure A3 shows the sign convention for the components of a wind acting on an aircraft; in stability axis co-ordinates the trim angle of attack is zero. An examination of each of these components shows its effect upon the aircraft and gives an indication of its relative importance to the total response to a windshear. The following analysis considers the free response from equilibrium of an aircraft flying straight and level. The Cessna 402B model is used for these simulations and the matrices of the state equations are given in Appendix A. [17]

An aircraft which encounters an increase in headwind or decrease in tailwind, when flying in equilibrium, shows an immediate corresponding increase in its airspeed. The aerodynamic forces vary as the square of the airspeed and so the lift and drag forces and pitching moment are all increased. As a result the aircraft pitches up and begins to climb. A statically stable aircraft develops a restoring pitching moment which reduces the angle of attack and the lift and, after a decaying oscillatory response, it returns to its original airspeed. The flight trajectory is now parallel to the original 'no shear' trajectory but at a higher altitude, and the aircraft's inertial speed is reduced by the magnitude of the shear. Figure 2.1 shows the initial response of the airspeed, u_a, the inertial speed, u, and the attitude of the Cessna 402B aircraft to a step change in the wind component, u_g, acting along the x-axis of the aircraft, and the effects of the same event over a longer duration. An increasing tailwind or decreasing headwind will produce the opposite result by reducing airspeed and hence the aerodynamic forces. The airspeed will again return to the equilibrium airspeed for a statically stable aircraft and the final flight trajectory in this case will be below the original equilibrium trajectory. It should be noted that the average microburst produces horizontal wind speed changes of approximately 50 knots over a short period and so the resulting effect without any control input could be approximately fifty times greater than those shown here. The effect of a shear (ramp) input rather than a step input is discussed next.

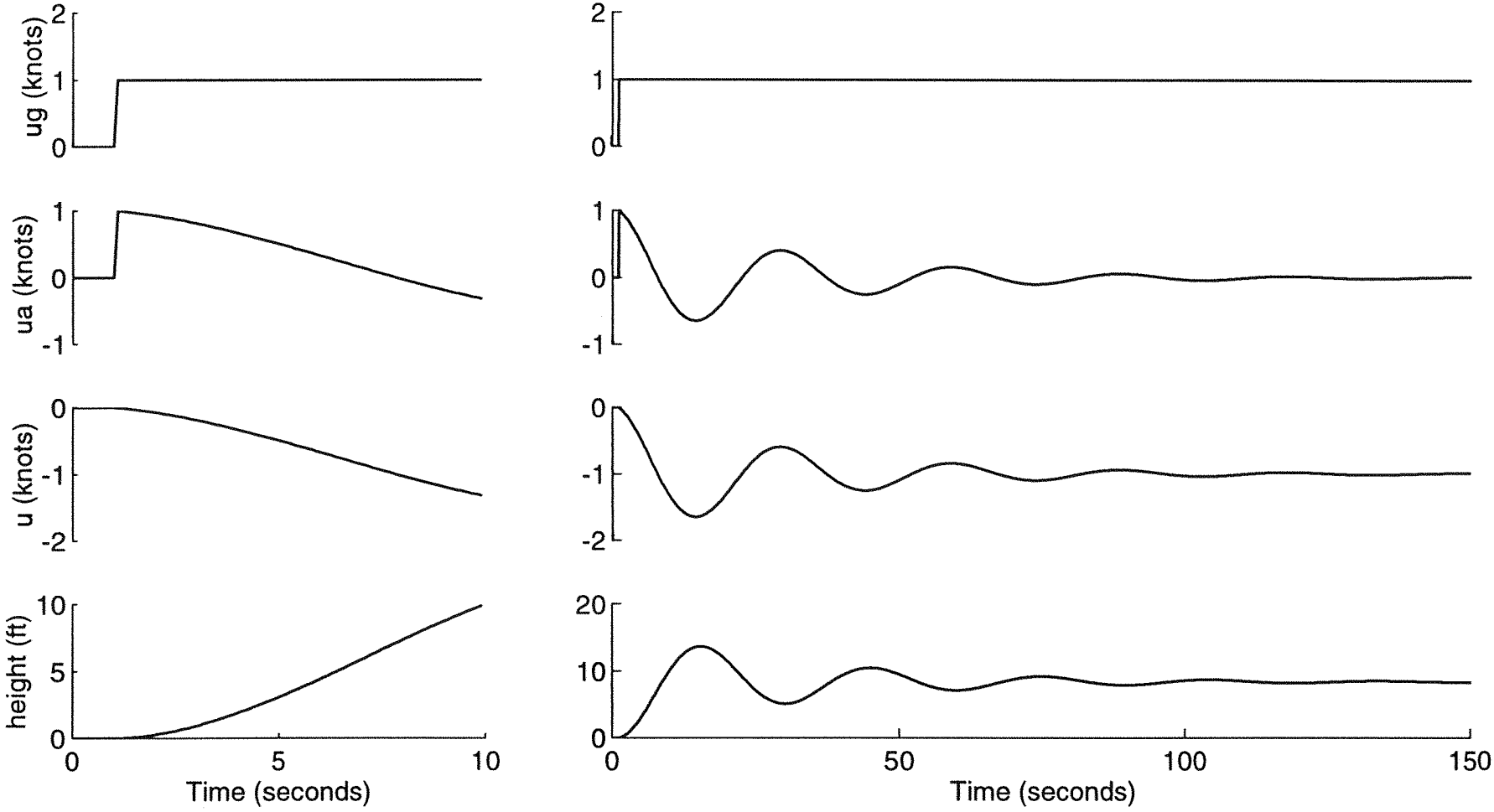

Figure 2.1: Effect of Unit Step in x-axis Wind on Airspeed, Inertial Speed and Height

Windshear may be described in terms of the resultant flight path improvement or deterioration: if the resulting trajectory is above the original path then the shear produces a flight path improvement and if it is below, there is a deterioration. Figure 2.2 shows a performance enhancing shearing wind of magnitude one knot per second. In this case the airspeed shows a larger variation than in Figure 2.1, but it still oscillates about the equilibrium value. However, the altitude shows a steady and significant increase of approximately 500 feet per minute. A performance decreasing shear of equal magnitude would result in a corresponding loss of altitude, and so a seemingly small rate of change of wind can cause serious hazards at low altitudes over a prolonged period. Both performance-increasing and performance-decreasing shears will cause problems for a pilot who is attempting to follow a fixed path e.g. a glideslope.

An updraft/downdraft shear affects the aerodynamic forces. The initial effect this time is a change in the angle of attack. An aircraft encountering an updraft experiences an increase in the angle of attack which increases the aerodynamic forces of lift and drag causing the aircraft to begin to gain altitude and the airspeed to reduce. Again, a statically stable aircraft produces a pitch down response which reduces the angle of attack and increases the airspeed and the aircraft returns to its equilibrium angle of attack and airspeed. Relative to an inertial reference, e.g. a ground-based observer, the aircraft is climbing. Figure 2.3 shows the initial step response of a typical aircraft to an updraft, w_g, acting the aircraft and the effects of the same event over a longer duration. It is particularly significant that a constant updraft produces a continuous change in altitude which is analogous to that produced by the shear of Figure 2.2, but of smaller magnitude. The updraft produces very little effect in the aircraft airspeed or ground speed. In contrast to an updraft, a downdraft reduces the angle of attack, reducing the aerodynamic forces and causing the aircraft to sink. The resulting motion returns to the original airspeed and angle of attack but the aircraft is descending relative to inertial references.

On a conventional aircraft, for which the X-Z plane is a plane of symmetry, a cross-wind shear from either direction has a similar effect. The shear affects the aerodynamics side force and the yawing and rolling moments causing the aircraft to yaw into the wind and roll away from it. The aircraft eventually stabilises with its wings level, but the heading is not restored and the aircraft

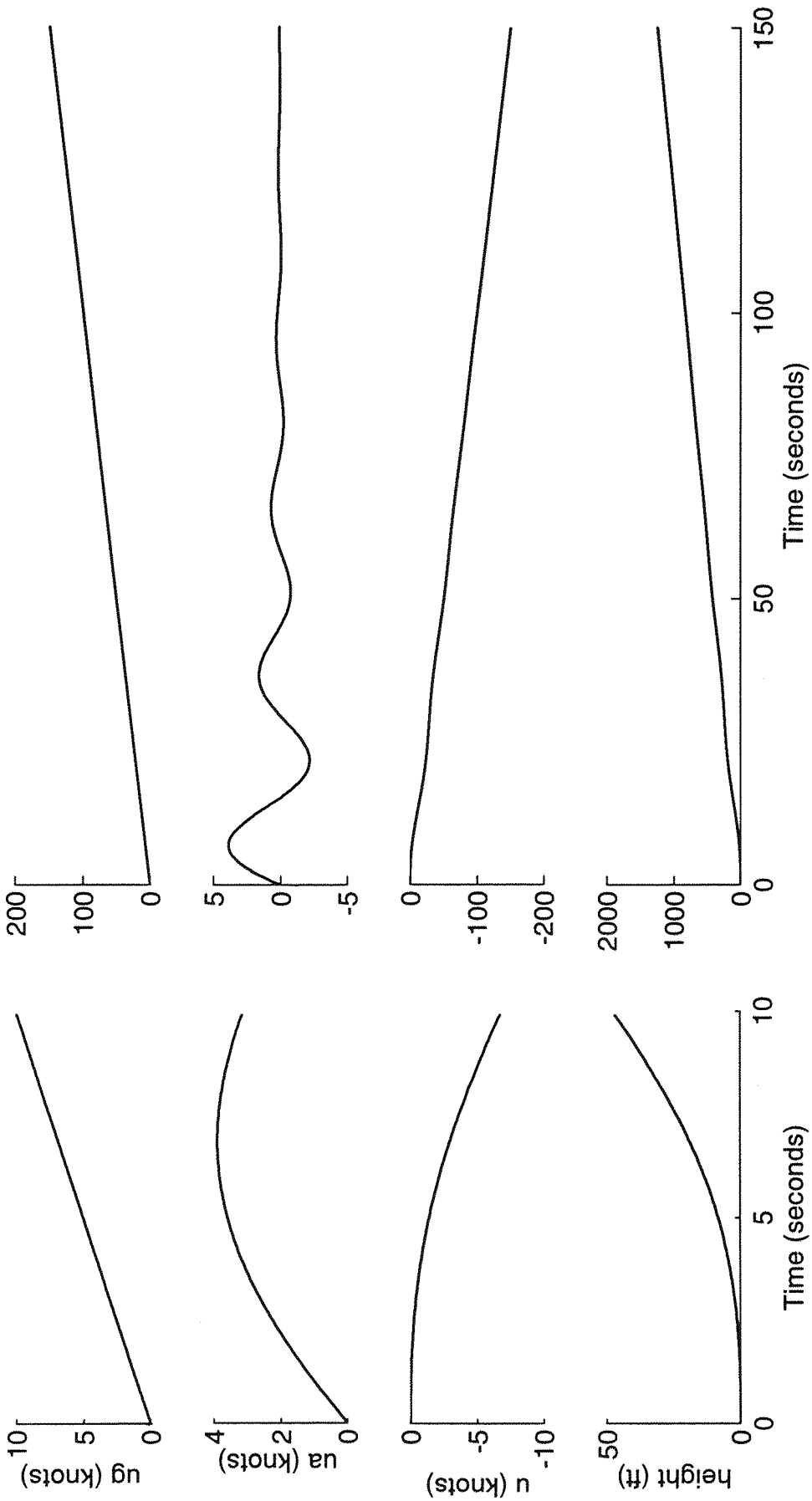

Figure 2.2: Effect of Ramp Input in x-axis Wind on Airspeed, Inertial Speed and Height

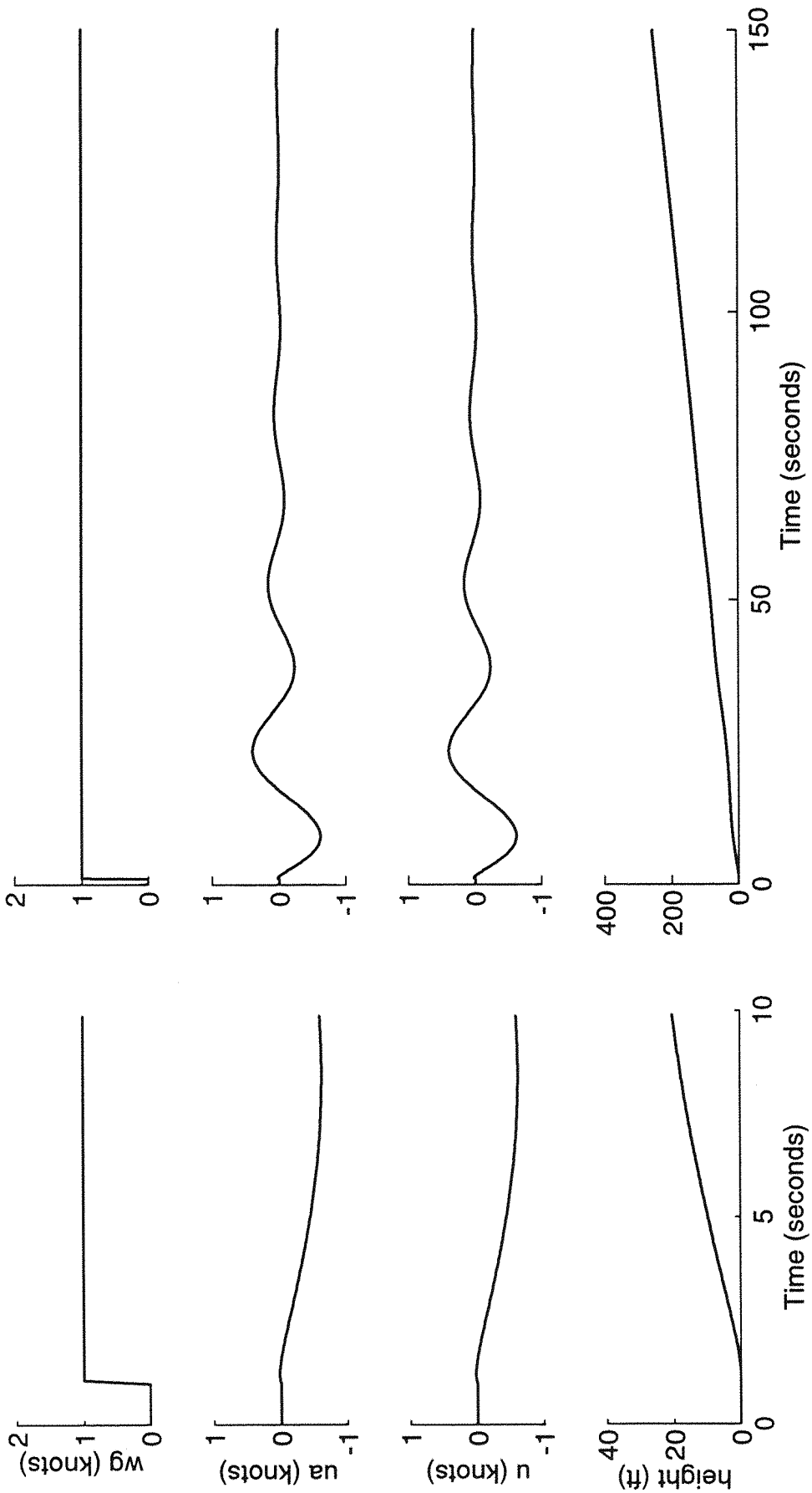

Figure 2.3: Effect of Unit Step in z-axis Wind on Airspeed, Inertial Speed and Height

flight path turns towards the upwind direction. The airspeed and altitude are not affected initially by a lateral shear, but may show a small variation if it is prolonged. The principal effect of the shear is to increase the pilot workload by requiring corrective action.

An analysis of aircraft performance in windshear has attempted to quantify the hazards. It is suggested that 75% of the microburst windshear hazard arises from the longitudinal component of the wind, 25% from the downdraft and only a small percentage from the cross-wind component. [18]

2.2.2 Microburst Encounter

An aircraft passing through a microburst while on approach to a runway experiences large and rapid changes in both longitudinal and vertical wind components. On entering the microburst, following a glideslope, the aircraft will first encounter the horizontal outflow which increases the headwind causing the aircraft to rise above its intended path as shown in Figure 2.4. [21] A pilot who is unaware of the situation will attempt to regain the intended glideslope and airspeed by lowering the nose of the aircraft and reducing the thrust. However the outflow is followed by the core of the microburst, the downdraft, which causes the aircraft to sink rapidly and then by the outflow which decreases the headwind component and again causes loss of altitude and airspeed. In a wet microburst, these effects may be exacerbated by the effect of heavy rain which can reduce the lift produced by the wings. [19] The ability of the aircraft to climb out of the microburst will depend on its intensity relative to the reserve power of the aircraft and the effectiveness and timing of the pilot's response to the changing situation. Analysis of windshear encounters indicates that typically only five to fifteen seconds are available to recognise and respond after an aircraft has entered a windshear. [20]

2.2.3 Aircraft Energy in Windshear

An aircraft's ability to manoeuvre freely to maintain its flight path depends on its having sufficient energy to achieve the manoeuvre. A measure of the severity of a windshear can be related to the change in aircraft energy. [21] The relationship is derived by considering the effect of wind on the ability of an aircraft to climb.

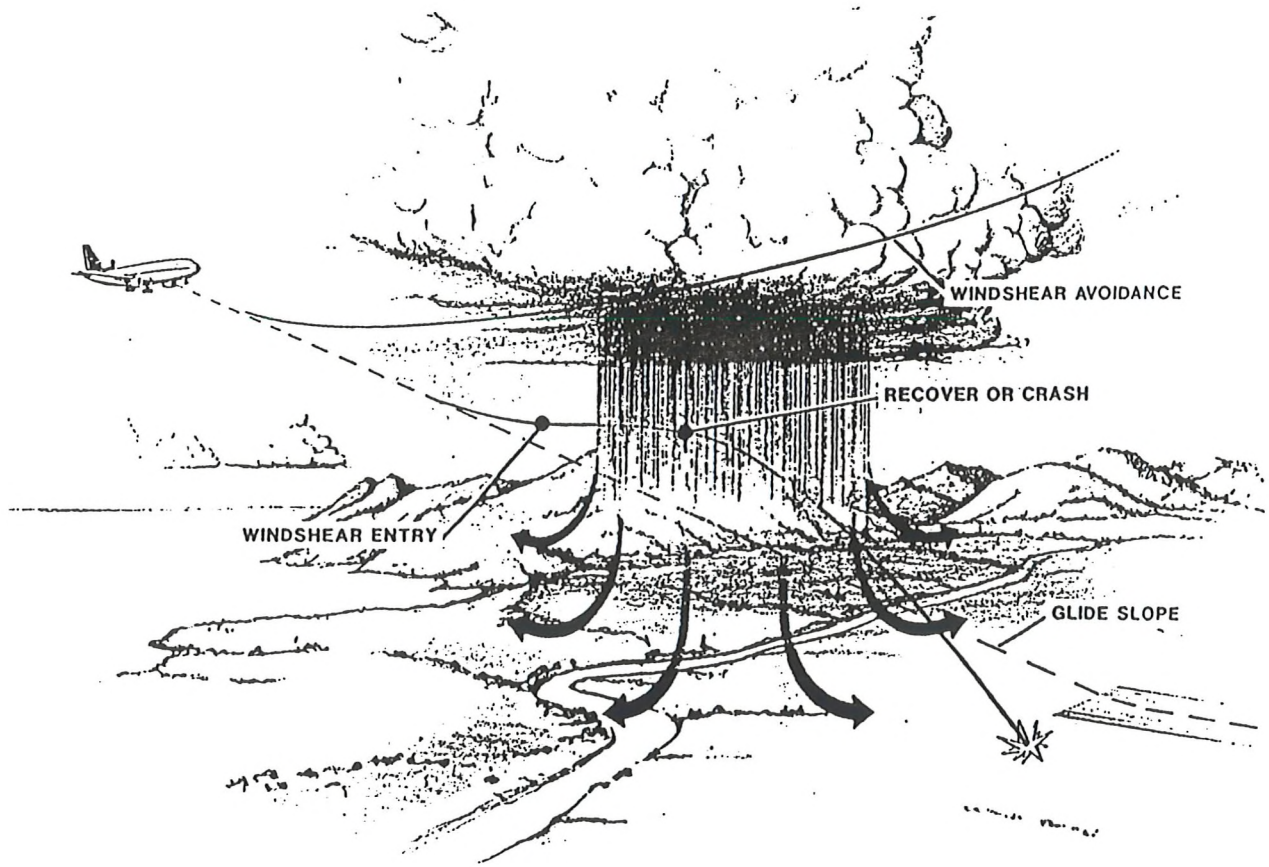

Figure 2.4: Flight Path through a Microburst

An aircraft's total energy comprises its kinetic and potential energies.

$$E = \tfrac{1}{2} m V_a^2 + mgh \tag{2.10}$$

where V_a is the true airspeed, m is the mass of the aircraft and h is the altitude. It is useful to express this in terms of the specific total energy, E_s, which is the energy per unit weight.

$$E_s = \frac{V_a^2}{2g} + h \tag{2.11}$$

It can be seen from this that the energy of an aircraft is distributed between its altitude and its airspeed so, for a given specific energy, a pilot is able to increase altitude only by allowing the airspeed to reduce and vice versa. Increasing the thrust of the aircraft will increase the specific energy allowing both parameters to be controlled.

The rate of change of specific energy, or specific power of the aircraft, is a measure of the potential rate of climb, $\dot{h}_p$.

$$\dot{E}_s = \dot{h}_p = V_a \frac{\dot{V}_a}{g} + \dot{h} \tag{2.12}$$

A windshear can have a significant effect on the specific energy and specific energy rate of an aircraft. A shear in the longitudinal plane affects both airspeed and altitude and so it produces a change in the specific energy. A windshear which causes flight path deterioration i.e. a decreasing headwind or increasing tailwind, or an increasing downdraft, reduces the specific energy of the aircraft. In contrast lateral shears have little, if any, effects on these parameters.

The air-relative flight path angle is most often considered in piloting situations as this relates the pitch attitude, θ, measurable from the aircraft instruments, to the angle of attack which governs the aerodynamic forces and moments acting on the aircraft. However, it is the inertial flight path angle which determines the rate of climb relative to the ground. The rate of climb and potential rate of climb can be related to the aircraft's inertial flight path angle, γ_i, by examining the co-ordinate system in Figure 2.5.

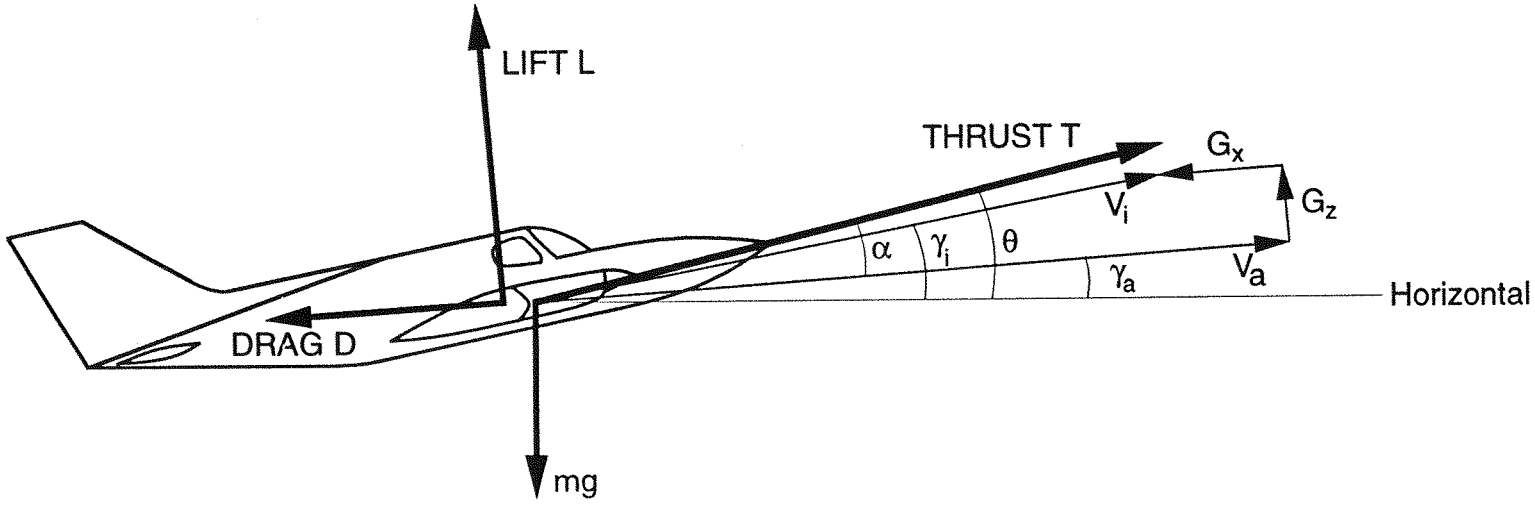

Figure 2.5: Axis System for Aircraft Energy Analysis

$$\dot{h} = V_i \sin\gamma_i \tag{2.13}$$

$$\dot{h}_p = V_i \sin\gamma_{ip} \tag{2.14}$$

V_i is the inertial speed of the aircraft. Substituting these expressions into equation 2.12 produces a relationship between the actual and potential inertial flight path angles and the aircraft's airspeed.

$$V_i \sin\gamma_i = V_i \sin\gamma_{ip} - V_a\left(\frac{\dot{V}_a}{g}\right) \tag{2.15}$$

The windshear affects the energy state of the aircraft and therefore alters the available energy which would enable it to gain height. The effect of a windshear on the air-relative inertial flight path angle can be examined by considering the rate of change of airspeed in the presence of a windshear.

$$\dot{V}_a = \frac{T}{m}\cos\alpha - \frac{D}{m} - g\sin\gamma_a + \dot{G}_x \tag{2.16}$$

where T and D are the aircraft thrust and drag respectively, α is the angle of attack and γ_a is the air-relative flight path angle. G_x is the component of wind parallel to the total airspeed vector.

Setting the airspeed change, $\dot{V}_a$, to zero allows the potential air-relative flight path angle to be found i.e. the potential air-relative climb angle if the airspeed is held constant.

$$\gamma_{ap} = \sin^{-1}\left(\frac{T\cos\alpha - D}{mg} + \frac{\dot{G}_x}{g}\right) \tag{2.17}$$

The relationship between air-relative and inertial flight path angle is:

$$\gamma_i = \sin^{-1}\left(\frac{V_a \sin\gamma_a + G_z \cos\gamma_a}{V_i}\right) \tag{2.18}$$

where V_i is the inertial speed of the aircraft and G_z is the component of wind orthogonal to the total airspeed vector. The equation can be simplified because the magnitude of the air-relative flight path angle is usually small and so $\cos\gamma_a$ can be set to unity.

The potential inertial flight path angle is derived by setting the airspeed rate of change to zero. In this case γ_{ap} from equation 2.17 can be substituted for γ_a in equation 2.18.

$$\gamma_{ip} = \sin^{-1}\left(\left(\frac{T\cos\alpha - D}{mg} + \frac{\dot{G}_x}{g}\right)\frac{V_a}{V_i} + \frac{G_z}{V_i}\right) \tag{2.19}$$

The relationship between the actual and potential inertial flight path angles has already been derived in equation 2.15. The expression for the potential inertial flight path angle can be substituted into this equation and the factors which affect the inertial flight path angle can then be derived.

$$\gamma_i = \sin^{-1}\left(\frac{T\cos\alpha - D}{mg} + \frac{\dot{G}_x}{g} + \frac{G_z}{V_a} - \frac{\dot{V}_a}{g}\right)\frac{V_a}{V_i} \tag{2.20}$$

The aircraft's ability to climb can be traded for airspeed as discussed earlier, and can be increased by increasing the thrust. The effect of the wind on the flight path angle can now be seen. The terms in equation 2.20 which relate the wind components to the flight path angle are known as the 'F-factor'.

$$F = \frac{\dot{G}_x}{g} + \frac{G_z}{V_a} \tag{2.21}$$

This factor is frequently used as a measure of the degree of hazard of a windshear. A large negative value indicates a significant performance decreasing shear whereas a positive value results from a performance increasing shear. It should be noted that the signs in the F-factor expression in this thesis differ from those from NASA references because the sign conventions used to define the wind co-ordinates differ.

The F-factor can be related to the parameters in the equations of motion already derived. The x-axis of the stability axis system points into the relative wind and so the trim angle of attack is zero. Therefore the total

airspeed is equivalent to the x-axis airspeed and the wind components are identical to those described in the stability axis co-ordinate equations:

$$V_a \equiv U_a \tag{2.22}$$

$$\dot{G}_x \equiv \dot{U}_g = \dot{u}_g \tag{2.23}$$

$$G_z \equiv W_g = w_g \tag{2.24}$$

The revised F-factor expression is given in equation 2.25.

$$F = \frac{\dot{u}_g}{g} + \frac{w_g}{U_a} \tag{2.25}$$

The use of this factor is discussed further in Sections 3.2 and 6.3.

2.2.4 Escape from a Windshear Encounter

The recommended action is to avoid all windshear situations, as some shears are too strong to be successfully traversed once entered. However, if a windshear is unintentionally encountered the pilot must act to maximise the possibility of surviving the shear. Normal piloting techniques place emphasis on maintaining airspeed to effect flight path control, but in a low altitude windshear such an approach is likely to worsen the outcome. The recommended action for a windshear encounter on either take-off or approach is to climb out of the shear by pitching up to an angle a little below the stall angle; the suggested target pitch attitude is 15°, and by maximising thrust. The altitude must be increased at the cost of airspeed and the pilot should therefore control the vertical flight path of the aircraft using pitch attitude control. No attempt should be made to regain airspeed until the aircraft has sufficient altitude and there is no risk of ground contact. [1, 22, 23, 24]

To familiarise airline pilots with these techniques an extensive programme of recurrent pilot training using simulators is undertaken. Without this training, a pilot may hesitate to respond in a way that differs from standard flying procedure. In addition, abnormal stick forces may be required to counter the loss of lift and the pitch-down tendency of the aircraft which is

caused by the loss of airspeed. [25] The Air Line Pilots Association (ALPA) in the USA disagreed with the recommendations and disliked the directive to fly at angles of attack which were approaching stall conditions. The association's preferred strategy was to hold some energy margin in reserve to prevent or soften ground impact. [26]

Alternative escape strategies have been analysed. [21, 27, 28] The results suggest that there is relatively little difference between strategies in the ability to escape a windshear. The best recovery strategy is to maintain the smallest rate of climb necessary for obstacle clearance, lowering the nose to reduce the rate of climb on take-off if necessary. However, the study showed that the most significant effect in enhancing survivability of a windshear was produced by providing an earlier time of alert. It was found that advancing the time of warning by five seconds had a far greater effect on the chances of surviving the windshear than a change in the escape strategy.

2.2.5 General Aviation Aircraft and their Response to Wind

General aviation aircraft differ from transport aircraft in their response to windshear in several significant ways. The principal differences arise from their lower flying speeds which means that a given windshear represents a larger proportion of the aircraft's airspeed and so the effect is more pronounced. The speed margin, i.e. the difference between the minimum operating speeds during take-off and landing and the aircraft's stall speed, is defined as a percentage of the stall speed and is therefore lower for general aviation aircraft; as a consequence general aviation aircraft are less able to penetrate strong wind shears such as those present in microbursts.

The lower airspeeds also mean that a general aviation aircraft will traverse a shear more slowly than a transport aircraft. This allows the pilot more time to recognise and respond to the shear but also makes the aircraft more susceptible to the z-axis component of the shear. From the discussions in Section 2.2.1 it can be seen that whilst an encounter with a decreasing headwind component at a slower speed reduces the rate of loss of airspeed, the z-axis component of the shear produces an increase in the loss of altitude at low airspeeds.

Although the speed margin of a general aviation aircraft is usually significantly lower than that of a transport aircraft, the difference in the acceleration margin is often much less. The ability of an aircraft to accelerate is not itself particularly important to an aircraft during a windshear encounter, provided stall speeds are avoided. However, the acceleration margin also indicates reserve capability to climb out of the windshear because, in energy terms, the acceleration can be exchanged for an improved rate of climb as shown in equation 2.12.

2.2.6 Windshear Susceptibility on Take-Off, Approach and Landing

Windshear is known to be a hazard during low-altitude phases of flight, but analysis of the flight phases shows that many more accidents occur during the final phases of flight than during take-off. This may arise for several reasons related to both aircraft performance and human factors. [2, 23, 29, 30]

During take-off the aircraft is at maximum thrust and set to climb away from the runway, whereas an aircraft on the approach phase of flight has a lower thrust setting and the airspeed is being reduced in preparation for landing; the windshear escape configuration is very much more closely allied to that required for take-off. The climb angle and glideslope angle, typically +7.5° and -3° respectively, mean that the aircraft spends a longer time at low altitude, and hence with a lower specific energy, during approach.

The pilot has a considerable workload on approach, not only in terms of controlling the aircraft, but also because of the very significant quantity of radio communications from the differing air traffic control/airport tower controllers who are responsible for the various phases of the approach and landing. The landing manoeuvre requires a greater precision from the pilot than the take-off, where the exact path of the aircraft is less important. In addition, the consequences for a pilot of a commercial aircraft of a missed approach causing a go-around manoeuvre and a delay in landing are more severe than those of a delayed take-off, and so the pilot is likely to feel a greater pressure to complete the landing. Finally, the pilot who is at the end of the journey may be considerably more fatigued and be slower to recognise the symptoms of windshear unless alerted to the situation in a clear and unambiguous way.

2.3 Mathematical Models of Atmospheric Disturbances

For analytical work on aircraft behaviour in wind it is useful to apply mathematical models of wind phenomena. Suitable models are developed in this section.

2.3.1 Classification of Atmospheric Disturbances

Atmospheric disturbances can be generalised for the purposes of aeronautics in three basic forms: turbulence, gusts and windshear. Turbulence is a high frequency, relatively small amplitude, random disturbance. Such air motion is always present to some extent in the atmosphere but it occurs at significant intensities as convective turbulence around clouds formations or as clear air turbulence. In contrast gusts are lower frequency, larger amplitude disturbances which can be reasonably accurately described for the purposes of wind-loading investigations as deterministic events. Windshear are again relatively low frequency, deterministic phenomena but they are generally of larger amplitude than gusts and are therefore considered to have a significant effect on the flight trajectory of an aircraft. The amplitude threshold between gusts and windshear is in the region of 15-20 knots. The distinctions between these three phenomena are made artificially for the purposes of simplifying the analysis; in practice the wind field encountered by an aircraft will contain some or all of these features.

The x-axis and z-axis wind components encountered by four transport aircraft can be seen in Figures 2.6 to 2.9. These exhibit qualities of turbulence, gust and windshear. The wind conditions encountered by Aircraft 1 which are shown in Figure 2.6 appear benign until the sudden loss of headwind combined with an updraft/downdraft shear which occurs after approximately 140 seconds. Aircraft 2, in Figure 2.7, is subjected principally to gusting winds, especially along the x-axis, with higher frequency turbulence superimposed. Aircraft 3 in Figure 2.8 encountered an initially increasing headwind and then a sudden reduction of approximately 60 feet per second over a two minute period followed by a further headwind increase and decrease. The z-axis component of the wind shows a considerable amount of high frequency, turbulent characteristics. Figure 2.9 shows that Aircraft 4 is subjected to some gusting wind in the first 100 seconds before the more violent windshear events which peak after approximately 330 seconds. In examining these figures it should be noted

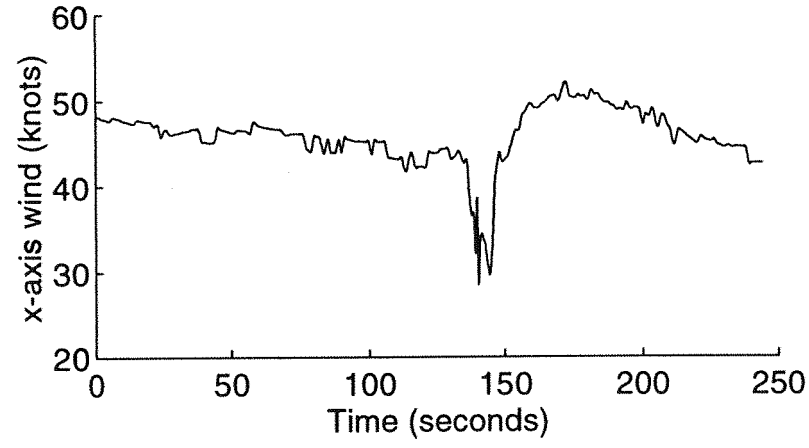

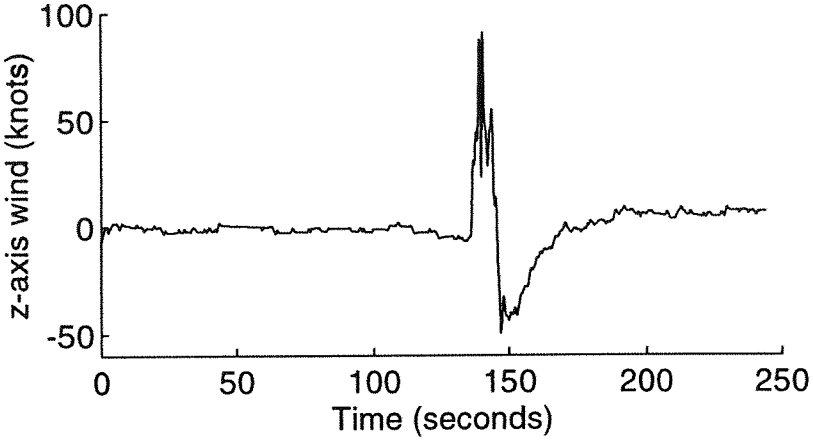

Figure 2.6: Winds Encountered by Aircraft 1

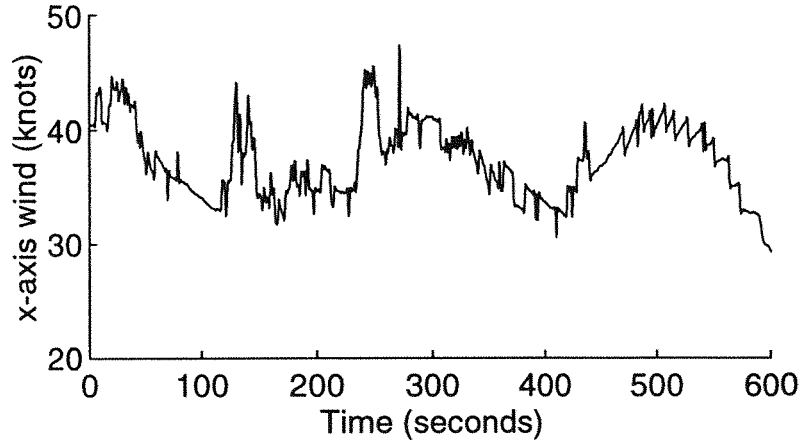

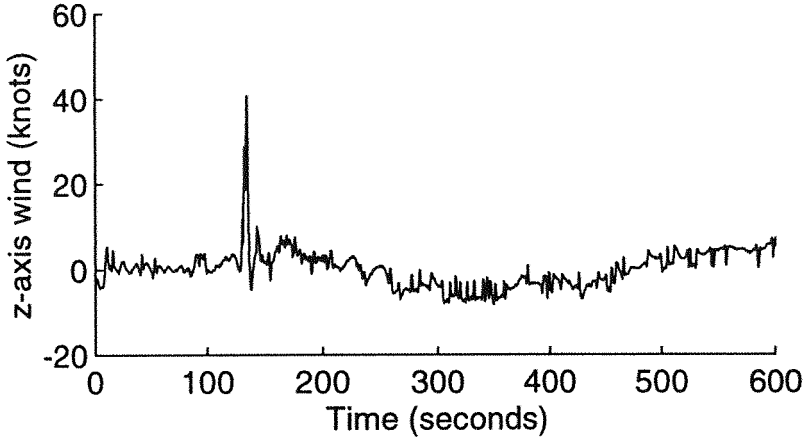

Figure 2.7: Winds Encountered by Aircraft 2

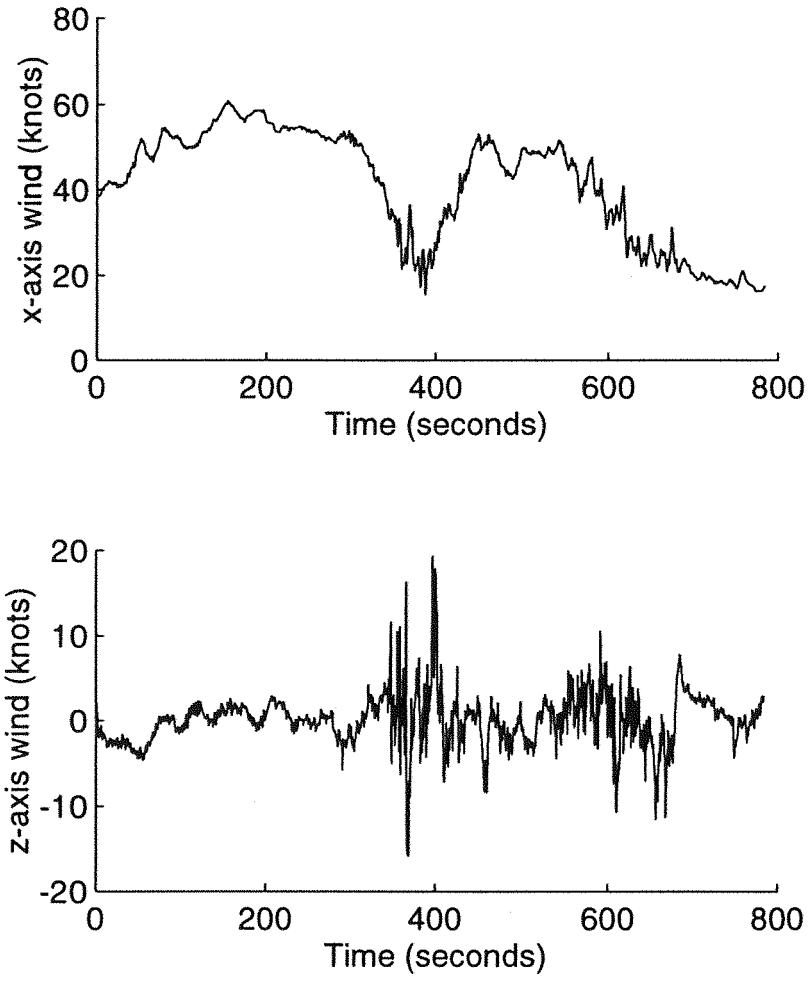

Figure 2.8: Winds Encountered by Aircraft 3

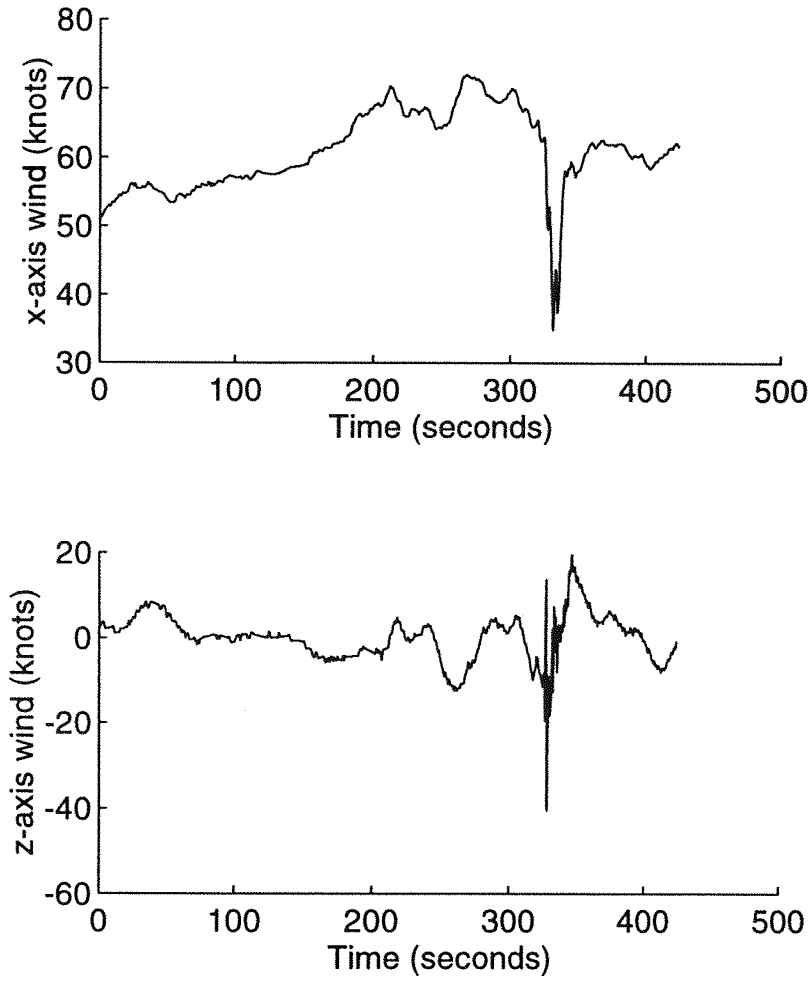

Figure 2.9: Winds Encountered by Aircraft 4

that all the aircraft were at cruising altitudes of approximately 33000 feet when these events were encountered whereas it is the low-level effects which are of most concern in windshear studies.

2.3.2 Gust models

As already described, a gust can be modelled as a deterministic function (although the timing of the occurrence may be random). The most widely used model for a discrete horizontal gust is the '1-cos' gust. The gust is described by equation 2.26 where A is half the resulting gust amplitude, ω is the frequency of the gust and t is the independent time variable.

$$Gust(t) = A(1-\cos\omega t) \tag{2.26}$$

The period of the gust is usually chosen to match that of the phugoid mode of the aircraft as this will maximise the dynamic loading. This is achieved by setting the frequency according to equation 2.27 where T_{ph} is the period of the phugoid mode.

$$\omega = \frac{2\pi}{T_{ph}} \tag{2.27}$$

This form of gust is specified in the FAA's Technical Standard Order [31] which specifies the required performance of an airborne windshear detection system for transport aircraft. It is used to test the systems to ensure that they are not triggered by non-hazardous gusts. For this purpose the peak amplitude ($2A$) is set to 15 knots and the frequency is set to values between 0.3 to 2 rads/sec which results in a duration of between 3 and 20 seconds.

2.3.3 Turbulence Models

Turbulence is a form of wind where the wind velocity is a random function of both space and time. It cannot therefore be represented as a deterministic process but requires the use of statistical methods. Two representations which model turbulence as a stationary, random process are widely used in aeronautical studies - the Von Karman model and the Dryden form. [4, 6, 32]

The Dryden model is a simpler representation and is therefore more frequently used. The FAA requires that windshear detection systems for

transport aircraft do not produce nuisance alerts when subjected to turbulence. The TSO [31] specifies that the systems must be tested using a Dryden turbulence model and the parameters which characterise this are defined at various different altitudes. The method by which the model is used to generate a turbulence profile is described in Appendix C.

Figure 2.10 shows the form of the x-axis and z-axis turbulence derived from the specification at two different altitudes and airspeeds (the same band-limited white noise sequence is used to generate the turbulence components at the two airspeed and altitude settings). The turbulence model for an aircraft at 1500 feet with an airspeed of 150 knots shows a slightly smaller intensity and greater amplitudes at low frequencies than the modelled turbulence at 100 feet and 150 knots airspeed.

2.3.4 Windshear Models

Models of typical wind components can be used to investigate the windshear problems, and these vary from the simple longitudinal models to complex '3-dimensional' models which are the type more frequently used for piloting studies in aircraft simulators. [13, 33] The models may be generated mathematically from a knowledge of windshear characteristics or by using data collected from aircraft, air traffic control (ATC), and meteorology sources after a windshear encounter to reconstruct the components of the wind.

Figure 2.11 shows a simple one dimensional mathematical representation of a symmetric microburst. The horizontal component models the characteristics of the microburst outflow using a sine function to simulate the initial headwind increase followed by a performance-decreasing shear. The vertical component is a '1-cos' function and represents the downflow at the core of the microburst. The model can be easily varied to provide differing test conditions and both components can be 'tuned' to the natural phugoid mode of the aircraft to cause resonance and maximise the induced load. The equations for the two windshear components are:

$$u_g(t) = A_x \sin(\frac{2\pi t}{T}) \tag{2.28}$$

$$w_g(t) = -A_z(1+\cos(\frac{2\pi t}{T})) \tag{2.29}$$

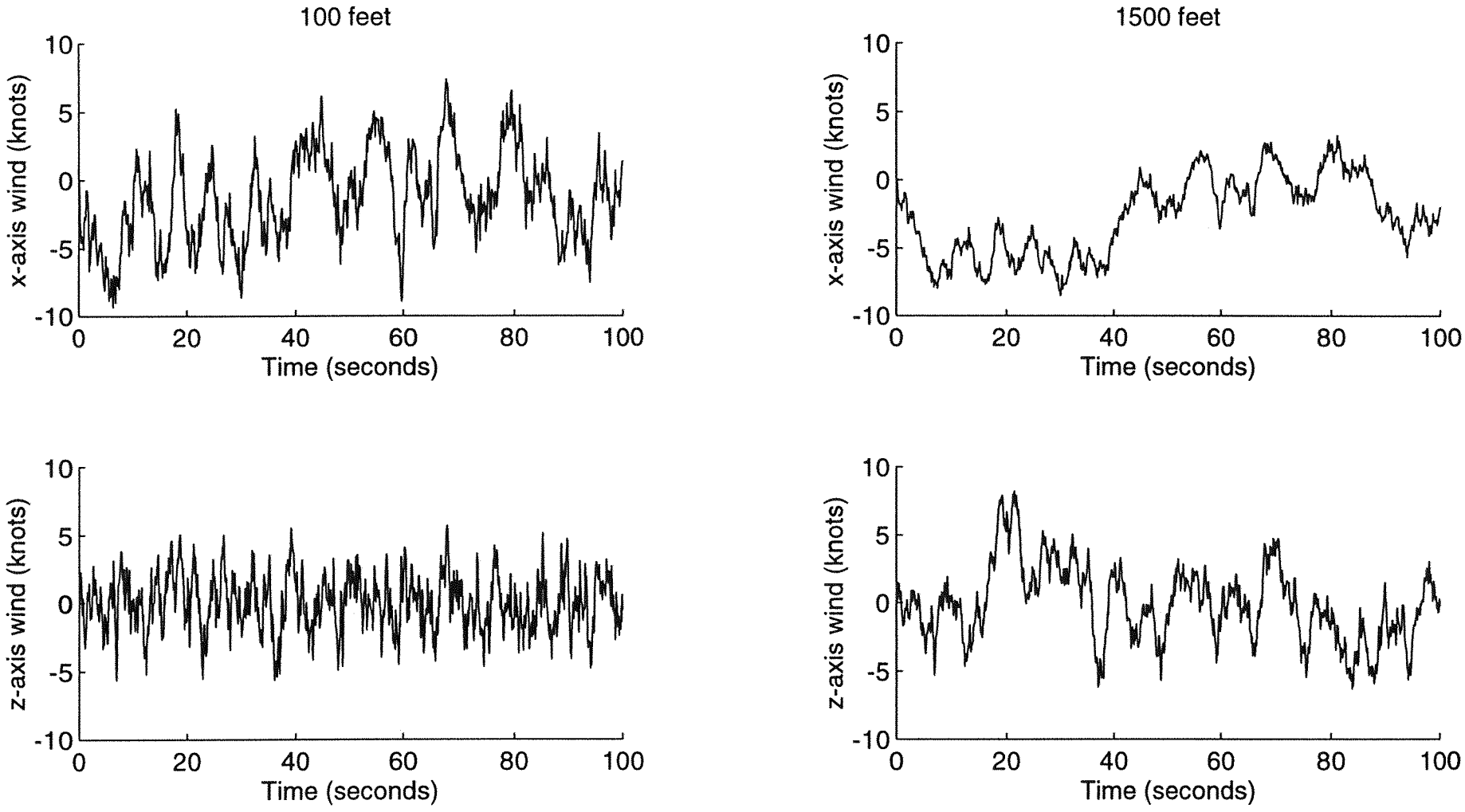

Figure 2.10: Dryden Turbulence Model at Altitudes of 100 feet and 1500 feet

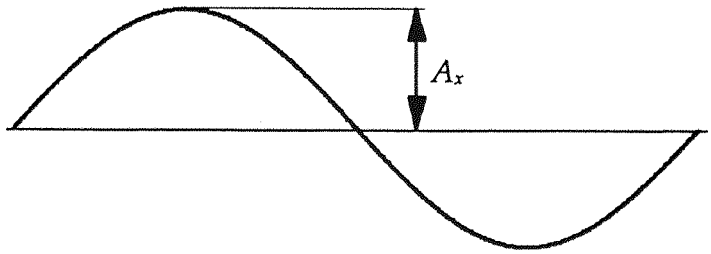

x-axis wind component

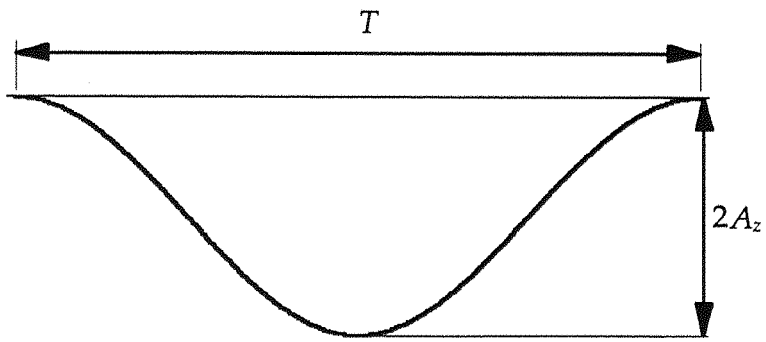

z-axis wind component

$$u_g(t) = A_x \sin(\frac{2\pi t}{T})$$

$$w_g(t) = -A_z(1+\cos(\frac{2\pi t}{T}))$$

Figure 2.11: Mathematical model of a Downburst

T is the period of the microburst and A_x and A_z are the amplitudes of the x-axis and z-axis components respectively.

Reconstruction of a windshear from recorded data was first achieved following the accident at John F. Kennedy Airport in 1975. Figure 2.12 shows a profile of the microburst and sea-breeze front which produced the strong wind variations and the trajectory of the aircraft. [6] The components of the shear are shown in Figure 2.13. The non-symmetric form of the microburst and the interaction of the sea-breeze front produce significant differences from the model in Figure 2.11. This is a useful windshear model because it is taken from an actual low-level windshear encounter and contains both rapid transitions and slow variations in both wind components.

The wind components shown in Figures 2.6 to 2.9 were reconstructed from data from flight data recorders and the Air Traffic Control radar records by researchers at NASA Ames. [34, 35] Parameters not recorded, such as angle of attack and sideslip, were calculated using the known parameters and the aircraft's performance characteristics and the wind components were then found using state estimation methods.

The digital flight data recorder on the L1011 aircraft which crashed at Dallas-Fort Worth Airport in 1985 and that on the following aircraft provided a very detailed set of flight data which, together with the ATC recordings, allowed the wind components to be estimated with a considerable degree of confidence. [36, 37] A number of models of the microburst which caused the accident have been generated. Figure 2.14 shows the substantial similarities between the wind components derived from the actual data and those from a model of a microburst using two vortex rings. [38] The use of mathematical models of this sort often has significant advantage compared with using the actual wind components because the location, intensity and form of the microburst can be easily altered to provide differing windshear conditions and the model provides a three-dimensional representation which causes the effect of the wind on the aircraft to vary depending on the aircraft course and the pilot's reaction. For this reason mathematical models of windshear derived from actual windshear encounters are often used in flight simulation. The ring vortex model of a microburst windfield defines the windfield in terms of the position relative to the vortex centre, the vortex radius, core diameter and circulation. By altering these parameters the intensity of the

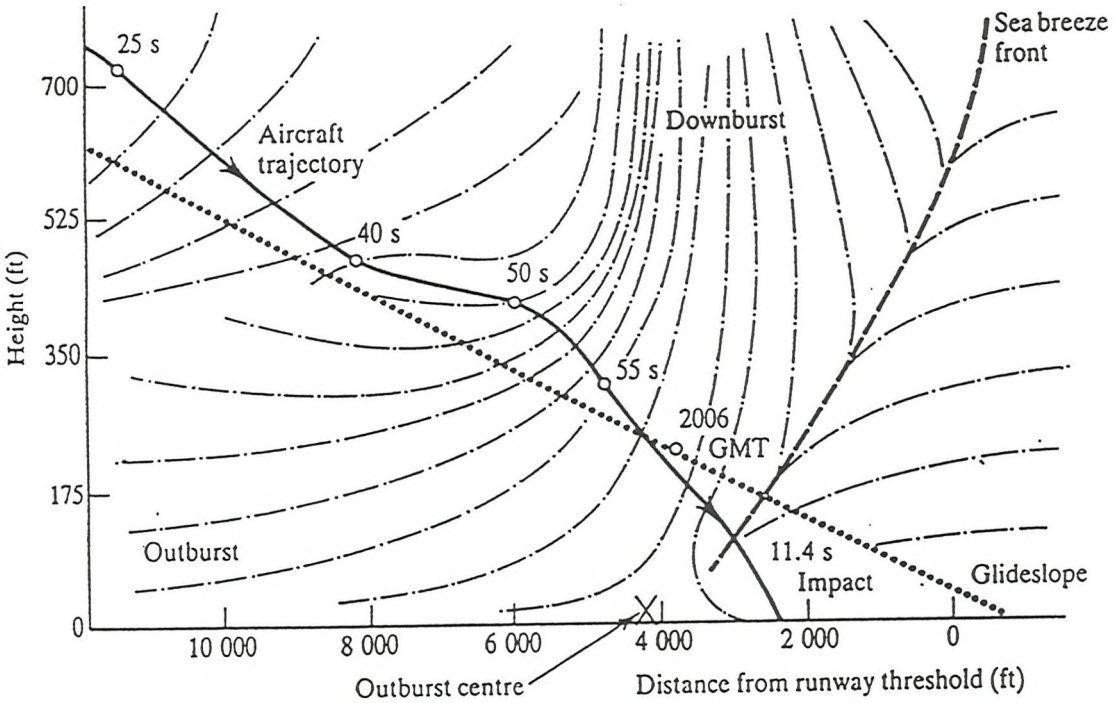

Figure 2.12: Cross-Section of JFK Windshear showing Aircraft Flight Path

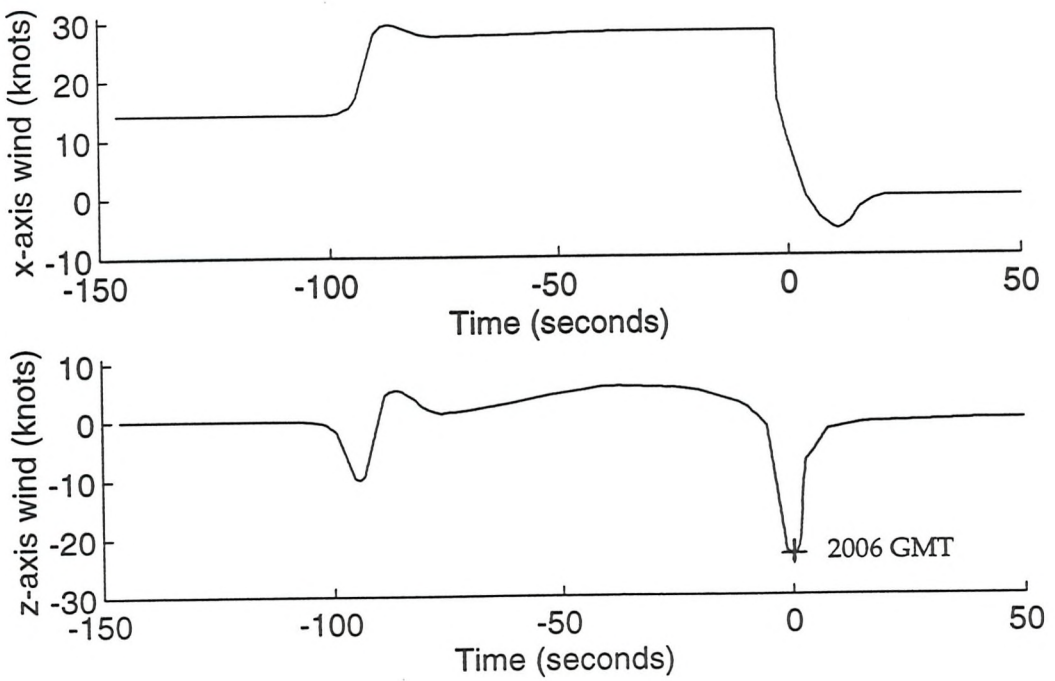

Figure 2.13: JFK Windshear Components

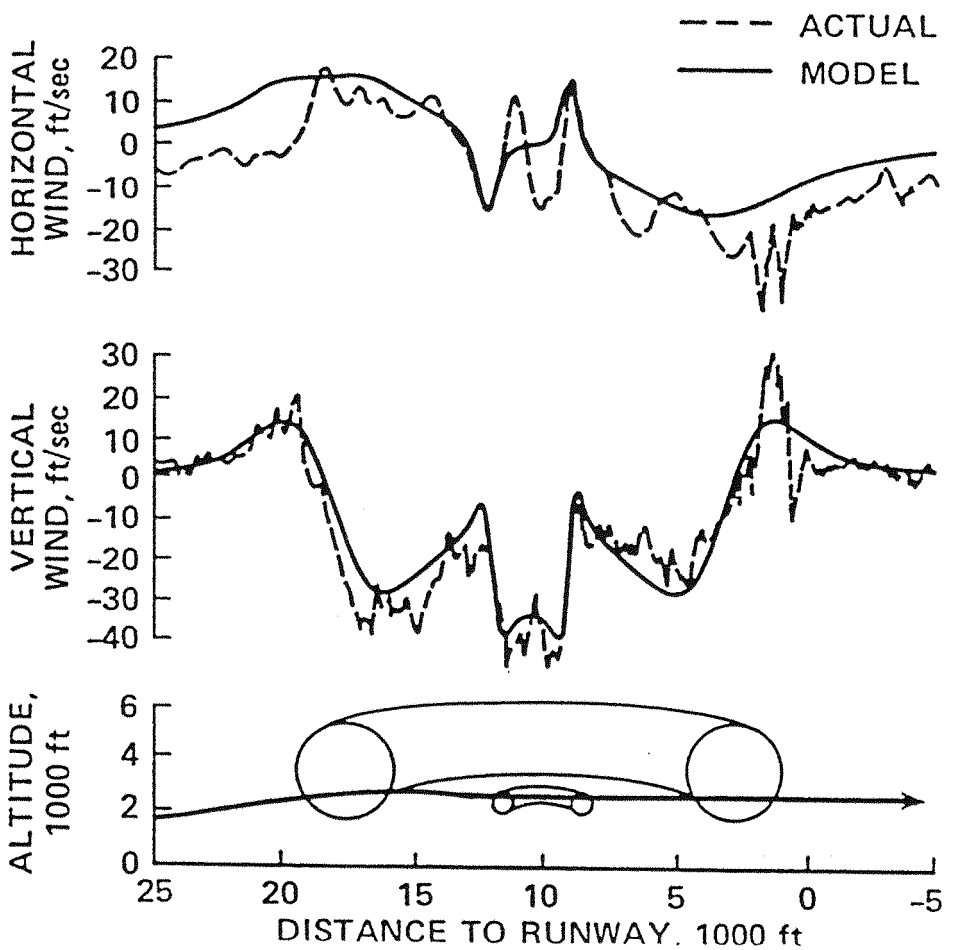

Figure 2.14: DFW Wind Components and Vortex Model of the Windfield

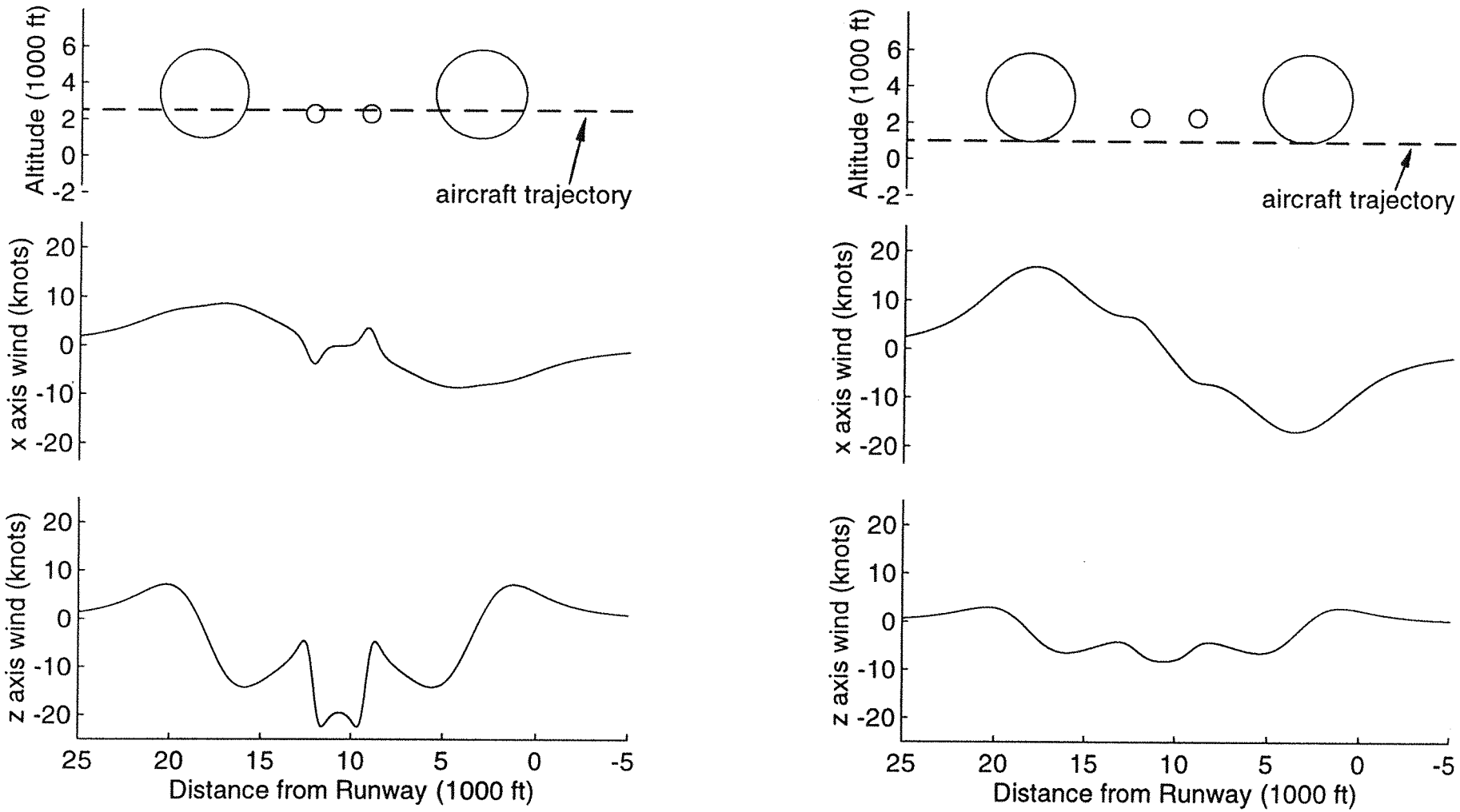

Figure 2.15: Wind Components of DFW Windshear at Two Altitudes

microburst and path of the aircraft through the shear can be varied to investigate warning and escape strategies. Figure 2.15 shows the wind encountered by an aircraft which traverses the microburst through the centre of the vortices at altitudes of 2500 feet (approximately the same as that encountered by the aircraft on go-around) and 1000 feet i.e. just below the large vortex ring. The trajectories of the aircraft relative to the vortex rings are shown in the upper diagram. It can be seen that the lower altitude path encounters larger horizontal changes as the aircraft passes through more of the outflow but the updraft/downdraft changes are reduced because the aircraft is not flying so close to the centres of the vortex rings.

3 WINDSHEAR DETECTION

As the awareness of the dangers associated with low altitude windshear increased the need for systems to detect these hazards became more apparent. Both ground-based and airborne windshear systems have now been developed and research into enhanced detection methods is still in progress.

3.1 Ground-Based Detection Systems

3.1.1 Low-Level Windshear Alert System

In the early 1970s the Federal Aviation Authority initiated the development of a network of anemometers situated on or near airports to monitor wind changes. The system, known as the Low-Level Windshear Alert System (LLWAS), was designed to detect gust fronts which at that time were considered to be the principal windshear hazard to aviation.

In its original form the system comprised a small network of six anemometers i.e. a centrefield anemometer and five outlying anemometers positioned three kilometres from the centre and linked to a minicomputer. The centrefield site was used to keep a two minute moving average of the wind velocity. Each outlying sensor was read every ten seconds and the reading compared with the centrefield average; a difference in excess of fifteen knots (7.5 ms^{-1}) caused an alert to be passed to the air traffic controllers. [39]

This system provided an operational means of monitoring wind velocities but had several inherent problems which reduced its reliability for detecting windshear. The most serious was the poor spatial resolution which enabled a gust front to be detected but could allow a microburst to pass between the anemometers and traverse the airport. The LLWAS system installed at Dallas/Fort Worth Airport in August 1985 failed to detect the microburst which caused the L1011 to crash until ten minutes after the accident had occurred because of inadequate resolution. [40, 41] In addition, the system appeared to produce alerts when aircraft did not experience adverse wind effects and this caused a loss of confidence in the system among pilots. [42] Yet another drawback was in the presentation of the data. The wind magnitude and direction at each anemometer were presented to the air traffic controllers, and read in the same format to the air crew. This made it difficult to relate the windshear in the vicinity to the hazard it presented for a

particular runway - a problem which was observed in the findings of the investigation into the accident at New Orleans International Airport in July 1982. [3, 43]

The LLWAS performance was measured during the Joint Airport Windshear Study (JAWS) which placed a large number of wind-measuring sensors over an area extending thirteen kilometres from Stapleton Airport, Denver, and monitored all windshear activity for a period of eighty days. The windshear occurrences recorded were compared with the LLWAS alarms and the correlation was found to be highly erratic, especially in the detection of microbursts. As a consequence, a programme to improve the system was begun.

The goals for the new program were to improve LLWAS by increasing the sensor density, by developing new algorithms which could specifically detect microbursts as well as other types of windshear and by improving the method of communicating a windshear event to the air traffic controllers. This resulted in the current enhanced system which consists of up to sixteen anemometers placed 2.5 km apart. The detection algorithm calculates the net airflow in each segment of the network grid which enables differentiation between the various forms of windshear. The warning display for the air traffic controllers gives specific information on the winds affecting the runways rather than information on the wind speed and direction at each anemometer. The microburst detection rate has improved from around twenty-five percent for the original system to eighty percent, and the number of false alarms is significantly reduced. [1, 2, 5] The upgraded system proved its effectiveness in July 1989 when a Boeing 737 received an alert of a 90 knot windshear on approach to Stapleton Airport, Denver. Although sceptical of the LLWAS warning, the pilot decided to execute a missed approach and began to climb and accelerate. The aircraft subsequently encountered a 95 knot windshear which caused a 50 knot airspeed loss and 400 feet loss of altitude. [44]

The upgraded LLWAS system is now deployed at over 100 airports is the USA. Although this provides useful and timely information on the surface windfield within the airport perimeter, the system has significant deficiencies in providing a comprehensive warning system. It is only able to measure the wind speed and direction at ground level and this prevents the

identification of a microburst until it has reached the ground and begins to rapidly intensify. A more significant problem, perhaps, is the restriction of the system to 'on-airport' measurements for determining levels of windshear hazard. A windshear at some distance from the airport may still be a considerable danger to aircraft which, during typical operations, are below 1000 feet (330 m) for 6 km on approach and for 2.5 km on takeoff - based on a 3° glideslope and a 7.5° climb respectively. [29]

3.1.2 Terminal Doppler Weather Radar

Radar has been used for many years to detect storms and other weather phenomena by measuring the radar returns from precipitation. Pulsed Doppler radar enables the velocity of the precipitation, and hence the airflows in which it is contained, to be measured and thus provides additional information on which to base weather predictions. A nation-wide network of Doppler radar for weather forecasting purposes has been installed in the USA to predict and track severe storms, and this system can provide some protection to aircraft at cruise altitudes. [45] A similar technology can be used for measurement of localised wind velocities around airports and a dedicated ground-based windshear detection system based on this principle, Terminal Doppler Weather Radar (TDWR), has been developed. [18, 46, 47, 48]

The radar scans the atmosphere above and around the airport and measures the radial component of wind velocity at a range of up to 80 km. The preferred location for the radar is at approximately 15 km from the airport and as close to the centrelines of the runways as possible. This positioning ensures that the measured winds correspond as nearly as possible to the headwind changes experienced by aircraft using the runways. Accurate estimation of a headwind component is most important for those systems where only a single component can be measured since headwind changes pose the greatest threat, as discussed in Section 2.2.1.

The system scans every minute at an altitude of approximately 100m and through an azimuth of 120° to detect the presence of any hazardous surface winds. In addition, a series of scans at varying elevations up to a height of 6 km are repeated every 2.5 minutes, and these are analysed by the system to ascertain whether the early symptoms of microburst formation exist. If this

is the case, and the characteristic surface wind patterns associated with a microburst are subsequently detected, a warning may be given even if wind velocities do not exceed the usual threshold in anticipation of the intensifying microburst. A 360° scan is made every five minutes which enables any frontal systems or storms at long range to be detected.

The system uses 5 cm wavelength 'C band' radar which was selected from considerations of the required compromise between performance factors viz. clutter suppression, range/velocity resolution, signal attenuation and size of antenna. Ground clutter, unwanted reflections from objects around the airport, was one of the major obstacles to be overcome in the development of the system.

The system performance differs for wet and dry microbursts. A wet microburst has significant precipitation and the radar reflection is stronger than that of a dry microburst. This difficulty was overcome by performing a series of trials in areas where wet or dry microbursts prevail and developing the algorithm to maximise the probability of detection while keeping the false alarm rate low. The design requirements for the system were for a 90% probability of detecting a reportable windshear in the vicinity of the airport and a false alarm rate of less than 10%. The performance achieved has been shown to be significantly better, with 97% of windshear detected.

The warnings are transmitted to the air traffic controllers who convey the whereabouts of the windshear to the pilots and adjust the airport operation, e.g. choice of runway, accordingly. An amalgamated airport weather information system which will principally comprise LLWAS and TDWR data is being developed and this will eventually have a transponder data link to the aircraft to fully automate the warning process.

3.1.3 Low-Cost Microburst Radar

The Terminal Doppler Weather Radar is being installed at 44 major US airports. The system is considered too expensive for other airports, being of the order of $3-$5 million. An alternative system for these sites is being evaluated. This uses technology developed for airborne detection systems discussed in Section 3.2.2. The 'Microburst Prediction Radar' uses X-band radar to scan a full hemisphere every twenty seconds. The system measures

the velocity of moisture particles to determine whether a downdraft is present and thereby evaluates the hazard. The system, which costs $500 000 - $700 000 was predicted to detect 96% of microbursts with a false alarm rate of 1%. Reports of testing of the system during 1992 indicate that during this evaluation the system detected 100% of microbursts with a false alarm rate of 1% and an average advance warning of 3.1 minutes. [49]

3.2 Airborne Detection Systems

3.2.1 Reactive Detection Systems

Airborne systems may be divided into two categories 'reactive' and 'forward-looking'. Reactive systems measure the response of the aircraft to its environment in order to determine whether windshear is present. Systems of this sort have been in service for some years, and legislation by the FAA, which required the installation of windshear detection systems in all transport aircraft with more than 30 seats by the end of 1993, resulted in the retrofitting of many such detection systems. [50, 51]

These systems aim to detect the windshear at least five seconds before the effects of the shear becomes apparent to a pilot from normal instrument displays and also to provide an unambiguous warning at this time. (This contrasts with standard flight instruments which do not effectively display the symptoms of severe windshear.) Most reactive systems alert the pilot with an aural warning which annunciates 'windshear' three time; a red light labelled 'windshear' on the instrument panel or electronic display is lit for the duration of the encounter. [31] Some systems advise the pilot of a significant 'performance enhancing' shear as well as hazardous performance-decreasing shears using an amber light and, in some cases, an aural caution alert. The pilot is then aware of abnormal wind conditions which may indicate the onset of a microburst.

Many systems provide escape guidance to the pilot and this is usually in the form of a moving pitch limit on the Attitude Direction Indicator. [52, 53] Immediate action by the pilot to climb out of the shear by maximising the thrust and increasing the pitch attitude can substantially improve the chances of surviving the encounter.

All the devices installed at present measure the velocity or acceleration of the airmass by comparing the inertial and air-relative motion variables in the longitudinal plane of the aircraft and thereby compute the headwind/tailwind and updraft/downdraft components of the wind. [54, 55, 56, 57, 58] This is accomplished by taking data from the onboard systems such as the Inertial Reference System (IRS) and the Digital Air Data Computer (DADC) as well as further inputs from angle of attack sensors and flap settings. Typical costs of the windshear detection modules alone are in excess of $30 000.

The Boeing wind shear detection criterion is based on the total energy methods as described in Section 2.2.3. The F-factor, which gives an indication of the specific rate of change of energy caused by windshear, is:

$$F = \frac{\dot{U}_g}{g} + \frac{W_g}{U} \tag{3.1}$$

A large negative value indicates a strong performance-decreasing shear. This equation can be simplified for the purposes of the detection system to an equivalent relationship

$$F = \frac{(\dot{U} - \dot{U}_i)}{g} + (\gamma_i - \gamma_a) \tag{3.2}$$

Figure 3.1 shows an implementation of this detection method for the Boeing 737-300, -400 and -500 aircraft. [20] The horizontal windshear component is calculated by comparing the rate of change of true airspeed with the inertial acceleration. The vertical wind contribution to the F-factor is derived by calculating the inertial and air-relative flight path angles and combining the result. The parameters required for the estimates of the horizontal and vertical contributions to the F-factor are taken from the on-board IRS, DADC and a vane measuring the angle of attack. The gain scheduling blocks are used to reduce the sensitivity of the algorithm when the aircraft is above 500 ft of radio altitude and the gust filtering reduces the likelihood of turbulence triggering the alarm; both of these measures reduce the probability of nuisance alerts.

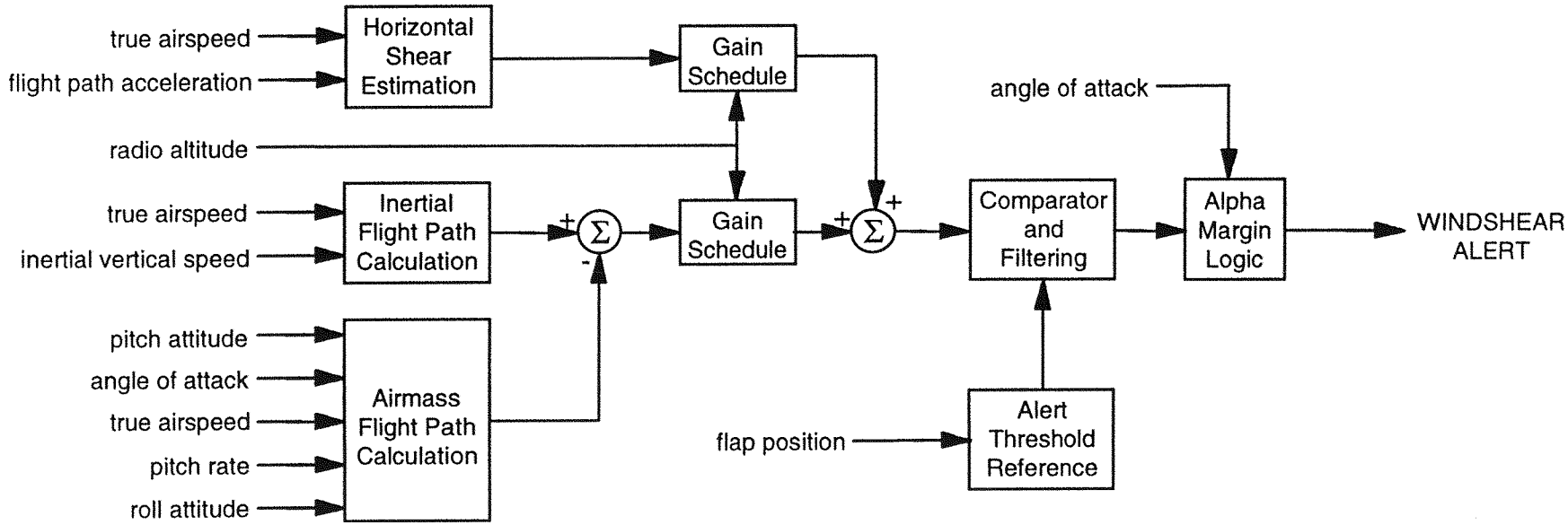

Figure 3.1: Boeing Windshear Detection System

A warning is given whenever the F-factor threshold is exceeded. The non-dimensional thresholds are 0.12 for take-off and 0.11 for approach. The 0.11 threshold corresponds to a pure longitudinal shear of 2.1 knots per second or a pure vertical downdraft of 11% of the forward speed.

The aural alert is in the form of two warning tones followed by a voice saying 'Windshear' three times. At the same time a visual warning is given with the word 'windshear' appearing in red on the Electronic Attitude Direction Indicator. This persists for the time that the aircraft is within four degrees of the stick shaker angle of attack and for a minimum of five seconds. The system is active up to an altitude of 1500 feet (~500m) above ground level. Flight guidance is provided by the system to assist the pilot in the control of the flight path during the windshear encounter; this targets pitch attitude instead of airspeed. [52]

The Honeywell Windshear Detection System also takes data from the IRS, DADC and angle of attack vane but it processes these data differently. [59] Instead of calculating the effect of the windshear on the aircraft energy, as is the case with the F-factor approach, the rate of change of both longitudinal and vertical wind are calculated directly and these are used to determine whether a hazardous windshear is present. Further inputs to the system viz. calibrated airspeed, pressure altitude and flap position plus knowledge of the 'weight on wheels' and 'take off/go around' (TOGA button) settings enable the windshear computer to determine the phase of flight and function accordingly. The system is only armed to warn of windshear during take-off, approach and go-around phases of flight, unless a pilot override is applied. Honeywell provide cautionary alerts during performance enhancing windshear encounters.

3.2.2 Forward-Looking Detection Systems

In contrast to the reactive systems, forward-looking systems are required to provide a predictive warning of events 2 km to 4 km ahead of the aircraft which, at typical speeds of approximately 150 knots, provides 30 - 60 seconds warning before the shear is encountered. Various technologies are being employed to achieve this and all of these primarily measure the headwind/tailwind component of the wind. The principle features of these are summarised below.

Doppler weather radar, already installed in aircraft, uses the change in frequency of the signal reflected from water droplets in the air to give a measure of the velocity of the atmosphere. However, these do not have the capability of detecting windshear effectively and so in recent years several manufacturers have enhanced or modified their units by increasing the power and altering the pulse widths to make them more suitable for this purpose. During the last few years three versions of Doppler radar systems, which scan the atmosphere ahead of the aircraft through a 40° azimuth, have been undergoing flight trials prior to seeking regulatory approval. [60] It is expected that such systems should be able to provide an advanced warning of 45 to 90 seconds which would enable the pilots to avoid the shear completely. The principal problems which faced this proposed solution were distinguishing the windshear from ground clutter and the requirement to predict dry as well as wet microbursts. Sophisticated signal processing algorithms have been developed to overcome the problem of ground clutter, which is much worse than for ground-based detection systems - airborne systems have reduced power, and the returns from the terrain can appear to move in a similar way to a weather return because of the aircraft motion. Research has shown that the X-band radar (8-12 GHz) used in all three of the systems works well in wet conditions but that K-band radar (12-18 GHz) performs better for dry microbursts. [61] In practice the advanced warning time generally reduces towards 45 seconds in less humid air: radar techniques are unable to detect shears in completely dry conditions, but such conditions are rare.

An alternative, but similar, technique being investigated is Doppler lidar. Light detection and ranging (lidar) measures reflections from tiny particles, or 'aerosols', in the atmosphere and it has been shown that even in clear conditions there is still sufficient backscatter for Doppler measurements to be made. [62] Early airborne research systems tested during the late 1970s and 1980s showed the potential of the technology to predict windshear 20 to 40 seconds ahead but required large apparatus. [63] Technological advances have reduced the volume of the equipment but it remains relatively bulky. The method is not subject to ground clutter problems, but it is attenuated by rain which reduces the performance. The systems use a carbon dioxide laser at present; the use of shorter wavelength lasers promise superior performance and smaller size in the longer term, but the technology is less

advanced. [64, 65] The cost of a lidar system would be of the order of $100 000.

A possible method of optimising the performance in both wet and dry conditions is to use a hybrid system which would comprise both radar and lidar detection. This has been put forward and discussed by the researchers in the field but is not being developed, perhaps because the cost is too great.

Infrared systems for windshear detection are also being developed. [1, 63, 66] These are based on the technology already used for turbulence prediction. The system samples infrared energy at two wavelengths, 14 and 15 microns, which measures the temperature of the carbon dioxide component of the atmosphere at 3.5 km and 0.5 km ahead of the aircraft respectively. The temperature is known to vary across a shear in relation to its intensity and so the difference in temperature gives an indirect measure of the shear intensity and can be associated with a hazard factor. The system is able to detect both wet and dry microbursts, but there is a large increase in attenuation of the signal in heavy rain. The sensors have a narrow field of view of a few degrees and so another sensor measures temperature outside the aircraft to detect windshear which approach unseen. It is anticipated that infrared system will be able to provide 30 to 60 seconds advanced warning of a shear and would cost in excess of $50 000.

The developers of forward-looking radar systems have not finalised the warning format. Present systems based on weather radar produce displays either on a dedicated radar display or on a multifunction display. A windshear alert consists of a red striped segment to show the position of the hazard and the word 'windshear' written in red at the top of the display. The pilot is also provided with an aural warning similar to that provided by reactive systems.

3.3 General Aviation Aircraft Windshear Requirements

General aviation aircraft usually do not have the sophisticated avionic systems, such as the inertial reference systems or the digital air data computers, installed on transport aircraft and therefore the methods already described cannot be applied to this class of aircraft. There is a requirement then for a low-cost system suitable for general aviation aircraft.

As described in Section 2.2.5, a general aviation aircraft is slower moving than a larger transport aircraft and as a result has a reduced stall margin and less excess power to climb out of the shear. The requirement to warn as early as possible is crucial.

A further reason for providing a warning system relates to general aviation operations as these may take place at remote airfields with minimal ground-based aids and none of the ground-based windshear detection systems described in Section 3.1. An average general aviation pilot flies relatively few hours per year and has little recurrent training. As a consequence the pilot is less likely to be able to identify a windshear from visual or instrument indications, or to react appropriately.

3.4 Aircraft Instruments

Aircraft cockpits are fitted with instruments which convey to the pilot the information required to fly the aircraft safely. The technology of the instruments and the quantity of information varies considerably depending on the class and age of aircraft. The instruments can be categorised according to their function viz.: primary flight instruments, navigation, communication and indicators which display settings and environmental information. The primary flight instruments provide the fundamental information required by the pilot to be able to control the aircraft effectively, and the parameters displayed are related to the aircraft's flight dynamics.

The standard primary flight instrument cluster comprises an Airspeed Indicator, an Attitude Indicator which is also known as an Artificial Horizon, an Altimeter, a Turn Co-ordinator, a Heading Indicator and a Vertical Speed Indicator. The measurements made by these aircraft instruments may also be of use in a low-cost windshear detection system and so the design of these instruments for small general aviation aircraft is discussed below.

3.4.1 General Aviation Flight Instruments

The term 'general aviation' covers a broad spectrum of aircraft types and costs, so that the instrumentation for this class of aircraft varies considerably and the more expensive and larger aircraft may have systems comparable with those for commercial aircraft. However, it is the less-sophisticated aircraft which have lower-technology instrumentation for which a windshear

detection system is intended; the aircraft used as a model in subsequent chapters, the Cessna 402B, is an example. The instrumentation for these general aviation aircraft is mostly of traditional design. A typical instrument panel is shown in Figure 3.2.

The effect of wind on the longitudinal and lateral motion of the aircraft was discussed in Section 2.2, where it was shown that it is the change in longitudinal motion of the aircraft which produces the greatest hazard and which is therefore most likely to be of use in detecting a windshear. The principal instruments which measure and display parameters which relate to the aircraft's longitudinal motion are described below. [67]

The Airspeed Indicator measures the aircraft's speed through the air. A Pitot-static gauge is fitted to the exterior of the aircraft and the total pressure and static pressure of the air is conveyed to the indicator via tubing. The subsonic calibrated airspeed in knots, U_c, is derived as a function of the difference between the two pressures, ΔP, measured in millibars, as shown in equation 3.3. [68]

$$U_c = 661.4876 \sqrt{5\left(\left(\frac{\Delta P}{1013.25}+1\right)^{\frac{2}{7}}-1\right)} \qquad (3.3)$$

The density of the air varies with altitude and so calculation of the 'true airspeed' requires correction for this. Such a correction is not made in the standard airspeed indicator and so the parameter displayed is the 'indicated airspeed' or 'calibrated airspeed' for which the reference density is that of standard atmospheric conditions at sea level. The derivation of the airspeed is traditionally achieved mechanically and the airspeed indicator has a capsule which deflects according to the Pitot-static pressure difference and drives a system of non-linear mechanical linkages and gears to produce an airspeed indication.

The attitude indicator shows the aircraft's pitch and roll angles. It traditionally uses a displacement gyro to maintain a 'level platform' within the instrument and this is used to indicate the position of the horizon relative to the aircraft. The gyro is either driven pneumatically or electrically.

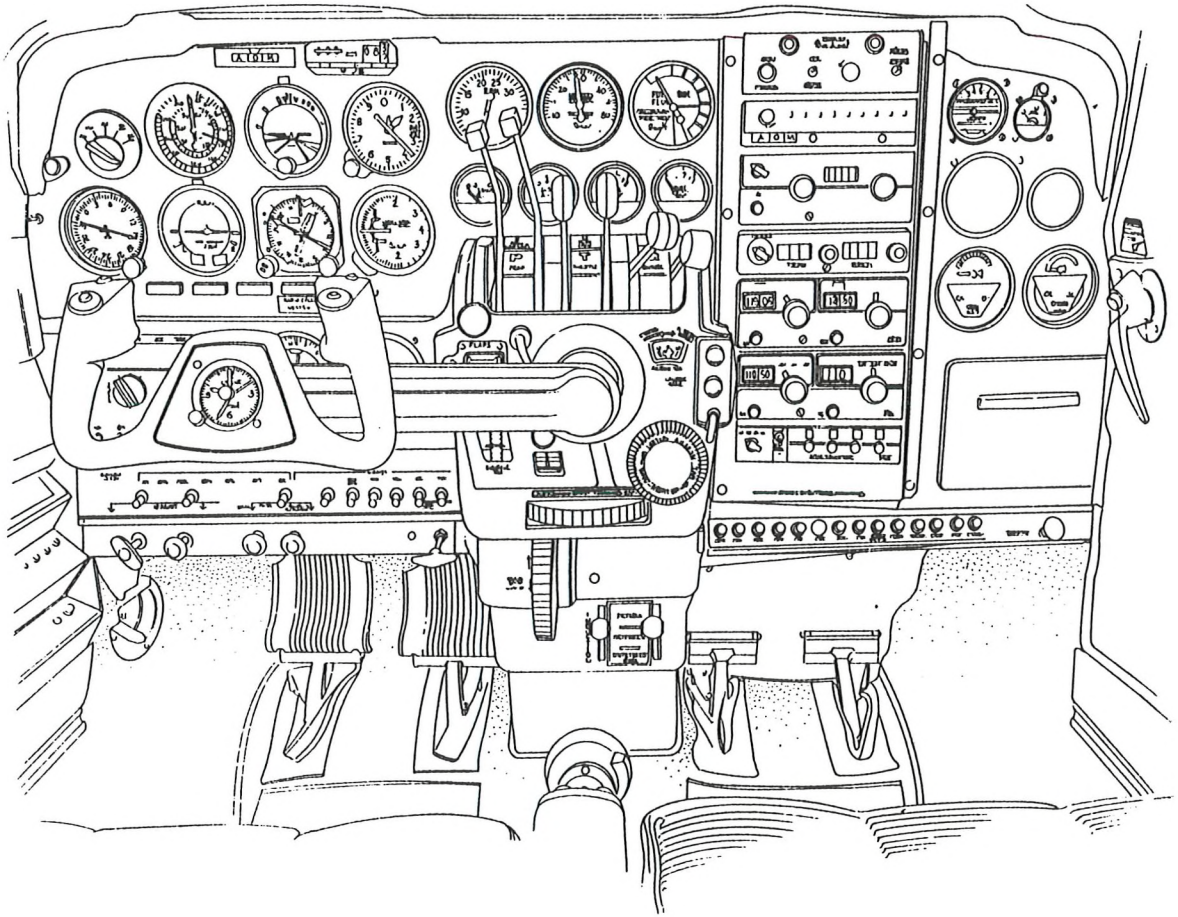

Figure 3.2: Typical Instrument Panel of a General Aviation Aircraft

The altimeter measures the altitude of the aircraft and displays it in feet. Atmospheric pressure varies with altitude and so by measuring pressure the altitude can be deduced. However, the barometric pressure also changes according to the weather and so the pilot must calibrate the altimeter to correct for this before each flight by applying an offset which relates to the ambient pressure. The altimeter is usually mechanical and uses linkages and gears to implement the altitude-pressure relationship. The equation relating static pressure, P_s, and altitude, h, is described in equation 3.4 for altitudes below 36000 feet. [68]

$$h = 145442\left(1-\left(\frac{P_s}{1013.25}\right)^{0.190263}\right) \tag{3.4}$$

The vertical speed indicator measures the rate of climb or descent of the aircraft in hundreds of feet per minute. The measurement is, again, based on pressure variation with altitude: the vertical speed is a function of the difference between the current static pressure and the static pressure which has been delayed for a short time. As a consequence of the time lag the instrument shows a small delay in displaying the vertical speed of the aircraft.

The turn co-ordinator and the heading indicator are concerned with lateral aircraft motion and need not be considered when studying longitudinal motion.

It is apparent from these descriptions that the traditional instruments are unlikely to provide outputs suitable for use in a detection system. Newer technologies are becoming available viz. solid-state sensors and efficient and low-cost microprocessors and systems. As instruments based upon these technologies replace the traditional instruments the likelihood of signals being available from such instruments is increased.

3.5 Aircraft Sensors

For windshear to be detected from the aircraft motion requires some means of measuring the dynamics of the aircraft. Some of these measurements may be available from instruments already fitted to the aircraft, but the discussion in

Section 3.4 indicates that it is likely, in general, that the measurements must be made independently by sensors incorporated in the detection system.

The change in the longitudinal motion of the aircraft produces the greatest hazard during windshear conditions and so to detect this hazard the system must measure some of the longitudinal flight parameters viz. inertial forward and heave velocity, air-relative forward and heave velocity, pitch rate, pitch attitude or angle of attack. These parameters are related by the equations of motion described in Section 2.1.

The linearised aircraft equations describe the motion of the aircraft in terms of small perturbations from a linearised 'trim' flight condition. It is, therefore, the small perturbation values of the parameters which are likely to be required. In a trim condition, the aircraft is either in unaccelerated steady climb, descent or level flight and so the aircraft has a constant pitch attitude and the pitch rate is zero. The air-relative and inertial airspeed and heave velocities are also constant but the inertial and air-relative quantities may differ if the aircraft is experiencing a steady wind such as might occur in a high altitude jet stream.

The extraction of the perturbed quantity from the total value of the parameter is usually achieved by using a high pass filter with a sufficiently low cut-off frequency that the frequencies related to the dynamic response of the small perturbation model of the aircraft are not attenuated but such that the more slowly-varying components of the signal are removed. This is commonly referred to as a 'washout' filter.

3.5.1 Pitch Rate and Pitch Attitude

The pitch rate can be measured directly using a rate sensor which measures the rate of angular motion about a fixed axis. As the trim pitch rate is zero the small perturbation values of the pitch rate are identical to the total measured pitch rate. The pitch attitude can then be obtained by integration.

A displacement gyro could be used as an alternative. The output of this would be the pitch attitude and the signal would require differentiation to derive the pitch rate, but this would generate inaccuracies for measurements made during turning manoeuvres.

3.5.2 Inertial Forward and Heave Velocity

Determination of the inertial forward and heave velocities can be most easily accomplished by the use of accelerometers mounted on the aircraft and aligned with the aircraft's body axes. The sensors would measure the acceleration of the aircraft in a body-fixed axis system. However, the measurement would include both the linear acceleration component, the centripetal components which arise because of the rotation of the body-fixed axis system in inertial space and the gravitational acceleration. The forward and heave accelerations about the centre of gravity are therefore:

$$A_{xcg} = \dot{U} + QW - RV + g\sin\Theta \tag{3.5}$$

$$A_{zcg} = \dot{W} + PV - QU - g\cos\Theta\cos\Phi \tag{3.6}$$

These can be reduced to a linearised form when considering small perturbations from a trim condition using the methods summarised in Appendix A and become:

$$a_{xcg} = \dot{u} + W_0 q + g\cos\Theta_0\theta \tag{3.7}$$

$$a_{zcg} = \dot{w} - U_0 q + g\sin\Theta_0\theta \tag{3.8}$$

For many flight requirements, because both the trim flight path angle and the pitch attitude are small, the gravity terms can be simplified using small angle approximations to give

$$a_{xcg} = \dot{u} + W_0 q + g\theta \tag{3.9}$$

$$a_{zcg} = \dot{w} - U_0 q \tag{3.10}$$

If the body-axis system were aligned with the stability-axis system then the equations would be further simplified by substituting $W_0 \equiv 0$. However such an alignment cannot be defined arbitrarily because, although the stability-axis system is body-fixed, the alignment with respect to the principal body-axes varies according to the trim condition. In practice, however, the error in making this assumption is usually small.

The inertial forward and heave velocities can now be derived as:

$$u = \int (a_{xcg} - g\theta)dt \tag{3.11}$$

$$w = \int (a_{zcg} + U_0 q)dt \tag{3.12}$$

The inertial forward velocity requires measurement of an estimate of the forward acceleration and the pitch attitude whereas the inertial heave velocity requires knowledge of the heave acceleration, the trim value of the inertial forward velocity and the pitch rate.

If the accelerometer is not mounted at the centre of gravity the equations for the x-axis and z-axis accelerations must include extra terms. For example, if an accelerometer, aligned with the z-axis, is mounted on the x-axis at a distance x_a forward of the centre of gravity, the acceleration measured is shown in equation 3.13.

$$a_z = a_{zcg} - x_a \dot{q} \tag{3.13}$$

3.5.3 Air-Relative Forward Velocity

The air-relative forward velocity can be determined using pressure measurements in an analogous method to that used in the Airspeed Indicator.

A measurement of the Pitot-static pressure differential will enable the indicated airspeed to be calculated from equation 3.3. If true airspeed is required the air density, or air pressure, variation with altitude could also be measured. However, at low levels where windshear is a hazard, the difference between the indicated and true airspeed is negligible.

For linear flight dynamics purposes it is often not the total airspeed, U_a, which is required but the trim value of the airspeed, U_{0a}, and the small variation, u_a, from that value.

$$U_a = U_{0a} + u_a \tag{3.14}$$

The small perturbation can be derived using a 'washout' filter and a low pass filter will extract the trim value. Alternatively, the trim value can be determined by subtracting the perturbed quantity from the total value or vice versa.

3.5.4 Angle of Attack

The angle of attack is related to the air-relative forward and heave velocities by the equation given below:

$$\alpha = \frac{W_a}{U_a} \tag{3.15}$$

The small perturbation equation expressed in the stability axis system becomes:

$$\alpha = \frac{w_a}{U_{0a} + u_a} \quad \text{or} \quad \alpha \approx \frac{w_a}{U_{0a}} \tag{3.16}$$

The angle of attack can be measured directly by a vane which is free to rotate in the airstream and is mounted on the exterior of the aircraft.

3.5.5 Vertical speed

Modern low-cost pressure sensors now have sufficient accuracy and resolution that the vertical speed could be calculated by measuring the rate of change of static pressure and calculating the rate of change of altitude using equation 3.4. The pressure change/vertical speed relationship varies with altitude but for the low altitudes with which hazardous windshear is associated the relationship can be assumed constant.

3.5.6 Performance of Sensors in a Windshear Environment

The performance of the sensors used in a windshear environment should not be significantly affected by the effects of the abnormal windfield. In a microburst the static pressure is likely to fluctuate and so it is no longer directly related to altitude according to equation 3.4. Sensors which use static pressure to derive flight parameters such as vertical speed are likely to have some inaccuracies on their output as a result. However, this effect does not induce errors in airspeed sensing where the difference between the total 'Pitot' pressure and the static pressure is measured, as the static pressure component of the total pressure will fluctuate in the same way.

4 THE WIND ESTIMATION ALGORITHM

4.1 Adaptation of Observer Theory to the Estimation of Unknown Inputs

This chapter derives methods for estimating the components of wind acting on an aircraft. The algorithms are based on observer theory, and the fundamentals of the theory are summarised in Appendix D. The Luenberger Observer enables the state vector of a system to be estimated if the system's matrices and the inputs to the system are known.

An inverse problem can sometimes exist; namely determining some of the inputs to the system. If the system's matrices are known and some, or all, of the state variables of the system can be found, then it may be possible to apply Luenberger Observer techniques to this problem.

The system equation D1 can be expressed in a slightly different form.

$$\dot{\mathbf{x}} = \mathbf{A}\mathbf{x} + \mathbf{B}\mathbf{u} + \mathbf{E}\mathbf{d} \tag{4.1}$$

where $\mathbf{x}$ is the state vector as before. The input to the system has been split into two vectors; $\mathbf{u}$ represents the known inputs and $\mathbf{d}$ is a vector of unknown inputs, which may be thought of as disturbances to the system. $\mathbf{B}$ and $\mathbf{E}$ are the matrices associated with the inputs $\mathbf{u}$ and $\mathbf{d}$ respectively. The division of the inputs in this way has not altered the generality of the system equation which can still be expressed with a single input vector as

$$\dot{\mathbf{x}} = \mathbf{A}\mathbf{x} + \left[\mathbf{B} \mid \mathbf{E}\right]\begin{pmatrix}\mathbf{u}\\ \hline \mathbf{d}\end{pmatrix} \tag{4.2}$$

The output equation is unchanged:

$$\mathbf{y} = \mathbf{C}\mathbf{x} \tag{4.3}$$

An observer can be constructed of the form:

$$\dot{\mathbf{x}}_e = (\mathbf{A} - \mathbf{K}\mathbf{C})\mathbf{x}_e + \mathbf{K}\mathbf{y} + \mathbf{B}\mathbf{u} \tag{4.4}$$

Although the observer equation appears identical to the standard equation of D18, the implementation differs. The disturbance input, **d**, being unknown, cannot be used as an input into the observer and so the observer representation is incomplete.

If the error between the system state vector and the observer state vector is defined as

$$\mathbf{e} = \mathbf{x} - \mathbf{x}_e \tag{4.5}$$

then the error can be calculated from equations 4.1, 4.3 and 4.4.

$$\dot{\mathbf{e}} = (\mathbf{A} - \mathbf{KC})\mathbf{e} + \mathbf{Ed} \tag{4.6}$$

This can be compared with the error equation for a standard observer.

$$\dot{\mathbf{e}} = (\mathbf{A} - \mathbf{KC})\mathbf{e} \tag{4.7}$$

It can be seen that there is an additional term in equation 4.6, caused by the unknown disturbance. Whereas the standard observer error decays to zero in the steady state, the steady-state error here is non-zero and is related to the disturbance input. If the dynamics of the disturbance are significantly slower than the dynamics of the estimator the steady error, found by setting $\dot{\mathbf{e}}$ to zero, is:

$$(\mathbf{A} - \mathbf{KC})\mathbf{e} = -\mathbf{Ed} \tag{4.8}$$

Provided that $\mathbf{A} - \mathbf{KC}$ is non-singular

$$\mathbf{e} = -(\mathbf{A} - \mathbf{KC})^{-1}\mathbf{Ed} \tag{4.9}$$

Alternatively, the disturbing input vector may be required and this can be determined as

$$\mathbf{d} = -\mathbf{E}^{+}(\mathbf{A} - \mathbf{KC})\mathbf{e} \tag{4.10}$$

where $\mathbf{E}^{+}$ is the pseudo inverse of the matrix **E**.

The equations 4.6, 4.9 and 4.10 relate the error in the observer state variables to the disturbance. The application of Luenberger observer techniques to this type of problem may therefore be used to find the disturbance itself. Any such method must rely, however, on having sufficient knowledge of the state vector.

4.2 Estimation of Wind acting on an Aircraft using a Single Aircraft State Variable

An aircraft with an unknown wind acting upon it may be considered as a specific example of the general problem described above; and so it may be possible to estimate the wind components using some technique derived from these methods. Such a method could then be used as a basis for windshear detection. A further restriction must be placed upon the method if it is to be practical, namely, that the number of state variables required as inputs to the detection algorithm should be a minimum. This restriction minimises the number of sensors required by the detection device and thereby limits the cost. The feasibility of measuring the aircraft state variables, and the sensors required, were discussed in Section 3.5. The design of any system using such a technique also assumes that the inputs applied to control the longitudinal dynamics of the aircraft are known, and so, for a conventional aircraft, knowledge of the elevator deflection and the engine thrust would also be required as a minimum.

The wind vector described in equation A26 comprises the x-axis, z-axis and pitching wind terms. It is the linear velocity components which are likely to be of most use in a windshear detection system. The pitching wind is related to the z-axis wind by equation A22.

The wind estimation method is discussed and evaluated in the following sections. The computer-aided design package MATLAB [69] and simulation package SIMULINK [70] were used to generate the results. The aircraft parameters were based on the Cessna 402B, and these are given in Appendix B.

A simplified wind estimation problem is addressed initially, in which the pitching wind term, and hence its effect on both the aircraft and observer, is

assumed to be zero. The consequences to the algorithm of a pitching wind term is considered later in the analysis in Section 4.5.

4.2.1 Airspeed Estimation using Pitch Rate

An observer can be constructed to estimate the state variables associated with the longitudinal dynamics of an aircraft. As a starting point, the pitch rate is chosen to be the state variable fed back from the aircraft to the observer because this can be measured directly using a pitch rate sensor, as described in Section 3.5. The equations for the aircraft are identical to those above, equations 4.1 and 4.3 with the disturbance input now expressed as the wind velocity components.

$$\dot{\mathbf{x}} = \mathbf{A}\mathbf{x} + \mathbf{B}\mathbf{u} + \mathbf{E}\mathbf{w}_{\text{ind}} \tag{4.11}$$

$$\mathbf{y} = \mathbf{C}\mathbf{x} \tag{4.12}$$

where

$$\mathbf{C} = \begin{bmatrix} 0 & 0 & 1 & 0 \end{bmatrix} \tag{4.13}$$

The wind vector and E matrix, which were defined in equations A26 and A29, are reduced because the pitching wind term is ignored

$$\mathbf{w}_{\text{ind}} = \begin{bmatrix} u_g \\ w_g \end{bmatrix} \tag{4.14}$$

$$\mathbf{E} = \begin{bmatrix} X_w & X_w \\ Z_u & Z_w \\ \tilde{M}_u & \tilde{M}_w \\ 0 & 0 \end{bmatrix} \tag{4.15}$$

Equation 4.11 is equivalent to equation 4.16

$$\dot{\mathbf{x}} = \mathbf{A}(\mathbf{x} + \mathbf{w}) + \mathbf{B}\mathbf{u} \tag{4.16}$$

where

$$\mathbf{w} \equiv \begin{bmatrix} \mathbf{w}_{ind} \\ \hline 0 \\ 0 \end{bmatrix} \tag{4.17}$$

since the input matrix, **E**, for the wind is a sub-matrix consisting of the first two columns of **A**. The values of the elements of the third and fourth columns of **A** do not affect the result, being multiplied by zero elements of the vector **w**.

The error equation for the difference between the observer state vector and the aircraft state vector is

$$\dot{\mathbf{e}} = (\mathbf{A} - \mathbf{KC})\mathbf{e} + \mathbf{E}\mathbf{w}_{ind} \tag{4.18}$$

so, if the wind variations are much slower than the observer dynamics, in steady state

$$\mathbf{e} = -(\mathbf{A} - \mathbf{KC})^{-1}\mathbf{E}\mathbf{w}_{ind} \tag{4.19}$$

$\mathbf{A} - \mathbf{KC}$ will be shown later to be non-singular.

The pitch rate is the only state variable being fed back to the observer, consequently the matrix **KC** is zero in every column except the third. The first two columns of $\mathbf{A} - \mathbf{KC}$ are identical to **E**, and so

$$(\mathbf{A} - \mathbf{KC})^{-1}\mathbf{E} = \begin{bmatrix} 1 & 0 \\ 0 & 1 \\ 0 & 0 \\ 0 & 0 \end{bmatrix} \tag{4.20}$$

This simplifies equation 4.19.

$$\mathbf{e} = -\begin{bmatrix} 1 & 0 \\ 0 & 1 \\ 0 & 0 \\ 0 & 0 \end{bmatrix} \mathbf{w}_{ind} \tag{4.21}$$

Expanding this, the first two elements of **e** can be expressed as

$$u - u_e = -u_g \tag{4.22}$$

$$w - w_e = -w_g \tag{4.23}$$

or

$$u_e = u + u_g \tag{4.24}$$

$$w_e = w + w_g \tag{4.25}$$

It can be seen by comparing equations 4.24 and 4.25 with 2.5 and 2.6 that u_e and w_e settle to the air-relative forward and heave velocities respectively after the transient response has died away. The magnitude and settling time of the transient response is determined by the observer gain matrix, **K**, which can be calculated using the optimal techniques described in Appendix E. The choice of weighting matrices in the performance index requires a compromise between those which result in a fast settling time and those which limit the magnitudes of the observer gains and transient overshoot to an acceptable level. The design of the observer gain is discussed further in Section 4.2.3. The robustness of the observer to variations in the matrix elements is examined in Chapter 5.

4.2.2 Calculation of the Wind Vector using Estimated Air-Relative Speeds

The knowledge of the approximate air-relative speeds alone is of little use in determining the wind components, but equations 2.5 and 2.6 show that the wind can be calculated as the difference between the air-relative velocities and the inertial aircraft velocities. A means of calculating or approximating the inertial aircraft velocities from the known variables is therefore required.

An examination of equation 4.16 shows that the inertial speeds and wind components can be combined as the air-relative speeds in the state equation. If it is assumed that the observer state variables are sufficiently accurate as measures of the air-relative speeds and that the pitch attitude can be readily calculated by integration of the pitch rate, then all the state variables required to evaluate equation 4.16 are available. The remaining variables which are required are the control inputs. These are used in the observer implementation and are, therefore, available to the estimation system. The full aircraft state equation including the effects of the wind vector can be modelled in the form

$$\dot{\mathbf{x}}_m = \mathbf{A}\hat{\mathbf{x}} + \mathbf{B}\mathbf{u} \tag{4.26}$$

where

$$\hat{\mathbf{x}} = \begin{bmatrix} u_e \\ w_e \\ q \\ \theta \end{bmatrix} \tag{4.27}$$

The model 'state' vector $\mathbf{x}_m$ approximates the aircraft state vector $\mathbf{x}$; therefore the first two state variables, u_m and w_m provide estimates of the inertial velocities of the aircraft. An estimate of the wind components can now be generated as the difference between the first two estimator state variables, which approximate the air-relative velocities, and the first two model 'state' variables. The observer and model are, therefore, being used to estimate an input disturbance and this contrasts with the standard use of observers which is to estimate unknown states. A block diagram representation of the aircraft, observer and model is shown in Figure 4.1. Plots of the resulting estimates for unit steps in each of the wind components are shown in Figure 4.2.

The plots show that the estimation of the wind components, especially the w_g estimate, is poor. The transient response has a duration of approximately fifteen seconds, during which time the errors are large. A significant feature of the both estimates is that, even after the initial transient has died, they do not achieve the desired steady value, but have a steady offset.

The effect of such errors on the estimation of wind during a windshear event is shown in Figure 4.3, which is the response of the estimation system when the 'JFK windshear' wind components are applied. (The JFK profile has been altered slightly by allowing the x-axis wind to initialise from zero using a half-period '1-cos' function. The time history of both components has been increased correspondingly. The maximum downdraft occurs after 176.2 seconds, which corresponds to time zero in Figure 2.13 and 2006 GMT in Figure 2.12.) The estimate of the x-axis component during a fast change in wind speed shows large errors and this corresponds with the errors observed in the transient response in Figure 4.2. The error is significantly less during the periods for which the wind is relatively steady. The effect of the offset in the steady state, which was observed in the previous figures, appears to be negligible. The z-axis wind estimate, in addition to exhibiting larger

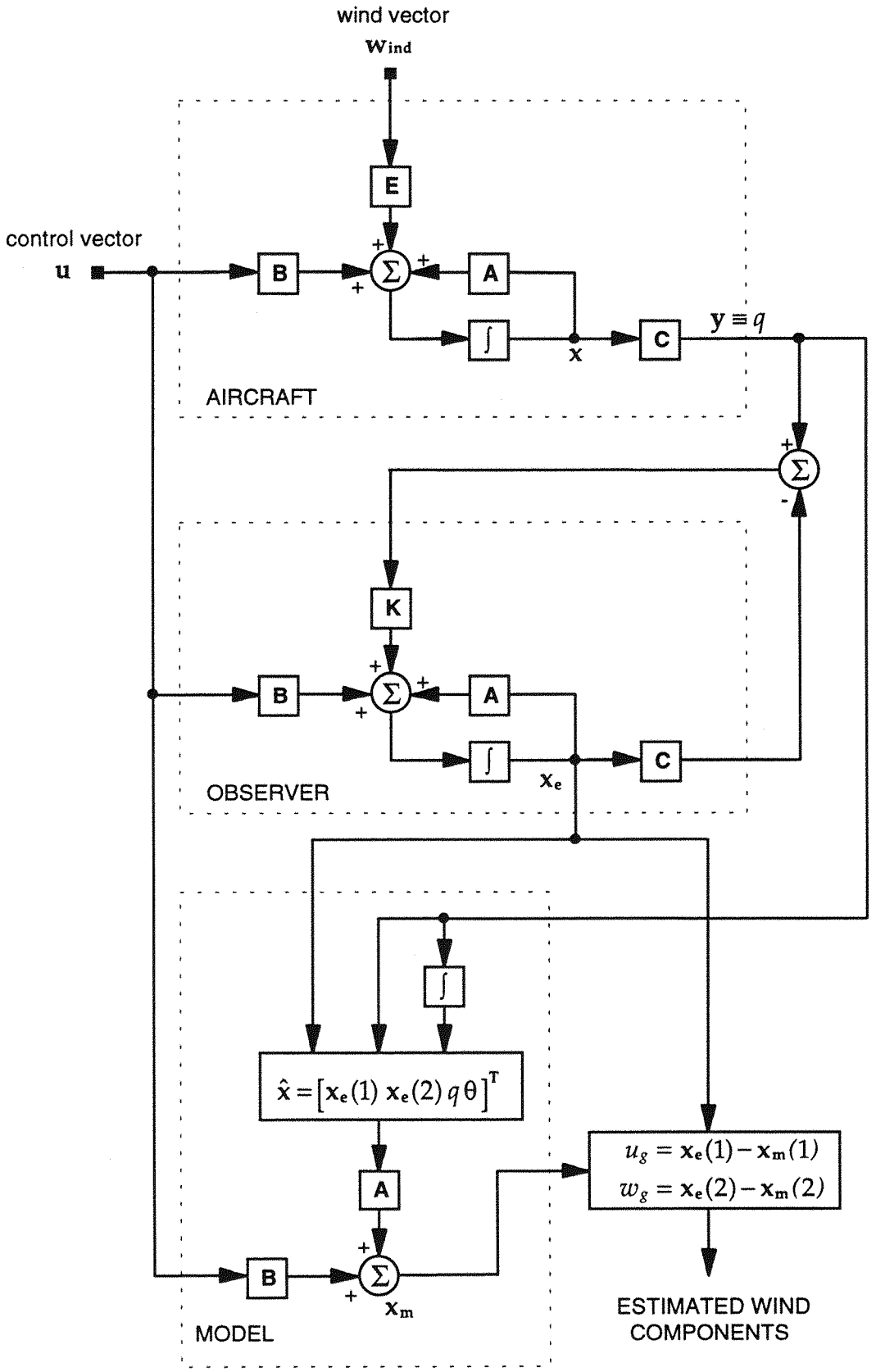

Figure 4.1: Schematic of Aircraft, Observer and Model

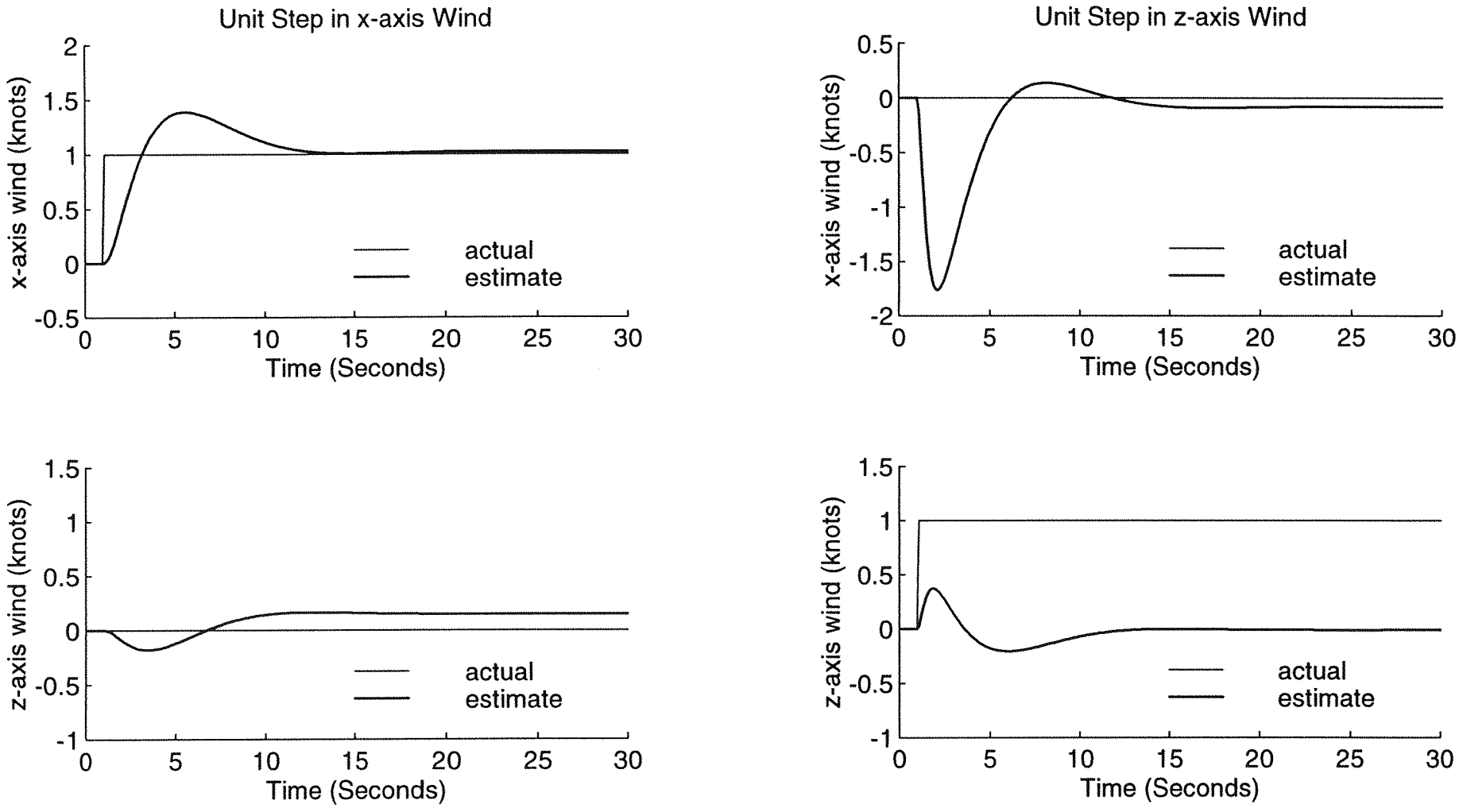

Figure 4.2: Estimation of Wind Components using Pitch Rate

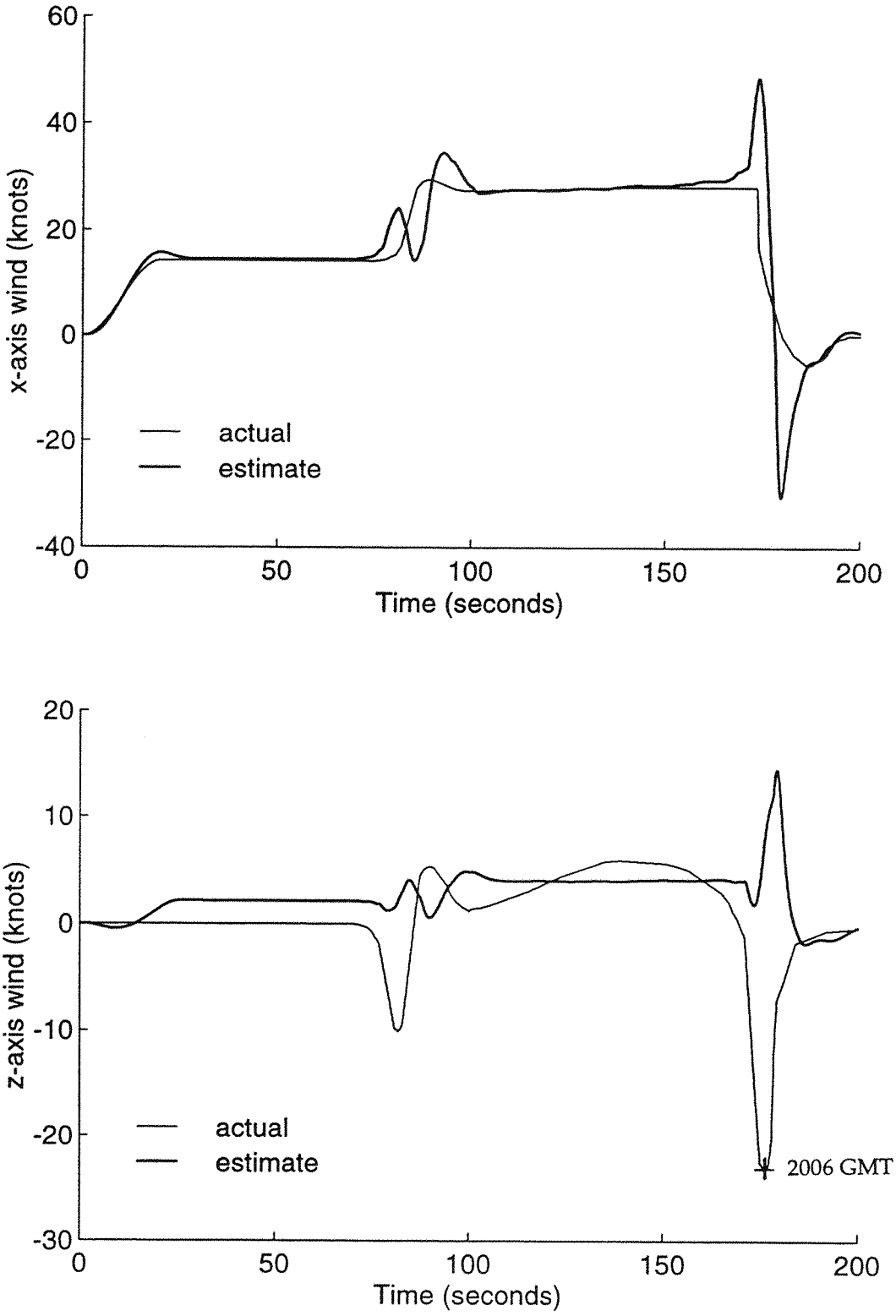

Figure 4.3: Estimate of JFK Wind Components using Pitch Rate

transient errors, is significantly worse during the phases when the wind is slowly-varying, and the steady state error is related not only to the wind component being estimated but also to the value of the x-axis component. A general examination of the plots shows that, despite these significant inaccuracies, the estimates give an indication of the nature and time of occurrence of the important features of the windshear.

The performance of the observer is demonstrated in Figure 4.4. These show the estimates of the air-relative velocities when the system is subjected to a unit step in each of the longitudinal wind components in turn. The actual air-relative velocities are also plotted, and it can be seen from this that the observer is functioning as expected and, after initial transients, the estimates settle to the aircraft's air relative speeds.

The errors in the estimation of the wind components must therefore arise from the errors in the observer state variables during the transient response. This has been confirmed by simulation. If the aircraft's air-relative velocities are fed into the aircraft model instead of the estimated air-relative velocities, then the inertial velocities, and hence the wind components, settle to their desired values, the only errors being the results of numeric resolution errors during simulation.

The contribution of the errors in each of the components of the estimated air-relative velocity to the resulting errors in the wind estimates was tested by passing into the aircraft model firstly the estimated air-relative forward velocity with the accurate air-relative heave velocity, and secondly the accurate air-relative forward velocity and the estimated air-relative heave velocity. The results showed that the inaccuracies in the forward velocity component yielded the greater errors in the wind estimation.

4.2.3 Examination of the Transient Errors in the Air-Relative Velocity Estimates

The errors in the wind estimation are produced as a result of the transient errors in the observer state variables. The transient response of the observer is determined by the eigenvalues of the observer state matrix, **A-KC**, which are determined by designing a suitable observer gain matrix, **K**, as discussed in Appendix E. The transient response will be faster for higher

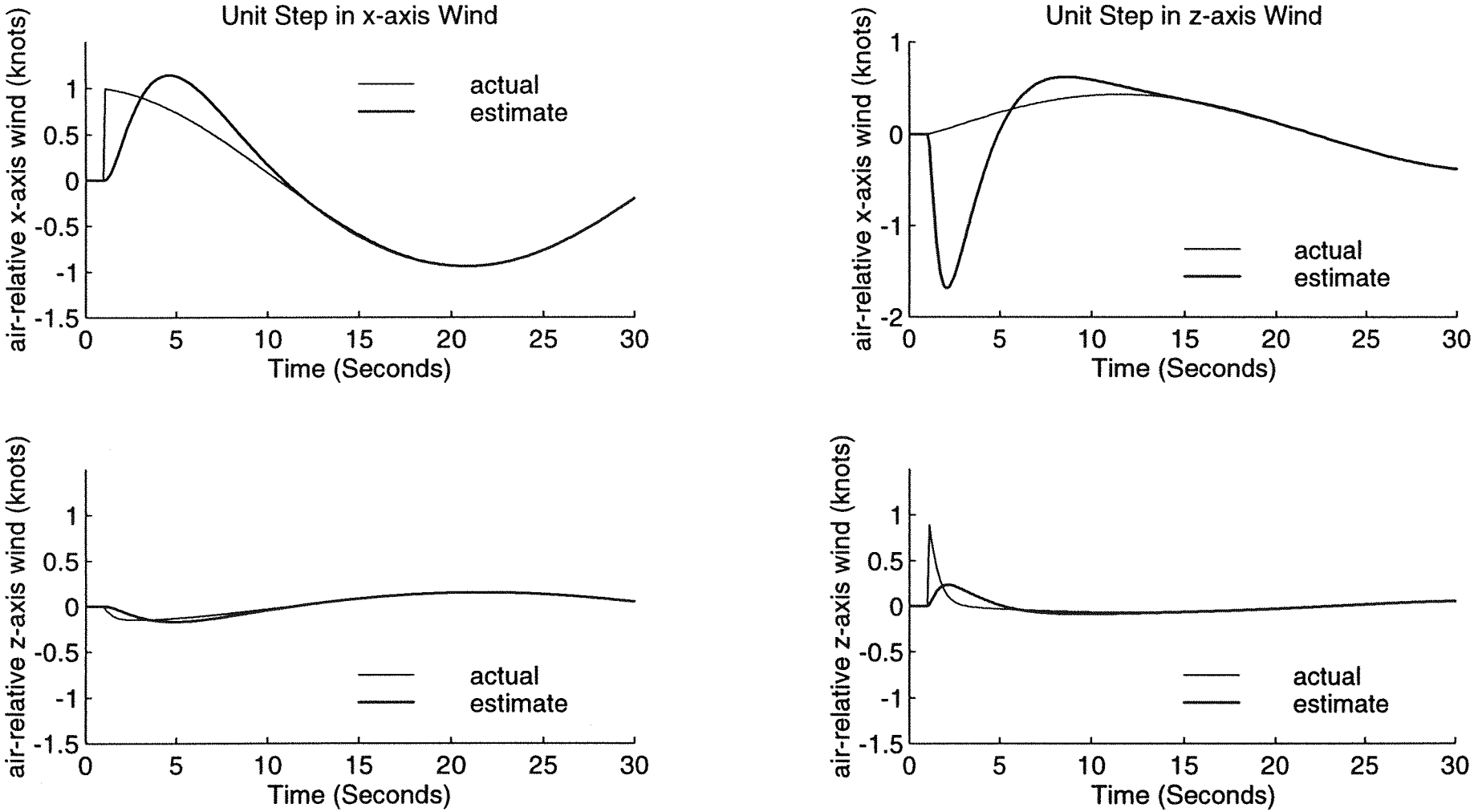

Figure 4.4: Observer Estimation of Air-Relative Velocities

gains, but the overshoot in the estimate and the amplification of any noise in the feedback will also be greater.

The gain matrix for the observer for the Cessna 402B was designed to be the result of optimising a performance index, J, of the form shown below.

$$J = \tfrac{1}{2}\int_0^\infty (\mathbf{e}^T\mathbf{Q}\mathbf{e} + \mathbf{y}^T\mathbf{R}\mathbf{y})dt \qquad (4.28)$$

The weighting matrix **Q** was chosen to be a diagonal matrix; **R** is a scalar. For the results shown in Figures 4.2, 4.3 and 4.4, the initial values of all the elements were selected by a standard method [89] but further improvements were achieved by varying the weighting and observing the effect on the transient response, so that it was largely a heuristic method. Such an approach can be efficient when using modern CAE packages and fast computers.

However, the transient response was found to be the principal source of error in the estimation technique described above and so the methods of designing the observer gain matrix and the choice of the weighting matrices were considered further.

It can be seen from Figures 4.2, 4.3 and 4.4 that the wind estimation error settles to a non-zero value although the observer error in estimating the aircraft's air-relative velocities settles to zero. This is because the model state vector is derived in part by integrating the estimates of the air-relative velocities, and the errors in those estimates are thereby integrated to produce offset errors in the derivation of the inertial aircraft velocities. It is desirable, therefore, in designing the observer gain, that the cumulative errors in the observer estimates are considered as well as the maximum error, settling time and size of the gains applied.

The settling time is related to the eigenvalues of the observer state matrix **A-KC**, which are the poles of the observer. Specifically, the rate of exponential decay of the error in the observer is determined by the real part of the eigenvalue for both complex and real eigenvalues. For the error to decay the eigenvalue must have a negative real part. The speed of decay is dependent upon the magnitude of the real part and, for the observer, a large negative real part is desirable because this indicates fast exponential decay of

the transient error associated with that eigenvalue. It follows that the duration of the transient response of the observer as a whole is governed by the eigenvalue with the smallest negative real part and so this gives a useful method for considering the settling time of the system.

The effect on the transient error, cumulative error, gain and settling time of varying each element of the weighting matrices, while holding the remaining elements constant, was monitored. The errors are expressed as a percentage of the magnitude of the step input applied. The cumulative errors were obtained by integrating the absolute value of the error over a 30 second duration, by which time the error had, in general, become negligible. The results are shown in Figures 4.5 to 4.9; Figures 4.5 and 4.6 have a linear ordinate scale whereas the other figures have a logarithmic x-axis. It is apparent from these plots that the variation of the weighting matrix elements produces, in general, a compromise between the requirement to have small maximum and cumulative errors in the observer transient, have a fast settling time and to keep the elements of the observer gain matrix to a reasonable magnitude. All the elements were varied over the same range of values and yet the magnitude of the effect in each of the parameters varies considerably. The element q_{44} appears to have the most significant effect and produces very large changes in the magnitude of the observer gain and in the settling time for the system, whereas the variation in $q_{11}$and q_{22} produced relatively little effect. Varying the single element of **R** produced large changes in the observer gain, but its effect on the other parameters was less significant.

It is interesting to compare these results with the weighting parameters for the observer used to produce the previous air-relative velocity estimates, which was designed by choosing the weighting matrices using heuristic methods to select the best performance. For the original design the single element of **R** was not altered from unity as similar optimisation of the performance index could be obtained by varying all the elements of **Q** by the inverse of any desired weighting element for **R**. The details of this design are given below.

Weighting Matrices:

$$\mathbf{Q} = \mathrm{diag}[1 \quad 0.001 \quad 0.001 \quad 100] \qquad (4.29)$$

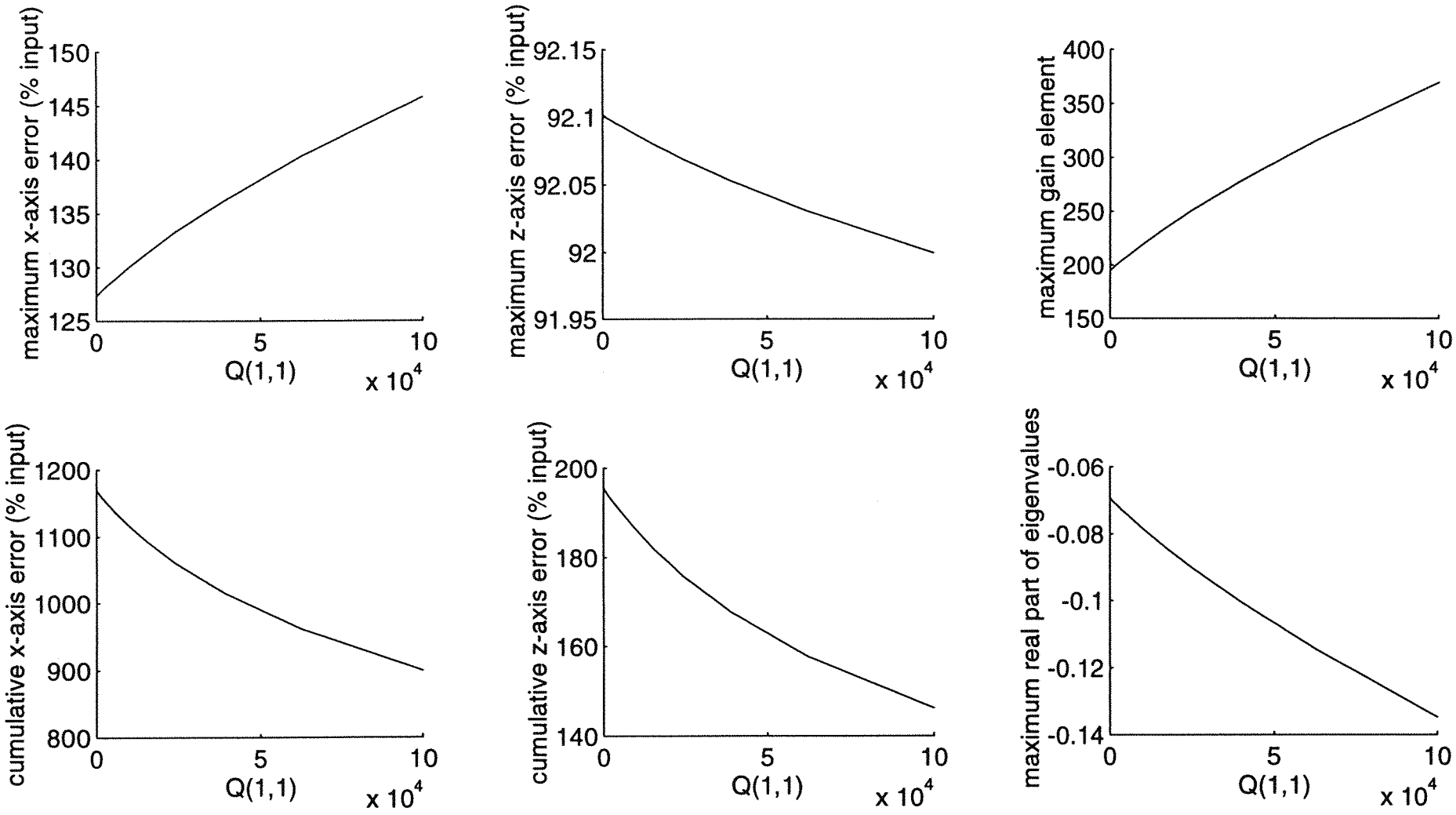

Figure 4.5: Effect of Varying Error Weighting Matrix Element Q(1,1)

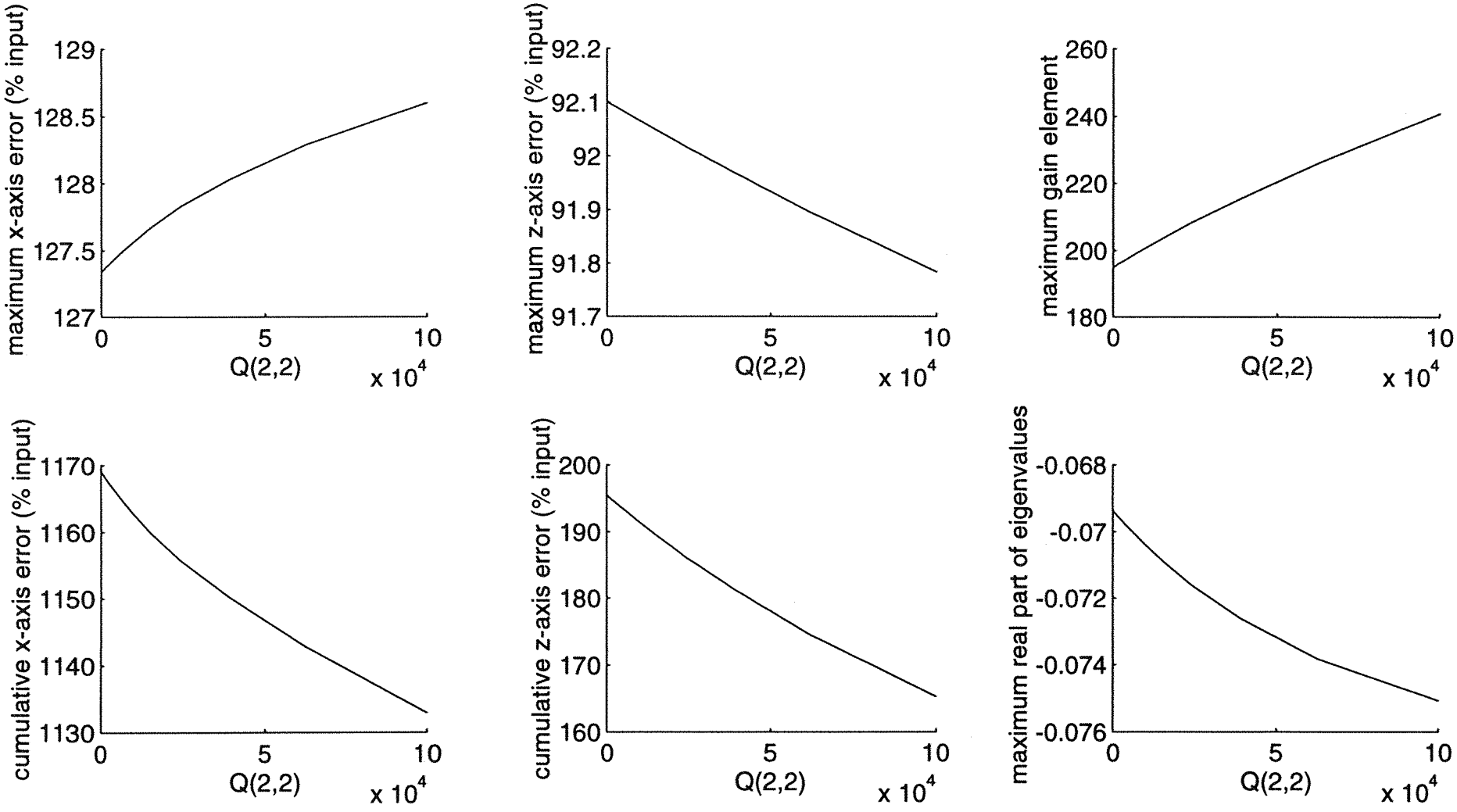

Figure 4.6: Effect of Varying Error Weighting Matrix Element Q(2,2)

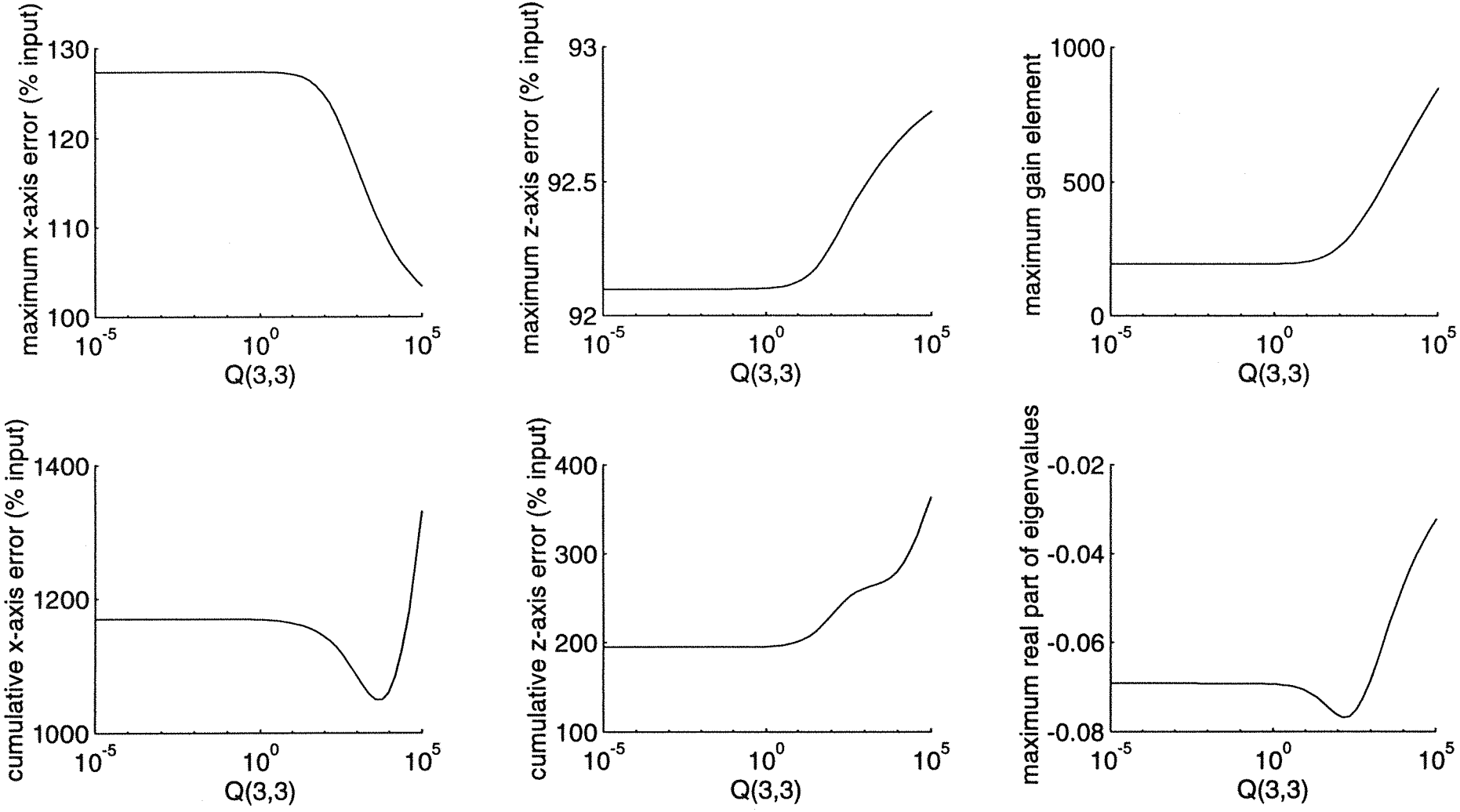

Figure 4.7: Effect of Varying Error Weighting Matrix Element Q(3,3)

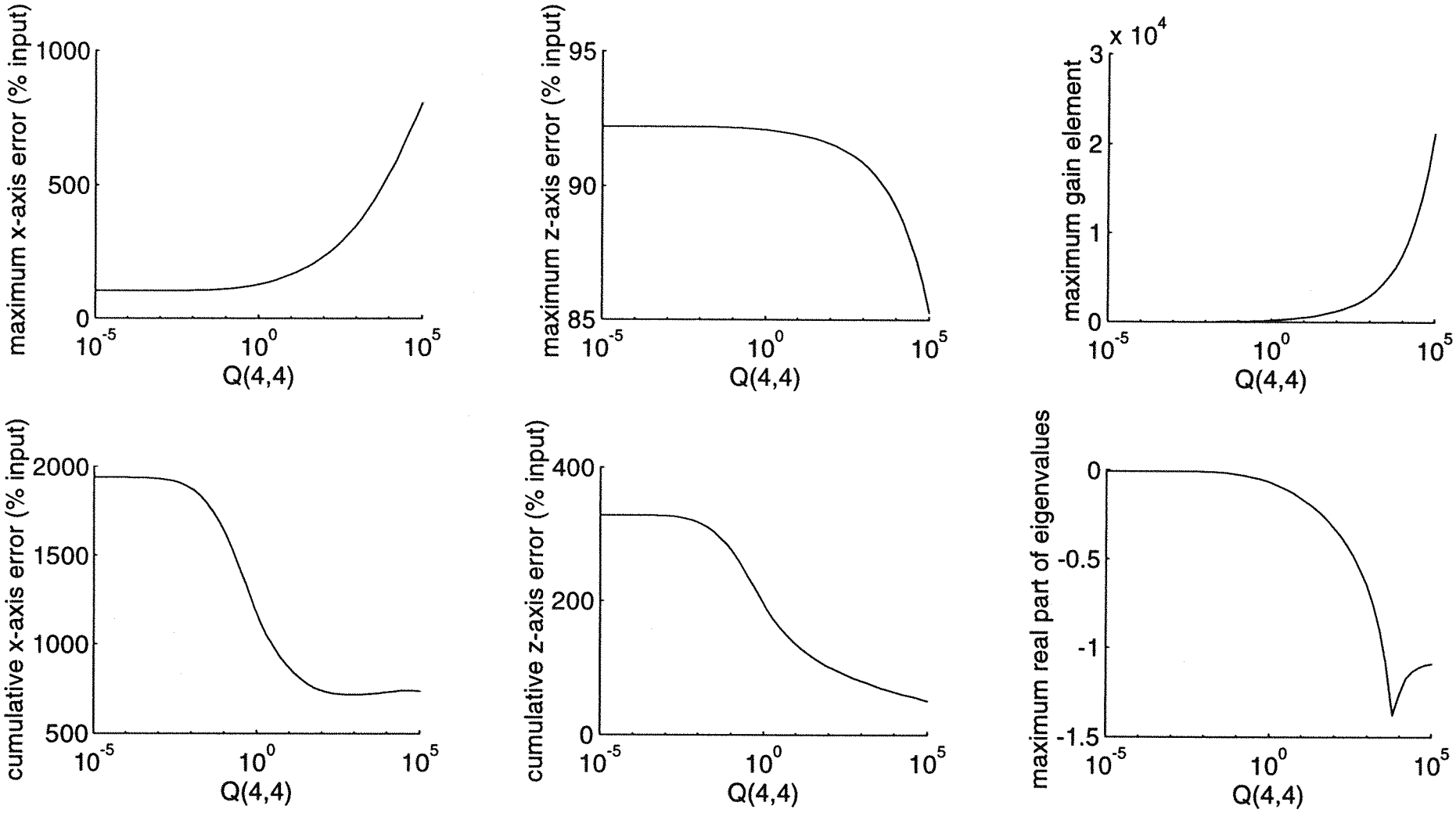

Figure 4.8: Effect of Varying Error Weighting Matrix Element Q(4,4)

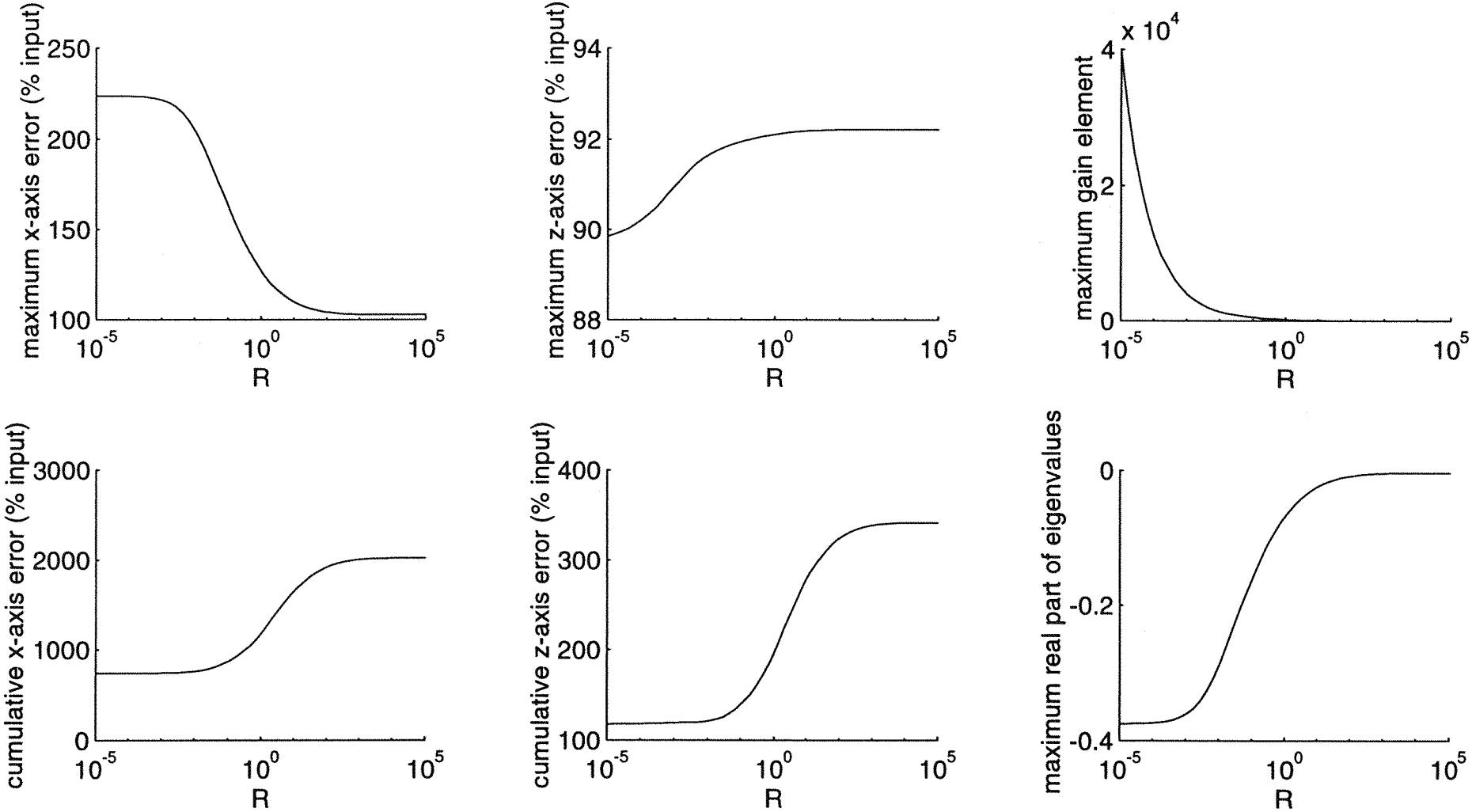

Figure 4.9: Effect of Varying Input Weighting Matrix

and

$$\mathbf{R} = [1] \tag{4.30}$$

Observer Gain Matrix:

$$\mathbf{K} = \begin{bmatrix} 1250 \\ 166 \\ 0.7 \\ -9.0 \end{bmatrix} \tag{4.31}$$

Table 4.1: Eigenvalues of the observer compared with those of the aircraft

Observer	Aircraft
−6.6167	−6.6174
−2.1034	−2.1092
$-0.3339 + 0.3415j$	$-0.0035 + 0.1504j$
$-0.3339 - 0.3415j$	$-0.0035 - 0.1504j$

Table 4.2: Errors in air-relative velocity estimates

	x axis velocity (% input)	z axis velocity (% input)
Maximum errors	234	92
Cumulative errors (30s)	739	101

The settling time associated with the complex eigenvalues of the observer is significantly faster when compared to the corresponding aircraft eigenvalues, which relate to the aircraft's phugoid mode. The remaining two eigenvalues show relatively little change, but remain relatively fast. In this application the similarity of the observer and aircraft eigenvalues does not cause problems in the performance of the observer, although this would appear possible from equation D10. However, it remains desirable that the observer dynamics settle faster than the aircraft dynamics. In this case the speed of settling has been achieved at the cost of relatively high gains in the observer gain matrix.

It was considered that little improvement could be gained by using the results from Figures 4.5 to 4.9 to make adjustments to the weighting matrices, and so the observer gain matrix was not changed.

4.2.4 Methods of Improving the Air-Relative Velocity Estimates

The estimation of the velocities has relied on the fact that the steady output of the observer is equivalent to the air-relative velocities, and an effort was made to reduce the errors induced by the transient response to a minimum. An alternative approach is to examine the observer 'error' equation, equation 4.6, as a whole and consider whether this can be applied in any way to improve the air-relative velocity estimates. If the effect of the transient can be approximated, then it may be possible to reduce the error in the observer estimation.

The difference between the observer and the aircraft state vectors, $\mathbf{e}$, is given by equation (4.6).

$$\dot{\mathbf{e}} = (\mathbf{A} - \mathbf{KC})\mathbf{e} + \mathbf{E}\mathbf{w}_{ind} \tag{4.32}$$

For the first two observer state variables to represent the air-relative velocities at all times is desirable that

$$\mathbf{e}(1) \equiv u_a = u + u_g \tag{4.33}$$

$$\mathbf{e}(2) \equiv w_a = w + w_g \tag{4.34}$$

The error equation, equation 4.32, represents four simultaneous equations. In order to solve for the two unknown wind components only two of the four equations are required. In matrix form the equations are

$$\dot{\hat{\mathbf{e}}} = \hat{\mathbf{G}}\mathbf{e} + \hat{\mathbf{E}}\mathbf{w}_{ind} \tag{4.35}$$

where $\hat{\mathbf{e}}$, $\hat{\mathbf{E}}$ and $\hat{\mathbf{G}}$ are subsets of $\mathbf{e}$, $\mathbf{E}$ and $\mathbf{A}-\mathbf{KC}$ representing the two simultaneous equations. The equation can be rearranged to give

$$\mathbf{w}_{ind} = \hat{\mathbf{E}}^{-1}\dot{\hat{\mathbf{e}}} - \hat{\mathbf{E}}^{-1}\hat{\mathbf{G}}\mathbf{e} \tag{4.36}$$

In order to perform this calculation two of the four possible equations must be chosen to satisfy the requirement that $\hat{\mathbf{E}}$ is not singular. Equation 4.37 shows that this precludes the use of the fourth equation representing $\dot{\theta}$, because the corresponding row of the $\mathbf{E}$ matrix contains only zeros, but any two of the first three row can, in general, be used.

$$\mathbf{E}=\begin{bmatrix} X_u & X_w \\ Z_u & Z_w \\ \tilde{M}_u & \tilde{M}_w \\ 0 & 0 \end{bmatrix} \tag{4.37}$$

In addition, not all the variables required to solve the equations are available and so, to maximise the known values, the third equation, $\dot{q}$, is used together with either the first equation representing $\dot{u}$ or the second representing $\dot{w}$. Using the first and third equations for $\dot{u}$ and $\dot{q}$ respectively, the $\hat{\mathbf{E}}$ and $\hat{\mathbf{G}}$ become

$$\hat{\mathbf{E}}=\begin{bmatrix} X_u & X_w \\ \tilde{M}_u & \tilde{M}_w \end{bmatrix} \tag{4.38}$$

and

$$\hat{\mathbf{G}}=\begin{bmatrix} X_u & X_w & -k_1 & -g \\ \tilde{M}_u & \tilde{M}_w & \tilde{M}q-k_3 & 0 \end{bmatrix} \tag{4.39}$$

where k_1 and k_3 are the first and third element of the observer gain matrix, **K**.

Equation 4.36 can be expanded to give

$$\begin{bmatrix} u_g \\ w_g \end{bmatrix}=\begin{bmatrix} f_{11} & f_{12} \\ f_{21} & f_{22} \end{bmatrix}\begin{pmatrix} \dot{u}-\dot{u}_e \\ \dot{q}-\dot{q}_e \end{pmatrix}-\begin{bmatrix} f_{11} & f_{12} \\ f_{21} & f_{22} \end{bmatrix}\begin{bmatrix} g_{11} & g_{12} & g_{13} & g_{14} \\ g_{21} & g_{22} & g_{23} & g_{24} \end{bmatrix}\begin{pmatrix} u-u_e \\ w-w_e \\ q-q_e \\ \theta-\theta_e \end{pmatrix} \tag{4.40}$$

where f_{ij} represents the (i,j)th element of $\hat{\mathbf{E}}^{-1}$.

As before, because of the relationship between **E** and **A**, the expanded equation yields a simple result for the first two columns of $\hat{\mathbf{E}}^{-1}\hat{\mathbf{G}}$,

$$\hat{\mathbf{E}}^{-1}\hat{\mathbf{G}}\equiv\begin{bmatrix} 1 & 0 & h_{13} & h_{14} \\ 0 & 1 & h_{23} & h_{24} \end{bmatrix} \tag{4.41}$$

here h_{ij} represents the (i,j)th element of $\hat{\mathbf{E}}^{-1}\hat{\mathbf{G}}$.

This enables the air-relative speeds to be separated from the rest of the equation, thus:

$$\begin{pmatrix} u_a \\ w_a \end{pmatrix} = \begin{pmatrix} u_g \\ w_g \end{pmatrix} + \begin{bmatrix} 1 & 0 \\ 0 & 1 \end{bmatrix} \begin{pmatrix} u \\ w \end{pmatrix} = \begin{bmatrix} f_{11} & f_{12} \\ f_{21} & f_{22} \end{bmatrix} \begin{pmatrix} \dot{u} - \dot{u}_e \\ \dot{q} - \dot{q}_e \end{pmatrix} - \begin{bmatrix} 1 & 0 & h_{13} & h_{14} \\ 0 & 1 & h_{23} & h_{24} \end{bmatrix} \begin{pmatrix} -u_e \\ -w_e \\ q - q_e \\ \theta - \theta_e \end{pmatrix} \quad (4.42)$$

The variables required to evaluate this expression are: the difference between $\dot{u}$ and $\dot{u}_e$, $\dot{q}$ and $\dot{q}_e$ and the last two elements of the error vector, $q - q_e$ and $\theta - \theta_e$. The observer parameters u_e, w_e, q_e, θ_e, $\dot{u}_e$ and $\dot{q}_e$ are known, as is the aircraft's pitch rate, q, which may be differentiated or integrated to yield $\dot{q}$ and θ respectively. The remaining unknown is therefore the rate of change of the aircraft's forward velocity, $\dot{u}$.

The aircraft model evaluates the approximate inertial velocities of the aircraft. If it is assumed that the air-relative velocity estimates can be improved by application of the algorithm above, then the inertial velocity approximations will show a corresponding improvement. The forward speed, u_m, may then be sufficiently close to the inertial forward speed, u, to feed back into the estimator improvement algorithm and reduce the observer errors.

This was implemented in simulation and the results for a step input in each of the wind components are shown in Figure 4.10. This can be compared with the results from the original method in Figure 4.2. It is apparent that not only has the technique failed to improve the transient, but it has significantly degraded it. For both wind components the errors in the estimate are now very much larger and the settling time appears unchanged. When a change in the x-axis wind is applied to the aircraft the steady state errors are larger, but the steady response of the z-axis estimate to a z-axis wind shows an improvement.

The performance of this method in estimating a typical wind shear profile, the 'JFK windshear', is shown in Figure 4.11 and this can be compared with Figure 4.3. As observed in the step response, the magnitude of the error in both wind components is very much larger, especially during the periods of rapidly varying winds. The estimate for the x-axis component during periods of steady wind conditions returns to zero and so is significantly

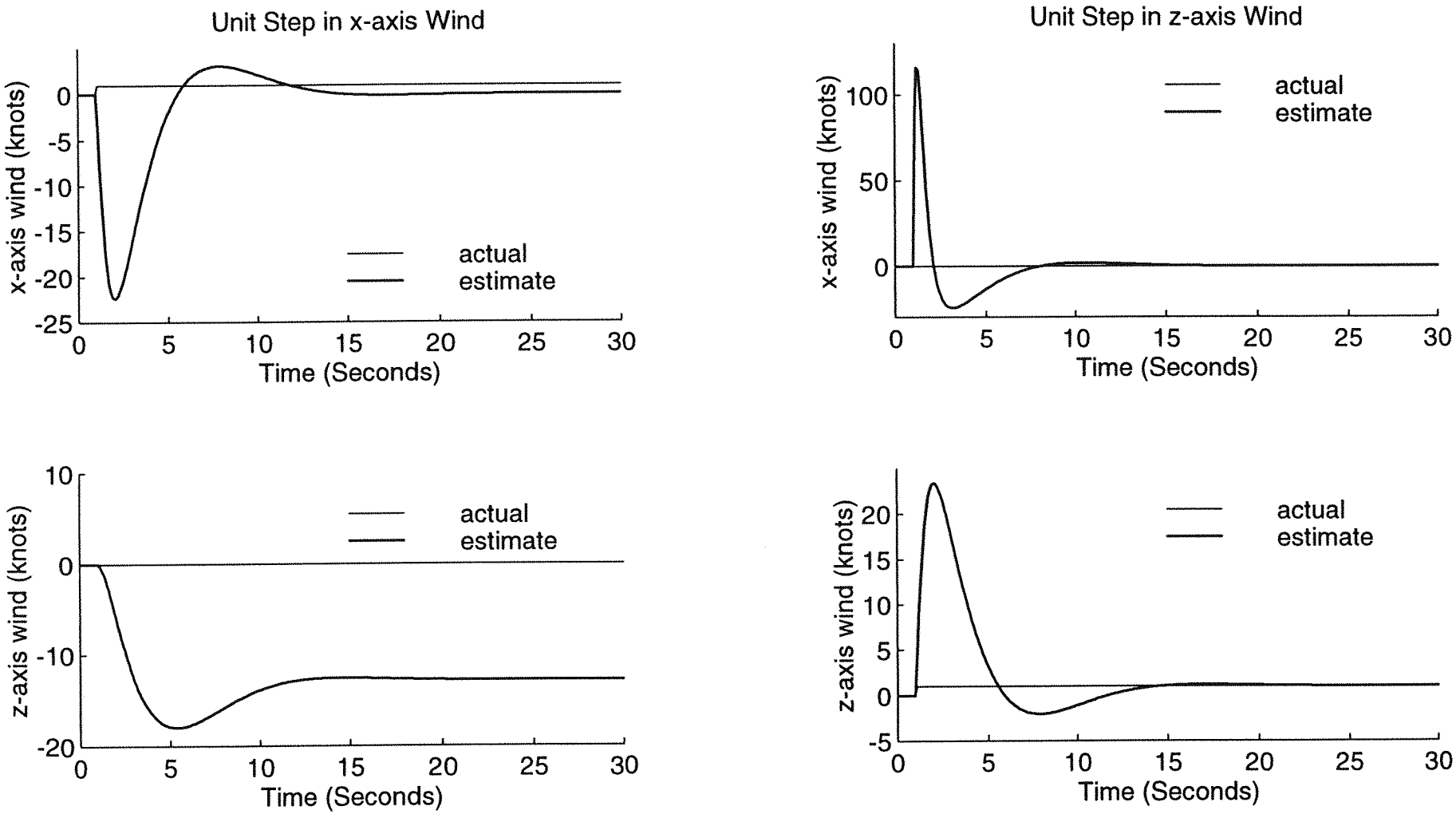

Figure 4.10: 'Enhanced' Estimation of Wind Components using Pitch Rate

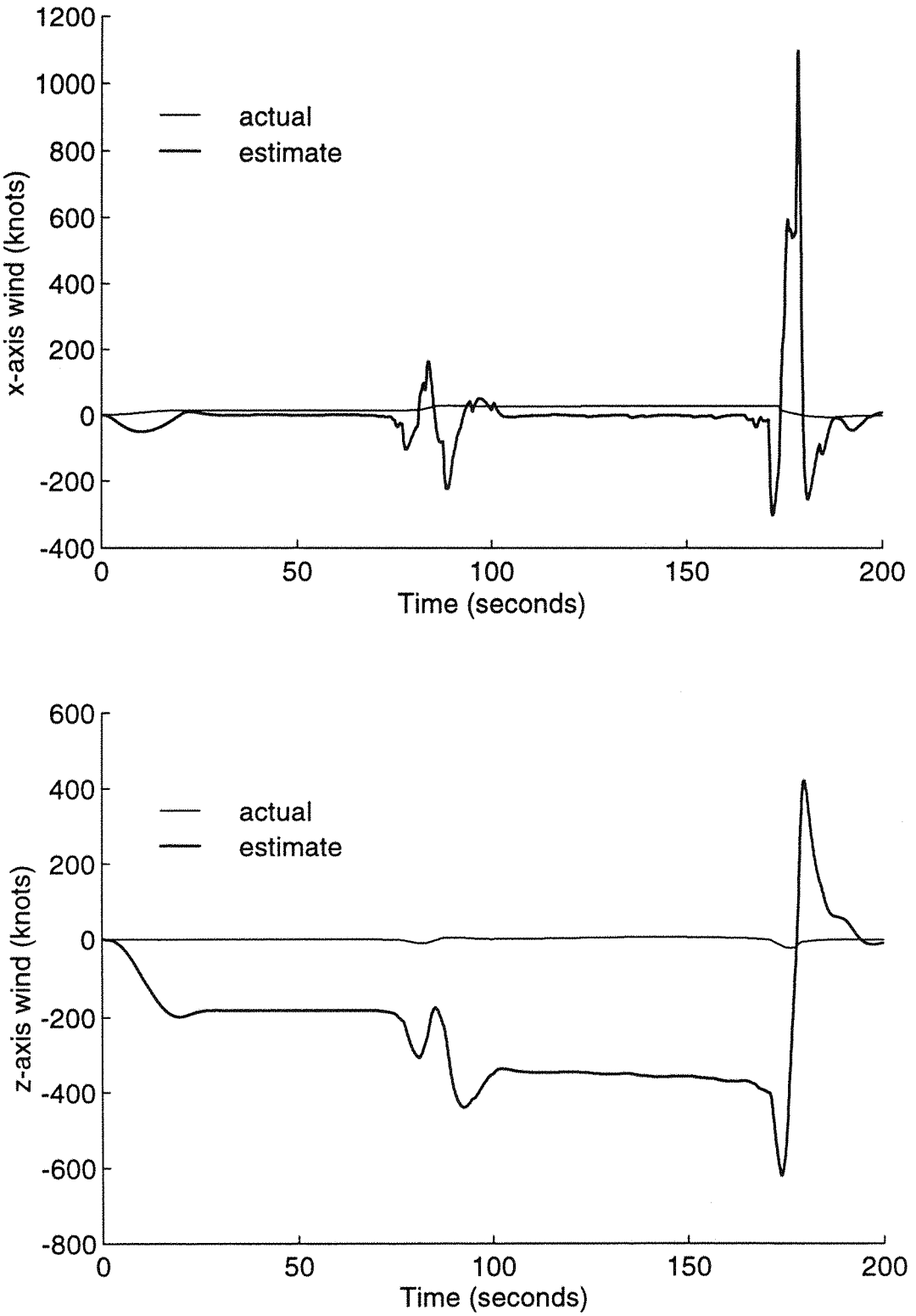

Figure 4.11: Estimate of JFK Wind Components using 'Enhanced' Observer

worse than the estimate of Figure 4.3 without the compensation for transients. The estimate of the z-axis wind component shows similarities to the x-axis wind profile, albeit inverted and magnified.

The results show that the method of improving the estimate by correcting for the transient errors is not having the desired effect. This is because the assumption that the inertial velocity derived from the aircraft model is a sufficiently accurate estimate of the actual inertial velocity is incorrect. The errors in the estimate in the inertial forward velocity from both x-axis and z-axis winds are shown in Figure 4.12. Although the estimate of the z-axis wind follows the actual parameters fairly accurately after the transient has passed there is a steady state error in the x-axis estimate in the inertial speed, these errors are passed into the transient-compensation algorithm and are sufficiently large to negate any improvement which could have been gained from the method. For such a technique to be of use requires a means of initialising the error in the inertial velocity estimate to zero and thereby reducing the error propagation caused by the feedback from the model to the transient compensation algorithm. The results, in Figure 4.13, are derived by passing the actual inertial velocity into the transient-compensation algorithm, rather the estimated velocity, and these show that the method could be used to improve the transient errors in the estimator if an accurate measurement of the inertial forward velocity were available.

4.3 Estimation of Wind acting on an Aircraft using Two Aircraft State Variables

The use of the pitch rate to estimate the wind velocities shows some approximation to the actual velocities but the resulting errors are too large to allow accurate windshear detection. However, the method shows that approximations, albeit poor, of both the air-relative velocities and the inertial velocities, can be made from a system by using a single state variable. The improvement which can be gained by measuring two aircraft state variables in now considered. This requires additional sensor data and so increases the cost of the device.

The acceleration acting along the z axis through the centre of gravity can be measured and this, together with the pitch rate allows the heave acceleration, $\dot{w}$, to be evaluated approximately. This acceleration can then be integrated

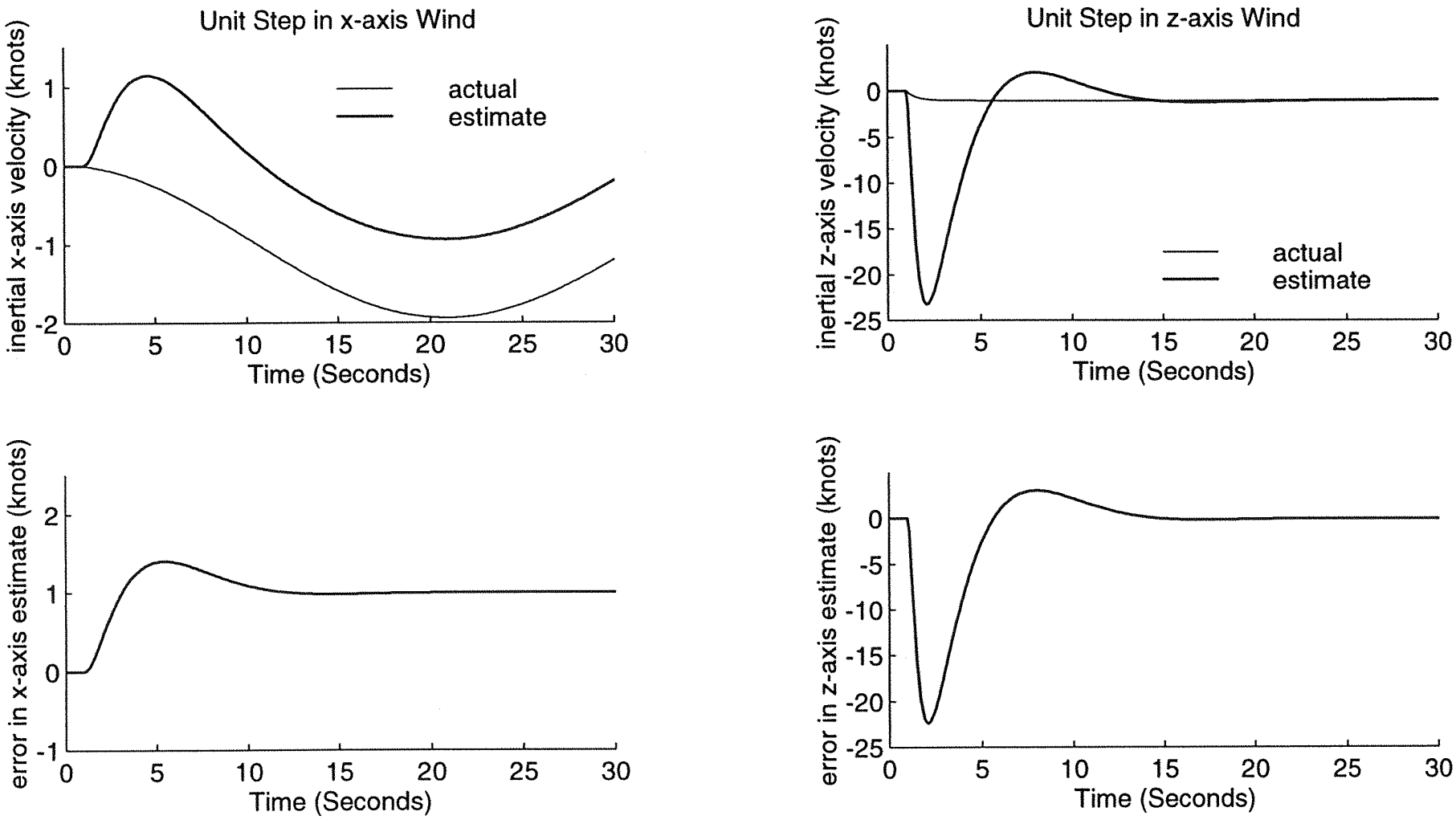

Figure 4.12: Estimation of Inertial Velocities by Model

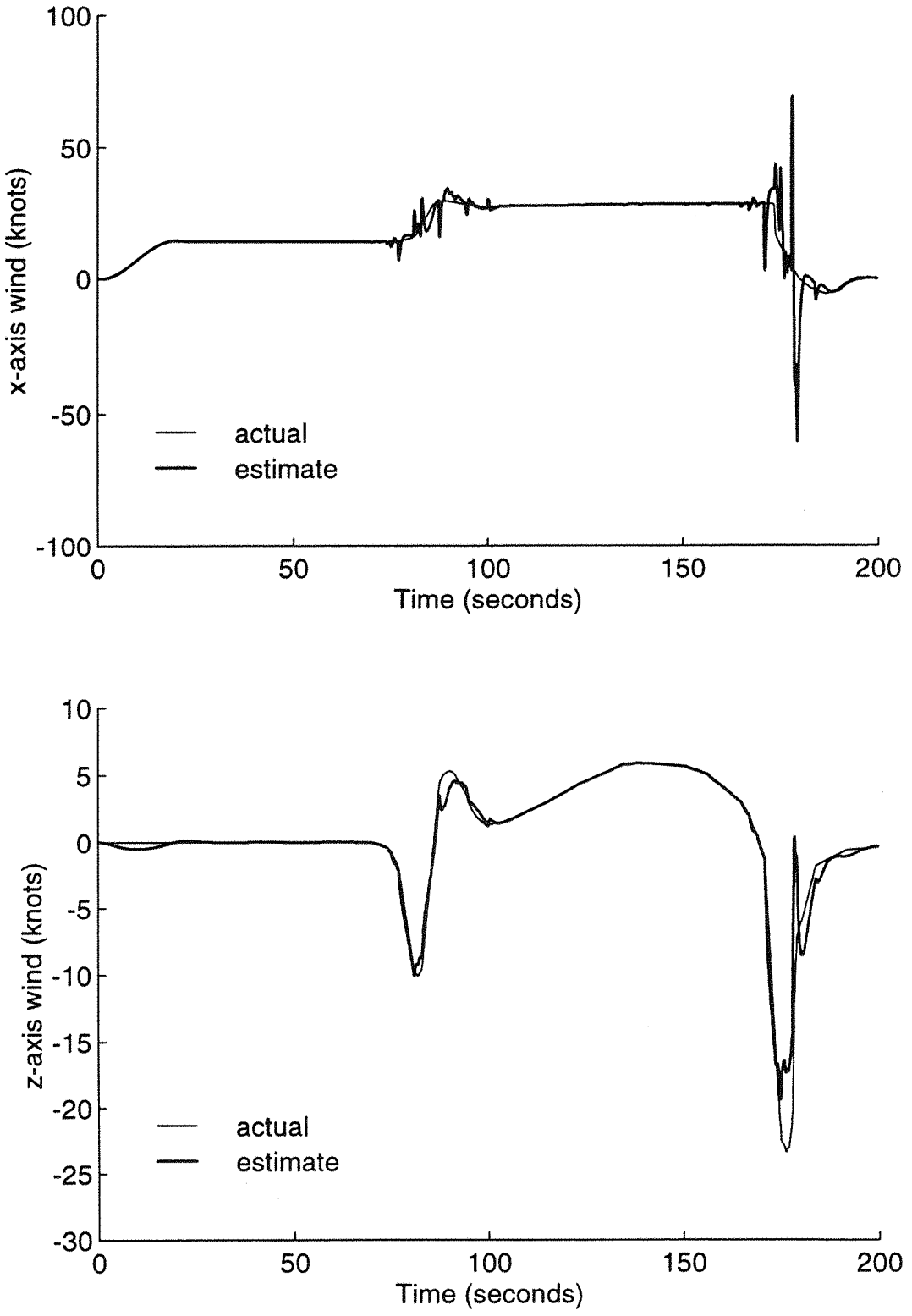

Figure 4.13: Estimate of JFK Wind Components using Actual Inertial Velocity

to give the heave velocity, w, which makes a second state available to the detection system. The practical implications of this were discussed in Section 3.5.

4.3.1 Observer Design

Two state variables are now available for feedback into an observer and these can be used to produce an observer to minimise the errors between the aircraft and observer state vectors. However, the purpose of the observer implementation is not to estimate the aircraft state vector but to facilitate a simple method of estimating the wind vector. The observer designed for the previous system fed back the pitch rate state variable only and produced estimates of the air-relative velocities. The same observer design can be used again in the new system so that the observer state variables representing the air-relative forward and heave velocities approximate these parameters as before. The errors produced by this observer are therefore unchanged and are shown in Figure 4.4.

Alternatively, both the heave velocity and the pitch rate can be considered for use as inputs to the observer. The output matrix then becomes:

$$\mathbf{C} = \begin{bmatrix} 0 & 1 & 0 & 0 \\ 0 & 0 & 1 & 0 \end{bmatrix} \tag{4.43}$$

The gain, $\mathbf{K}$, of the observer is designed using optimal techniques and produces a matrix of dimensions [4x2]. The steady state error of the observer is, as before, given by equation 4.44.

$$\mathbf{e} = -(\mathbf{A} - \mathbf{KC})^{-1}\mathbf{E}\mathbf{w}_{\mathbf{ind}} \tag{4.44}$$

However, the performance of the observer in differs from that when only the pitch rate is used, since the matrix $\mathbf{KC}$ is non-zero in both the second and third columns. and therefore equation 4.20 is not applicable. As a consequence the first two observer states do not settle to the air-relative velocities, but to a combined function of the wind inputs, viz.

$$u - u_e = -u_g - n_{12}w_g \tag{4.45}$$

$$w - w_e = -n_{22}w_g \tag{4.46}$$

where n_{ij} represents the (i,j)th element of $(\mathbf{A}-\mathbf{KC})^{-1}\mathbf{E}$.

The air-relative velocities cannot be readily derived from these equations and therefore this form of the observer was not implemented. The observer already designed, which uses a single input, pitch rate, was used for the remaining analysis of the wind estimation using pitch rate and heave velocity.

4.3.2 Compensation of Transients in the Air-Relative Velocity Estimates

The transient error in the observer estimation was found to be the significant source of inaccuracies in the estimation of the air-relative speeds and therefore the wind vector. Section 4.2.4 described a method designed to improve the observer estimate by modelling the effects of the transient response as closely as possible. A similar technique can be applied for the present system where $\dot{w}$, and hence w, are available.

The difference between the aircraft and observer state vectors was given in equation 4.32, which represented four simultaneous equations. It was shown in equation 4.36 that the wind vector could be related to the error vector by using just two of these four simultaneous equations. Equation 4.42 then showed the relationship between the air-relative velocities and the observer and aircraft parameters when the first and third simultaneous equations in $\dot{u}$ and $\dot{q}$ were used.

The system using two state variables measures, indirectly, both pitch rate and heave velocity and, as a consequence, it is more suitable to solve for the air-relative velocities using the second and third of the simultaneous equations in $\dot{w}$ and $\dot{q}$. Use of this equation means that the air-relative velocities can be evaluated directly without requiring feedback from the aircraft model.

$$\begin{pmatrix} u_a \\ w_a \end{pmatrix} = \begin{pmatrix} u_g \\ w_g \end{pmatrix} + \begin{bmatrix} 1 & 0 \\ 0 & 1 \end{bmatrix} \begin{pmatrix} u \\ w \end{pmatrix} = \begin{bmatrix} f_{11} & f_{12} \\ f_{21} & f_{22} \end{bmatrix} \begin{pmatrix} \dot{w}-\dot{w}_e \\ \dot{q}-\dot{q}_e \end{pmatrix} - \begin{bmatrix} 1 & 0 & h_{13} & h_{14} \\ 0 & 1 & h_{23} & h_{24} \end{bmatrix} \begin{pmatrix} -u_e \\ -w_e \\ q-q_e \\ \theta-\theta_e \end{pmatrix} \quad (4.47)$$

where f_{ij} and h_{ij} now represent elements derived from the second and third simultaneous equations following the methods derived in Section 4.2.4.

There is still a further simplification which can be made to the transient-compensated estimation. Both the air-relative and the inertial heave velocities are available and so it follows that the z-axis wind component can be calculated directly.

$$\begin{pmatrix} u_a \\ w_g \end{pmatrix} = \begin{bmatrix} f_{11} & f_{12} \\ f_{21} & f_{22} \end{bmatrix} \begin{pmatrix} \dot{w} - \dot{w}_e \\ \dot{q} - \dot{q}_e \end{pmatrix} - \begin{bmatrix} 1 & 0 & h_{13} & h_{14} \\ 0 & 1 & h_{23} & h_{24} \end{bmatrix} \begin{pmatrix} -u_e \\ w - w_e \\ q - q_e \\ \theta - \theta_e \end{pmatrix} \tag{4.48}$$

The results of this algorithm in enhancing the observer's estimates of the velocities is shown in Figure 4.14. This shows the x-axis airspeed estimates and the z-axis wind component estimates when the aircraft is subject to a unit step in the x-axis and z-axis wind components separately. The error in the estimate of airspeed when an x-axis wind is applied can only just be distinguished from the actual airspeed and so the estimate is a large improvement on the basic observer response shown in Figure 4.4. The estimate of airspeed with a z-axis wind shows a small transient error which has become insignificant within two to three seconds.

Considering now the z-axis wind estimates in the lower plots, the magnitude of the error resulting from an x-axis wind is negligible when compared to the size of the wind applied. The z-axis component again shows a small, transient error which decays to become negligible within two seconds. Both these estimates show a very large improvement compared to the estimates obtained with the system using a single state variable shown in Figure 4.2.

The compensation stage of the algorithm cancels the transient errors in the observer and therefore reduces the design requirement to optimise the transient performance. The optimisation was originally achieved by a suitable choice of the observer gain using optimal techniques which involved careful selection of the weighting matrices. However, a stable observer can be designed with the weighting matrices both set to be equal to the identity matrix. The gain matrix then becomes:

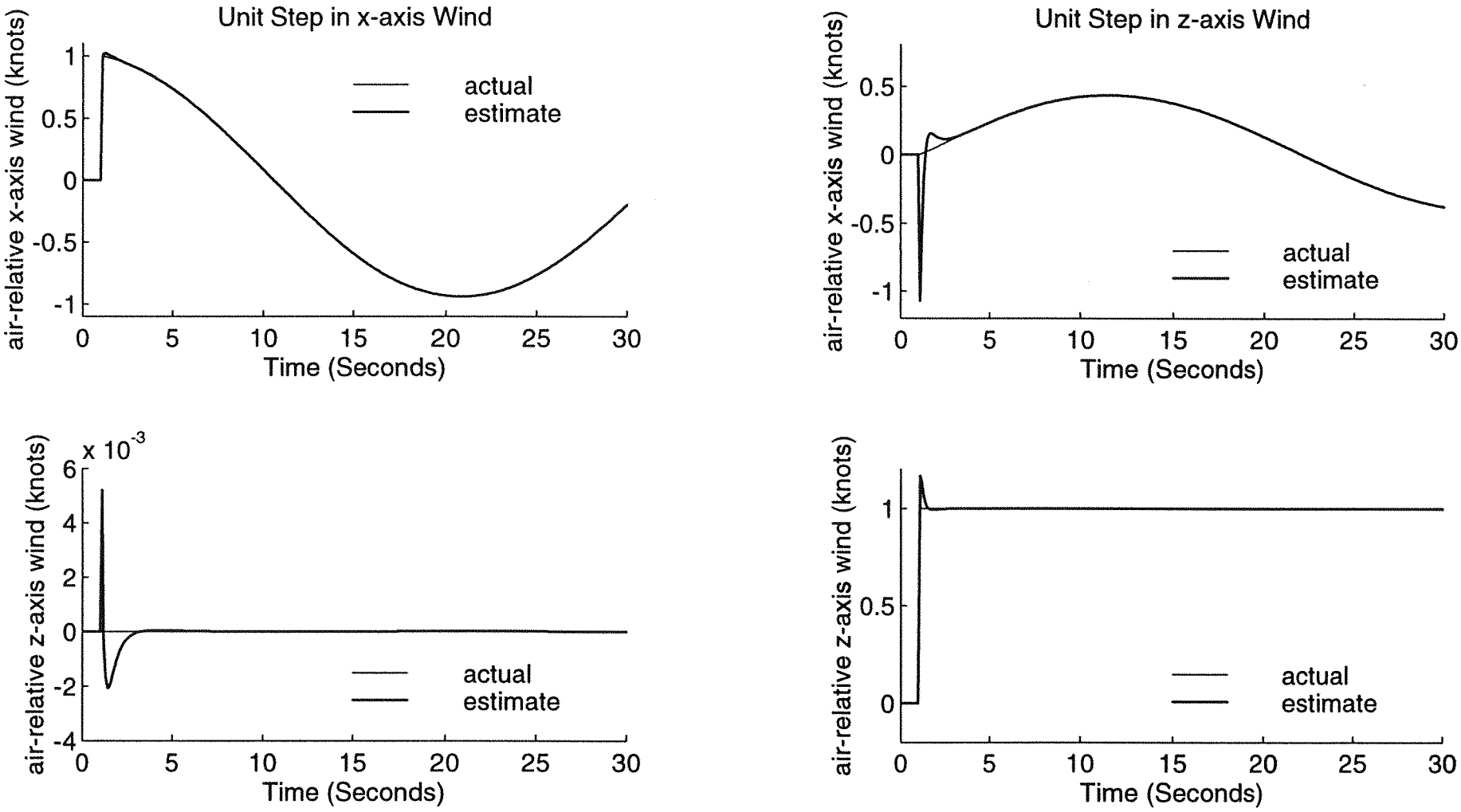

Figure 4.14: Output of 'Enhanced' Observer using Pitch Rate and Heave Velocity

$$\mathbf{K} = \begin{bmatrix} 194.92 \\ -29.41 \\ 0.19 \\ -0.41 \end{bmatrix} \tag{4.49}$$

If this observer gain is implemented in the wind estimation method, the transient-compensated observer produced similar errors to these shown in Figure 4.14. The non-optimal design of the observer has a negligible effect on the errors produced when this method is used.

A block diagram of the transient compensation method, based on equation 4.48, is shown in Figure 4.15.

4.3.3 Calculation of the x-axis Wind Component

It remains to determine the inertial forward velocity of the aircraft to evaluate the x-axis component of the wind. The inertial forward speed, u, can be found from a simulated aircraft 'model' as before.

Figure 4.16 shows the resulting estimates for unit step changes in both wind components (the z-axis wind estimates are repeated from Figure 4.14). The errors in the x-axis wind estimates are of similar magnitude and duration to those for the air-relative forward velocity estimates of Figure 4.14 and so the inertial velocity estimate can be seen to have contributed negligible errors.

The response of the system to a typical windshear is shown in Figures 4.17, which show the estimates of the wind components and the corresponding errors when the 'JFK' windshear profile is applied to the aircraft. It can be seen that the errors remain very small even when there are large wind transients. This method of wind estimation is, therefore, likely to be suitable for windshear detection.

4.4 Estimation of Wind acting on an Aircraft using Pitch Rate and Airspeed Measurements

The system described in Section 4.3 uses two state variables; pitch rate was chosen as one of the state variables as this can be measured directly, and the second state variable was chosen to be the inertial heave velocity which can

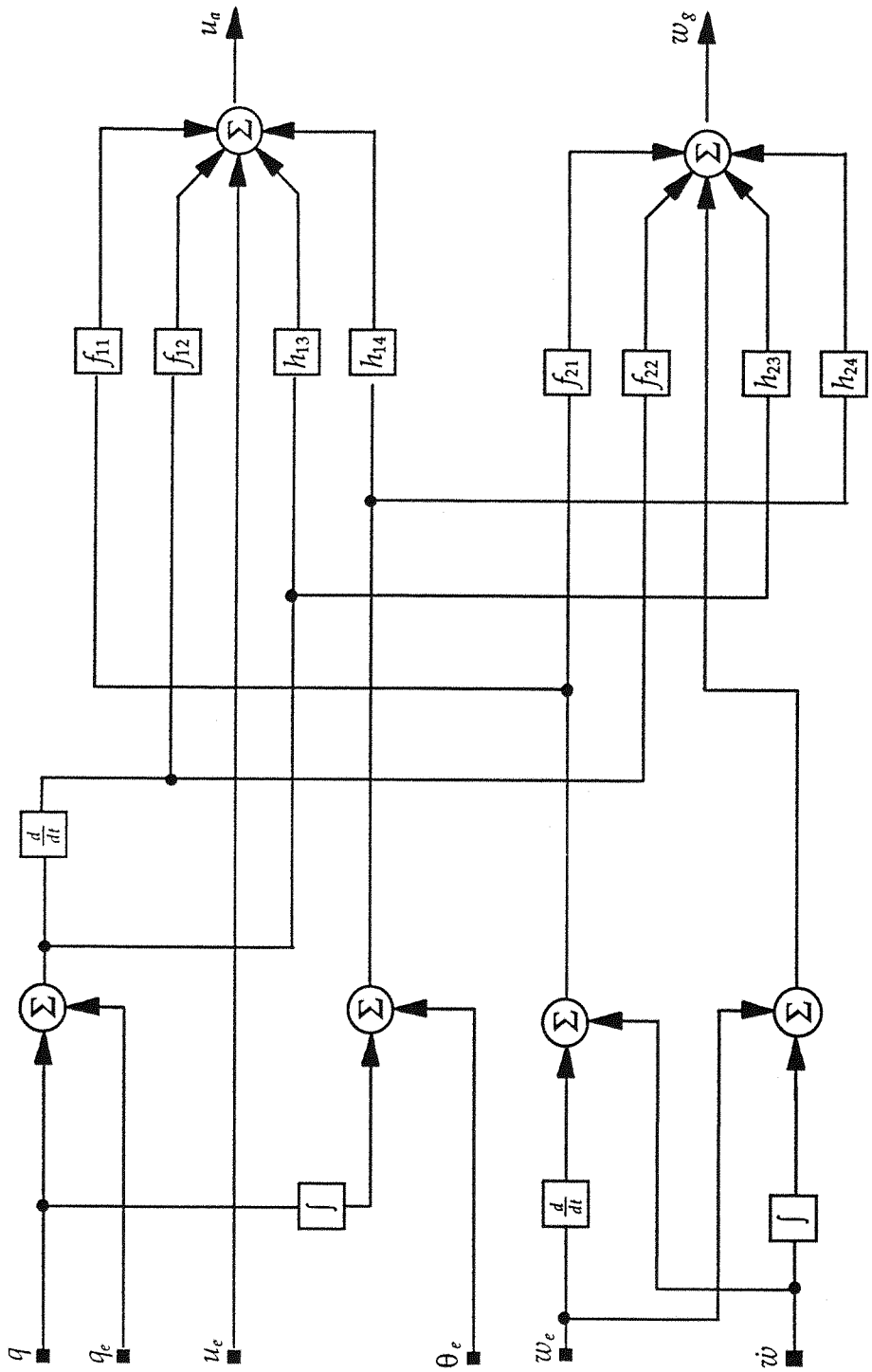

Figure 4.15: Schematic of Transient Compensation

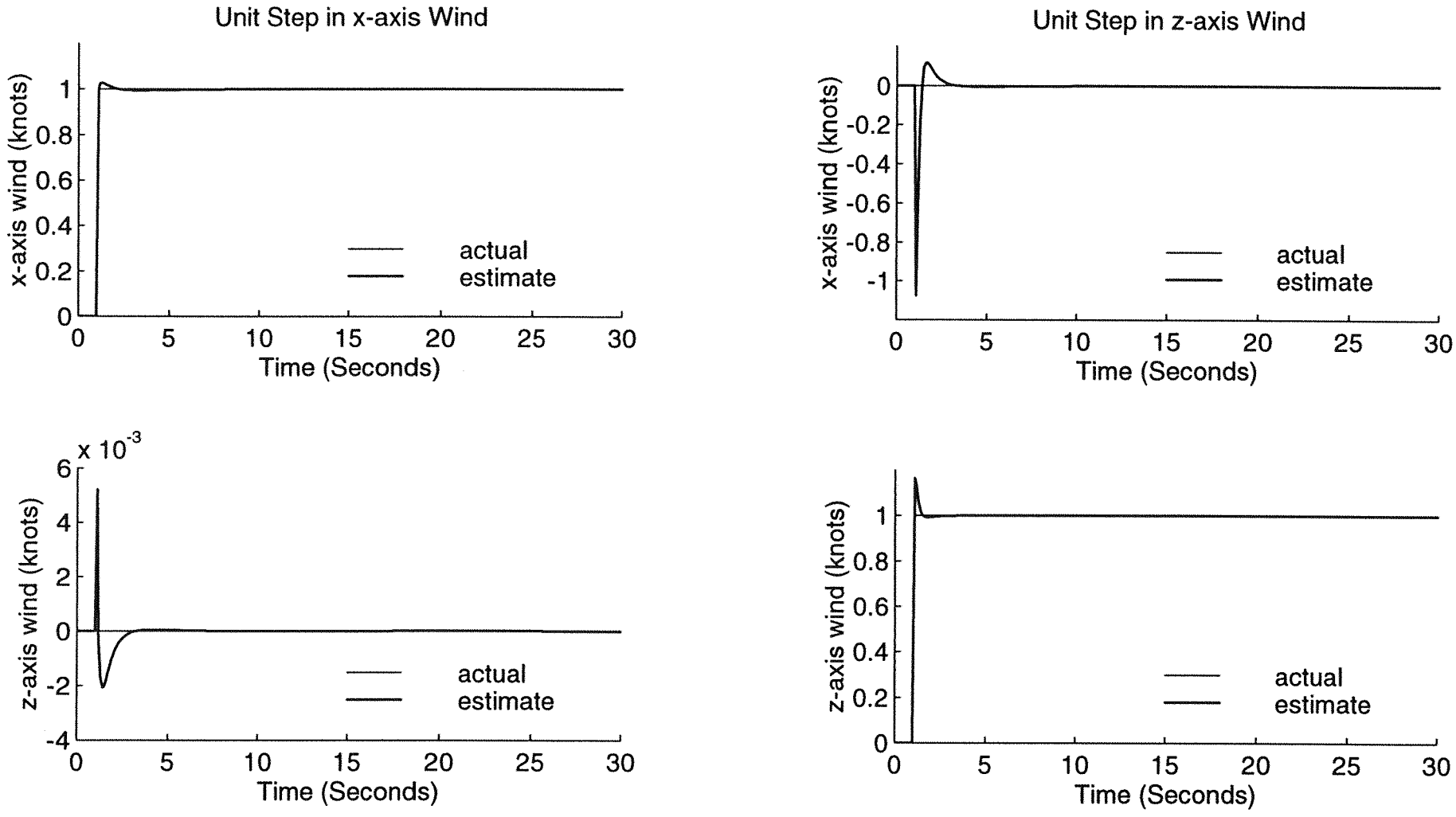

Figure 4.16: Estimation of Wind Components using Pitch Rate and Heave Velocity

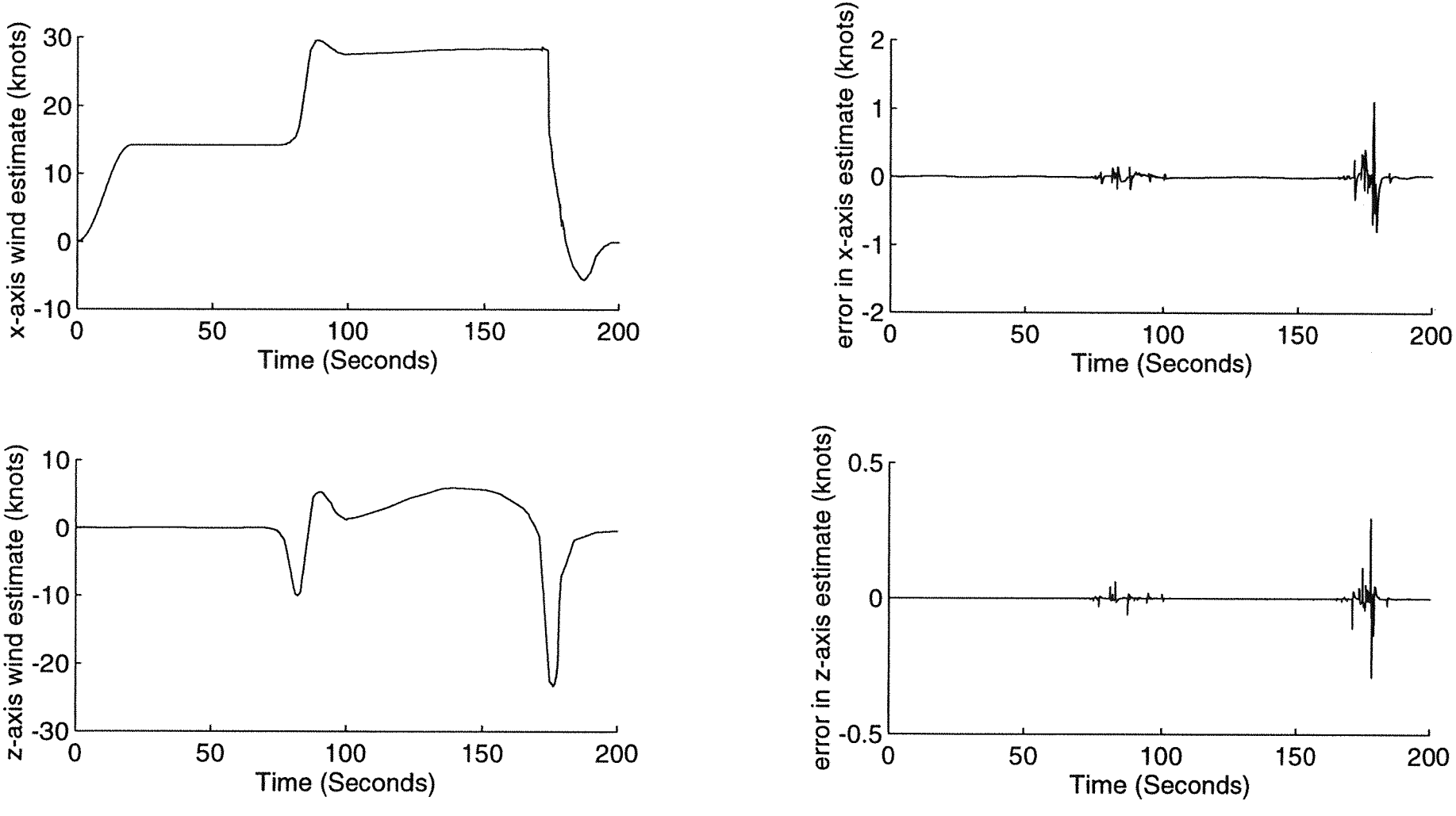

Figure 4.17: JFK Wind Component Estimates using Pitch Rate and Heave Velocity

be derived using a relatively simple accelerometer as the sensor. As an alternative the airspeed could be measured, and the method for doing this to obtain the trim airspeed, U_a, and the perturbed quantity, u_a, is discussed in Section 3.5. Although the airspeed is not an aircraft state variable, it is related to inertial forward velocity by the x-axis wind component, and so may be of use in the wind estimation. This system will be useful for consideration in Chapter 5 and so the design of the estimation algorithm, which is analogous to the two input system already described, is summarised below.

The system and output equation for the aircraft are:

$$\dot{\mathbf{x}} = \mathbf{A}\mathbf{x} + \mathbf{B}\mathbf{u} + \mathbf{E}\mathbf{w}_{ind} \tag{4.50}$$

$$\mathbf{y} = \mathbf{C}\mathbf{x} + \mathbf{D}\mathbf{w}_{ind} \tag{4.51}$$

where

$$\mathbf{C} = \begin{bmatrix} 1 & 0 & 0 & 0 \\ 0 & 0 & 1 & 0 \end{bmatrix} \tag{4.52}$$

and

$$\mathbf{D} = \begin{bmatrix} 1 & 0 \\ 0 & 0 \end{bmatrix} \tag{4.53}$$

The same observer as used in the previous designs can be implemented, and this uses only the measured pitch rate as an input. However, it is also possible to configure a two input observer using the additional airspeed input. The observer equation is:

$$\dot{\mathbf{x}}_e = \mathbf{A}\mathbf{x}_e + \mathbf{B}\mathbf{u} + \mathbf{K}\mathbf{y} - \mathbf{K}\mathbf{y}_e \tag{4.54}$$

and when using both airspeed and pitch rate as inputs, the error equation becomes:

$$\dot{\mathbf{e}} = (\mathbf{A} - \mathbf{K}\mathbf{C})\mathbf{e} + (\mathbf{E} - \mathbf{K}\mathbf{D})\mathbf{w}_{ind} \tag{4.55}$$

As the first two columns of **(A-KC)** and **(E-KD)** are identical, the steady state error of the system now becomes:

$$\mathbf{e} = -(\mathbf{A}-\mathbf{KC})^{-1}(\mathbf{E}-\mathbf{KD})\mathbf{w}_{ind} = -\begin{bmatrix} 1 & 0 \\ 0 & 1 \\ 0 & 0 \\ 0 & 0 \end{bmatrix}\mathbf{w}_{ind} \tag{4.56}$$

The first two states of the observer settle to the air-relative forward and heave velocities and so this observer is suitable as part of the detection system.

The observer gains were optimised using similar techniques to those of Section 4.2.3 (although the advantage gained, when using the observer transient compensation, is small). The weighting matrices used were:

$$\mathbf{Q} = \text{diag}[1 \quad 1 \quad 1 \quad 10] \tag{4.57}$$

$$\mathbf{R} = \text{diag}[3 \quad 1] \tag{4.58}$$

The gains required to optimise the observer were significantly smaller then those for the system using pitch rate and heave velocity viz.

$$\mathbf{K} = \begin{bmatrix} 10.8 & -0.05 \\ 0.56 & 0.81 \\ 0.02 & 0.06 \\ -1..83 & 0.02 \end{bmatrix} \tag{4.59}$$

The observer estimate can be compensated for transient errors in a similar manner to that described in Section 4.2.4 using the simultaneous equations in $\dot{u}$ and $\dot{q}$ to yield equation 4.42. For this to be possible requires that the inertial forward velocity be known to the transient compensation algorithm and, although this is not available as a measured value, the model produces an estimate of this parameter which can be fed back into the transient compensation algorithm (as was attempted for the system using a single state variable in Section 4.2.4).

The airspeed is a measured quantity and so the observer and transient compensation are only required to generate the air-relative heave velocity

estimate. This parameter is then passed into aircraft model with the airspeed, pitch rate and pitch attitude as the vector $\hat{\mathbf{x}}$ so that the equation for the model is, as before:

$$\mathbf{x}_m = \mathbf{A}\hat{\mathbf{x}} + \mathbf{B}\mathbf{u} \tag{4.60}$$

The model produces estimates of the inertial forward and heave velocities and so the wind components can be estimated as the difference between the airspeed and the inertial forward velocity, and the air-relative and inertial heave velocity estimates.

The system was simulated and the results when using the 'JFK' wind components as input are shown in Figure 4.18. The transient errors are most noticeable when the wind components are rapidly changing, but they are small when compared to the wind magnitudes. There was no discernible offset in the estimates of the two wind components.

4.5 Effect of Pitching Wind Component

The estimation techniques which have been developed have assumed that the wind is composed only of a x-axis and z-axis component and that there is no contribution from a pitching wind component. In practice, such a component will also affect the longitudinal dynamics of the aircraft. A pitching wind can be represented as a scaled rate of change of the z-axis wind as derived in Appendix A.

$$q_g = -\frac{\dot{w}_g}{U_0} \tag{4.61}$$

The pitching wind component can be calculated, therefore, from the wind components already used to test the algorithm, and its effects can be included in the simulation.

The system matrices now include the terms associated with the pitching wind component. These are the state equations summarised in Appendix A. The wind vector and its associated input matrix are:

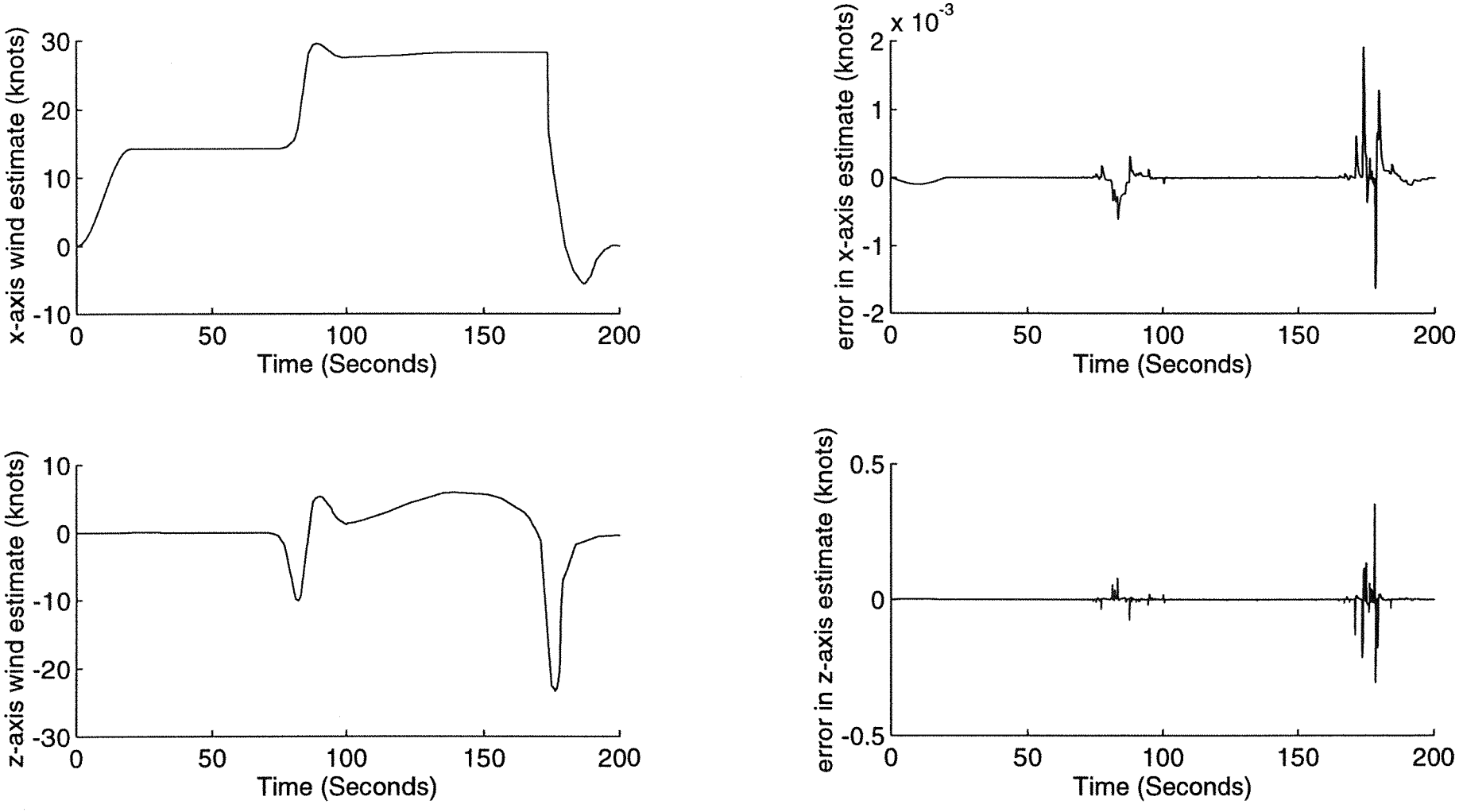

Figure 4.18: JFK Wind Component Estimates using Pitch Rate and Airspeed

$$\mathbf{w}_{\text{ind}} \equiv \begin{bmatrix} u_g \\ w_g \\ q_g \end{bmatrix} \tag{4.62}$$

$$\mathbf{E} = \begin{bmatrix} X_u & X_w & 0 \\ Z_u & Z_w & Z_q \\ \tilde{M}_u & \tilde{M}_w & \tilde{M}_q - 2M_{\dot{w}}U_0 \\ 0 & 0 & 0 \end{bmatrix} \tag{4.63}$$

The additional terms in the matrix affect the estimation of the x-axis and z-axis wind components.

4.5.1 Estimation using Pitch Rate and Heave Velocity

The results produced by the wind estimation algorithm when the pitch component of the wind is included in the simulation are shown in Figure 4.19. Although the estimates of both components follow the general profile of the actual components, there are significant errors which are associated with the periods when the z-axis components are changing most rapidly and, therefore, when the component of pitching wind is significant. The errors in the x-axis wind component, in particular, are very significant. These errors can be explained by examining the error equation of the observer:

$$\dot{\mathbf{e}} = (\mathbf{A} - \mathbf{KC})\mathbf{e} + \mathbf{E}\mathbf{w}_{\text{ind}} \tag{4.64}$$

This equation can be rearranged by dividing the input matrix, $\mathbf{E}$, to clarify the analysis:

$$\dot{\mathbf{e}} = (\mathbf{A} - \mathbf{KC})\mathbf{e} + \mathbf{E}_{\text{uw}} \begin{bmatrix} u_g \\ w_g \end{bmatrix} + \mathbf{E}_{\text{q}} q_g \tag{4.65}$$

where $\mathbf{E}_{\text{uw}}$ represents the first two columns of $\mathbf{E}$, which is identical to the $\mathbf{E}$ matrix used in the earlier derivations, and $\mathbf{E}_{\text{q}}$ represents the third column, which comprises the elements associated with the pitching wind.

The steady errors in the observer are:

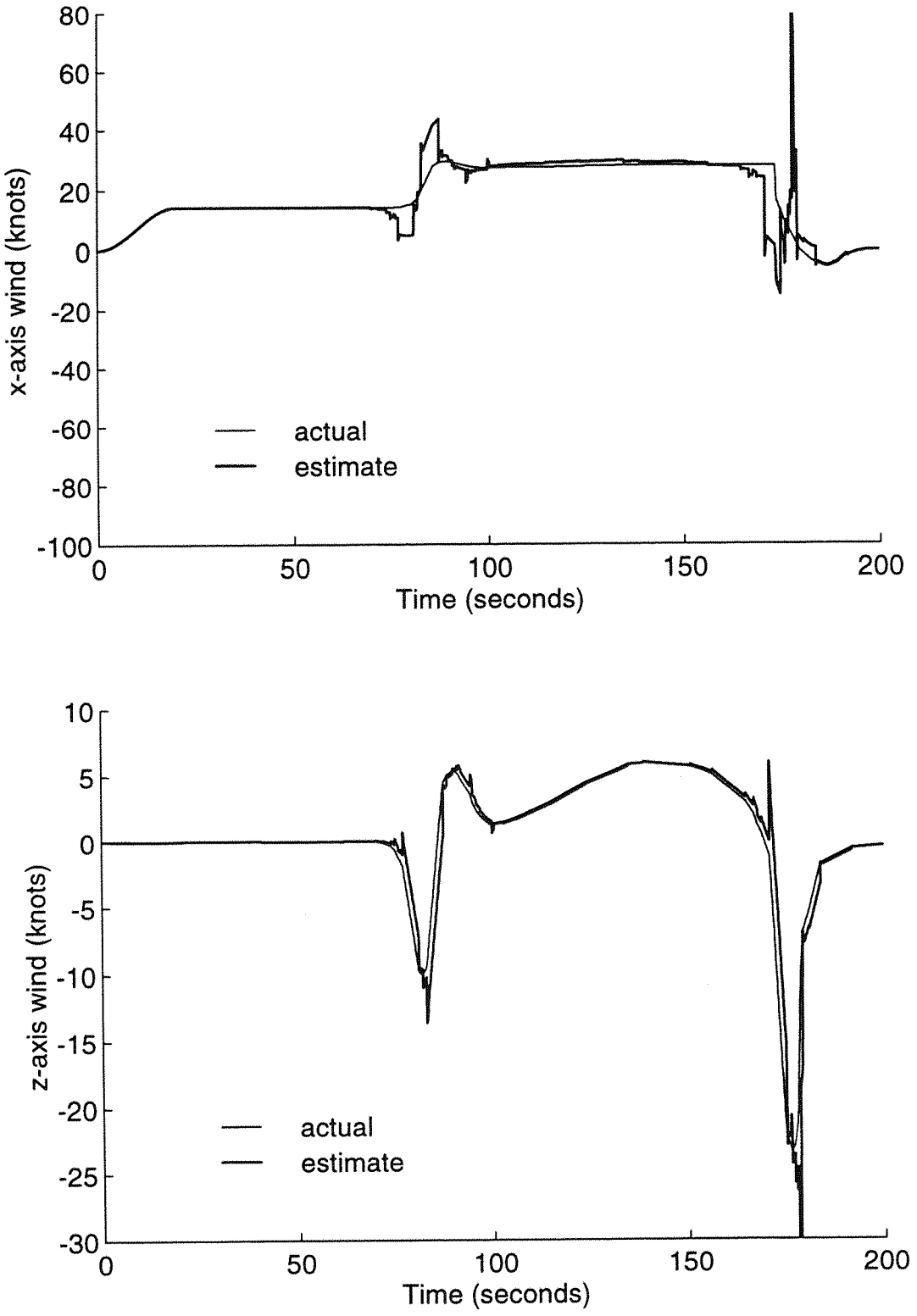

Figure 4.19: Effect of Pitching Wind on Estimation using Pitch Rate and Heave Velocity

$$\mathbf{e} = (\mathbf{A} - \mathbf{KC})^{-1}\mathbf{E}_{uw}\begin{bmatrix} u_g \\ w_g \end{bmatrix} + (\mathbf{A} - \mathbf{KC})^{-1}\mathbf{E}_q q_g \tag{4.66}$$

This can be compared with the error in the observer using pitch rate and heave velocity but when the pitching wind was ignored, equation 4.44. There is an additional term in the steady error, which is related to the pitching wind input. It is desirable that the observer states settle to the air-relative velocities, but in this case there is an additional steady error resulting from the pitching wind which produces an offset in the estimation. (If the z-axis wind is steady, the pitching wind component is zero because of the relationship in equation 4.61, and no offset will be produced. However, some turbulence is present during all flights and this will cause the z-axis wind to vary. The components of pitching wind generated may be significant.)

The effect of the pitching wind component on the transient-compensation algorithm of the observer can be derived from equation 4.65 using the two simultaneous equations in pitch rate and heave velocity. This produces additional terms in equation 4.48 as shown:

$$\begin{pmatrix} u_a \\ w_g \end{pmatrix} + \begin{bmatrix} p_1 \\ p_2 \end{bmatrix} q_g = \begin{bmatrix} f_{11} & f_{12} \\ f_{21} & f_{22} \end{bmatrix} \begin{pmatrix} \dot{w} - \dot{w}_e \\ \dot{q} - \dot{q}_e \end{pmatrix} - \begin{bmatrix} 1 & 0 & h_{13} & h_{14} \\ 0 & 1 & h_{23} & h_{24} \end{bmatrix} \begin{pmatrix} -u_e \\ w - w_e \\ q - q_e \\ \theta - \theta_e \end{pmatrix} \tag{4.67}$$

Here p_i represents the ith element of $\hat{\mathbf{E}}_{uw}{}^{-1}\hat{\mathbf{E}}_q$.

Whereas the transient compensation previously produced an accurate estimation of the airspeed and z-axis wind, the output is now confused with the effects of the pitching wind component. The relationship between the pitching wind component and the z-axis wind means that the right-hand side of equation 4.67 can be simplified as follows.

$$\begin{pmatrix} u_a \\ w_g \end{pmatrix} + \begin{bmatrix} p_1 \\ p_2 \end{bmatrix} q_g \equiv \begin{pmatrix} u_a - \dfrac{p_1}{U_o}\dot{w}_g \\ w_g - \dfrac{p_2}{U_o}\dot{w}_g \end{pmatrix} \tag{4.68}$$

The time derivatives can be expressed in Laplace terms where s is the Laplace operator. w_g is the small perturbation value of the z-axis wind component from the trim value and the initial value of this is assumed to be zero.

$$\begin{pmatrix} u_a \\ w_g \end{pmatrix} + \begin{bmatrix} p_1 \\ p_2 \end{bmatrix} q_g = \begin{pmatrix} u_a - s\frac{p_1}{U_o} w_g \\ w_g\left(1 - s\frac{p_2}{U_o}\right) \end{pmatrix} \tag{4.69}$$

The equation for the z-axis wind must be solved first. If the sign relating the functions of w_g and $\dot{w}_g$ were additive then the z-axis wind could be calculated by applying low-pass filtering to cancel the effect of the pitching wind component, since:

$$w_g = \left(\frac{1}{1 + s\frac{p_2}{U_0}}\right)\left(w_g + \frac{p_2}{U_0} s w_g\right) \tag{4.70}$$

However, w_g cannot be derived from equation 4.69 in this way because dividing the equation for w_g by the term $\left(1 - s(p_2/U_0)\right)$ implements an unstable filter. An alternative, approximate method must be used instead. A low-pass filter was found to improve the z-axis wind estimate by reducing the high-frequency effects of the pitching wind component. The estimate of a z-axis wind produced by this method when using a first order filter with a 0.1 Hz cut-off frequency can be seen in Figure 4.20.

Equation 4.69 implies the airspeed estimate could be improved by adding the pitching wind term of equation 4.69 to the airspeed estimate produced by the transient compensation because:

$$u_a = \left(u_a - \frac{p_1}{U_o}\dot{w}_g\right) + \frac{p_1}{U_o}\dot{w}_g \tag{4.71}$$

In practice this is not possible. The filter used in the estimation of the z-axis wind introduces a time lag. As a result, the compensation derived from this parameter is not in phase with the airspeed estimate, and so the estimate is degraded.

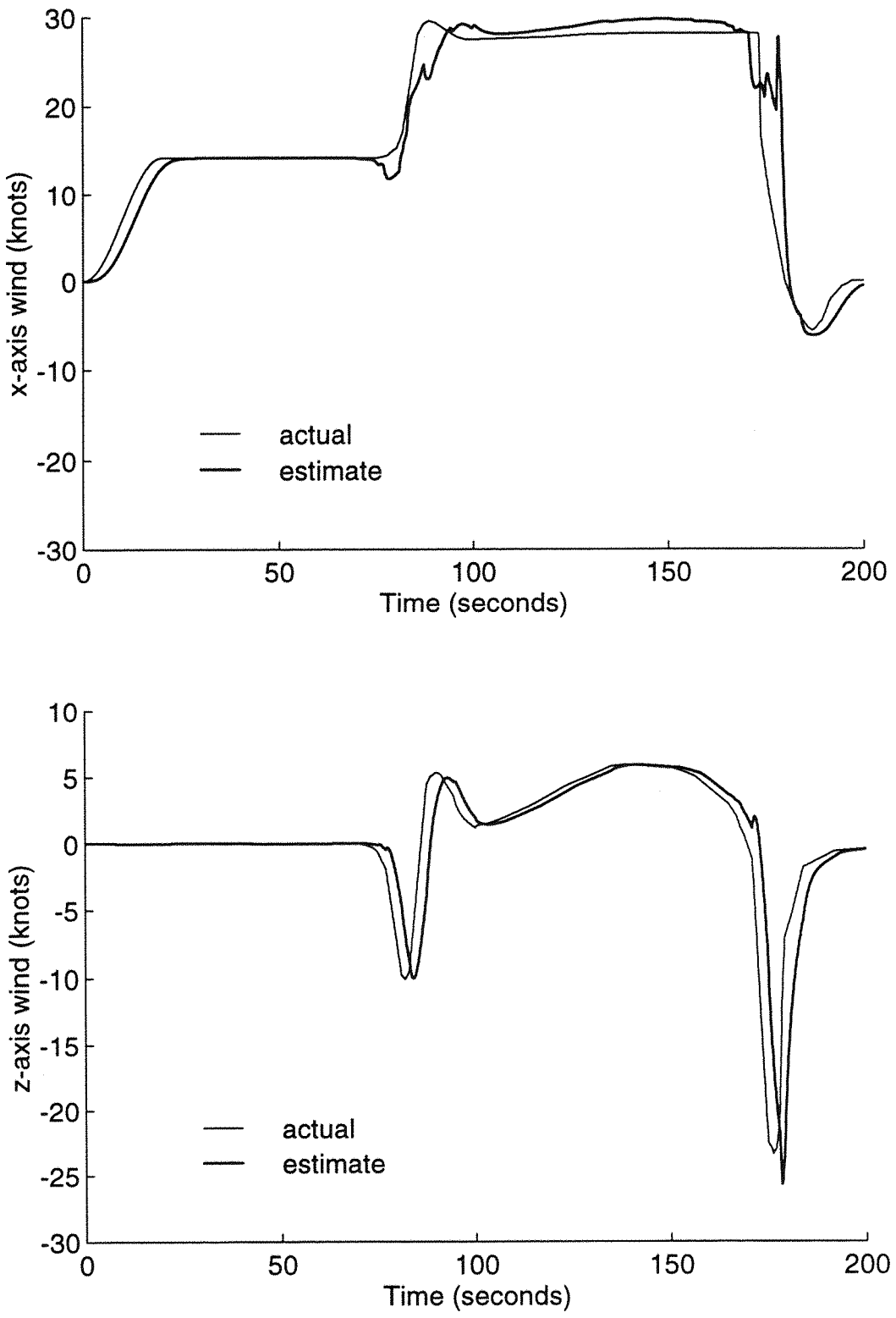

Figure 4.20: Improved JFK Estimation using Pitch Rate and Heave Velocity

However, the x-axis wind estimate is derived by subtracting the inertial aircraft velocity from the airspeed and so the error in the airspeed caused by the pitching wind component is present in the estimate, albeit with further errors introduced by the aircraft model. It seems likely, therefore, that the estimate of this wind component could be improved by application of compensation at this stage.

The x-axis wind compensation was tested and found to require the following several stages. A low pass filter stage is required to produce a delay in the estimation of the x-axis wind component to matched that in the z-axis component. The compensation term of equation 4.71, $(p_1/U_0)\dot{w}_g$, can then be added to the x-axis wind estimate to reduce the errors arising from the effects of the pitching wind component. A further low-pass filter stage is required to remove high frequency transient errors in the estimation introduced by the differentiation of the z-axis wind in the compensation. This was also selected to be a first-order filter with a cut-off frequency of 0.1 Hz.

The result of the simulation of the revised algorithm with the pitching wind component present produced the results shown in Figure 4.20. The estimates of both wind components show a delay which is caused by the low-pass filtering - the filter characteristics were chosen to be a compromise between the elimination of the transient errors caused by the pitching wind component and the delay produced in the estimated wind component. The implications of the delays in the estimation for timing of the alert are considered in Chapter 6. The z-axis wind estimate still exhibits a small 'overshoot' error during the periods when the wind changes rapidly, but this is significantly smaller than the errors shown in Figure 4.19. The x-axis estimate follows, in general, the actual wind component, but shows discrepancies during periods when the pitching wind component is significant. These are caused by residual errors in the compensation and also by the errors in the estimate of the inertial velocity.

A block diagram of the system incorporation the pitching wind compensation is shown in Figure 4.21.

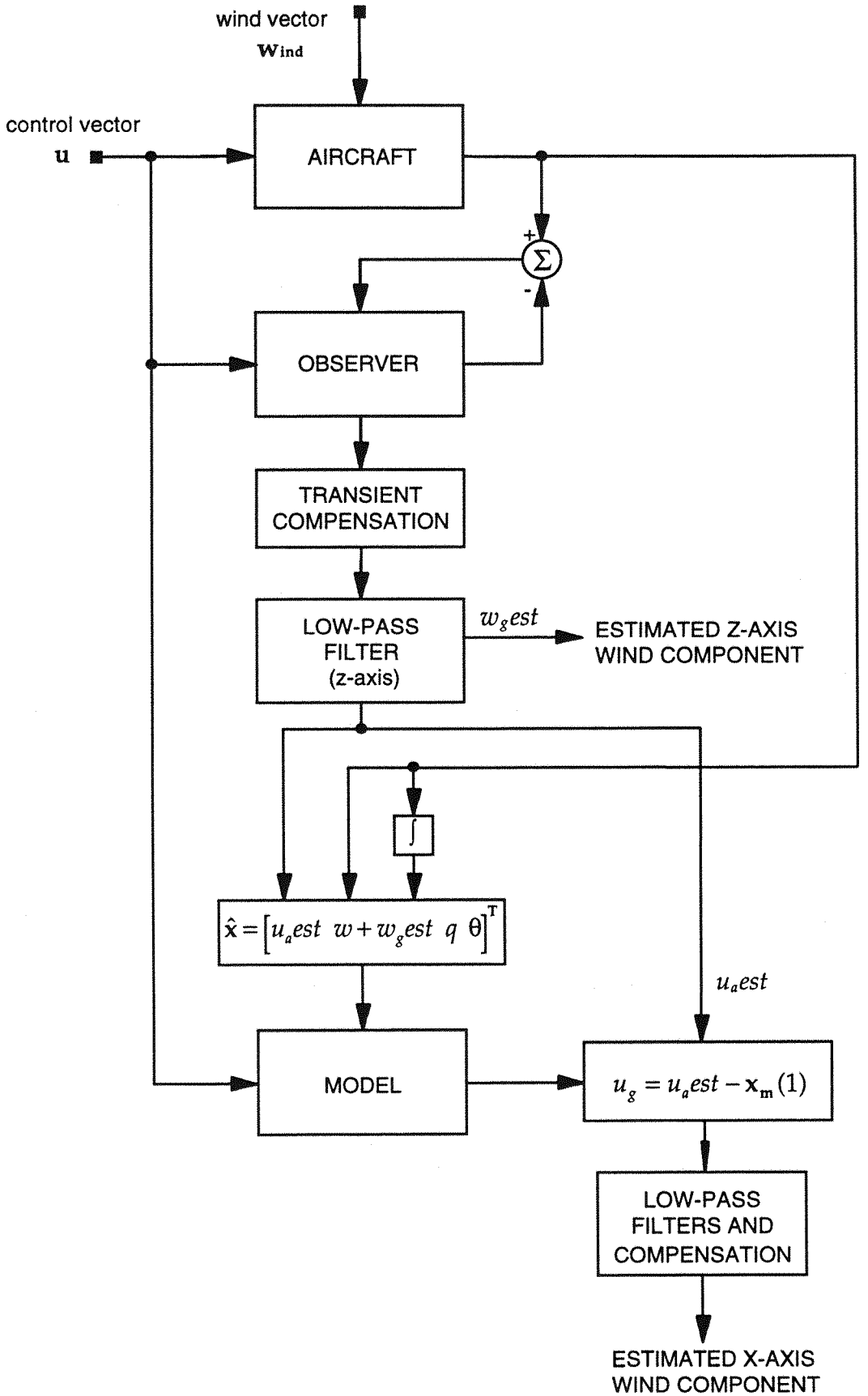

Figure 4.21: Schematic of Revised Wind Estimation Method

4.5.2 Estimation using Pitch Rate and Airspeed

The inclusion of the pitching wind terms in the wind estimation algorithm which uses pitch rate and airspeed produces the results shown in Figure 4.22. The x-axis wind estimate remains a reasonably accurate estimate of the wind component. The pitching wind component produces very significant errors in the estimation of the z-axis wind. The estimate appears to be similar to the inverted wind profile but with additional transient and oscillatory errors.

The equation for the observer's transient compensation, analogous to equation 4.67, becomes:

$$\begin{pmatrix} u_a \\ w_a \end{pmatrix} + \begin{bmatrix} p_1 \\ p_2 \end{bmatrix} q_g = \begin{bmatrix} f_{11} & f_{12} \\ f_{21} & f_{22} \end{bmatrix} \begin{pmatrix} \dot{w} - \dot{w}_e \\ \dot{q} - \dot{q}_e \end{pmatrix} - \begin{bmatrix} 1 & 0 & h_{13} & h_{14} \\ 0 & 1 & h_{23} & h_{24} \end{bmatrix} \begin{pmatrix} -u_e \\ -w_e \\ q - q_e \\ \theta - \theta_e \end{pmatrix} \quad (4.72)$$

The pitching wind component can be replaced by the equivalent z-axis wind, in accordance with equation 4.61. However, the right-hand side of the equation cannot be simplified to produce a relationship in w_g and $\dot{w}_g$, as was achieved in Section 4.5.1, because it the air-relative heave velocity not the z-axis wind which is being estimated. Therefore it is not possible to implement a compensating filter to extract w_g, as was attempted for the algorithm using pitch rate and heave velocity.

Although the estimate shows some resemblance to the wind component being estimated, the errors are large and so it is unlikely the approximate methods for improving the estimate would yield satisfactory results. The method of wind estimation using pitch rate and airspeed is, therefore, suitable for use in estimating only the x-axis wind component, whereas the method of estimation using pitch rate and heave velocity produces promising x-axis and z-axis wind estimates.

4.6 Summary

The technique for measuring the wind components acting on an aircraft could be based upon methods used in the design of observers for time-invariant linear systems.

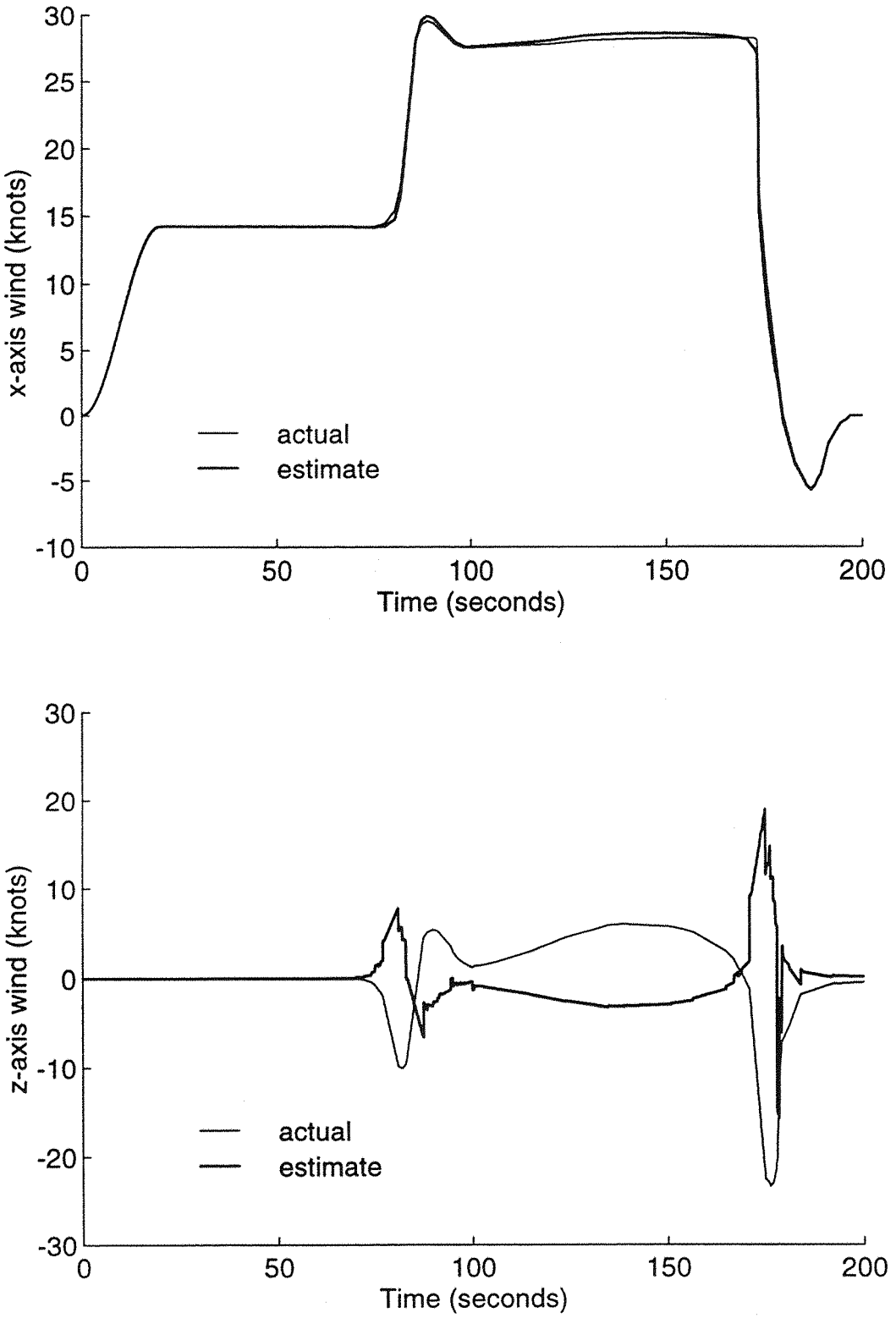

Figure 4.22: Effect of Pitching Wind on Estimation using Pitch Rate and Airspeed

The problem of estimating the x-axis and z-axis wind components, without a pitch component, was considered first. The use of a single state variable, the pitch rate, in the estimation algorithm produced large errors in the estimation. These arose principally as a result of transient errors in the observer and could not be satisfactorily compensated. A system using two state variables, heave velocity and pitch rate, to estimate the wind components produced better results which could be further improved using a transient compensation algorithm to reduce the effects of the transient errors. A similar technique produced good estimates when a system measuring the pitch rate and airspeed was simulated.

Incorporation of a pitching component introduces errors in to the estimates of the wind components. The effect on the estimation method which uses pitch rate and airspeed is to produce a significant error in the z-axis estimate. When the pitch component is incorporated into the algorithm using pitch rate and heave velocity measurements it produces transient errors in both the translational wind components. However, these errors can be compensated by adding further stages to the transient compensation algorithm, although this causes a delay in the estimation process.

It should be emphasised that the purpose of such an algorithm is not to find the wind components accurately, but to allow an assessment of the magnitude of the wind variation over a short period, to decide whether there is a windshear hazard. The result above show that, in principle, such methods are likely to be adequate for these purposes. The practical implications of both of the methods are discussed in the next chapter.

5 PRACTICAL DESIGN OF THE WIND ESTIMATION ALGORITHM

5.1 Effect of a Change in Flight Condition on the Estimation

The wind estimation algorithms described in Chapter 4 were designed for a specific aircraft flight condition viz. takeoff at sea level. However, aircraft dynamics differ with each flight condition and these differences are evident in the changes in the stability derivatives. Therefore, the differences result in variations in the elements of the matrices associated with the state equation of the aircraft, viz.

$$\dot{\mathbf{x}} = \mathbf{A}_i\mathbf{x} + \mathbf{B}_i\mathbf{u} + \mathbf{E}_i\mathbf{w}_{ind} \tag{5.1}$$

where i is an index which indicates the corresponding flight condition.

If flight conditions other than take-off at sea level are considered then the matrices of the observer and the model will no longer be identical to those assumed here for the aircraft and hence the dynamics of the aircraft and the wind estimation system will cease to be matched. Such a mismatch can induce errors in the estimation, a situation which can be demonstrated by changing the aircraft matrices in the system designed in Chapter 4 to model different flight conditions. The stability derivatives and parameters corresponding to a number of flight conditions for the Cessna 402B are given in Appendix B. Data are available for five flight conditions viz. take-off, climb at sea-level, approach at sea-level, climb at 5 000 feet and cruise at 20 000 feet. As windshear is most hazardous at low altitude it is the sea-level flight conditions which are most relevant to this work.

Alternative wind estimation techniques using the pitch rate and either the heave velocity or the airspeed were described in Chapter 4 and both were found to be feasible methods, although further development would be required before the method using airspeed and pitch rate could be used. It is the performance of these methods at low altitudes with differing flight conditions which is now considered.

5.1.1 Change in Aircraft Modes with Flight Condition

The matrices which define the state equation, 5.1, for the various flight conditions are shown in Appendix B, together with their associated eigenvalues and the frequency and damping of the corresponding modes.

It was seen in Section 2.1.2 that the short-period mode governs the high frequency dynamic response of the aircraft and the phugoid mode results in a long-period oscillatory motion. From an examination of the Cessna 402B data in Appendix B it can be observed that the real parts of all the eigenvalues are negative, hence the aircraft possesses dynamic stability. For most of the flight phases the short period mode has two real eigenvalues and does not produce an oscillatory response. The response is composed instead of two exponentially decaying transients and the speed of decay is determined by the magnitude of the eigenvalue. Only in the condition of cruise at 20 000 feet is the short period mode oscillatory (just), with a period of 1.4 seconds and a very heavy damping factor of 0.94, which results in a very rapidly damped oscillation. The speed of decay of the response means that the short-period mode is unlikely to contribute significantly to the errors in the wind estimation algorithm, even if the mode is poorly modelled. In contrast, because the phugoid mode has both low frequency and damping, any errors in the modelling which affect this mode can contribute to errors in the estimation to a far greater extent and over a longer duration. A summary of the phugoid data is tabulated in Table 5.1.

Table 5.1 Cessna 402B - Phugoid Modes

Flight Phase	Period (seconds)	Damping
sea-level take-off	41.9	0.023
sea-level climb	41.6	0.044
climb at 5 000 feet	43.3	0.040
cruise at 20 000 feet	59.8	0.082
sea-level approach	42.5	0.148

All the sea-level flight conditions have a very similar phugoid period of approximately 42 seconds. The climb at 5000 feet condition is comparable at approximately 43 seconds and so the cruise condition is once again the exception, with a period of nearly 60 seconds. However, it is not necessary to take this mode into account when modelling the aircraft dynamics for a

windshear detection system because although the phenomenon of windshear, and particularly the microburst, occurs at heights greater than 1000 feet it is only regarded as hazardous to aircraft below that height. The phugoid mode is lightly damped for all conditions but there is some variation; the difference in damping between the sea-level conditions of take-off and approach being particularly relevant. The effect on the estimation algorithm of changing the flight condition of the aircraft is likely to be related to these modal variations.

5.1.2 Wind Estimation using Pitch Rate and Heave Velocity

Figure 5.1 shows the results of a simulation of the wind estimation algorithm using pitch rate and heave velocity measurements, with flight conditions different from the design condition of sea-level take-off viz. climb at sea-level, approach at sea level and climb at 5000 feet. Although it is beyond the bounds of the microburst hazard, the latter condition is included because it represents a flight condition above sea-level and so prevents the analysis from being too restricted. The plots will be discussed when a further modelling requirement resulting from the changing flight conditions has been incorporated, which is now examined.

The simulations use the derivative of the heave velocity from the aircraft model as an input to the estimator although it is not available as a direct measurement. In practice this input is likely to be derived from the z axis component of acceleration as described in Section 3.5, i.e.:

$$\dot{w} = a_{zcg} + U_0 q \tag{5.2}$$

The aircraft trim inertial speed, U_0, varies with the flight condition, but the value which is used to calculate the derivative of the inertial heave velocity for use in the estimation remains unchanged, and so further inaccuracies arise. Figure 5.2 show the results of repeating the simulations after changing the calculation of the derivative of the inertial heave velocity to include the inaccuracies resulting from the use of the nominal trim airspeed.

A comparison of the results from the simulation of climb at sea level show that there is a very small error caused by the changes in the elements of the aircraft matrices, as may be seen from Figure 5.1. When the approximation

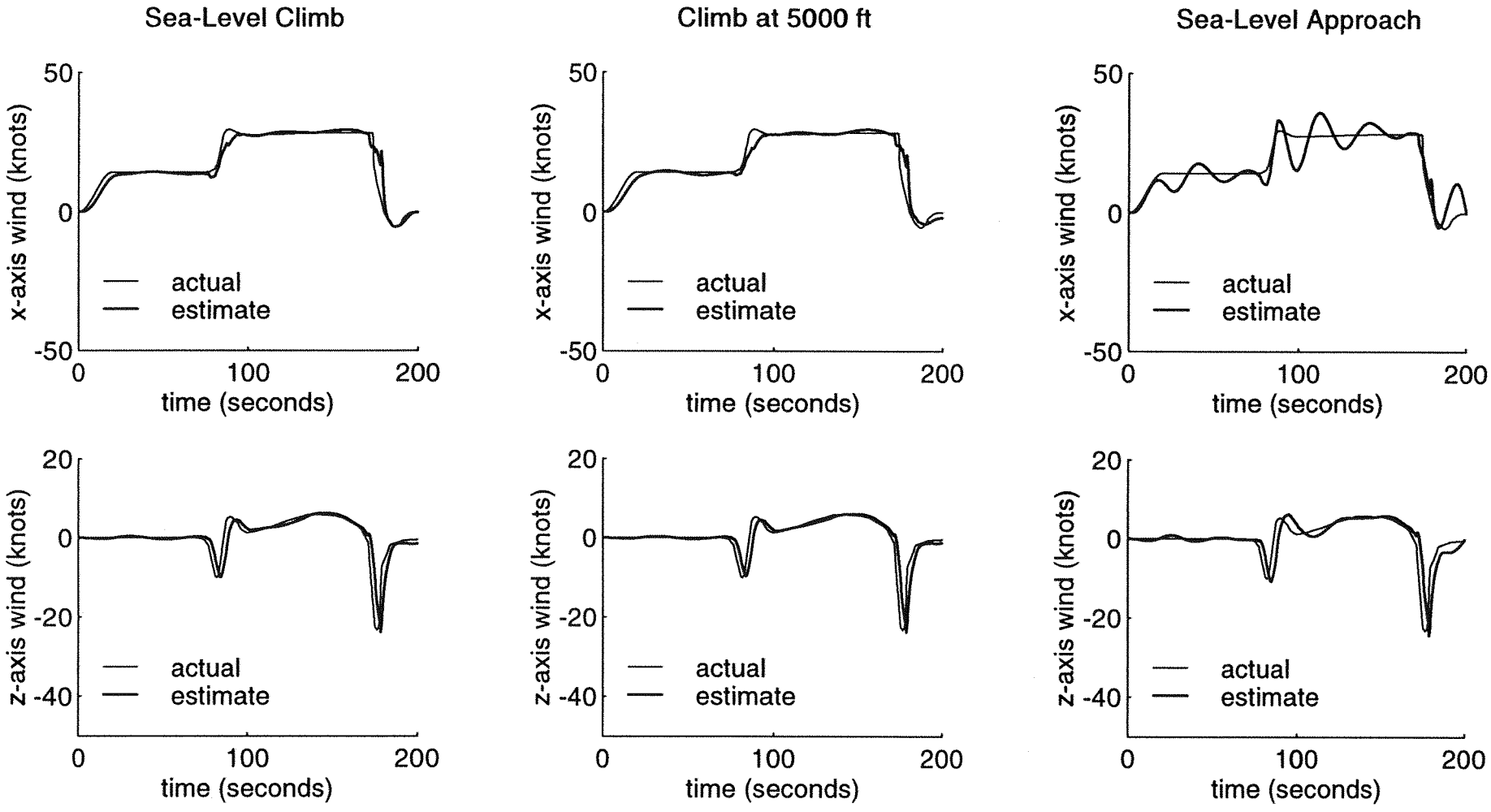

Figure 5.1: Effect of Change of Flight Condition on Estimation using Pitch Rate and Heave Velocity

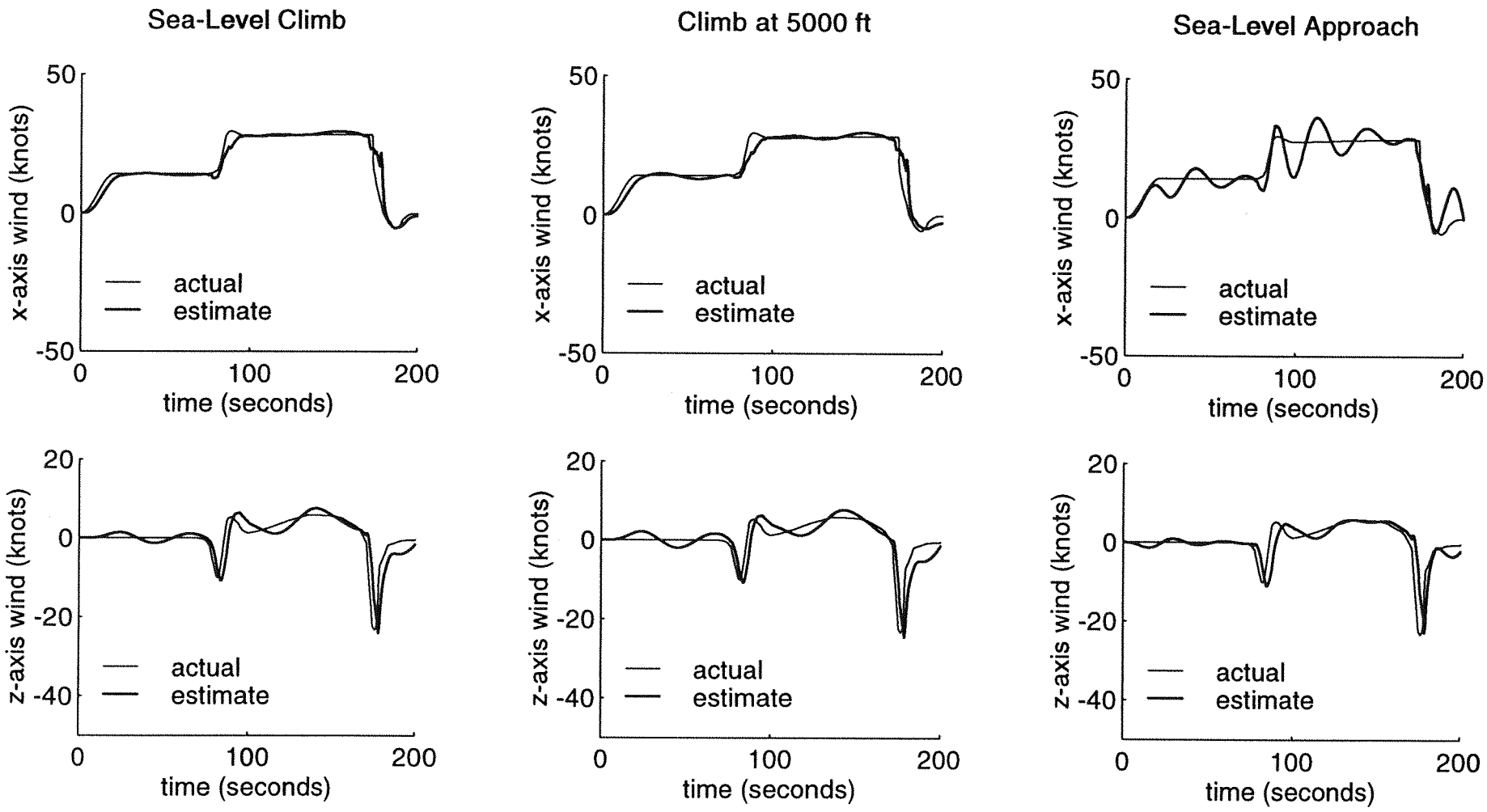

Figure 5.2: Estimation at Different Flight Conditions with Derived Heave Velocity

error in the derivation of the heave velocity is included the total error in the z-axis wind estimate is increased and exhibits a modal characteristic of approximately the same period as the phugoid mode of the aircraft, see Figure 5.2.

The flight condition which represents climb at 5000 feet indicates that the change in the elements of the matrices produces a result similar to that for sea-level climb, although the errors are greater. An oscillatory error can just be distinguished in the x-axis estimate in Figure 5.1.

In the simulations for a sea-level approach, the errors are significantly larger for the x-axis wind component. The oscillatory errors are much greater in this case because the sea-level approach flight condition has a relatively heavily-damped phugoid mode compared to the mode corresponding to the sea-level take-off condition which was modelled in the observer. The errors induced by the derivation of the heave velocity appear to be relatively insignificant when compared to those which arise from the change in the elements of the aircraft matrices. It should be noticed, however, that despite the large oscillatory errors, the mean estimate still follows the wind profile.

5.1.3 Wind Estimation using Pitch Rate and Airspeed

Figure 5.3 shows the result of changing the flight condition when the estimation algorithm is based on the use of pitch rate and airspeed. This includes the effect of the pitching wind which produced estimation errors when the aircraft and observer matrices were matched, as shown in Figure 4.22. In general, the estimate of the x-axis component is satisfactory and exhibits only small oscillatory errors. The estimate of the z-axis component is poor, as would be expected since the method failed to produce a satisfactory estimate when the estimation and aircraft matrices were matched.

The errors in the z-axis estimate are caused in part by the effects of the pitching wind, but some significant errors are generated by the mis-matching of the aircraft and estimator matrices. Figure 5.4 shows the effect of the change in flight condition on the estimation using pitch rate and airspeed when the pitching wind is forced to be zero throughout the simulation. The estimate of the z-axis component shows large oscillatory errors which are

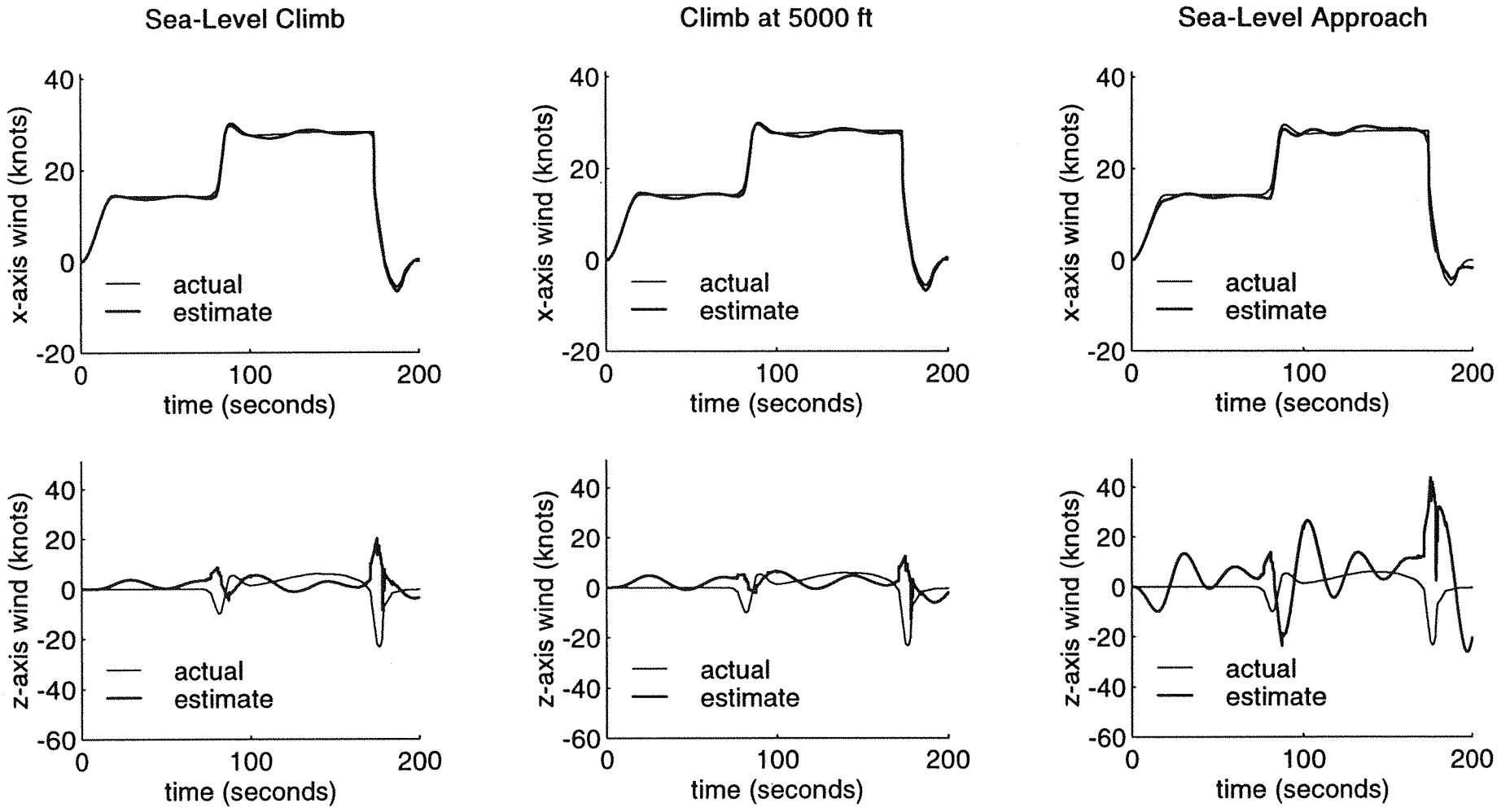

Figure 5.3: Effect of Change of Flight Condition on Estimation using Pitch Rate and Airspeed

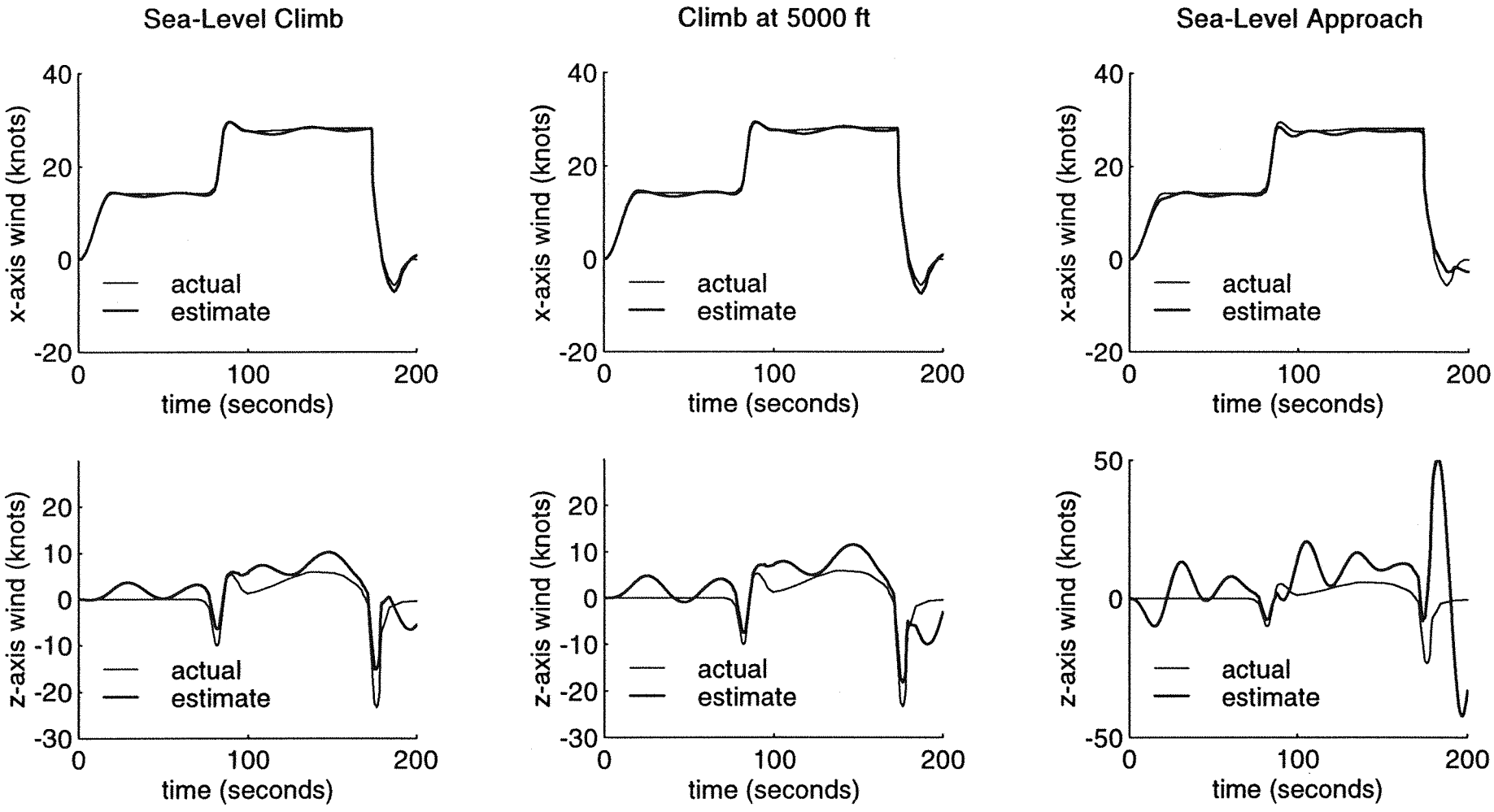

Figure 5.4: Estimation using Pitch Rate and Airspeed with no Pitching Wind Input

once again related to the phugoid response of the aircraft. In addition, the z-axis component exhibits an offset error, particularly in the central region of the plots i.e. between 80 and 180 seconds. The sea-level approach condition produces the largest errors in both the x-axis and z-axis components. It is the variation in the damping factor produced by the change in flight condition which appears to govern the magnitude of the errors in the estimation.

5.1.4 Variation of Stability Derivatives as a Function of Airspeed

The derivation of the elements of the coefficient and driving matrix elements was summarised in Appendix A where they were found to depend principally upon the stability derivatives of the aircraft. Equations A9 to A12 show the general form of the linearised longitudinal aircraft dynamics and equation A27 shows the matrix elements, for an aircraft flying straight and level, derived from the linearised model. The stability derivatives are determined from the aerodynamic forces and moments acting on the aircraft and these vary according to the aircraft's configuration and flight phase. The aircraft response is dependent upon various parameters and a significant one is the velocity of the aircraft relative to the air i.e. the airspeed. Almost every element varies with airspeed to a greater or lesser extent: element A(2,3), for example, is directly related to the airspeed and other elements are functions of the aerodynamic forces and moments (which are themselves proportional to the square of the airspeed, as shown in equation A7). As the estimation method of Section 5.1.3 already uses a measurement of the airspeed, this parameter can be used to vary the stability derivatives according to the flight condition.

The variation of the elements of the state matrix with airspeed for the Cessna 402B is shown in Figure 5.5. (For clarity, the units of each element of the A matrix are not shown, but these can be derived from Appendix B and they are provided in the relevant texts. [16]) It can be seen from these plots that some of the elements could be represented relatively accurately as a function of airspeed whereas there appears to be little correlation for others. From an examination of the aerodynamic force equation (equation A7) it would be expected that the elements would vary with the square of the airspeed, with air density and with other factors, such as configuration and attitude of the aircraft. However, the plots indicate that, for some stability derivatives, it may be a reasonable approximation to consider that any variation is entirely

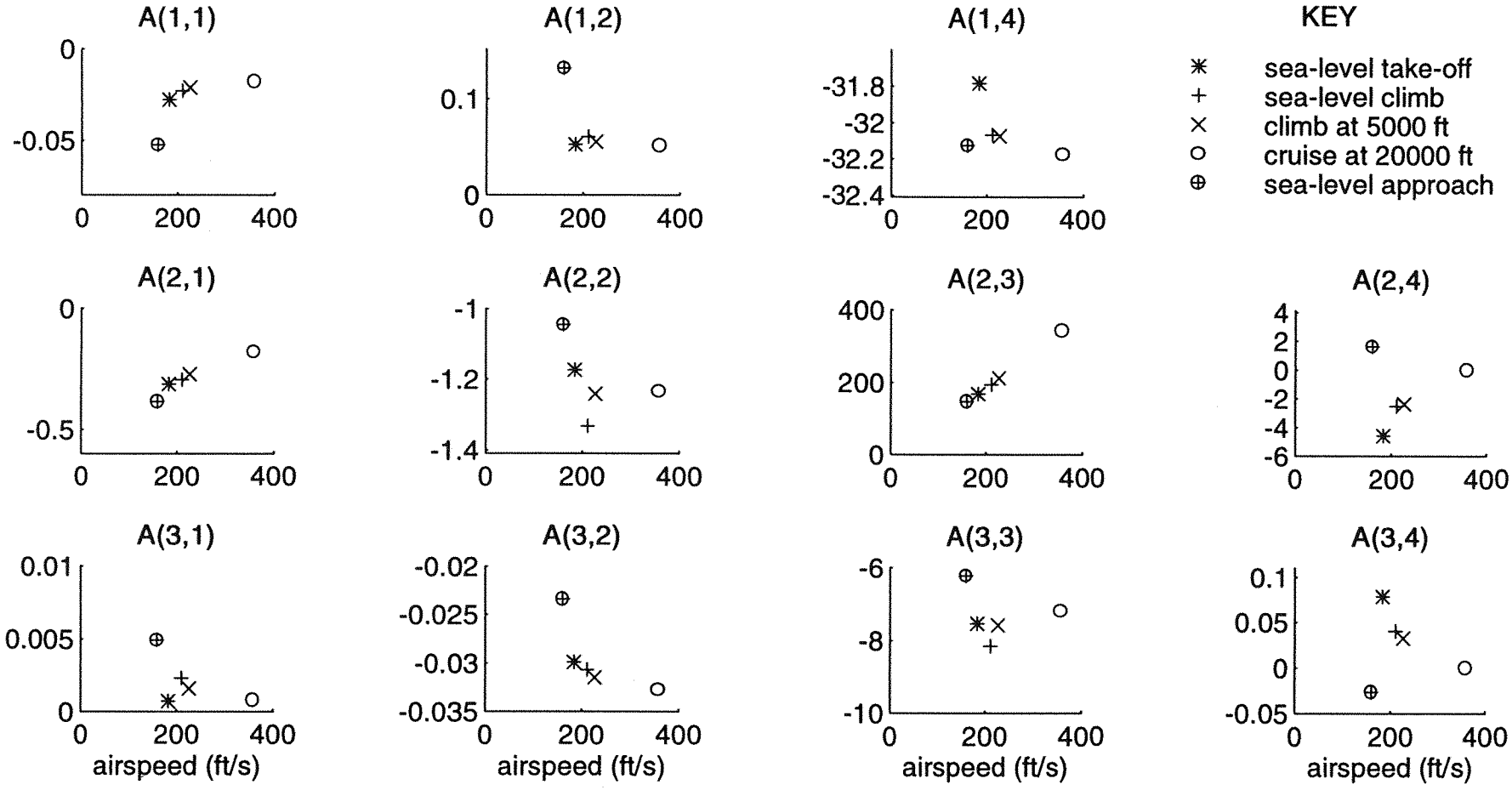

Figure 5.5: Variation in the Elements of Matrix A with Airspeed

caused by changes in airspeed, as the air density and other factors produce relatively little effect, especially for the low altitude conditions. Therefore, as a practical approach, the airspeed could be used to 'schedule' these matrix elements to improve the accuracy of the aircraft parameters used in the estimation process and thereby reduce the errors. For other stability derivatives the effect of changes in the aircraft configuration is significant. This can be seen by comparing the values of the stability derivatives for sea-level take-off and approach, for which the trim airspeed is comparable.

Those elements of the A matrix which appear to be related to the airspeed were varied according to the airspeed; the remaining elements were set at constant values which were approximately the median values of these elements for the three sea-level flight conditions. The varied elements were A(1,1), A(2,1), A(2,3) and A(3,2). These elements were varied with airspeed, according to a least-square error fit of the elements against airspeed, for the four lower-speed flight conditions, viz. sea-level take-off, sea-level climb, climb at 5000 feet and sea-level approach. A linear fit proved to be adequate for these flight conditions. The remaining flight condition of cruise at 20000 feet could have been included in these approximations. In this case the relationship, as seen in the plots of Figure 5.5, would have been best represented by using a second order fit in airspeed which corresponds to the factor of the square of the airspeed in the aerodynamic force equation.

In Figure 5.6 are shown the results of simulations of this method of wind component estimation when the pitching wind is set, once again, to zero. The figure can be compared with Figure 5.4. The results for the flight condition of take-off at sea-level are now included because there are now errors between the estimation matrices and the aircraft matrices for this condition. The estimates of the x-axis wind show some improvement, especially for the flight condition of approach at sea-level. Although there is a slight improvement in the offset errors in the z-axis wind estimates, when compared to those made using airspeed and pitch rate without the scheduling of the principal airspeed-dependent matrix elements, Figure 5.4, large oscillatory errors remain. The pitching wind would cause further significant errors. It is likely, nevertheless, that this method could be used to detect the x-axis wind component in order to distinguish adequately between a gust for which no alert is needed and a dangerous microburst.

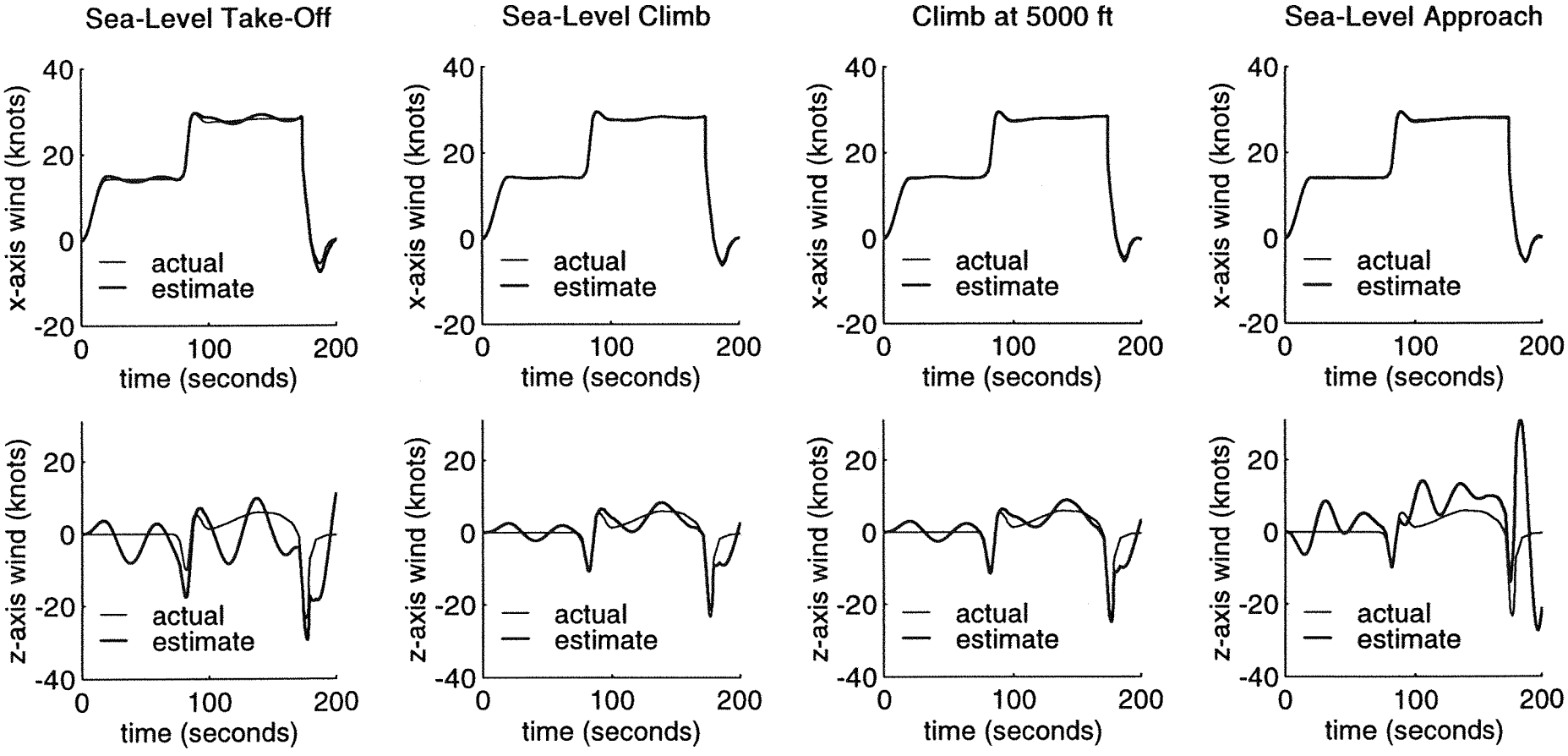

Figure 5.6: Estimation using Airspeed-Scheduled Parameters with no Pitching Wind Input

5.1.5 Wind Component Estimation using Airspeed, Heave Velocity and Pitch Rate.

It is apparent from the results obtained that the estimation technique using the heave velocity and pitch rate has produced a good estimate for the vertical wind component but provided poorer results for the horizontal wind estimate when the flight conditions were varied. In contrast, the method using airspeed and pitch rate produced a relatively accurate estimation of the horizontal component but, had very significant errors in the estimate of the vertical component. Therefore, either component could be estimated to good accuracy by measuring two variables. The forward-looking airborne windshear detection systems, described in Chapter 3, only measure, in general, the x-axis wind component and establish the hazard based upon this measurement. Using this approach, a windshear detection system could be developed using two measured flight variables.

Alternatively, the use of airspeed, heave velocity and pitch rate in the estimation algorithm can produce an estimation method which determines both wind components with relative accuracy and is robust to changes in flight condition. There are several possible configurations for a system using the three measured variables. The simplest form can be achieved by combining the two estimation methods and eliminating redundancies by selecting the method which gives the best performance.

The combined system comprises the observer as used in the airspeed and pitch rate method of estimation, where both these parameters are passed into the observer. The transient compensation algorithm is taken from the heave velocity and pitch rate method because this configuration does not require the feedback of any parameters from the aircraft model, and it can provide an estimate the z-axis wind component directly. The aircraft model requires the airspeed, pitch rate and air-relative z-axis component as inputs. The first two parameters are measured, and the air-relative z-axis component is found by adding the estimated z-axis wind and the measured heave velocity.

Scheduling of the observer and model matrix elements with airspeed is also possible, hence, the effects of changes in flight conditions can be reduced, as described in Section 5.1.4. The results obtained from this system, with the pitching wind included, are shown in Figure 5.7. It is apparent that this

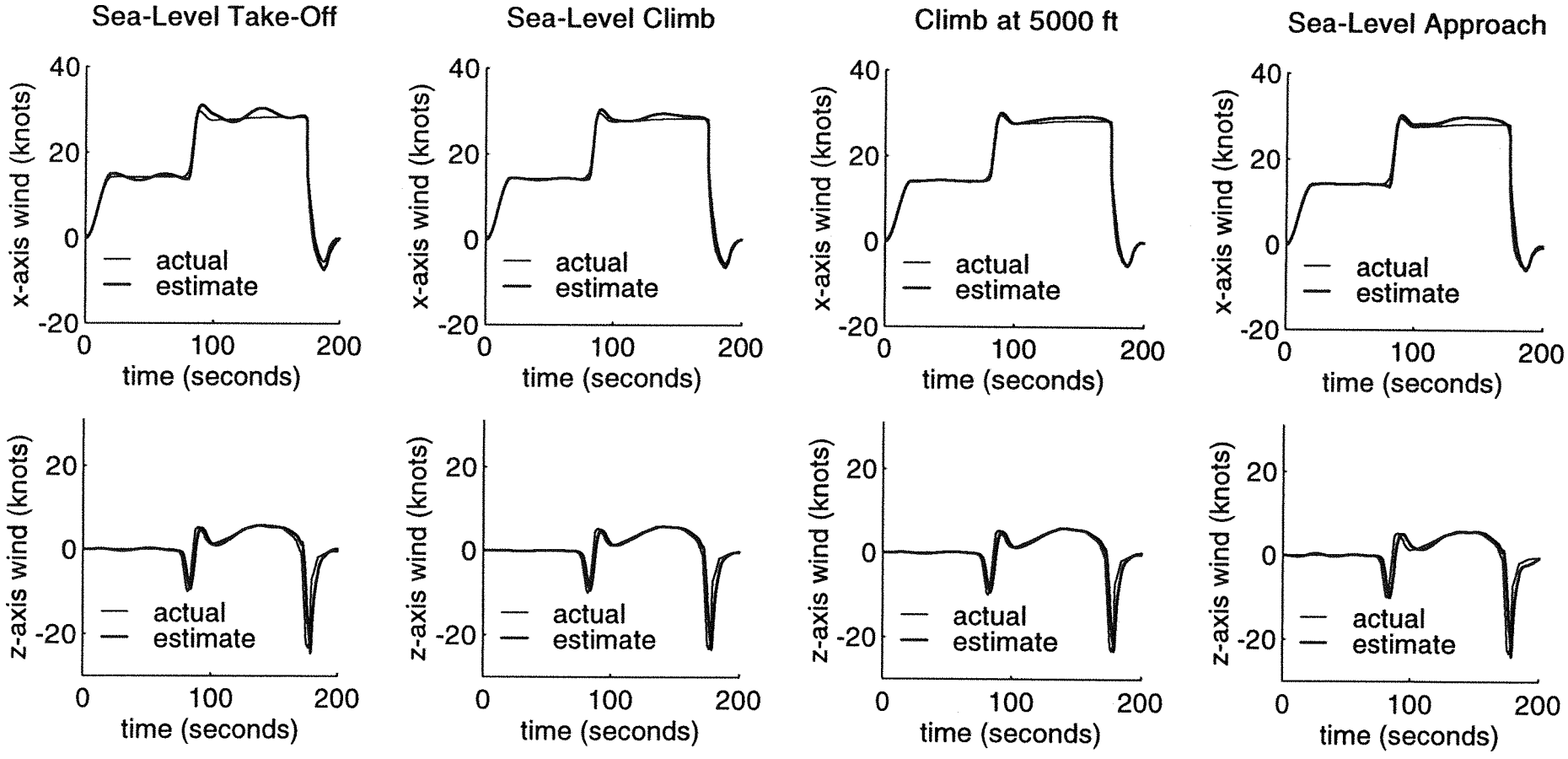

Figure 5.7: Estimation using Pitch Rate, Heave Velocity and Airspeed

approach is very much more robust to the changes in flight condition, for there are no discernible offset errors and oscillatory errors introduced by the mis-matching of the phugoid mode are greatly reduced. The system has sufficient accuracy to enable the development of an algorithm which can distinguish windshear from smaller gust inputs without excessive nuisance alerts being generated.

5.2 Measurement of Required Parameters

The algorithm to estimate both wind components requires a knowledge of the aircraft's pitch rate, heave velocity, airspeed and any control inputs. The practical implications of sensing these will now be considered.

The instruments and sensors commonly used in the measurement of aircraft motion have already been discussed in Sections 3.4 and 3.5. Sensors which can be used to measure the airspeed, heave velocity and pitch rate are now considered. The process of sensing must have inherent errors which will arise from such sources as non-ideal performance of the sensors, mounting or location inaccuracies, and sensor and measurement noise.

It is the small perturbation values of the parameters which the algorithm requires. These can be obtained from the total value of the parameter by means of a washout filter. A well-designed washout filter removes any steady and slowly-varying components of the sensor signal, with minimal transient offset errors in the perturbation value it produces. Figure 5.8 shows the characteristics of the small perturbation flight parameters during an encounter with the JFK wind component during a take-off at sea-level.

5.2.1 Airspeed Measurement

Airspeed is measured as a pitot-static pressure difference and converted to knots using equation 3.3. The small perturbation value of airspeed is required by the estimation algorithm and the trim value is needed for scheduling the aircraft matrices and to compute the heave velocity from the accelerometer measurement. These two values can be found from the total value by means of a washout filter.

The pitot-static pressure difference can be measured either by a single differential pressure sensor, or as the difference between two absolute

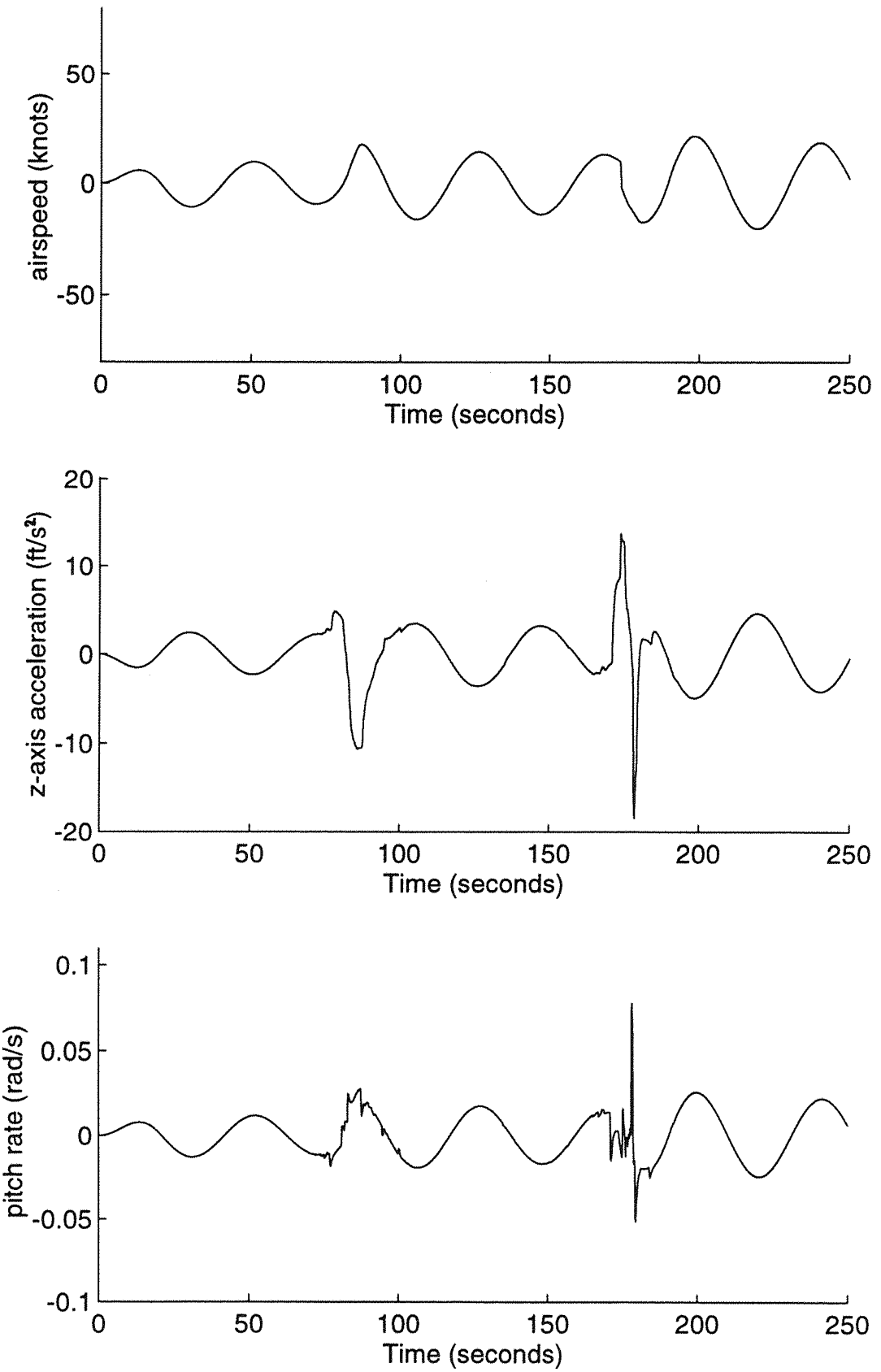

Figure 5.8: Small Perturbation Flight Parameters during JFK Windshear Encounter

pressure sensors. Pressure sensors using solid-state piezo-resistive or capacitive technology have high performance and resolution and are relatively low-cost devices. Therefore, the use of a second sensor may yield advantages. A static pressure measurement would enable the altitude of the aircraft to be calculated which, in determining when the aircraft is below 1000 feet, could have significant advantages for the system operation. The altitude is not available as a signal to the system because, unlike transport aircraft, general aviation aircraft are not fitted with air data units.

Important considerations for choosing pressure sensors include the offset and scale errors of the device, temperature effects, and the presence of noise in the output. However, with the increasing use of microprocessors in sensing systems, the ability to compensate for many of these errors has become much greater. The principal concerns in the choice of sensor are now related to stability, repeatability and hysteresis. A sensor can be characterised by calibration and any errors removed by applying compensation algorithms to the output, provided that the characteristics do not change appreciably with time.

After compensation any remaining errors in the pressure are the result of residual errors in the compensation and these are considerably smaller than the original errors. It is the effect of these errors which is now considered briefly. For simplicity of analysis, any residual hysteresis and non-linearities in the sensors are regarded as scale effects. Steady offset errors in the perturbed parameter values are gradually removed by the washout filters and so only occur while the filter is settling. The analysis examines the effects of scale errors on the small perturbation values; the sea-level take off condition is used for both aircraft and estimation process, and the matrices are matched.

A scaling error in the perturbed airspeed measurement produces a small oscillatory error in the x-axis wind estimation - see Figure 5.9. The effects on the z-axis wind estimate are negligible. A scale error of five percent is assumed for this figure chiefly to ensure that the error is clearly visible; calibration techniques which can be applied to low cost sensors are able to reduce scale errors to values significantly below this figure.

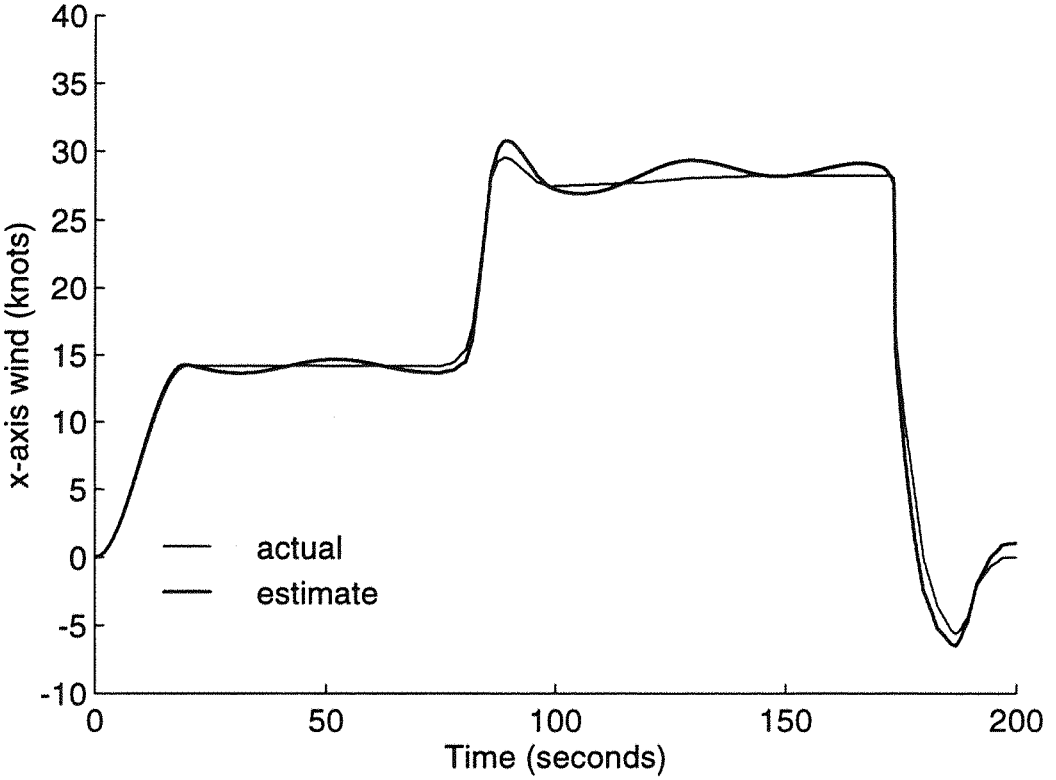

Figure 5.9: 5% Scale Error in Perturbed Airspeed Value - JFK Windshear

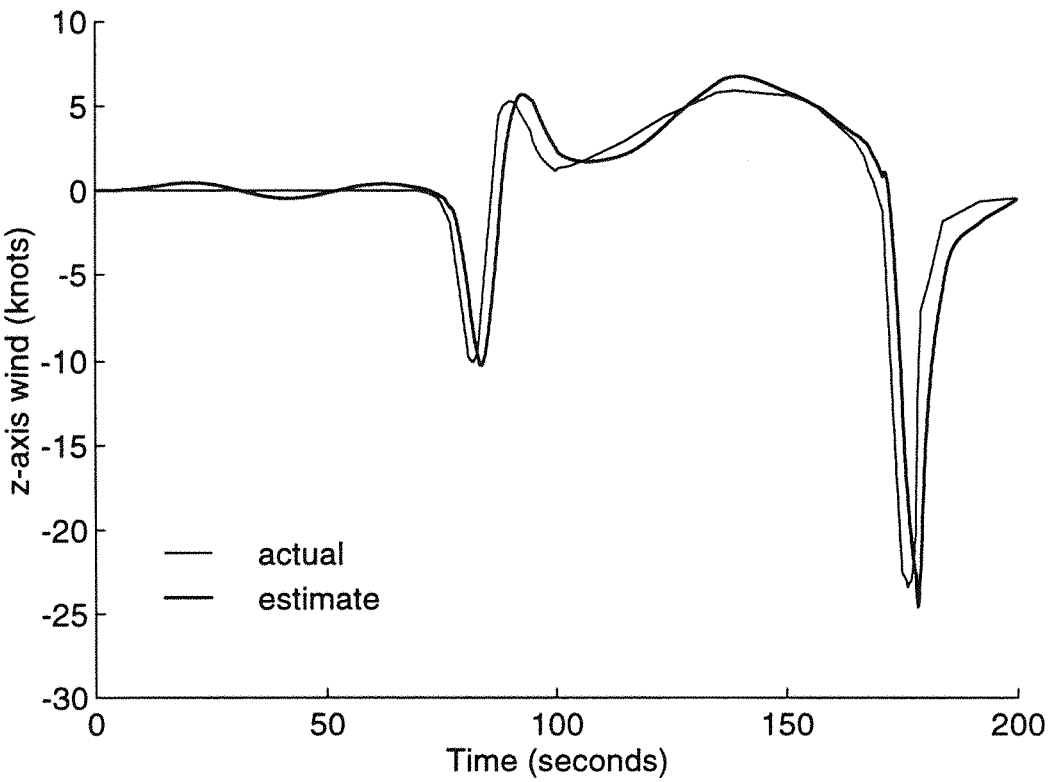

Figure 5.10: 5% Scale Error in Perturbed Acceleration - JFK Windshear

Residual offset errors in the sensor calibration are removed by the high-pass effect of the washout filter. However, during start-up of the system, the response of the filter to a sudden change in the total airspeed value would result in large transients in the perturbed airspeed value. These errors can be reduced because the wind estimation algorithm is not valid until the aircraft is airborne and, therefore, the system does not begin to compute the wind components until rotation is completed. The washout filter can be initialised to the airspeed value at the time of rotation, thus avoiding a sudden 'step' input to the airspeed washout filter.

Finally, the trim airspeed must be derived in some fashion. It can be calculated as the difference between the total airspeed and the perturbed value from the washout filter. The wind estimation is relatively insensitive to small inaccuracies in trim airspeed (which was observed in Section 5.1.3 and Figures 5.2 and 5.3 where the errors resulting from changes in flight condition and associated trim airspeeds were found to be acceptable).

5.2.2 Heave Velocity Measurement

An accelerometer is used to measure the heave velocity. Low-cost, high-performance accelerometers, using similar technology to the pressure sensors, are now available. The implications for the mounting of the accelerometer were discussed in Chapter 3 where it was shown that is desirable to place the accelerometer on or as close as possible to the centre of gravity.

The output from the accelerometer can also be calibrated and compensated to minimise any errors. If the accelerometer has not been mounted at the centre of gravity, but is significantly offset along the x-axis, any error induced could be computed from the pitch rate signal and from knowledge of the approximate distance from the centre of gravity of the aircraft. This error could be applied as a correction at this stage. Any misalignment of the accelerometer with the aircraft z-axis could produce cross-axis errors in the measurement which would appear as transient offsets, however, these are likely to be small.

The perturbed value for the heave velocity is washed out from the total value; the effect of residual scaling errors is shown in Figure 5.10. Again, a 5%

error in the scale factor has been used to illustrate the effect more clearly; any error in a calibrated sensor would be significantly smaller.

5.2.3 Pitch Rate Measurement

A rate sensor is likely to be the most cost-effective choice for the pitch rate measurement, although a displacement gyro could be used. The sensor does not have to be mounted on the centre of gravity, but the sensitive axis should be carefully aligned with the y axis of the aircraft to avoid cross-axis effects.

The measured pitch rate is passed into the observer, and it is also integrated as part of the heave velocity calculation and to generate the pitch attitude to feed into the 'model' stage of the algorithm; it affects therefore both the x-axis and z-axis wind estimates. Although the trim value of the pitch rate is zero, it may still be useful to washout the perturbed value from the sensor signal to remove any offset errors. This approach also assists in reducing the effects of any drift: any remaining pitch rate signals exhibit themselves as small scaling errors. The effect of these errors is shown in Figure 5.11.

Sensor drift is a potential source of error, which manifests itself as a change in the sensor offset with time. Low-cost pressure sensors and accelerometers can now be obtained which have very good long-term stability. (Drift is described in units of parts-per-million (ppm) of the full-scale output per year; a drift figure of below 200 ppm per year can be obtained.) Such low drift rates do not cause problems during the period for which the system is operating and the effect can be eliminated during initialisation. However, the rate sensors, which are relatively more expensive even for the low performance models, have some inherent drift which can become significant in minutes, rather than years.

A significant value of drift in pitch rate would be integrated to produce increasingly large errors in the heave velocity and any pitch attitude variables which are derived from it, unless some form of compensation is applied. A high pass (washout) filter does prevent the build-up of the drift in the pitch rate input, but the drift rate must be slower than any pitch perturbations which are of relevance to the algorithm. Parameters derived from the integrated pitch rate could also require high pass filtering to remove the integrated effects of any transients which feed through from the pitch rate

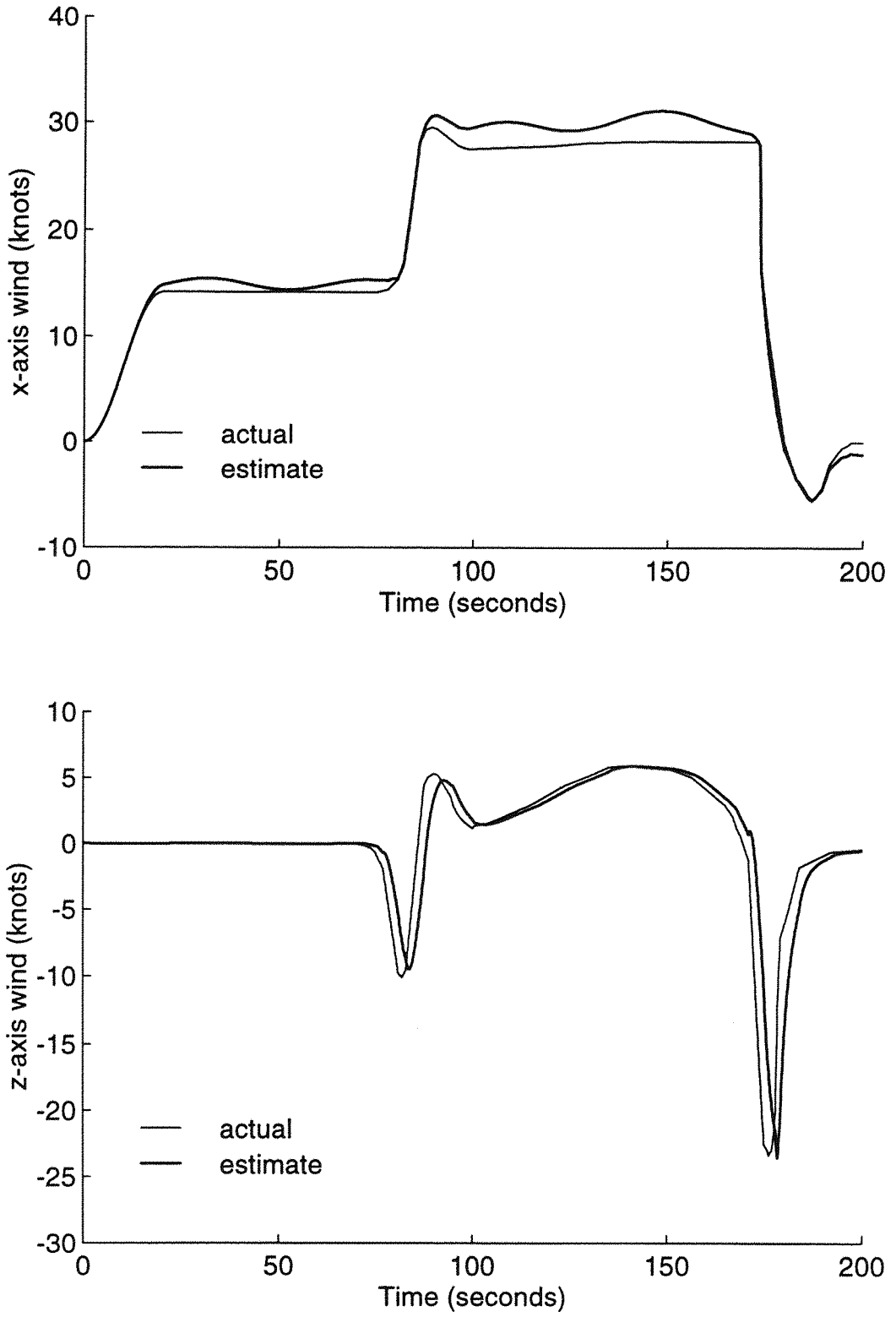

Figure 5.11: Effect of 5% Error in Pitch Rate Measurements- JFK Windshear

drift compensation. The compensation could be initialised during the start-up period before take-off when the aircraft is nominally stationary. The exact form of such a system would depend on the drift characteristics of the rate sensor.

The effect of the drift of the rate sensor could also be counteracted by attempting to improve the performance during periods of steady flight i.e. when the acceleration and airspeed are relatively stable and the pitch rate is expected to be nominally zero. The pitch attitude of the aircraft will not be changing and so inherent drift in the computed pitch attitude could be calculated and compensated in a manner similar to the drift compensation techniques used for gyro-based inertial navigation systems. These concepts, and other possible techniques such as Kalman filtering, or adaptive methods, are subjects for further study once the errors induced by actual sensors have been established.

If a pitch attitude sensor were used instead of a pitch rate sensor any inherent drift would cause less problems, for its output need not be integrated to derive the attitude. In contrast, the differentiation of the signal to obtain the pitch rate could induce noise and the effects of this noise on the estimation algorithm would have to be established.

Noise is a further time-variation which will be evident in the all the sensor outputs, but it is likely to be more significant in the pitch rate measurement since these sensors are inherently noisier. It differs from drift in being a relatively high frequency phenomenon. In a microprocessor-based system some of the noise can be eliminated when the analogue signals are digitised, as anti-aliasing filters are required to reduce the bandwidth of the signals to frequencies which are compatible with the sampling rate of the system. Further digital filtering could also be used to reduce any noise which passes through the anti-alias filters but which is above the frequencies of interest for the estimation algorithm. Sensors should be selected so that the remaining noise produces a negligible effect on the algorithm.

5.2.4 Control Setting Measurements and Sensing Errors

The sensors which were discussed in Sections 5.2.1 to 5.2.3 are used to measure parameters related to the flight dynamics of the aircraft. The wind

estimation algorithm also requires a knowledge of the commanded changes to the longitudinal aircraft motion: this knowledge is achieved by estimating, or measuring, the longitudinal control surface settings. The parameters related to the longitudinal control surface settings may be available as signals from the aircraft but, for smaller aircraft in particular, this is unlikely. Therefore, thrust and elevator deflection applied by the pilot, and possibly other control settings, must be derived by other means.

In conventional aircraft longitudinal control is achieved primarily by the use of an elevator which varies the pitch attitude of the aircraft and by changes in the throttle setting which causes changes in thrust level. It is the small perturbation values of the controls which are needed by the algorithm and these can be extracted by using a washout filter.

The elevator deflection is controlled by the fore/aft motion of the control yoke in the cockpit and, therefore, a measure of elevator deflection can be obtained by attaching an angular displacement transducer to the elevator torque tube. Any error in the measurement of elevator deflection affects the estimations of both the x-axis and z-axis wind components.

For a system in which the parameters describing aircraft and estimator are matched, any change in the control inputs will be cancelled and will not, therefore, affect the estimated wind components, as can be seen in equation 4.18. However, sensor or modelling inaccuracies will cause changes in the control settings to generate errors in the estimation process. The control inputs are independent of the aircraft response in windshear; hence, any errors can not be simulated in the same way as the flight parameter errors. To assess the effects of scale errors on the system a typical control input is required. Control settings are likely to be steady for much of the take-off approach and landing phases of flight, and any change is likely to be in the form of a small step input. The effect of an exaggerated scale error in the yoke position calibration is shown in Figure 5.12. A step change in elevator deflection of 3 degrees was implemented at the beginning of the simulation to generate this result. In practice, the steady error would be gradually removed by the effects of the washout filter which has not been implemented here.

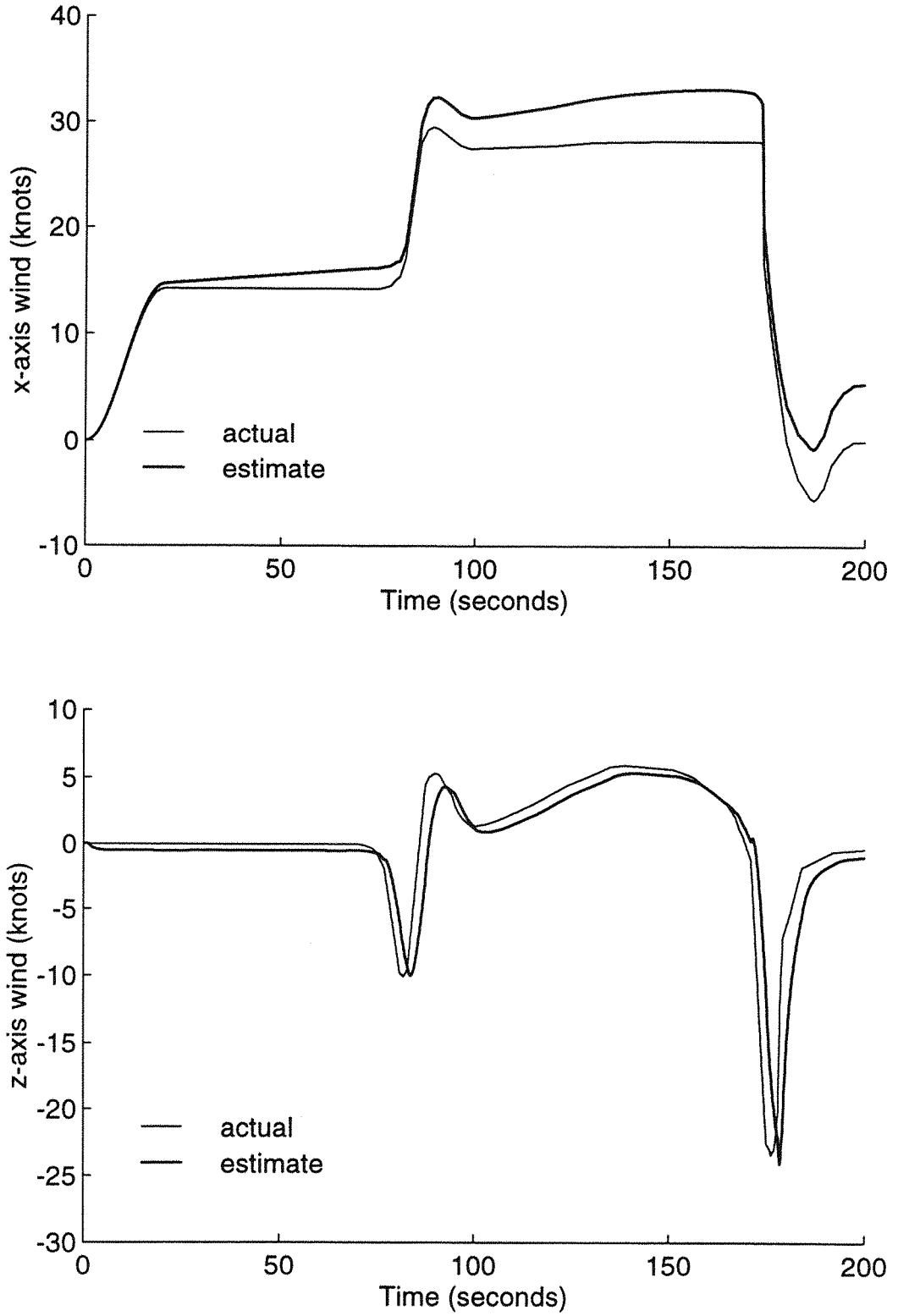

Figure 5.12: 5% Error in elevator sensor Scale Factor - 3 degree elevator change

Changes in thrust are also required by the algorithm. There is a 'trim' thrust value for each flight condition and it is deviations from these values which affect the linearised equations of motion. For low altitude flight these deviations are likely to be small as a pilot rarely adjusts the throttle during these phases - on take-off, the aircraft is at maximum thrust, and on approach the thrust is maintained at a steady, low value until just before touch-down.

Thrust cannot be measured directly without a specialised system. For a piston-engined aircraft, thrust depends on the mixture and propeller control settings, as well as the throttle setting. The mixture is varied with altitude; at low altitudes it is set to be relatively rich because of the higher air density. The propeller pitch can be varied to maintain the maximum engine efficiency and, in cruising flight, a propeller efficiency of up to 85% can sometimes be obtained with a well-designed propeller; however, at lower speeds, the efficiency is less. [71] In practice, the propeller and mixture settings are secondary effects and the small perturbations from the trim thrust setting is affected principally by the throttle position. Therefore, if a position transducer can be fitted to the throttle lever the setting can be calibrated to provide a signal which closely approximates the applied thrust.

Figure 5.13 shows the effect of an exaggerated scale error in throttle position measurement when a step change of 5% thrust is applied at the beginning of the simulation. A small drift in the estimate of the x-axis wind component is noticeable; this would be removed slowly by a washout filter.

The additional controls which affect the aircraft's longitudinal motion e.g. the flap settings, can be significant. The steady-state flap positions are included in the aircraft and control matrices which describe each phase of flight. However, a deployment of the flaps, or a change in their position, during low-altitude phases of flight will produce sudden changes in the aerodynamic forces which will affect the small perturbation values of the sensed parameters. Some of the early designs of windshear detection system only generated windshear alerts on take-off until the flap were retracted, and the systems were reactivated when the flaps were extended for landing. [58] An example of the problems associated with the operation of flaps during periods when windshear detection is operational is the recent accident involving a DC-9 at Charlotte, North Carolina. [72, 73] The accident has

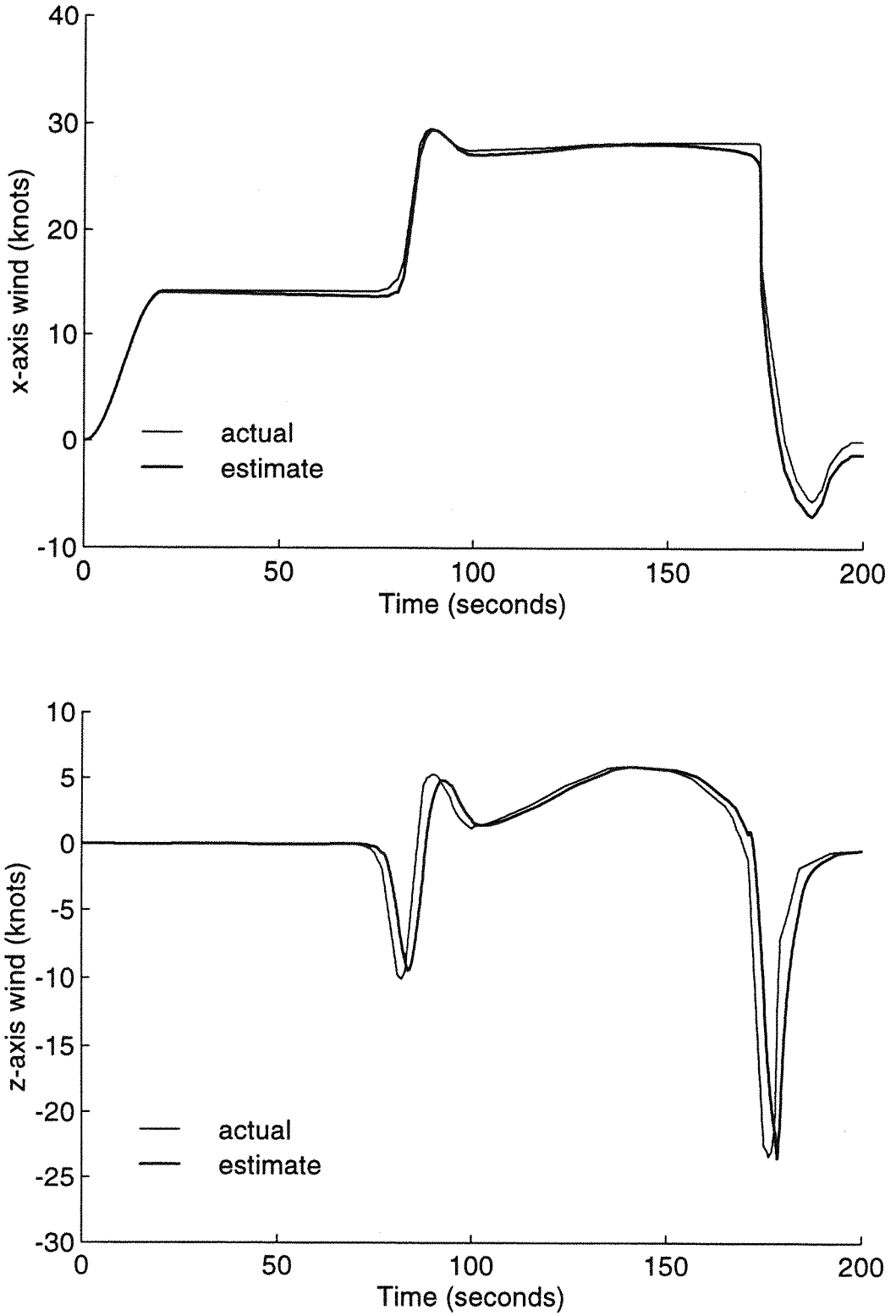

Figure 5.13: 5% Error in Throttle Sensor Scale Factor - 5% Thrust Change

been attributed to a microburst encounter on approach to the airport. The aircraft was fitted with a reactive windshear detection system, designed by Honeywell, but this failed to provide a windshear alert, despite a headwind shear of 61 knots. This is because the windshear was encountered as the flaps were being deployed: to avoid the generation of nuisance alerts caused by the variation in the lift, the system inhibits warnings while the flaps are in transit.

The windshear detection system requires, therefore, an indication of the flap settings and, possibly, other configuration settings, e.g. undercarriage position. The effects of these settings can then be included in the aircraft model in a similar fashion to the modelling of the changes in the elevator and thrust level.

5.3 Discussion and Summary

The alternative methods for implementing the estimation algorithm were shown in Chapter 4 and gave a reasonable estimate of the wind acting on the aircraft when the observer model matched that of the aircraft itself. Section 5.1 examined the performance of the algorithm when the modelling was not identical - a situation which arises with during the differing phases of flight. It was found that the x-axis wind component could be estimated when measuring only the pitch rate and airspeed and the z-axis component could be determined from the heave velocity and pitch rate, but to estimate both wind components to a reasonable accuracy required all three flight parameters to be measured. Scheduling of the observer and model matrices associated with the linear aircraft equation of motion, using the measured airspeed, produced improved estimates.

Section 5.2 considered briefly the practical problems of sensing the parameters required by the algorithm. The forms of errors inherent in sensors were considered and the probable effect on the algorithm was examined. The principal requirements for the sensors are good resolution and stability as other effects can be removed during calibration or compensation can be applied. Small errors in the form of oscillation and slow drift were introduced but these did not show a significant effect upon the wind component estimates.

A more comprehensive examination of the effects of sensing errors is required before the performance of the algorithm with 'real' sensors can be fully assessed and this would include more detailed modelling of the sensors. Such an investigation should be conducted using a 'full' dynamic model of the aircraft, rather than a small-perturbation model, which could be achieved using, for example, a flight simulator. This would enable the washout filtering, compensation techniques and gain scheduling of the airspeed to be evaluated more effectively.

6 HAZARD EVALUATION AND WARNING METHODS

6.1 Hazard Evaluation and Warning Requirements

The wind estimation algorithm discussed in the previous chapters gives an estimate of the wind components acting on an aircraft. These components can be used as part of the windshear detection system, but to do this requires criteria for evaluating the hazard presented by the varying winds.

The requirements of the hazard evaluation are twofold; to determine whether a hazardous windshear exists and to trigger a timely alert. The risk imposed by a wind condition will be determined by pre-set criteria and the thresholds for this must be chosen to maximise the detection of any dangerous winds while minimising alerts for which there is no significant hazard; that is, the system must respond to windshear but not to smaller magnitude gusts or turbulence. Possible criteria could be defined by considering the wind magnitudes, wind changes or the effects of the wind on the aircraft. In addition, the time required by the windshear evaluation algorithm to assess the situation must be short so that the alert is provided as early as possible giving the pilot maximum time to respond to the alert and to manoeuvre the aircraft to escape from the windshear.

The warning system must provide a clear and unambiguous warning. The method and format of alert must be such that the pilot is provided with the necessary information to enable a rapid decision to be taken and the appropriate reaction to be made. The design of such a warning system involves consideration of several human factors and the study of the appropriateness of differing forms of alert includes an examination of these considerations.

6.2 Effect of Wind on Airspeed and Vertical Speed

A windshear is a change in the wind vector, and the definition given in Chapter 1 describes a hazardous windshear as one which induces a change in excess of 15 knots in airspeed or 500 feet per minute in the vertical speed of an aircraft. The magnitudes of the wind components which generate these responses depend upon the temporal properties of the wind components and upon the aircraft dynamics. Some insight into the relationship can be

determined from transfer functions which describe the responses of the airspeed and vertical speed to the winds.

6.2.1 Transfer Functions relating Airspeed and Vertical Speed to Wind Inputs

The transfer functions for the airspeed and vertical speed of the aircraft are derived from the state equation (2.23) by considering the response of the aircraft to wind inputs solely i.e.

$$\dot{\mathbf{x}} = \mathbf{A}\mathbf{x} + \mathbf{E}\mathbf{w}_{ind} \tag{6.1}$$

$$\mathbf{y} = \mathbf{C}\mathbf{x} + \mathbf{D}\mathbf{w}_{ind} \tag{6.2}$$

Here the **C** and **D** matrices are different from those used in earlier chapters and reflect the fact that the output variables have been selected to be the airspeed and vertical speed of the aircraft. The airspeed is derived from equation (A14) as

$$u_a = u + u_g \tag{6.3}$$

The inertial vertical speed can be found by considering the relationship between the z-axis acceleration and the state variables from equation 3.10.

$$a_z = \dot{w} - U_0 q = -\ddot{h} \tag{6.4}$$

From this the vertical speed, measured positive for an upward motion and negative for descent, is:

$$\dot{h} = -w + U_0\theta \tag{6.5}$$

Hence the matrices for the output equation 6.2 are:

$$\mathbf{C} = \begin{bmatrix} 1 & 0 & 0 & 0 \\ 0 & -1 & 0 & U_0 \end{bmatrix} \tag{6.6}$$

$$\mathbf{D} = \begin{bmatrix} 1 & 0 \\ 0 & 0 \end{bmatrix} \tag{6.7}$$

where

$$\mathbf{y} \equiv \begin{bmatrix} u_a \\ \dot{h} \end{bmatrix} \tag{6.8}$$

The transfer function is given as a function of the Laplace operator, s, by:

$$\mathbf{G}(s) = \mathbf{C}(s\mathbf{I} - \mathbf{A})^{-1}\mathbf{E} + \mathbf{D} \tag{6.9}$$

The frequency response from each input to each output can be derived by substituting $s = j\omega$ into equation 6.9. Figure 6.1 shows the magnitude of the frequency response of the airspeed and vertical speed to the wind inputs. The transfer functions were evaluated using the data for the Cessna 402B using the flight condition which relates to take-off at sea-level. The frequency range used was chosen to show the principal features of the aircraft response. In some parts of the analysis it may be more convenient to consider the wind period rather than the frequency. The period is the reciprocal of frequency, and so any decrease in frequency will correspond to an increase in period.

The first plot shows the magnitude of the frequency response of the airspeed to the x-axis wind. At frequencies above approximately 0.2 Hz, which relates to winds variations with a period of five seconds or less, the gain is 0 dB. The wind change causes a change of equal magnitude in airspeed, but, as the restoring dynamics of the aircraft (discussed in Chapter 2) are slower, their effect is not exhibited in the response at these frequencies. As the frequency of the x-axis wind decreases the magnitude of the response increases until it reaches a maximum of approximately 23 dB at 0.024 Hz (42s period). At this frequency the magnitude of the response is fourteen times greater than the magnitude of the wind, and the frequency of the wind corresponds to the phugoid frequency of the aircraft: thus the wind is exciting the natural mode of the aircraft, which causes the significant amplification. Below this frequency the response of the aircraft again decreases, and at frequencies below 0.017 Hz (60s period) the aircraft produces an increasingly attenuated response to the wind input - the

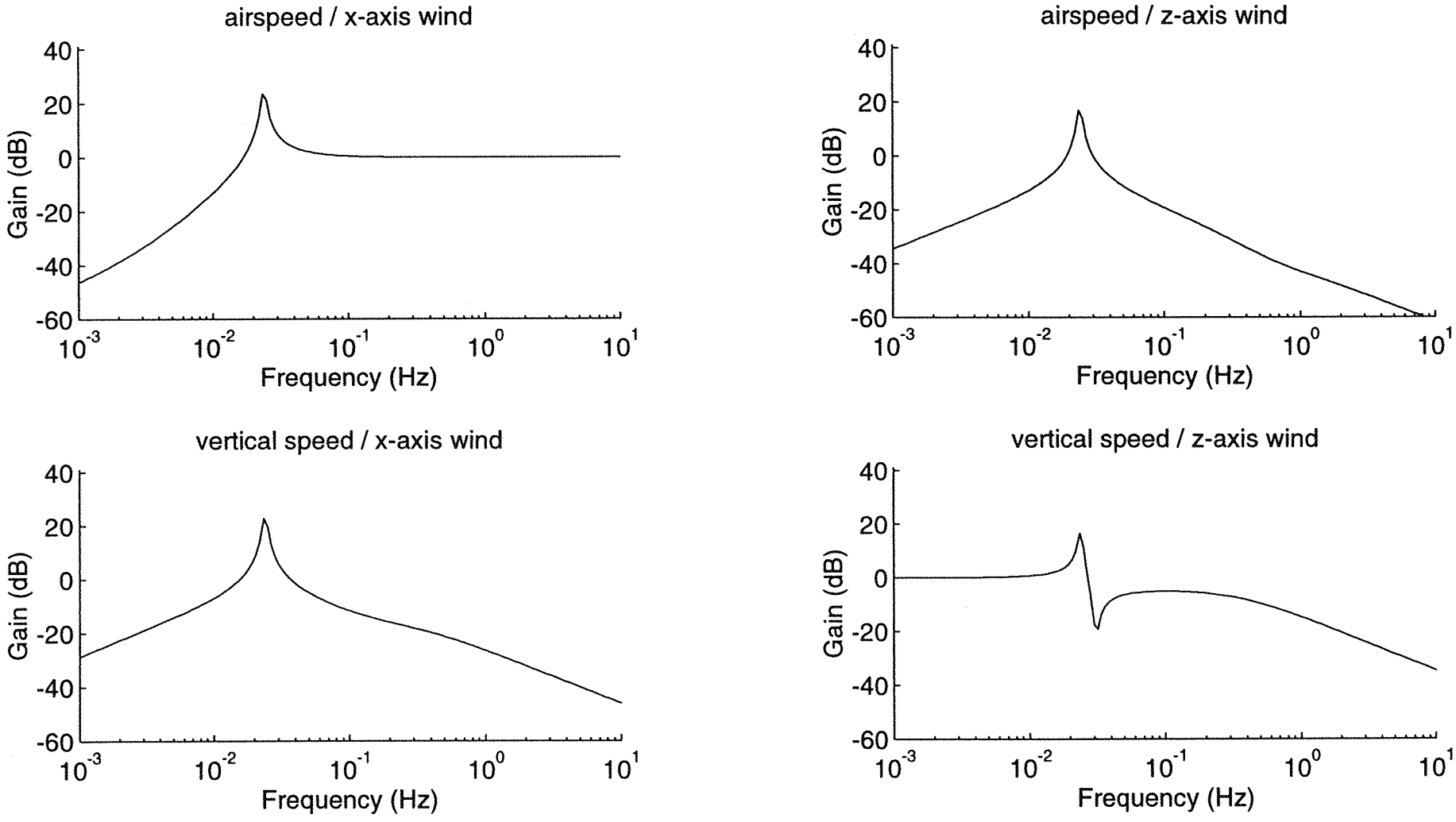

Figure 6.1: Frequency Response of Aircraft to Wind Inputs

restoring dynamics counteract the effects of the changing wind. This agrees with the analysis of Chapter 2, where it was shown that an aircraft subjected to a change in airspeed eventually returned to the equilibrium airspeed, albeit with a change in altitude and ground speed.

The low frequency response of the airspeed to a z-axis gust is similar to that produced by the x-axis gust, although the magnitude of the response is small. The resonant effect at the phugoid frequency is apparent and the response decreases as the frequency decreases. However, at frequencies above the phugoid frequency the response also rolls off continuously, so that high frequency changes in the z-axis wind produce negligible response in the airspeed.

The effect on the inertial vertical speed of a horizontal gust is similar in form to the response in the airspeed to an z-axis wind. A significant response occurs at frequencies close to the phugoid frequency and above and below this frequency the response rolls off. At the phugoid frequency the magnitude of the response is approximately 17 dB.

The effect of a z-axis gust on the inertial vertical speed of the aircraft is more complex. A pole and zero in the transfer function are close together in the region of the phugoid frequency which causes the large magnitude change exhibited in the figure. The plot again shows a maximum response at the phugoid frequency with little effect at higher frequencies. At low frequencies a change in the vertical wind produces an equivalent change in the vertical speed of the aircraft.

6.2.2 Frequency Characteristics of Hazardous Windshear

The hazard posed by winds of differing frequencies on the Cessna 402B aircraft can be summarised.

High frequency winds are classified as turbulence and the characteristics of turbulence were described in Chapter 2. Although winds at these frequencies can be seen to affect the airspeed, the dynamic response of the aircraft is slow and, consequently, they do not have a significant effect on the flight path. At very low frequencies an x-axis wind component has

negligible effect, while a low-frequency z-axis wind causes an equivalent change in vertical speed.

For wind periods between 5 and 64 seconds (frequencies 0.015 Hz to 0.2 Hz) the amplitude of the free response of the aircraft is greater than that of the wind causing the excitation. At these frequencies, and particularly at the phugoid frequency, the changing wind produces large airspeed and vertical speed deviations from a trim condition. A significant wind speed change in this bandwidth could result in large airspeed and flight path deviations which, at low airspeed and altitude, could cause a stall condition and, subsequently, ground impact.

The results show the free response of the aircraft to a wind. In practice, a pilot would act to correct any observed flight path deviations. The phugoid period of an aircraft is sufficiently long to allow a pilot to apply corrective control inputs and, as a consequence, the flight path and airspeed deviations could be significantly reduced. This has been demonstrated in piloted simulation studies where flight path deviations were reduced by a factor of four. [74]

The implications for a windshear detection system are that the hazard criterion must function according not only to the magnitude but also to the frequency distribution of the wind acting on the aircraft. Wind periods in excess of 5 seconds are amplified by the aircraft dynamics and cause sudden changes in airspeed and vertical speed. These may cause large flight path deviations before the pilot becomes aware of the situation and reacts. Frequencies around that of the phugoid mode of 0.024 Hz (42 second period) allow the pilot more time to respond, but the effects upon the aircraft dynamics are greater. More slowly varying winds provide a longer time for the pilot to react to a change and to control the flight path, as well as producing a smaller effect, but the change itself is also prolonged and may produce a large total change in the residual energy of the aircraft. For each of these cases a timely windshear warning to alert the pilot to the windshear condition could increase the survivability of the event.

6.3 Hazard Evaluation Methods

The method used to determine whether a hazardous windshear has been encountered could be based on the wind components themselves or on the aircraft's performance margins in the wind conditions. For transport aircraft the FAA have specified a detection criterion based on the F-factor, which is derived from the aircraft's energy margin and, therefore, its ability to climb out of the shear. However, general aviation aircraft have lower take-off and landing speeds than transport aircraft and so the speed margin of the aircraft must also be considered carefully; even moderate windshear may cause airspeed losses which could induce a stall condition.

Three alternative methods for defining hazard criteria are discussed here. The first method examines the change in the wind components, thereby measuring windshear directly, whereas the second method considers the aircraft response in windshear. Finally, the F-factor evaluation method is discussed. Section 6.4 will then discuss the problem of setting thresholds levels for each method and will compare their performance.

6.3.1 Wind Change Thresholding

The windshear hazard must be evaluated in real-time and this means that time domain techniques are the most appropriate. A method of measuring wind changes which occur over short periods of time is considered first. The time period can be determined using observations of the aircraft and pilot frequency responses made in Section 6.2.2. This suggests that wind changes with periods between approximately 5 and 60 seconds are most hazardous. Low-pass filters can be used to attenuate frequencies above this range in the estimated wind component. The most recent 30 seconds of data can then be examined and the wind changes which occur during that period can be found. This duration is chosen because it represents the time for a half-period swing from maximum to minimum, or vice versa, of the slowest wind variation being considered, i.e. a wind period of 60 seconds. When the wind changes have been extracted they can be compared with a chosen threshold value and, if this level is exceeded, an alert is triggered. A flowchart showing the method of implementing this method is given in Figure 6.2. Figure 6.3 shows the wind changes extracted when the wind components from the JFK windshear are fed directly into the algorithm.

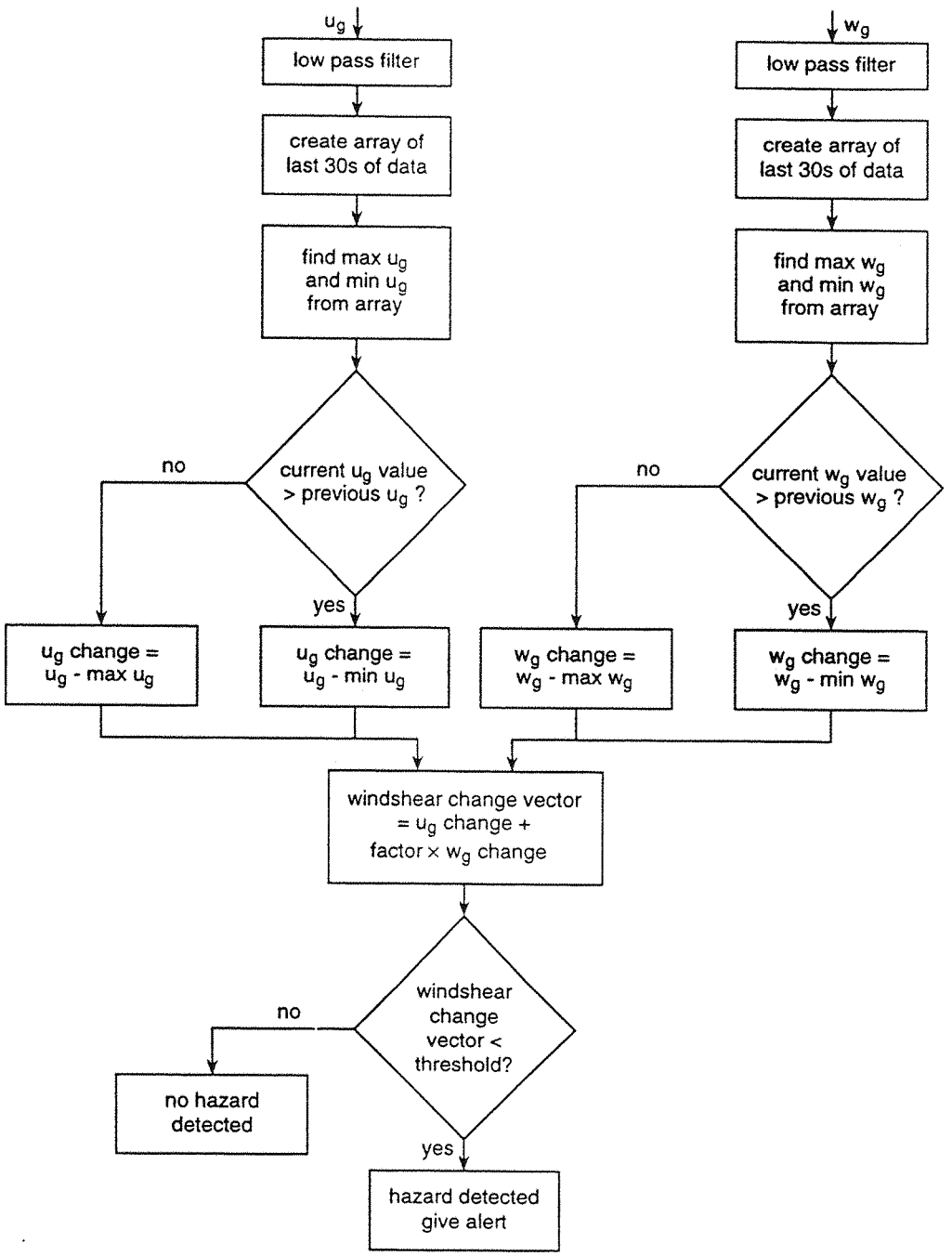

Figure 6.2: Flowchart of Wind Change Thresholding Method

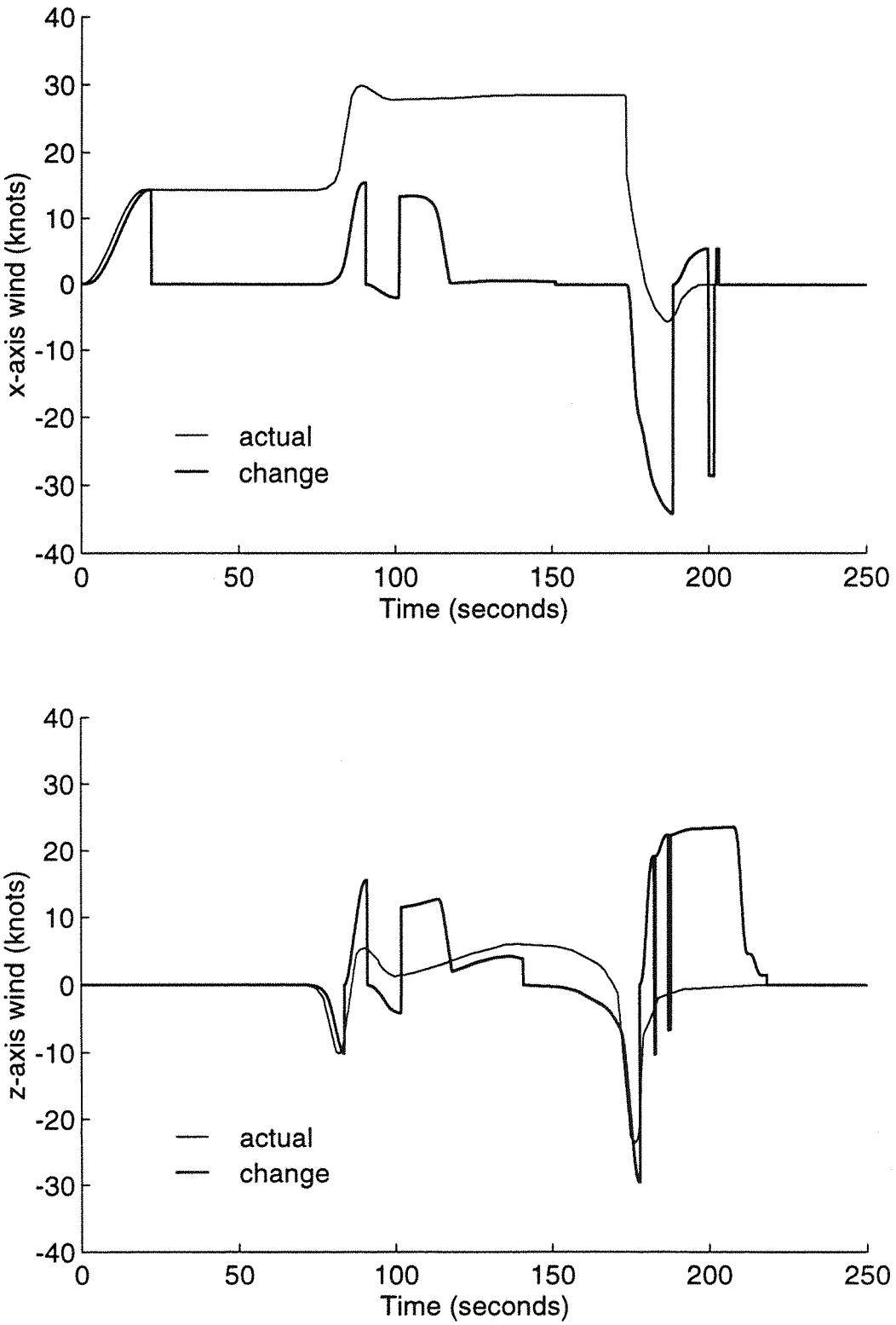

Figure 6.3: Extraction of Changes in Wind Components - JFK Windshear

The algorithm will also detect wind changes which have a period greater than 60 seconds, but the magnitude of the change which causes an alert will be larger, as the wind must change by the threshold quantity within the 30 second time interval to produce a warning. Thus the windowing technique has an inherent high-pass filter characteristic which limits the detection bandwidth.

6.3.2 Performance Margin Thresholding

The change in the performance margins of the aircraft itself could be considered; for example, a speed margin method may be suitable as the aircraft's airspeed is being measured directly. In this case, a threshold could be set at a fixed margin above the 1g flight speed (the minimum speed to sustain level flight) or the stall speed, and if the x-axis wind component is sufficiently large to cause a degradation in airspeed to below this level, the windshear alert system could be triggered.

This simple method does not take account any z-axis winds. These could be included by evaluating their relative effect, and an approximation of this can be calculated by considering the aircraft's energy state which is the sum of its potential and kinetic energy.

$$E = \frac{1}{2} m U_a^{\,2} + mgh \tag{6.10}$$

The change in energy can be calculated and set to zero, and the kinetic and potential energy change can then be equated. It was observed in Section 6.2 that a 'steady' or very low frequency vertical wind component produces an equivalent sink rate in the free-response of the aircraft, but at slightly higher frequencies around the phugoid mode it produces a gain factor of up to seven. The height change resulting from a z-axis wind can be replaced by the wind component and an associated frequency-dependent gain, k_1.

$$U_a \dot{U}_a = g k_1 w_g \tag{6.11}$$

The change in the x-axis wind component produces a change in airspeed, but this varies according to the gain in the transfer function at each wind

frequency. Using a second gain factor, k_2, the effect on the aircraft's energy of the x-axis and z-axis winds can be related by:

$$w_g = \frac{k_2 U_a \dot{u}_g}{k_1 g} \tag{6.12}$$

or

$$u_g = \frac{k_1 g}{k_2} \int \frac{w_g}{U_a} dt \tag{6.13}$$

This equation provides an approximate relationship between a z-axis and x-axis wind component. The gain, k_1/k_2, is the ratio of the gain, at a particular frequency, of the z-axis wind to vertical speed transfer function to that of the x-axis wind to airspeed transfer function. This varies from 1 to 2 in the frequency range for detection when the free response of the aircraft is considered. However the piloted response, discussed in Section 6.2.2, is likely to produce a smaller transient deviation in flight path and airspeed, and so the effective gain could be reduced, especially in the region of the phugoid frequency. Estimates made from the piloted simulation results suggest that the phugoid oscillation can be controlled to approximately a quarter of the amplitude of the uncontrolled oscillation. [74] Hence, a gain factor of unity is used as a reasonable initial estimate, so that the final relationship becomes

$$u_g = g \int \frac{w_g}{U_a} dt \tag{6.14}$$

To implement this method the z-axis wind is passed through a low pass filter, or a moving-average technique is used, to extract the low frequencies which represent a windshear hazard. The output is then converted to an 'energy equivalent' x-axis wind change using equation 6.14. For example, from this relationship, a z-axis wind with a magnitude of 1% of the aircraft's airspeed and a duration of a fifty seconds is approximately equivalent in energy change to a x-axis wind change of 16 ft/s for the Cessna 402B.

Figure 6.4 shows a method of implementing the algorithm. Different performance margins could be considered using this method. When

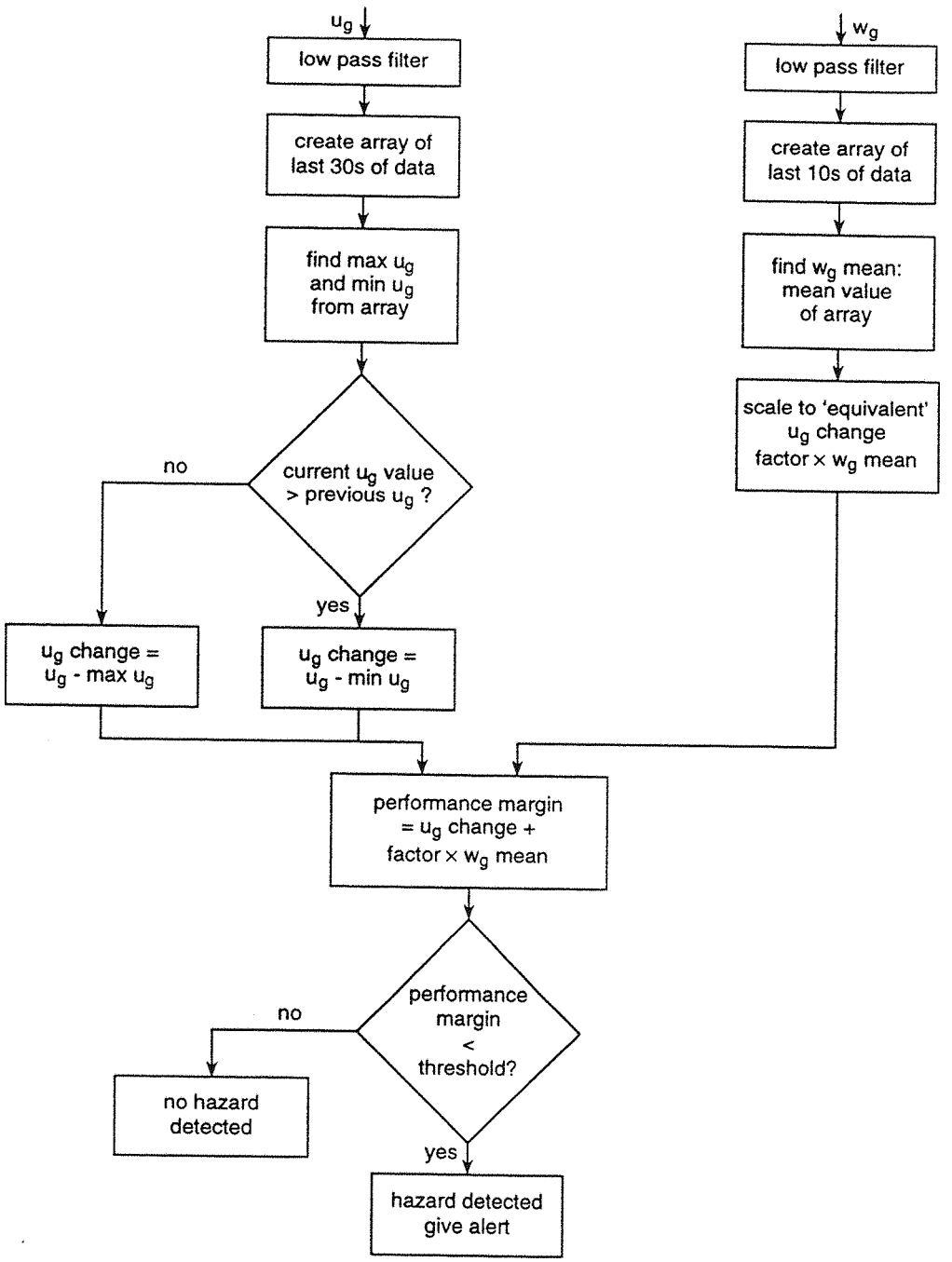

Figure 6.4: Flowchart of Performance Margin Thresholding Method

equation 6.14, which was derived using a relatively intuitive approach, is compared with the F-factor in equation 2.25 it can be seen that the energy method used in both cases has yielded similar results.

6.3.3 F-factor Thresholding

The FAA produced a Technical Standard Order for reactive windshear warning systems for transport aircraft. [31] This document specifies the method by which the risk associated with the sensed wind conditions can be evaluated, and it is based on the F-factor. The F-factor and its derivation are discussed in Section 2.2.3. This showed that the F-factor was related to the x-axis and z-axis winds according to Equation 2.25 viz.

$$F = \frac{\dot{u}_g}{g} + \frac{w_g}{U_a} \tag{6.15}$$

Here g is expressed in the same units as $\dot{u}$ and U_a is the true airspeed. The sign of the F-factor differs from that used in the reference because of differences in sign conventions; in all cases a negative F-factor represents a performance decreasing wind condition.

Figure 6.5 is based on Figure 1 from the reference and shows the criteria for which an alert must be given. [31] The abcissa is a time axis and represents the duration, τ, over which the wind is being assessed. The ordinate shows the average value of the F-factor over the period, τ, which is calculated as:

$$F_{av,\tau} = \frac{1}{\tau}\int_0^{\tau} F(t)dt \tag{6.16}$$

(The signs of the abscissa scale of the graph in the reference are assumed to be incorrect and have been inverted in Figure 6.5, as the document states that the figure is intended to relate to performance decreasing conditions.) For durations of less than five seconds no alert is required, regardless of wind intensity. A wind which generates an average F-factor less than -0.21 over a five second duration must produce an alert. As the thresholding duration is increased the threshold value decreases so that a warning is given if the relationship of equation 6.17 is true, viz.

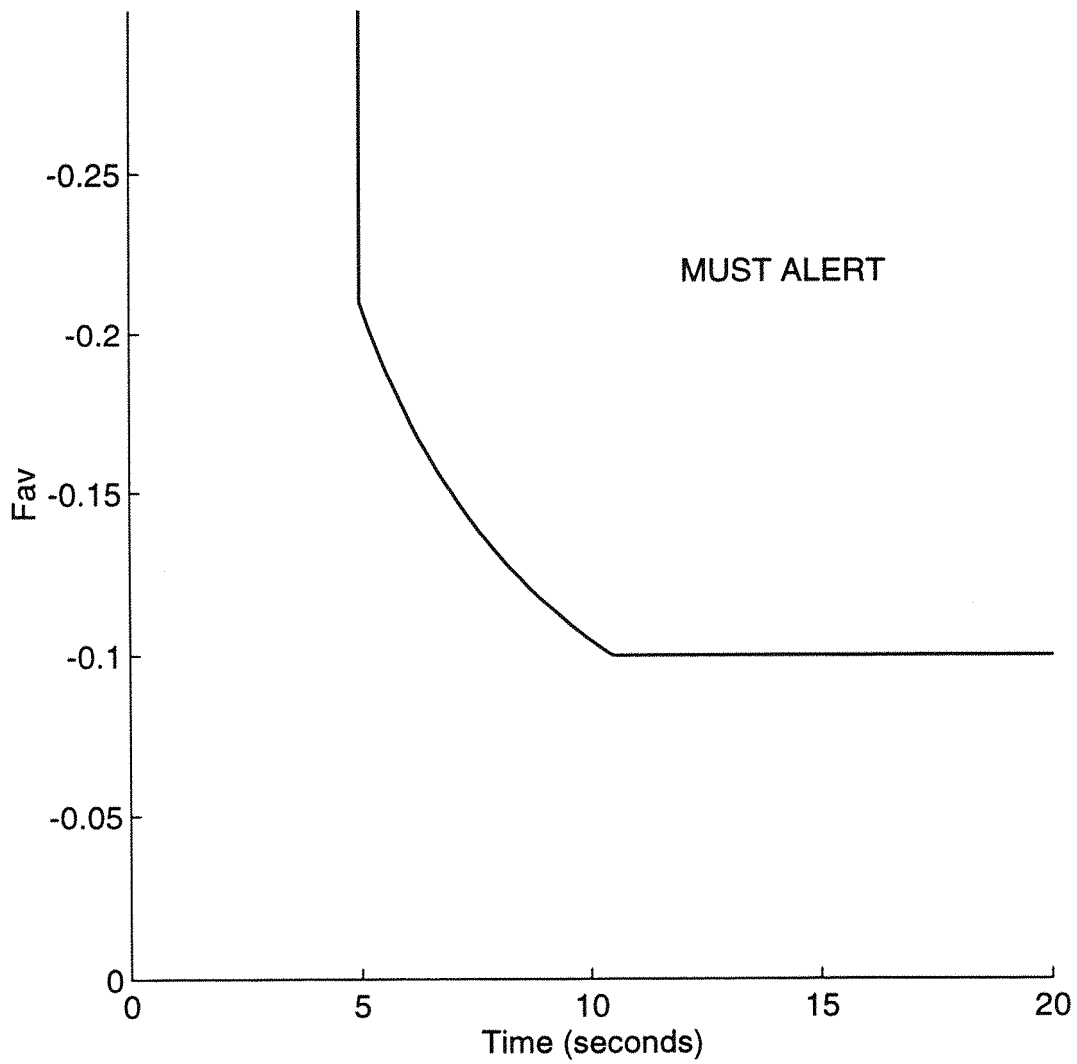

Figure 6.5: FAA F-factor Threshold Requirements

$$F_{av,\tau} <= \frac{-1.049}{\tau} \qquad (6.17)$$

This criterion applies for periods up to ten seconds, when the threshold is -0.105. For averaging durations longer than ten seconds the 'must alert' threshold is shown in the figure to be constant at -0.105. Such a criterion is, in practice, included in the criterion for the 10s averaging period because an event for which the average F-factor is more than -0.105 during any ten second period cannot be below this threshold over a longer period.

The implementation of this form of windshear thresholding in a real-time system requires some simplification of the method; in particular the calculation of F_{av} over a continuously varying period could impose a large computational requirement. However, as the frequencies of the wind which may be a hazard are relatively low, averaging the F-factor over periods of, for example, 5, 6, 7, 8, 9 and 10 seconds is likely, at worst, to result in a marginal warning being delayed by up to a second. The averaging process is a compromise, therefore, between computational complexity and warning promptness.

A flowchart which shows a method of implementing the FAA criteria numerically using the averaging periods discussed is shown in Figure 6.6.

6.4 Comparisons of Thresholding Levels

A comparison of the three techniques can be made by comparing their warning effectiveness using differing wind magnitudes and profiles. The form of windshear was discussed in Chapter 1 and possible models were presented in Chapter 3. In addition, the discussion of Section 6.2 revealed the temporal characteristics of hazardous windshear. However the magnitude of a wind which constitutes a hazard has not been considered and this will vary, as it is dependent on the performance of the particular aircraft. The means of determining a suitable magnitude will be considered in Sections 6.5 and 6.6, but, for the present comparison, the threshold levels defined by the FAA for transport aircraft will be used. [31] It will be attempted to match these threshold levels using the other two methods.

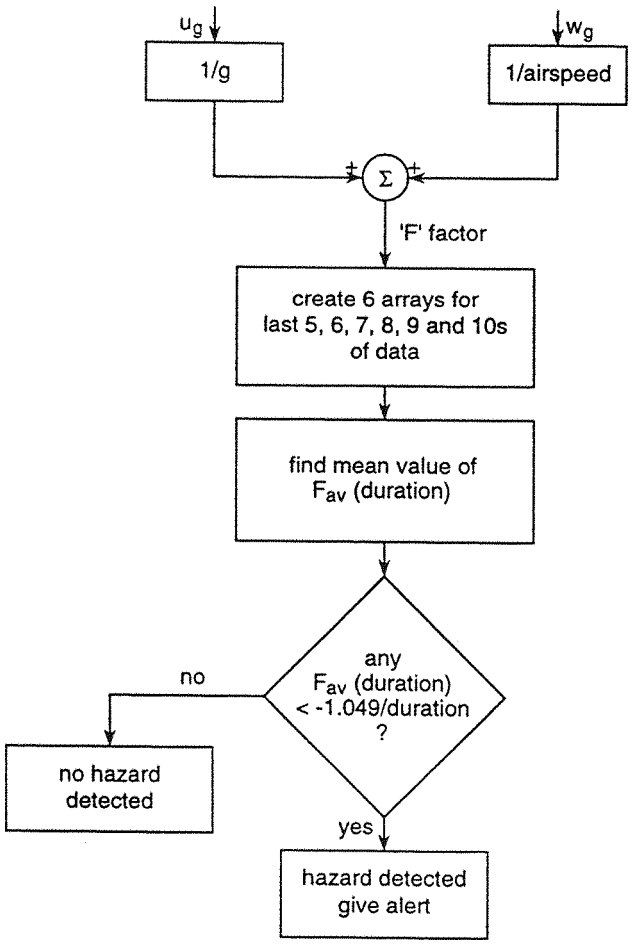

Figure 6.6: Flowchart of F-factor Thresholding Method

6.4.1 FAA Threshold Levels

The FAA specification requires that an alert is given when the relationship of equation 6.17 is satisfied for time periods between 5 and 10 seconds. An equivalent x-axis wind speed change can be found from the values of F_{av} for these periods:

$$\Delta u_g = \int_0^\tau \dot{u}_g(t)dt = F_{av,\tau} g\tau \tag{6.18}$$

1g is 19.1 knots/s. For any averaging period between 5 and 10 seconds the equivalent x-axis wind speed change for which an alert is required is a constant 20 knots. Above this time period the F_{av} threshold is held constant and so the wind change which would be required to trigger an alert increases linearly. As mentioned in Section 6.3.3, such a wind changes would be detected as a 20 knot change over a ten second time period.

The z-axis wind threshold is more complex. For a z-axis wind only, the equation for F_{av} is:

$$F_{av,\tau} = \frac{1}{U_a \tau} \int_0^\tau w_g dt \tag{6.19}$$

If the z-axis wind is constant over the period of interest the z-axis wind threshold as a ratio of the total indicated airspeed can be found.

$$F_{av,\tau} = \frac{w_g}{U_a} \tag{6.20}$$

The decreasing threshold defined for averaging periods between 5 and 10 seconds means that the z-axis wind component required to trigger an alert will decrease correspondingly from a downdraft with a magnitude of 21% of the airspeed for a 5 second duration to one of magnitude 10.5% for a 10 second averaging period.

6.4.2 Performance Margin Threshold Levels

The x-axis wind threshold used by the F-factor method of Section 6.4.1 is 20 knots detected over durations of up to ten seconds and therefore for winds of

periods up to 20 seconds. The same duration could be used for the performance margin method, but the analysis of the frequency response of the aircraft suggested that wind period of up to approximately 60 seconds should be considered and so the 'window' for detection of the half-period peak-to-peak change will be set initially to 30 seconds instead.

The equivalent z-axis wind threshold can be found from equation 6.20. A ten second moving average is used to extract the 'steady' z-axis wind component and therefore the threshold is set to be 10.5% of the airspeed to equate to the F-factor threshold for a ten second averaging period.

6.4.3 Wind Change Threshold Levels

This method considers the magnitude of the *change* in both the x-axis and the z-axis wind components. The x-axis criterion is therefore exactly the same as that for the performance margin method and so the same threshold of 20 knots and window length of 30 seconds is used.

The definitions of the hazardous windshear as 15 knots horizontal wind change or 500 ft/min (5 knots) vertical change suggest that the z-axis wind change threshold should be set to be one third of that for the x-axis wind, but the transfer function plots of Figure 6.1 indicate that for changes within the bandwidth of interest, the x-axis wind has approximately twice the effect of a z-axis wind of similar magnitude. Therefore the z-axis threshold is initially set equal to that of the x-axis wind and the alert is triggered if a 20 knot z-axis wind change is detected.

6.4.4 Threshold Tests

The first test uses the simple model of a microburst discussed in Section 2.3.4 and shown in Figure 2.11 to examine the thresholding levels of each of the hazard assessment methods. The model parameters were varied during the test to simulate windshear of differing amplitude and period. The three thresholding methods were each tested for x-axis and z-axis windshear conditions separately using microburst periods of between one and one hundred seconds. The amplitude of the wind was gradually increased until a warning condition was detected.

6.4.5 Threshold Test Results

Figure 6.7 shows the plots of the amplitudes of the modelled microburst at which an alert was triggered by each of the thresholding methods, plotted as a function of the period of the gust. It should be noted that for both wind components, the amplitude of the wind used in the tests represents a wind change of twice that value, as can be seen in Figure 2.11.

The results for an x-axis wind are discussed first. Only two traces are shown on the plot because the wind change criterion and the performance margin method both use an identical method of thresholding for x-axis windshear. The plot can be divided into three distinct regions; a 'low-pass' filtering region between one and ten seconds, a 'pass band' between ten and twenty seconds and a 'high-pass' filtering region for windshear periods in excess of twenty seconds.

In the first region the low-pass characteristics of each method are achieved in different ways. The thresholding level for the wind change algorithm is governed by the nature of the low-pass filter through which the wind components are passed before the thresholding algorithm is applied. Here a fourth-order Butterworth filter has been used with a 0.25 Hz (4 seconds) cut-off frequency. In contrast, the low-pass filtering for the F-factor algorithm is effected by the averaging process for which the minimum period is six seconds, so that any winds with periods below twelve second are attenuated.

The two methods show a good match within the 'pass band' region where they both trigger an alert for an amplitude of 10 knots (a 20 knot wind speed change). The differences in the high-pass region are caused by the differences in the length of the 'data window' for the two algorithms. The F-factor method has a maximum averaging time of ten seconds and so the maximum period of the wind within the pass band is twenty seconds. The window length for the wind change algorithm was originally set to be thirty seconds so that the pass band would extend to sixty second and thereby correspond to the bandwidth of hazardous wind as discussed in Section 6.2. This was found to give a very slow increase in the thresholding levels above the sixty seconds 'cut-off', i.e. the filter roll-off was slow, and so the window length was reduced to twenty seconds and the high-pass filtering this produces begins to roll-off at forty seconds. The attenuation at periods of up

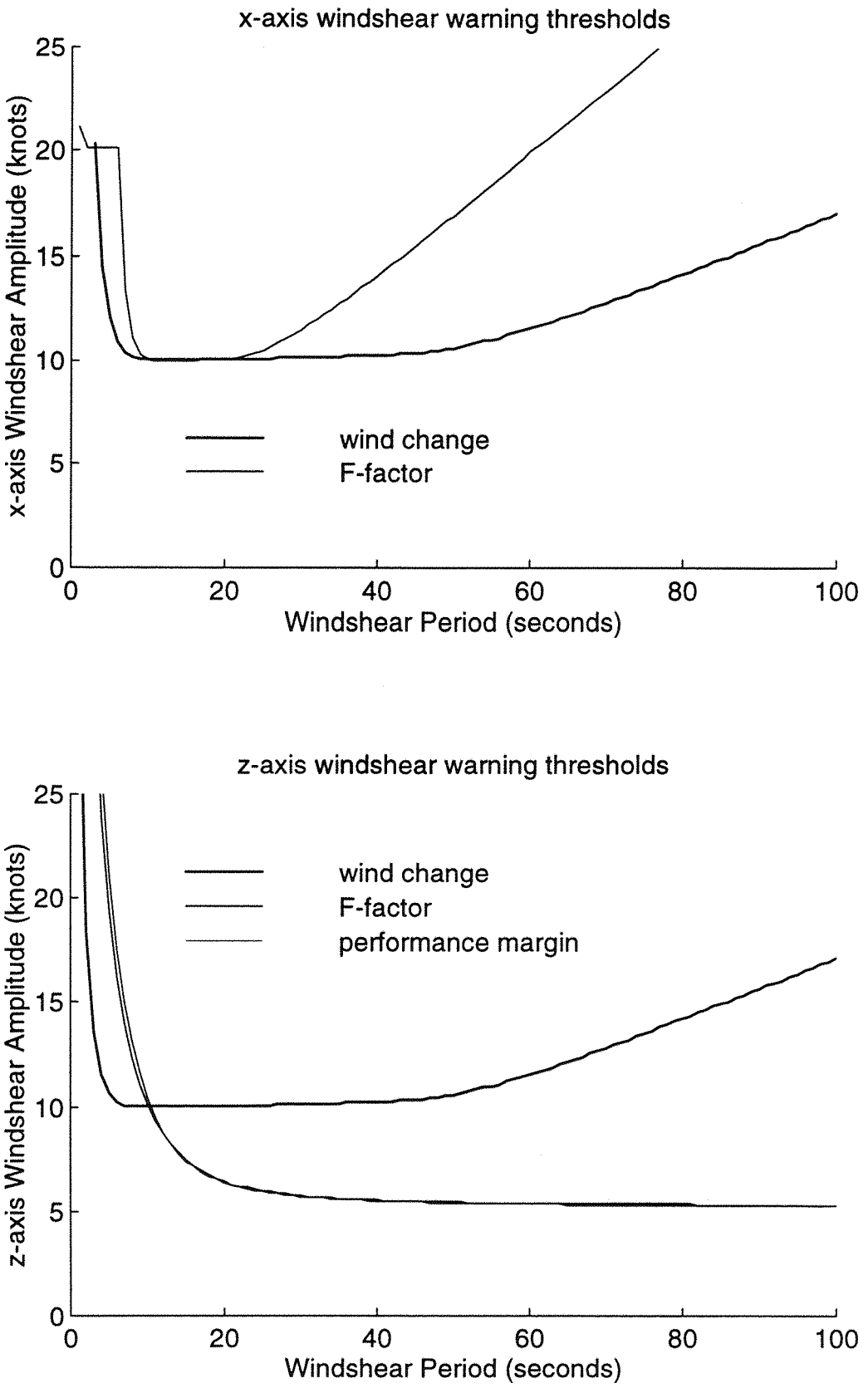

Figure 6.7: Comparison of Windshear Alert Thresholds

to sixty seconds is slight, as can be seen in the figure. Reducing the algorithm data window further would cause the threshold levels for periods above twice the window length, and the rate of 'roll-off' in this region, to increase; therefore, a ten second window would be likely to produce similar 'high-pass' results to those from the F-factor algorithm.

The second plot shows the z-axis wind thresholds as a function of wind period for each of the three methods. Here a fourth-order Butterworth filter is used to extract the high frequency components from both the 'performance margin' method and the 'wind change' algorithm, with a cut-off frequency set to 0.1 Hz (10 seconds).

It was attempted to match the threshold levels of the F-factor and performance margin methods and the two plots show a close agreement. Both show similar low-pass filtering effects and neither method shows an increase in the threshold as the period increases.

In contrast the z-axis threshold level produced by the 'wind change' algorithm differs from the other two. The low-pass filtering characteristic is produced by the Butterworth filter. The threshold and window length for this method were set to be the same values as those for the x-axis wind change and the response in at low frequencies is the same, although the differences in the x-axis and z-axis components of the test profile produce an apparent difference in the results.

6.4.6 Comparison of Hazard Criteria using Windshear Profiles

The tests in Section 6.4.4 compared the wind intensities at which a windshear warning was given. However, the time taken to evaluate the hazard and trigger an alert is also significant, and so tests were performed to compare this. The windshear profiles derived from records obtained from aircraft accidents, described in Chapter 3, were used. These profiles were passed into each of the three algorithms and the elapsed time from the beginning of the windshear profile to when the hazard criteria were first satisfied was recorded. The methods were initially tested using the 'JFK' profile and then using the 'DFW' wind history.

Figure 6.8 shows the JFK wind components and the alerting periods for each of the thresholding methods. The origin of the time axis corresponds to the time when the aircraft passes through the core of the downburst and experiences the maximum downdraft. Here the F-factor threshold produced the earliest warning at -1.6 seconds, 0.3 seconds ahead of the wind-change thresholding method (-1.3 seconds) and 1.9 seconds ahead of the performance margin method (0.3 seconds).

The 1.9 second delay between the F-factor and the performance margin methods was investigated and was found to arise, in part, from the effect of the low-pass filtering. The moving average technique used by the performance margin method itself produces a low-pass filter effect, and so the pre-filtering was removed from the performance margin algorithm and the threshold levels for the algorithm were re-tested. There was no distinguishable difference, showing the pre-filtering to have been superfluous. The method was tested again using the JFK profile and this time the alert was given by the performance margin algorithm after 175.9 seconds of exposure to the JFK windshear.

A further cause for differences between the methods is because the F-factor has a series of thresholds and averaging periods between five and ten seconds, whereas the performance margin method has a single ten-second averaging period. The different averaging periods affect the time taken to measure the 'steady' z-axis wind component and as a consequence the F-factor method will detect a deterioration in the z-axis wind component earlier than the performance margin method.

Differences in the alerting conditions between the wind-change method and the other methods are likely to arise because of the different concept used to define a windshear condition. The plot shows that the wind-change algorithm produces a series of short duration alerts corresponding to the sudden changes in the wind components, whereas the other two methods result in single alerts of longer duration.

The small time difference between the alerts of the F-factor method and the wind-change method were investigated and were also found to be produced in part by the low-pass pre-filtering applied to the estimated wind components for the latter method. If the cut-off frequency of the filter is

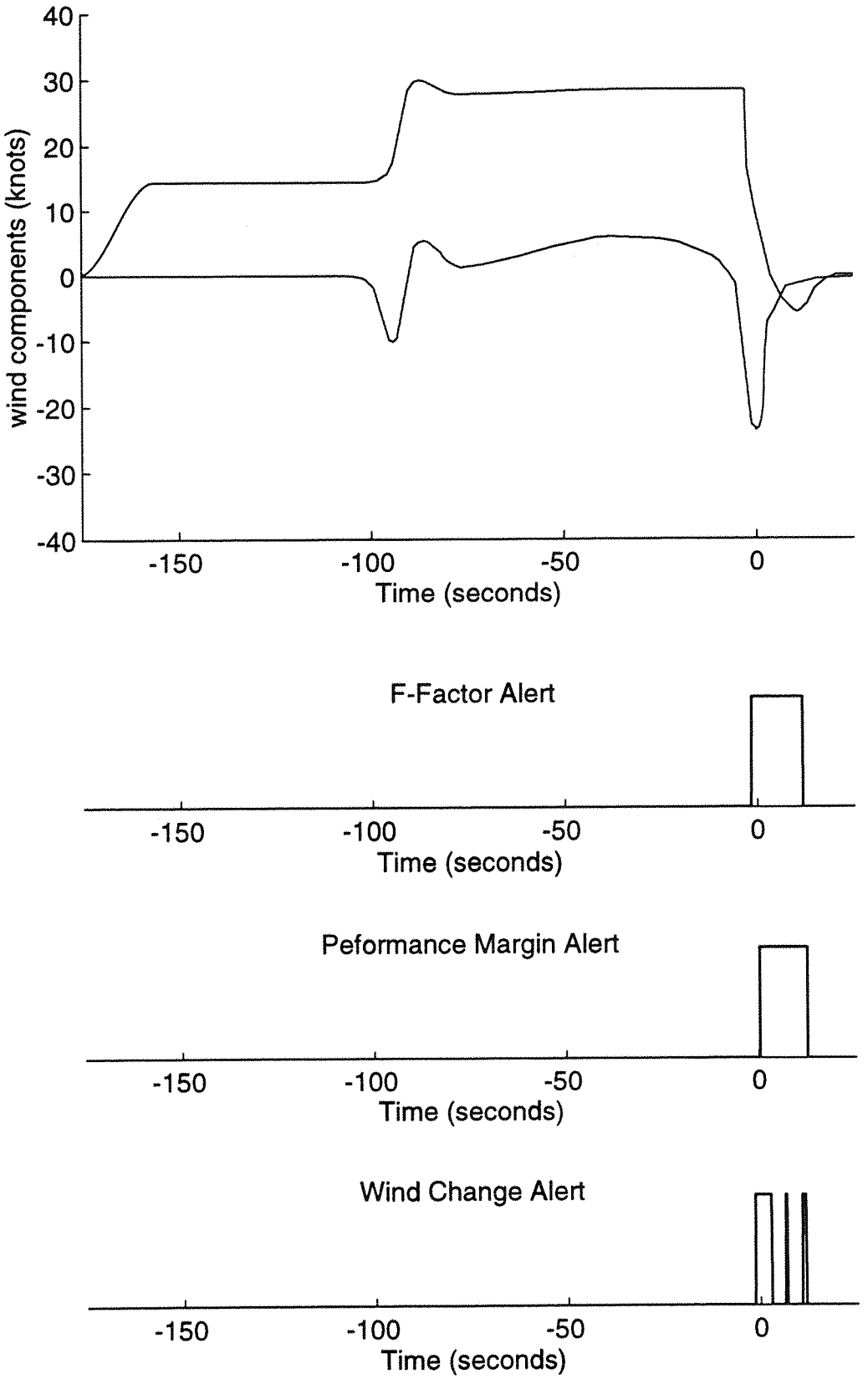

Figure 6.8: Alert Generation by Thresholding Methods - JFK Windshear

changed to a higher frequency the delay is reduced, but this also produces a lower threshold in the high frequency region and therefore less turbulence rejection.

A further contribution to the differences between the F-factor and the wind-change threshold method is the chosen level of threshold. At present z-axis threshold used in the wind-change method is significantly larger than that for the other methods and a decrease in this would enable the wind change method to alert after a smaller wind change. This would decrease the time to alert, but it could result in an increased number of false warnings.

The DFW windshear profile was also used for testing. The pre-filtering was not applied to the z-axis component when testing the performance margin method, in accordance with the observations made from the results of the JFK tests. The other two methods were unchanged, with the cut-off frequency of the pre-filter for the x-axis and z-axis wind changes remaining at 0.25 Hz and 0.1 Hz respectively, and the thresholding level at 20 knots wind speed change.

Figure 6.9 shows the DFW windshear components and the periods during which the hazard criteria were satisfied for each of the evaluation methods. For this case, the wind change criterion gave the earliest alert at -22.0 seconds and the warnings from the F-factor and performance margin methods were made at -15.4 seconds and -13.3 seconds respectively.

The z-axis wind component is the principal cause of the exceedance of the hazard threshold. The differences in the warning times between the wind change method and the other method arise because this component exhibits a small updraft before the onset of the downdraft - a characteristic of a symmetric microburst. Therefore the threshold of the wind change method is triggered by the large negative wind change before the methods which use the magnitude of the z-axis wind as part of the criterion. An extra 6.6 seconds are available for the pilot to respond using the wind-change threshold as configured here.

If the warning times for the two wind profiles are compared it can be seen that the warning for the DFW windshear is given before the central core of the microburst with its very large wind changes is encountered, enabling the

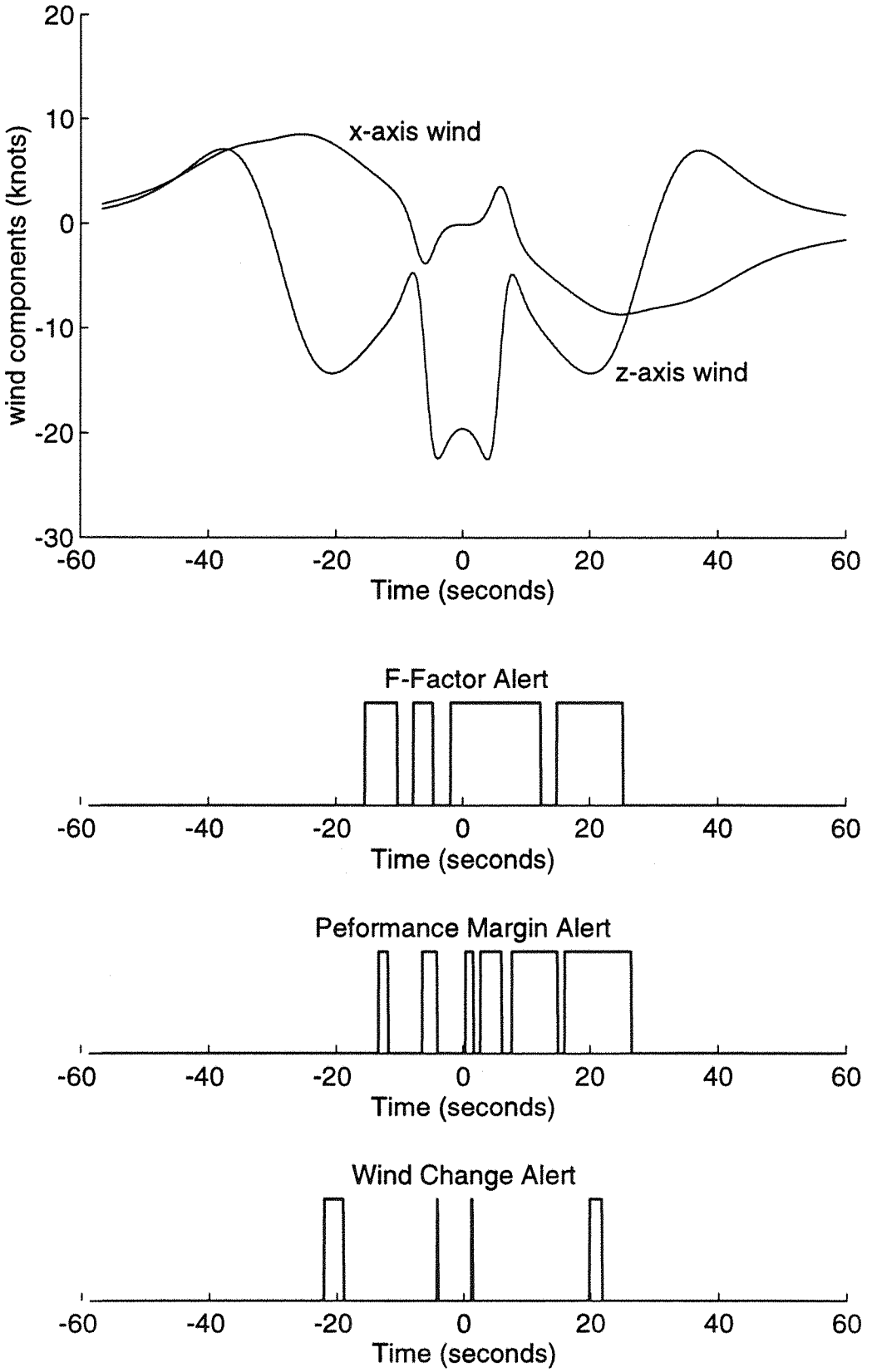

Figure 6.9: Alert Generation by Thresholding Methods - DFW Windshear

pilot to maximise altitude in advance. In contrast, the JFK alert is given as the aircraft experiences the maximum wind changes for this profile and so the pilot receives a less useful warning.

6.5 Discussion of Hazard Criteria

The performance of the three methods of defining a hazardous wind were examined using two windshear profiles in Section 6.4.6 and all three produced an alert within a few seconds of each other. The F-factor and performance margin methods were similar in design and produced similar alert characteristics, although the performance margin method showed a delay, mainly because of its longer averaging period for z-axis windshear detection.

The wind-change criterion was based upon a different method of defining the hazard. This showed comparable results, giving a warning 0.4 second after the F-factor method for the JFK windshear but 6.6 second ahead for the DFW windshear. All the criteria examine the x-axis wind change and, therefore, the differences arise mainly from the z-axis thresholding. The relative hazards of a z-axis and x-axis wind change are difficult to define and were reasoned to be approximately equivalent in Section 6.4.3; as a consequence a significantly larger z-axis wind change is required before an alert is triggered when compared with the threshold levels for a steady downdraft used by the other two methods.

The performance of the wind change algorithm differs from that of the F-factor hazard criterion. In the tests using the DFW and JFK profiles the differences are exhibited in the timing of the alerts, but, for some wind profiles, one criterion could produce an alert whereas the other might not detect a windshear. This could occur when an updraft changes suddenly to a downdraft in a similar way to the first thirty second of the DFW profiles in Figure 6.9. If no further deterioration in the wind condition occurred only the wind change algorithm would generate a warning. In contrast, if an aircraft is flying slowly relative to the rate of change of the z-axis wind component, the wind change algorithm is less likely to detect a windshear as the apparent period of the wind would be less and the high-pass effect of the windowing could, therefore, attenuate the change. However, the F-factor calculates the z-axis wind hazard as a ratio of the wind component to the

aircraft's airspeed and so the slower transition of the shear is taken into account. Design changes to the wind change algorithm would allow the airspeed to be incorporated in the z-axis wind change evaluation, and could enable the data window for the z-axis wind to be increased; both these changes would reduce the difference in the performance for this case.

The selection of the most suitable criterion for use in the detection system is complex. The wind-change and F-factor methods gave the best results in the limited tests performed but these results were dependent on the thresholds and filtering used. Further design of both of these aspects could yield performance improvements. The thresholds must be set to detect the maximum number of hazardous windshear while minimising false alerts and the filters must optimise turbulence rejection while giving a timely response to a windshear condition.

One of the problems of choosing the best hazard criterion is in defining the characteristics of hazardous windshear to use as a reference. This has been achieved to some extent in this analysis by considering the effects of wind on an aircraft and defining bandwidths for the wind hazard. A study conducted to evaluate methods principally intended for ground-based and forward-looking windshear detection systems provides an alternative approach to evaluation of the relative merits of different forms of hazard criteria. [75]

The evaluation was achieved by simulating the dynamics of a piloted aircraft flying several different approach trajectories through a modelled microburst windfield. An approach degradation factor was defined as being the root mean square of the sum of non-dimensional values related to the deviation of the flight path below the glideslope and the airspeed loss relative to the stall speed, and this factor was integrated over the whole approach to give an overall 'microburst impact' factor for that approach. Five different hazard criteria were defined and these were intended to assess the criteria used by such systems as the Terminal Doppler Weather Radar and forward-looking airborne windshear detection as well as those for reactive systems; they comprised:

1. Total Divergence - the headwind-to-tailwind shear, measured along the glideslope.

2. Mean Shear - total divergence divided by the distance between the headwind and tailwind peaks.

3. The Peak F-factor.

4. The largest F-factor exceeded for a given distance, using distances from 1500 feet to 6000 feet.

5. The largest mean F-factor over a given distance, using distances from 1500 feet to 6000 feet.

The value of each of the hazard criteria was evaluated for the approaches. The correlation with the microburst impact factor was calculated and this was then taken as a measure of the effectiveness of the criteria in determining a hazardous windshear.

The criteria which showed the best correlation were the mean shear, the largest F-factor exceeded over 1500 and 3000 feet, and the largest mean F-factor over 4500 feet. The last two criteria are intended primarily for forward-looking airborne systems but because the reference distance can be related to a reference time period at a given aircraft velocity, these methods could also be applied to reactive systems. Distances of 1500 to 3000 feet would relate to time periods of between five and fifteen seconds for a typical range of transport aircraft speeds. The F-factor exceedance criterion would be implemented by setting a threshold for the F-factor and triggering an alert if this were exceeded for the whole of the reference distance (or time). In contrast, the largest mean F-factor criterion is analogous to the method recommended in reference 31 and used in the F-factor analysis in Section 6.3.3. From the results in the reference it would seem likely that a method analogous to the F-factor exceedance criterion may yield an improved performance.

The mean shear criterion gave the best correlation of all the methods but the divergence alone gave the worst. This was accounted for by the fact that the divergence method measures only the along path component of the shear, i.e. the x-axis wind, whereas the mean shear method measures the rate of shear, and this is a better indication of the effect of the wind on the aircraft. In addition, because continuity of mass applies to the airflow, it was argued

that the rate of headwind change gives some measure of the magnitude of the downdraft. The wind change criterion tested in Section 6.4.4 measure the change in both components and to take account of the rate of shear to some extent by defining the bandwidth and roll-off characteristics of the method at high and low wind frequencies. It would seem likely, therefore, that the wind change criterion may relate more closely to the results from the mean shear method than those for total divergence. A similar study to test this criterion would not only indicate whether this is correct, but could also assist in defining a factor to relate the x-axis and z-axis wind change threshold. This could be achieved by varying the factor to optimise the correlation.

The study in reference [75] took no account of the time taken by the hazard assessment algorithm to perform the evaluation and long averaging periods will cause a delay in the alert, as observed in the tests of Section 6.4.4. For a reactive detection system this is of the greatest importance. In addition, the computational intensity of each algorithm and, therefore, the time taken to perform the evaluation, is an additional factor which must be considered when selecting the most appropriate method for any real-time system.

Finally, reference [75] makes no attempt to define the threshold levels for each criterion, as these would depend on the type of aircraft for which the system is being designed. A hazardous windshear could be defined in a similar way to the approach degradation parameter viz. in terms of the induced flight path and airspeed deviations, and the optimum threshold levels could then be found using similar simulation techniques.

6.6 Thresholding Levels for the Cessna 402B

The task of defining suitable hazard criteria and threshold levels for use in a windshear detection system for general aviation aircraft is a subject for study and verification as discussed in Section 6.5. The evaluation of the detection system performance need not be dependent on these threshold levels because an assessment can be made by comparing the alerts provided by the detection system with those generated by applying the same criteria to the wind profile itself. Nevertheless, it would be useful to set some more realistic thresholding levels than those defined for transport aircraft which were used in the earlier tests.

Various parameters describing the flight dynamics of the Cessna 402B for the different flight phases are given in Appendix B. Further information relating to the Cessna 402C, which is similar in performance to the 402B, can be derived. [76] The relevant performance data derived from these sources are given in Table 6.1.

Table 6.1: Cessna 402 Performance Parameters

sea-level take-off airspeed	110 knots(184 ft/s)
sea-level climb airspeed	126 knots (211 ft/s)
sea-level approach airspeed	96 knots (160 ft/s)
stalling speed (flaps up)	78 knots (130 ft/s)
stalling speed (flaps down)	68 knots (114 ft/s)
max. rate of climb at sea level	1450 feet/min (24.2 ft/s)

The difference between the approach speed and the stall speed (flaps down) is only 28 knots and so suitable thresholds for this aircraft must be significantly lower than the 20 knot wind speed change threshold for transport aircraft.

The threshold level could be defined by considering the airspeed margin alone, or by examining the effect of the winds on the rate of climb - the performance margin from which the F-factor is derived.

The effect of wind on an aircraft's rate of climb can be derived directly from equations 2.13, 2.20, 2.23 and 2.24 as

$$\Delta\dot{h} = \frac{U\dot{u}_g}{g} + w_g \qquad (6.21)$$

where $\Delta\dot{h}$ is the change in the aircraft's rate of climb and U is the true airspeed. The ratio of airspeed to g, lies between 3.5 and 6.5 for the Cessna 402B at low altitude using the airspeed values in Table 6.1.

If the change in the rate of climb induced by the wind is equivalent to the maximum rate of climb of the aircraft of 24.2 ft/s (1450 ft/min), then the aircraft will not have sufficient power to climb and escape the shear. This occurs for z-axis winds of magnitude 24.2 ft/s (14.4 knots) or for x-axis rates of change of wind of between 2 and 4 knots/s.

For the purposes of windshear detection thresholding, a hazardous windshear condition could be described as one which severely restricts the aircraft's ability to climb for more than a few seconds. If the detection threshold were set when the potential rate of climb had reduced to zero the pilot would be unable to trade airspeed for altitude and so the warning would be too late. A further related requirement therefore is that the threshold must allow an airspeed margin above the stall airspeed.

A 10 to 20 knot wind speed change is induced by a rate of horizontal airspeed change of 2 to 4 knots/s for five seconds, during which time the aircraft's potential rate of climb is reduced to zero. Rates of change of wind speeds of such magnitude reduce the aircraft's stall margin to between 8 and 18 knots on approach. An x-axis wind change threshold of between 10 and 15 knots is likely to provide a reasonable setting for the hazard criteria, and a level of 12 knots is chosen for the remaining work. The z-axis threshold for each hazard evaluation method can be calculated using the methods of Section 6.4.

6.7 Warning Methods

6.7.1 Warning Requirements

The warning system is required to alert the pilot to an event requiring his immediate attention, to enable him to understand rapidly that windshear has been detected and, if possible, to initiate an appropriate reaction. The following section discusses the 'human factors' or ergonomic implications of the design of the warning system.

A pre-requisite of the design of the warning system is that an alert is only given when there is a significant hazard. A system which provides an alert during benign conditions will cause a pilot to lose confidence in the system and, as a consequence, the pilot may hesitate to respond to a genuine warning until he has assessed the credibility of the alert. The early GPWS systems suffered from this effect, with as many as 65% of the warnings provided before 1982 having subsequently been found to be false alarms, in that no significant hazards were present. [77] The lack of pilot confidence in the early designs of the LLWAS system, described in Chapter 3, was also caused by high false alarm rates.

A pilot receives information on his situation from visual, aural, kinesthetic (motion) sense and tactile cues in that order of significance. [14] Of these, the two practical forms of presentation of a windshear alert are through vision and hearing. These could be used individually or in combination to provide a warning. There are two conflicting theories on the most suitable form of message to reduce the pilot's distraction from the primary task. Stimulus - central processing - response compatibility theory suggests that if the form of the warning, the task and the response are similar the performance will be increased, and so, for example, a warning which affects an aircraft system and requires a physical response should be presented in a spatial, visual form. In contrast, multiple resource theory suggests that several independent resource 'pools' exist and performance will be degraded only if tasks share the same pool. The primary flight task is essentially a visual and spatial process of controlling the aircraft and so a verbal alert is less likely to cause a resource conflict than a visual warning. The aim in designing the warning system is to minimise the response time without distracting the pilot from essential tasks. Studies carried out on the response time following visual and vocal warnings show conflicting results but in general suggest that a concise aural alert produces a faster response time. [14, 78, 79] The implications of both visual and aural alerts are discussed below.

6.7.2 Visual Alerts

A visual display can be used to draw the pilot's attention to a situation. A visual alert provides spatial information relevant to the nature of the alert; for example, in the case of an engine fire, a schematic of the aircraft showing the location of the malfunction and a symbol representing fire may convey the warning clearly and concisely. A second example of the use of visual warnings is provided by the forward-looking windshear detection systems which were described in Chapter 3. The location of the windshear is shown on a CRT display in the weather radar format familiar to the pilot. The hazardous area is shown by red bars across that part of the map which enables the pilot to quickly assess whether evasive action is required.

For a reactive windshear detection system the aircraft will have already entered the windshear when the alert is triggered and the required response from the pilot will always be the same viz. to maximise the rate of climb of

the aircraft and fly out of the windshear. Although it is possible to show the required reaction visually in some form - some existing systems for transport aircraft, for example, have a pitch director to aid the pilot in optimising the pitch angle while avoiding stall - the added requirements and processing would be impractical for a low-cost general aviation instrument, as well as requiring recurrent pilot training.

A visual warning in the form of a warning light could be used to draw the pilot's attention to the windshear condition. By convention, aircraft alert lights have three colours depending upon their level of urgency. Those of high urgency which demand immediate pilot attention are coloured red. Alerts which are cautionary in nature, warning of a situation which may become hazardous, are amber and advisory alerts, the lowest priority, are coloured green. Although it has been shown that the human eye is most sensitive to colours in the mid-range of the visual spectrum, i.e. blue/green rather than those at the periphery such as red/orange shades, the convention is so well established that it remains the standard. [77] A red warning light could be used, therefore, to give a visual windshear alert. The optimum location for the light would be in the instrument panel close to the altimeter, airspeed and vertical speed indicators.

6.7.3 Aural alerts

An aural alert has the advantage that the warning is not directional and so the pilot is alerted irrespective of his eye position, and no change in his gaze is necessary to receive the alert. The disadvantages are that the aural alert may distract the pilot's attention and, especially in the case of a vocal alert, it may interrupt other communications and cause 'auditory clutter'. This situation is less likely to arise in a smaller general aviation aircraft than in an aircraft with a larger flight crew. [14]

A warning can be provided to the pilot either in the form of a tone which the pilot could be trained to identify as a windshear alert, or as a vocal warning. Warning tones are the longest established forms of aural alert with bells, buzzers and horns being sounded for different hazardous situations; but vocal alerts have become increasingly popular following the rapid advances made in speech synthesis technology over the last two decades. The tone has the advantage that it need not mask other communications, but it requires

memorising so that the alert can be associated with the relevant hazard. As general aviation pilots have little recurrent training and a windshear encounter is a rare event, the significance of the tone could easily be forgotten unless the tone was made familiar by providing a sample alert. This could be provided during system initialisation and the possibility of doing this is discussed further in Chapter 7. Even with reminders of the warning tone, the pilot must still mentally process the sound to associate it with the hazard which may occur during take-off, approach or landing phases of flight when the workload is already high. In contrast, a vocal alert can be much more informative about the hazard so that the mental processing is reduced.

The most suitable forms of tone for a cockpit alert have been investigated and the results suggest that a warning should have the following characteristics. [80] It should be sufficiently loud so that it can be clearly heard above the ambient cockpit noise but it should not be so loud that it startles the pilot. The recommended sound level is 15 dB to 25 dB above the ambient cockpit noise, with the more urgent alerts having louder tones. The optimum form of sound was considered to be a series of pulses of differing formats. The rise times of these pulses would be limited so that the pilot would not be startled by a sudden noise and the recommended duration of each pulse was between 100 ms and 150 ms to enable the pulses to be perceived but prevent the interruption of other auditory communications. The time intervals between the pulses should be designed to provide a unique sound with an urgent alert having closer pulse spacing. The fundamental frequencies of the tones should be designed to take account of the hearing ranges of typical pilots.

Vocal alerts provide a message to enable the pilot to quickly identify the problem. The information conveyed must be concise as a speech message is conveyed in a serial format and almost the whole message is usually required before it is understood. It has been shown that long messages are both inefficient in time and may easily be forgotten, at least in part, during a high stress situation. [81]

A vocal warning can be given from a recording of human speech, by means of a digitised speech message or as synthesised speech. Pilots are found to prefer synthesised speech to the other two forms, provided that it is

intelligible. The speech need not sound natural, indeed, a synthesised speech message is not confused with other crew and radio communications; it is recognised as a 'system' message and this provides a cue to the nature of its contents. [14] The response to a synthesised message has been found to be faster than a message spoken by a person.

The factors to be considered in designing a system using synthesised vocal message include the method of speech synthesis, speech rate, vocabulary, pitch, volume and signal to noise ratio. If the synthesised speech is not sufficiently intelligible the listener is focuses on understanding each word and the comprehension of the whole message deteriorates. Developments in speech synthesis during the last decade have enabled each phonetic element of the message to be controlled for both pitch and speech rate and this form of speech generation has been found to be effective in the cockpit environment. Airline pilots have found phonetic synthesised speech to be equal to, if not better than, Air Traffic Control radio communications. [75]

The rapid increase in the use of synthesised speech in the cockpit has prompted several studies into the design and implementation of vocal alerts, which have helped to identify desirable features of these systems. Tests are carried out on subjects who are performing a primary task, and for which the response to the warning is a simple secondary task. In most cases the experiment was designed using standard flight-combat computer games as the primary task: these provide the subject with a relatively high workload which corresponds with the more intense flight phases. The response to the message was usually acknowledged by a simple action from the pilot such as pressing a selected button. The testing methods assumed that the response to the warning was a secondary task whereas a windshear alert requires an immediate change in the primary (flight control) procedure. Nevertheless, the pilot must still comprehend the alert during a period of high workload and so the investigations into the comprehension and reaction time of the subjects are likely to yield useful conclusions for a windshear situation despite the difference in the required response. The method of calculating the response time varied, with some researchers using the time from the end of the message until the initial pilot response, known as the comprehension time, and others using the time from the onset of the message until the pilot's first reaction, the 'system' time. The second method is most relevant for the design of a warning system as it measures the overall time from when an

alert is triggered. In addition, the comprehension time is only representative if it is assumed that the subject does not assimilate any of the message while it is being received.

The form of the message was found to be important. The message could be in the form of keywords or a partial sentence, and these formats differ in their linguistic redundancy. The tests investigated the effect of this redundancy on the response time of the subjects. [81] The results showed that a polysyllabic keyword format produced a faster response, which is consistent with the concept that a shorter message reduces the requirements on the short-term memory and so is easier to retain under a high workload. Also some subjects considered a shorter message to sound more urgent. An optimal length was found to be four or five syllables, with messages shorter than this being less intelligible.

The effect of speech rate has been investigated using three different rates of 123, 156 and 178 words per minute. [78] The results showed that a faster speech rate gave a faster system time. Subjects expressed a preference for the moderate rate of 156 words per minute and said that the faster rate was less intelligible, although there was no degradation in performance. The slowest rate was found to distract the subjects from the primary task.

The pitch of the voice was also tested in the same study. Early speech systems used a higher-pitch female voice, but research conducted subsequently has shown that the pitch, or apparent sex of the speaker, has no perceived effect on either intelligibility or user confidence. However speech with a higher pitch than other messages can convey a greater urgency.

In all the tests the subjects were given time to familiarise themselves with both the primary task and the warning responses separately. Initial sessions enabled the user to become familiar with the messages and it has been found that familiarity with a warning greatly increases intelligibility. [14, 78, 81, 82] As a windshear warning will be rarely heard, provision must be made for the general aviation pilot to familiarise himself with the message.

6.8 Warning System Design

The ergonomic factors described in Section 6.7 can help to define the most suitable form of alert. A complex visual warning system giving guidance to the pilot is not feasible for a simple, low-cost system. However, a visual alert using a red warning light identifiable as a windshear warning would be possible.

The design of an aural alert could be based upon observations from the studies and these suggest the following requirements. The aural alert should be a phonetic synthesised voice providing a message of four to five syllables in length which should include polysyllabic words. The pitch should be selected to give a sense of urgency to the speech and the rate should be approximately 156 words per minute to optimise the response rate.

The form of the message is more difficult to define; the alert could be composed of a simple message 'Windshear Windshear' or could include further information such as 'Windshear Thirty Knots Tailwind Change'. The research suggests that it is necessary to provide sufficient information for the pilot to make a full assessment of the situation but that excess information is not helpful and can reduce performance. The pilot is required to respond immediately to the alert by climbing out of the windshear. Any details of the shear strength could therefore be considered superfluous as they do not contribute significantly to the task of optimising the rate of climb of the aircraft. The message would inevitably be longer and so is likely to be less comprehensible and may cause the pilot to hesitate while assessing the situation. A further alternative would be to include basic advice viz. 'Windshear Windshear Climb Climb' to remind the pilot that he should attempt to maximise the altitude at the cost of airspeed. This message and the simple alert 'Windshear Windshear' both conform closely to the ergonomic requirements of a warning system with the former being more likely to provoke the correct response whereas the latter is more concise. The message which results in the fastest reaction time and most suitable pilot response could be found using similar research techniques to those described in Section 6.5.

A combination of a red warning light and a synthesised message would allow for the advantages of both systems at the cost of some added

distraction of the pilot. As both alerts would be relatively simple and the requirement to draw attention to the situation is urgent, the advantages of a combined system are likely to outweigh the disadvantages. This concept is given support by the Technical Standard Order (TSO) for reactive windshear detection systems on transport aircraft. [31] On detection of a windshear a message 'Windshear Windshear Windshear' is required together with a red warning light labelled 'windshear' which remains lit for the duration of the shear or for three seconds, whichever is greater.

The TSO also allows for a cautionary alert if an abnormal performance enhancing shear is encountered, but this is not mandatory and is at the discretion of the system designers. This is displayed visually as an amber warning light and an aural alert may be provided. The merits of a cautionary warning are a topic for debate. A caution may provide an advanced warning of a shear condition, for example, when an increasing headwind component in encountered by an aircraft on entering a microburst, and will increase the alertness of a pilot to a potential windshear, but it may not be followed by a performance-degrading shear and so may simply distract the pilot and reduce the credibility of the system.

6.9 Summary

The windshear detection system must evaluate the wind conditions and establish the degree of hazard. A dangerous wind cannot be determined solely by examining the magnitude of the wind as the frequency distribution must also be taken into account. The analysis of Section 6.2 considered the effect of winds of different frequencies acting on the aircraft and found that windshear with periods of between five and sixty seconds were most dangerous to general aviation aircraft, based upon the response of the Cessna 402B.

Three methods of evaluating the windshear hazard were discussed. One method, the 'wind change' method, considered the change in both the x-axis and the z-axis wind components and derived a detection criterion based upon the magnitude of the changes at different frequencies whereas the 'performance margin' method was a simple technique based upon the effect of the wind components on the aircraft's energy. These criteria were tested together with the criterion required by the FAA for airborne windshear

detection systems for transport aircraft. The time at which an alert was provided by the three criteria was tested using two windshear profiles. The wind change criterion and the F-factor method produced comparable results but the performance margin method was slower to provide an alert.

The level of windshear which is hazardous to general aviation aircraft was derived from the performance data of the Cessna 402B. A x-axis wind change of 12 knots was considered to be a suitable threshold level. The z-axis threshold related to this value differs depending on the criterion used for the hazard evaluation.

The method of providing an alert to a pilot was discussed in Section 6.7. The human factors affecting the choice of warning method were reviewed and used as a basis for the selection. A warning system with both an aural and visual alert was chosen. The aural warning provides the pilot with a synthesised vocal message; the messages 'Windshear Windshear' and 'Windshear Windshear Climb Climb' were both considered to be feasible alternatives. The visual warning is in the form of a red light labelled 'Windshear' and mounted on the instrument panel close to the instruments most relevant for a windshear escape manoeuvre.

7 THE WINDSHEAR DETECTION SYSTEM

This chapter examines the performance of the proposed windshear detection system by combining the wind estimation and hazard evaluation methods. It then considers other operational requirements which are important for an airborne windshear detection system. Possible methods of implementing the system are then described before the research which has been described in this dissertation is summarised. Further aspects of the research are then discussed. Conclusions are drawn from the results described here and, finally, suggestions are made for further work which would assist in the development of the system.

7.1 Evaluation of the Windshear Detection Method

The method for detecting windshear comprises both the algorithm which estimates the components of wind acting on the aircraft and the hazard evaluation for determining whether the wind conditions constitute windshear. In Chapter 6 the hazard criteria were shown to perform well when they were verified using actual windshear components; however, the performance of the system with estimated wind components, derived from the estimation algorithm, also requires testing.

Wind estimation and hazard evaluation algorithms were tested using simulation. The wind conditions used for these tests were the JFK and DFW windshear profiles. These should cause a warning to be generated. Moderate levels of turbulence should not cause the system to produce false alerts and this was also tested using the Dryden model. The aircraft was simulated at the four different low-altitude flight conditions described in Chapter 5, so errors caused by any mis-matching of the modelled dynamics would be present in the estimation process. The errors which may arise from sensor inaccuracies, which were also discussed but not quantified in Chapter 5, were not included.

For the results generated in Chapter 6, the value at which the warning threshold was activated was set at 20 knots for x-axis wind speed change (or the 'equivalent' value for a combination of x-axis and z-axis winds). (The corresponding z-axis wind was defined differently for each of the three hazard criteria.) However, in Section 6.6, a 12 knot x-axis wind speed

change, or its equivalent, was considered to be a more appropriate threshold for general aviation aircraft. This revised value was used for the performance evaluation of the whole system.

7.1.1 Combination of Wind Estimation and Hazard Evaluation Methods

When the wind estimation method designed in Chapters 4 and 5 is combined with the hazard criteria established in Chapter 6 there is some redundancy in the system. Low-pass filtering was applied to the z-axis wind estimate to reduce transient errors introduced by the effect of the pitching wind component. However, the estimates of the wind components are passed through low-pass filters, or an averaging process, as the initial stage of the hazard evaluation to restrict the bandwidth of the wind to that considered to be hazardous. These stages serve, therefore, similar purposes in rejecting the high frequency components of the wind.

The low-pass filter at the output of the z-axis wind estimate and the restriction of the bandwidth at the input of the z-axis wind hazard evaluation were compared. It was found that both the Butterworth filter and the averaging methods used to reject turbulence also served to reduce the transient error, and so the additional filter on the z-axis component in the estimation stage was superfluous. The filter was removed from the simulation and the results in this chapter were obtained by feeding the unfiltered z-axis wind estimate directly into the various thresholding criteria.

7.1.2 JFK Windshear Profile Tests

The JFK windshear profile was passed through both stages of the system viz. the wind estimation and the hazard evaluation algorithms. The wind profile acting on the aircraft was the same for every flight condition: no adjustment was made to account for the differing airspeeds of the aircraft at each flight condition and, hence, for the duration of the encounter. The estimated wind components generated by the estimation algorithm, which are the same as the components shown in figure 5.7, were passed through the hazard evaluation algorithm and the time at which an alert was provided was recorded.

Although the time history of the wind input is the same for each flight condition, the airspeed value varied. This parameter was used in the calculation of both the F-factor and the performance margin hazard criteria and it was expected that a change in the flight condition would produce some change in the time taken to produce a warning using these methods.

The results of the simulations for each of the hazard criteria at each flight condition are tabulated in Tables 7.1 and 7.2.

Table 7.1: JFK Windshear - Time to alert using estimated winds (in seconds)

Hazard Criterion	Flight Condition			
	S.L. Take-off	S.L. Climb	Climb 5000 ft	S.L.Approach
F-Factor	-2.1	-2.2	-2.2	-2.2
Perf. Margin	-0.6	-0.6	-0.6	-0.8
Wind Change	-1.5	-1.7	-1.8	-1.8

Table 7.2: JFK Windshear - Time to alert using actual winds (in seconds)

Hazard Criterion	Flight Condition			
	S.L. Take-off	S.L. Climb	Climb 5000 ft	S.L.Approach
F-Factor	-2.3	-2.3	-2.3	-2.3
Perf. Margin	-0.9	-0.8	-0.8	-1.0
Wind Change	-2.4	-2.4	-2.4	-2.4

In Chapter 6, the performance of the hazard evaluation algorithm with the actual JFK wind components and using a 20 knot x-axis wind change threshold was shown in figure 6.12, for a flight condition representing take-off at sea-level. By comparing the results for the sea-level take-off flight condition in Table 7.2 with those shown in figure 6.12, the effect of the change in threshold on the time of alert can be seen. The change from a 20 knot x-axis wind change threshold to 12 knots has produced only a very small improvement of between 0.5 and 1.5 seconds in the timing of the warning: for this particular profile, both wind components change very abruptly to performance-decreasing conditions.

When the performance of the system using the estimated wind components in Table 7.1 is compared with the results in Table 7.2 using the actual wind profile, it can be seen that the errors in the estimation produce, in general, only a minimal change in the timing of the alert. The severe and sudden

changes in the wind components causes the timing of the alert to be less susceptible to small inaccuracies in the wind estimates thereby producing only small differences. The largest difference of 0.9 second is produced for the flight condition representing take-off at sea-level when using the wind change criterion and is likely to be caused by the oscillatory error in the estimation reducing the apparent change in the z-axis wind component.

A comparison of the performance of the three hazard criteria shows that the performance margin method is consistently slower in providing an alert than the other two methods. The F-factor provides the earliest warnings being up to 0.6 seconds ahead of the wind change criterion.

The variation in the alert times of the performance margin criterion at different flight conditions see in Table 7.2 is caused by the variation in airspeed. The z-axis wind hazard is calculated as a function of the airspeed for both the performance margin and the F-factor hazard criteria, although it does not appear to affect the F-factor results in this case.

7.1.3 DFW Microburst Tests

The detection system was also tested with the DFW microburst model, described in Section 2.3.4. In contrast to the JFK simulations, the differences in the timing and duration of the encounter, caused by the different airspeeds, were taken into account. The time scale of the wind profile varied for each of the flight conditions - a lower airspeed caused the wind encountered by the aircraft to be lower in frequency and of longer duration.

The times taken for the system to generate an alert from both the estimated and actual wind profiles and for each flight condition were generated using the same method used for the JFK windshear tests. The results are shown in Tables 7.3 and 7.4.

Table 7.3: DFW microburst - Time to alert using estimated winds (in seconds)

Hazard Criterion	Flight Condition			
	S.L. Take-off	S.L. Climb	Climb 5000 ft	S.L.Approach
F-Factor	-33.6	-28.5	-25.9	-40.3
Perf. Margin	-31.5	-26.2	-23.7	-38.5
Wind Change	-35.1	-30.4	-27.5	-42.7

Table 7.4: DFW microburst - Time to alert using actual winds (in seconds)

Hazard Criterion	Flight Condition			
	S.L. Take-off	S.L. Climb	Climb 5000 ft	S.L.Approach
F-Factor	-34.5	-29.1	-26.4	-40.8
Perf. Margin	-32.4	-26.9	-24.2	-38.6
Wind Change	-35.4	-30.2	-27.7	-41.4

By comparing tables 7.3 and 7.4 it can be seen that the times taken to provide an alert using estimated wind components are very similar to the alert times resulting from the use of the actual DFW profile. The errors in the estimation of the wind components produce delays in the alert time of up to 0.9 second. The timing differences produced by the simulation of take-off at sea-level are significantly larger, however, than those generated using other flight conditions.

Once again, the performance margin hazard criterion shows the slowest alert time. The F-factor and wind change algorithms vary in their timing of alerts by up to 2.4 seconds. For this profile the wind change algorithm provides a warning consistently earlier than the F-factor method.

7.1.4 Dryden Turbulence Tests

It is important that the detection system does not generate false alarms, i.e. provide an alert, when the wind conditions are not hazardous. The Dryden turbulence model was used to confirm that the hazard evaluation criteria do not respond to this form of wind condition when it is injected into the system at the specified, non-hazardous intensities. In order to verify the operation of the whole system, the hazard evaluation algorithm had to be tested using the wind components obtained from wind estimation algorithm.

The detection system was tested again therefore, but with turbulence acting on the aircraft. The threshold level for generating a warning had been reduced from 20 knots x-axis wind change to 12 knots and so the Dryden gust amplitude was reduced in proportion, by scaling the output of the turbulence filters described in Appendix B. As the parameters defining the turbulence characteristics are described as functions of both altitude and

airspeed the form of the turbulence generated differed for each flight condition.

The turbulence was injected into the estimation system and the estimated components then passed into the hazard evaluation algorithm. A total duration of 360 minutes of turbulence was applied at each flight condition but no alerts were generated by any of the hazard criteria.

Further tests were performed for each flight condition to establish the margin in the warning threshold. The maximum threshold level which could be used before an alert was generated was tested over a 360 minute duration using each flight condition. The threshold values were compared and the worst case was found to be 17 knots for the condition representing take-off at sea level. This allows a margin of 40% of the design threshold of 12 knots for any further errors resulting from sensor errors and the system implementation.

7.1.5 System Performance

The hazard evaluation algorithms seemed to perform satisfactorily when tested using the estimated wind components: all gave alerts within a similar time and none was susceptible to turbulence. However, the performance margin algorithm was consistently slower in providing an alert than the other two methods. The thesholding of the x-axis wind is identical for both the performance margin method and the wind change method and the difference must arise, therefore, from the method of assessing the z-axis wind hazard. The ten second moving-average filter used in the performance margin method to reduce the z-axis wind bandwidth is the cause of the delay, and the alert time could be improved by reducing the averaging period.

All the hazard evaluation methods filter the wind components to reduce their bandwidth either directly or indirectly using averaging techniques. The low-pass filters reduce the susceptibility of the system to generating false alerts from turbulence, but they also introduce a time lag in the estimated wind component which delays the time at which an alert is provided. The time variances produced by differing cut-off frequencies are of the order of seconds and can, therefore, be significant for this system. The warning

system must be optimised to obtain the best compromise between the time to alert and the rejection of false alarms.

7.2 The Operation of the Windshear Detection System

The wind estimation and hazard evaluation algorithms are the principal constituents of the windshear detection system and these have been discussed in some detail in the preceding chapters. The method of operation of the whole system is now considered.

7.2.1 Warning Envelope

The detection system is required to operate at altitudes of less than approximately 1000 feet to provide warnings of windshear during the take-off, climb, approach and landing stages of flight. Although these phases of flight could be associated, in general, with the periods of flight at lower airspeeds, the limits of operation of the system can be determined more accurately by other means.

One method, used by other airborne detection systems, is to restrict the warning envelope to those phases on take-off and landing when the flaps are extended. This method has the advantage that it is relatively simple and avoids the problems of inaccuracies in the wind estimation while the flaps are in transit, but the activation of the detection system is not directly related to the aircraft's altitude.

Alternatively, the use of airspeed and altitude enables the system to begin calculating the windshear hazard once the airspeed has exceeded the rotation speed of the aircraft (the pitch rate sensor could also be used to ascertain when rotation is completed), and to suppress the windshear detection when the altitude has changed by 1000 feet from its initial value after take-off. Limits for warnings during landing are more difficult to determine as the altitude of the landing runway cannot be assumed to be the same as that of the take-off runway and the barometric pressure at the landing runway, set by the pilot on the altimeter, is unlikely to be available as a signal to the system. However, by combining the trends of both airspeed and altitude it may be possible to estimate the flight phase, and this could then be used to limit the warning function.

7.2.2 System Initialisation

Sensors for use in the detection system were considered in Chapter 5. The parameters used in the algorithms were derived from the sensor measurements and it was perceived that the errors in these parameters could be significantly reduced by initialisation. The pitch rate measurement is initialised while the aircraft is stationary to determine the offset and, possibly, any drift characteristics. The other sensor measurements are initialised as the wind hazard calculation begins after the aircraft has rotated. The mean value of each of the parameters, measured over a short interval, immediately after rotation is used as the initial estimate of the trim value.

The sensor signal conditioning and compensation, and extraction of the small perturbation values all continue to operate throughout the flight, although the sensed parameters are not passed through the wind estimation algorithm unless the aircraft is within the warning envelope.

7.2.3 Self-Test Function

Windshear is a rare event and a pilot is unlikely, therefore, to ever experience a windshear warning. A self-test function, which allows the algorithm and warning method to be tested while the aircraft is on the ground, enables a pilot to confirm that the system is operational and to become familiar with the warning message. This is achieved by passing digitally stored windshear components through the windshear detection and evaluation algorithm and checking that appropriate alerts are provided.

7.3 Summary of Research

7.3.1 The Windshear Hazard

Windshear is a sudden change in the wind velocity which can adversely affect the aircraft flight path. A departure from the intended flight path is particularly hazardous to aircraft when they are in the low-altitude phases of flight viz. take-off, climb, approach and landing.

An examination of an aircraft's dynamics shows that it is most susceptible to changes in the wind component which acts along the x-axis of the aircraft, as a headwind decrease or tailwind increase initially causes a corresponding

loss in airspeed and, unless control action is taken, this can result in a significant loss in altitude. A performance-decreasing wind change along the z-axis can also be hazardous for this causes the aircraft to sink steadily, unless the effect is compensated. A lateral wind, which acts along the aircraft's y-axis, affects the heading and requires control from the pilot, although it has little effect on altitude and is, correspondingly, less hazardous.

Windshear can be generated by a variety of weather conditions. It is the small-scale, localised weather phenomena which are most dangerous as these are difficult to predict and detect. The microburst is a particularly hazardous form of windshear, being short-lived and very localised; it is a phenomenon which has resulted in several major accidents in recent years. An encounter with a symmetric microburst initially causes an increase in headwind which results in the aircraft rising above the intended flight path, but it is then followed by a downflow of air and a decreasing headwind component, both of which reduce the performance of the aircraft. A pilot who is unaware of a windshear situation may initially attempt to regain the original flight path by reducing the aircraft's height, only to experience difficulties when the later stages of the microburst are encountered. There are differing philosophies about whether pilots should be warned when performance-increasing windshear are encountered. Provision of a warning under these conditions is likely to increase the number of false alarms generated by a detection system, but would be advantageous in providing a significantly earlier warning for the microburst situation described here.

Pilots are trained to identify weather conditions in which windshear may be present. The recommended action is to avoid all windshear, as some shears are too severe for an aircraft to successfully penetrate when flying at low altitude. An inadvertent encounter with a windshear requires abnormal piloting techniques. A pilot usually attempts to control the flight path by maintaining airspeed whereas in a windshear situation it is the altitude which must be maximised by allowing the airspeed to reduce. The approved action, albeit controversial, is to pitch the aircraft to an angle a little below the stall angle and to maximise thrust.

A windshear encounter is characterised indirectly in the changes in the airspeed, altitude and vertical speed. However, windshear can only be

identified by a combination of these effects and it may take some time for the pilot to recognise the trends that are associated with them. It has been found that an early recognition, sometimes by as little as a few seconds, can significantly improve the survivability of the windshear event, and this has led to the development of airborne systems specifically for providing a warning of windshear.

7.3.2 Windshear Detection

Both ground-based and airborne windshear detection systems are now deployed. Ground-based systems are located on or near airports and provide a warning to aircraft in the vicinity if hazardous windshear is found. The original system was the Low-Level Windshear Alert System (LLWAS) which used anemometers to measure wind speed and direction at different locations around the airport. This has been developed to improve its ability to recognise microbursts, but its capability is limited to the detection of these events on the airport site and at ground level. A better system uses Doppler radar techniques to scan the atmosphere around and above the airport for adverse wind conditions, but this method is in use at only a limited number of sites, principally because of the cost of such systems.

Airborne detection systems are now installed on all transport aircraft in the USA with more than thirty seats. These systems are reactive, i.e. they measure the response of an aircraft to its environment, in order to ascertain whether windshear is present. The wind acting on the aircraft is evaluated in a dedicated unit by comparing the inertial and air-relative motion of the aircraft using measurements from the Inertial Reference System and Digital Air Data Computer which are installed on this class of aircraft.

Forward-looking detection systems which measure the characteristics of the air ahead of the aircraft to determine whether there is a hazard are becoming available. Doppler radar and lidar technologies measure the motion of the wind along the x-axis of the aircraft directly. Radar techniques are the most advanced and the first detection systems of this type are now being fitted to aircraft. They provide an advanced warning up to ninety seconds ahead of the encounter; however, their performance is reduced in dry conditions. Forward-looking infrared (FLIR) systems measure the temperature at two locations in the atmosphere ahead of the aircraft to determine whether a

temperature change of a magnitude which is characteristic of a windshear is present.

General aviation aircraft are also susceptible to windshear and their response to wind varies from transport aircraft. The principal differences arise because they fly at lower speeds and so have a correspondingly lower speed margin. General aviation aircraft traverse the shear more slowly and this means that they are more sensitive to the z-axis wind component. Although there are few records of general aviation accidents caused by windshear this is likely to result from the inability to positively identify such causes rather than their lack of occurrence - general aviation aircraft are not required to carry flight data recorders. The general aviation pilot, in general, flies fewer hours, has less flying expertise and receives less recurrent training than a commercial airline pilot. However, the total hours flown annually by all general aviation pilots greatly exceed those of transport aircraft pilots. There is, therefore, a requirement for an airborne windshear detection system suitable for this class of aircraft.

The windshear detection systems already described are not economical for general aviation use. The forward-looking sensors are only viable for large transport aircraft and the reactive units require costly inertial and air data systems. A system for general aviation aircraft must use a minimum number of sensors in order to minimise the cost. The utilisation, where possible, of sensors already installed on the aircraft for other purposes is desirable. Although there is unlikely to be many available signals on aircraft that are currently operational, the increased use of solid-state sensors and microprocessor-based systems means that sensor output from other instrumentation may become more easily available in the future. Meanwhile, low-cost additional sensors can be installed for windshear detection purposes.

7.3.3 Methods for Wind Estimation

Techniques based on the theory of observers can be used to estimate an unknown state vector provided that the vectors describing the input and output of the system are known. These techniques were adapted to attempt to estimate the x-axis and z-axis components of wind acting on an aircraft using knowledge of a limited number of flight parameters and the control

inputs. The technique used an observer to estimate the air-relative x-axis and z-axis wind velocities and an aircraft 'model' to derive the corresponding inertial velocities, from which the wind components could be derived.

Results obtained by simulation when only one state variable, the pitch rate, was measured showed large errors in the estimations. These errors were found to be caused by transient errors in the observer. A method of compensating for the transients was devised, but was not effective because it relied on the feedback of the estimated inertial x-axis velocity which was itself inaccurate.

Measurement of a further aircraft flight parameter was incorporated into the estimation algorithm. Both velocity and airspeed were considered to be suitable parameters because they could be measured with relatively simple sensors. When the effects of only the x-axis and z-axis winds were simulated accurate estimates of these components were obtained using either pitch rate and heave velocity or pitch rate and airspeed as the measured aircraft parameters. However, the estimates were degraded when the pitching wind component was also included in the simulation.

When the estimation method using pitch rate and heave velocity was considered, the errors introduced by the pitching wind component could be reduced by using low-pass filters. These produced acceptable estimates of the x-axis and z-axis wind components but the filtering introduced a time lag into the estimates. However, it was subsequently found that when the estimation algorithm was combined with the hazard evaluation algorithm, the low-pass filters in the estimation algorithm were no longer required. For the algorithm using pitch rate and airspeed, only the x-axis wind estimate was satisfactory.

The development of the estimation algorithm assumed that the measurement and modelling of the aircraft was exact whereas, in practice, inaccuracies in the measurements occur, and changes in the aircraft's flight phase cause the parameters to differ. When the changes for different low-altitude flight conditions were incorporated, the estimation of the wind components showed oscillatory errors which were caused primarily by differences in the damping factor of the phugoid mode of the aircraft. It was found that estimation using pitch rate and airspeed produced good estimates of the

x-axis wind component for all low-altitude flight phases, but the estimation of the z-axis component remained very poor. In contrast, the algorithm using pitch rate and heave velocity produced a good z-axis wind estimate but, for some flight conditions, the oscillatory errors in the x-axis estimate were large.

It seemed likely that a combination of the algorithms using pitch rate, airspeed and heave velocity would yield acceptable estimates for both wind components. A revised system combining the methods was simulated and good estimates of both the x-axis and z-axis wind components were obtained. The measurement of airspeed produces a further advantage, that of enabling the model of the aircraft to be varied according to the trim airspeed. It was observed that, at low altitudes, changes in some elements of the state matrix of the aircraft corresponded closely to the variations in the airspeed, and this was used to reduce the differences between these parameters for the aircraft and the algorithm, and thereby reduce the errors in the estimation.

The sensors which are required to measure the pitch rate, airspeed, heave velocity and control inputs were considered. The principal requirement is for stable and repeatable sensors which, therefore, enable calibration and compensation to produce highly accurate measurements. Washout filtering, which is used to extract the small parameter values from the measured quantity, also serves to drive any offset errors to zero. Residual errors in the calibration were modelled and these were found to produce small offset or drift effects which would be compensated by the filtering.

7.3.4 Defining the Windshear Warning

The wind estimation algorithm provides a measure of the wind acting on an aircraft, but the nature of a hazardous windshear must also be defined before the detection system can determine the risk. The requirements for the warning system were that it should provide reliable warnings while minimising false alarms and its hazard evaluation method must distinguish, therefore, between windshear and turbulence. This was achieved by considering the effect on the aircraft's airspeed and vertical speed of winds at differing frequencies, from which it was found that, for the Cessna 402B, the greatest hazard is presented by winds having period of between five and sixty seconds. Turbulence is a higher frequency wind phenomenon and,

therefore, a low-pass filter with suitably chosen cut-off frequency is used to attenuate any turbulence content of the estimated winds. In a similar way, winds of periods greater than sixty seconds are also attenuated by using either a high pass filter or averaging methods.

Three techniques for evaluating the windshear hazard were tested. The F-factor method was recommended by the FAA for use on windshear detection systems for transport aircraft. The method is based upon the effect of a windshear on the aircraft's energy and a similar energy-based technique devised as an alternative and flexible means of evaluating the loss in performance of an aircraft was described as the 'Performance Margin' criterion. The third method simply considered the change in the x-axis and z-axis wind components and triggered an alert if the combined change exceeded a pre-determined threshold.

The level at which to set the threshold level for an z-axis wind when compared to an x-axis wind was determined either directly from energy considerations or, in the case of the wind change algorithm, by considering the relative effect of each wind component on the airspeed and vertical speed of the aircraft. A warning threshold of 12 knots of airspeed change, or the equivalent z-axis wind change, was chosen for the Cessna 402B by examining relevant performance data.

When a windshear is detected a clear and unambiguous warning is required to enable the pilot to respond to the situation as rapidly as possible. The form of the alert can have an effect on the speed with which the pilot comprehends a situation and this has been the subject of several human factors studies. The conclusions from the studies were evaluated to ascertain the optimum design of warning system. The proposed system is for a simple combined aural and visual alert. The visual alert is simply a red light labelled 'windshear', located near to the airspeed indicator, altimeter and vertical speed indicator. The aural alert is produced by a speech synthesiser and generates a message in the form of either 'Windshear Windshear' or 'Windshear Windshear Climb Climb'.

7.3.5 Performance of the Detection Algorithms

The performance of the estimation and hazard determination stages of the algorithm was tested by passing estimated wind components through the hazard evaluation algorithms. The time at which an alert was provided when winds, estimated at each of the low altitude flight conditions, were passed through the three hazard criteria were recorded. These were compared with the time of warnings generated using the actual winds under the same conditions and produced only small delays of less than one second.

When the combined system was tested with Dryden turbulence, no alerts were produced for any flight condition using any of the hazard criteria.

7.4 System Implementation

The algorithms for detecting windshear have been discussed in the preceding chapters, but the possible methods for implementing the system have not been addressed. These are now considered.

7.4.1 Implementation Method

The requirements for the implementation of the windshear detection system are most likely to be satisfied by a digital system. Although the basic wind estimation algorithm could be implemented using analogue electronics, the size of the algorithm of whole system and the additional requirements such as the scheduling of matrix elements with airspeed and the sensor compensation mean that this is impracticable.

The digital algorithm could be implemented using a microprocessor, transputer or digital signal processor. The choice of the most suitable device depends not only on its meeting the performance requirements of the algorithm but also on the cost and the number of additional peripherals, such as memory and control devices, required.

The sensor data is required in digital form for use by the algorithm, and this can be achieved using an analogue to digital converter (ADC). The signals must be passed through filters before digitisation to prevent aliasing of the data. The calibration, compensation and extraction of perturbed parameters,

which were discussed in Chapter 5, is accomplished digitally before the data is passed into the wind estimation and hazard evaluation stages of the algorithm.

The simulation of the system throughout this thesis have been performed using a cycle time of 100 ms (10 Hz sample rate), which allows a 5 Hz signal bandwidth, and this has been demonstrated to be adequate for the algorithm requirements. In practice, the sample rate may be required to be a little higher than this because of filtering requirements.

7.4.2 Warning System

If a windshear is identified by the hazard estimation algorithm a warning is triggered. The warning system comprises a warning light on the instrument panel and a vocal alert. The speech message can be conveniently generated in one of two forms, either as using a speech synthesis chip in which the message is generated phonetically from digitally stored data, or by recording a spoken message in an analogue form using capacitive storage device. Both of these provide relatively low cost solutions. The human factors research discussed in Chapter 6 found that the response time was improved when using synthesised speech.

7.4.3 Self-Test Function

The self-test function injects a digitised wind profile into the system. The profile can be stored in an EPROM or other suitable device. An EPROM 'smart card' would enable a variety of different profiles to be easily tested by inserting the appropriate card into the system. When the system is in test mode data can be read from the card and processed as if they were the small perturbation data from the sensors. This method could appear to the pilot to be a more evident self-test and induce, therefore, greater confidence in the system.

7.5 Discussion and Conclusions

The aim of the research has been to investigate the feasibility of adapting the theory of observers to enable a low-cost airborne detection system suitable for use on general aviation aircraft to be developed. A method has been derived

which can estimate the wind components acting on the aircraft to suitable accuracy, and further algorithms have been designed which then evaluate whether the components constitute a windshear hazard. The robustness of the system to changes in the aircraft's flight conditions and to atmospheric turbulence has been established, and the errors which may be introduced by sensor inaccuracies are not expected to cause a significant deterioration in the performance of the system.

The estimation technique can estimate a single wind component by measuring only two aircraft parameters plus the control inputs, whereas the estimation of two wind components requires a further measured aircraft parameter. Thus the lowest cost system could use only a pitch rate and an airspeed sensor to measure the aircraft dynamics, and this would provide an estimate of the x-axis wind component which is the most important component for evaluating the windshear hazard. Forward-looking airborne detection systems evaluate the risk based solely on this component. However, as these systems are able to measure the wind movement ahead of the aircraft, they have more time available to calculate the hazard and the algorithm used in the evaluation can be more complex. The contribution of the z-axis wind component to the windshear hazard is significant, particularly at the low airspeeds at which general aviation aircraft fly; therefore, for a rapid evaluation of the risk presented by a wind event, the measurement of both the x-axis and z-axis wind components is desirable for a reactive windshear detection system.

The three alternative hazard evaluation algorithms all performed reliably, but the F-factor and the wind change algorithm had the faster response times. These two methods were based upon differing concepts of how a wind hazard is defined. The F-factor is determined by considering the change in aircraft energy because it is the reserve energy of the aircraft which determines its ability to climb when in shear conditions. In contrast, the wind change method extracted the change in each wind component over a short period of time and based the hazard evaluation on the magnitude of the shear. In practice, the principal difference between the methods was in the assessment of z-axis wind component: the F-factor method examined the magnitude of this component and not the magnitude of the z-axis wind change. The F-factor criterion has a well-established theoretical basis and it is a widely accepted method of determining the windshear hazard for

transport aircraft. However, the wind change method can provide an advantage by producing a prompt warning when a windshear encounter is preceded by an updraft, a phenomenon which is a characteristic of microburst encounters. Both the evaluation methods only produce a warning when severe performance-decreasing conditions are experienced by the aircraft.

The evaluation of the probable sensor errors suggested that any offset or drift errors produced in the estimates of the wind components would be small and transient, but this is dependent on the choice of sensors and the filtering methods employed. The wind change algorithm is less susceptible to such errors because it uses the change in the z-axis wind rather than the steady component in the evaluation, and this could reduce the requirements on the sensor performance and thereby reduce the cost of the detection system.

The research suggests that an airborne windshear detection system suitable for general aviation aircraft can be developed. The characteristics of the aircraft, i.e. the parameters required for the observer and aircraft model, must be known although the method has been shown to be robust to moderate inaccuracies in these parameters. The system requires, as a minimum, sensors to measure the pitch rate, airspeed, z-axis acceleration, elevator and throttle settings and may require further measurements of, for example, flap setting. The probable method of implementation of the system was described in Section 7.4. The feasibility of developing the system is dependent largely on the cost and the major constituent of this is likely to be the sensors - low-cost standard integrated circuits are likely to be sufficient for the acquisition, processing and warning requirements. The prices of solid-state sensors and devices continue to decrease while their performance increases and so in volume production the system may be viable. The perceived risk of a windshear encounter by general aviation pilots is a significant factor which will affect the market for an airborne windshear detection system and the price at which it can be sold, unless such a system becomes mandatory. A marketing study would be required to ascertain the demand for the product.

Alternatively, the detection algorithm could be implemented as part of a larger system which has common functions or requirements. Solid-state aircraft instruments are now being produced and many of these would be

suitable for integration with the windshear detection system. For example, attitude indicators provide an accurate measure of the aircraft's pitch attitude and newer solid-state versions may employ a pitch rate sensor for this. These instruments may also require measurements of the aircraft's z-axis acceleration, and so integrated system could combine a significant part of the sensing requirements. The detection system could be also be combined with a longitudinal control system where this is used. Some of the regulatory authorities are considering the feasibility of requiring some general aviation aircraft to be fitted with data recorders and it is likely that a flight data recorder would also have common sensing requirements.

7.6 Suggestions for Further Work

7.6.1 Further Investigation of Hazard Evaluation Methods

Three methods of evaluating the windshear hazard were discussed in Chapter 6 and analysed using windshear models to determine the time at which an alert was provided. A more thorough investigation into the performance of the evaluation algorithms could be achieved by further simulation of general aviation aircraft in windshear situations using a pre-defined index to classify the windshear hazard. This would be particularly valuable for establishing the relative threshold levels for warning of the x-axis and z-axis wind components.

There is some support for the concept of providing a warning for an abnormal wind event and not just a performance-decreasing encounter, particularly because this is likely to improve the speed of response of a reactive system to a microburst. However, general aviation pilots are likely to be less familiar with windshear procedures than commercial pilots and may therefore be more sceptical of the risks. If the system provides a warning when the aircraft performance is improved, and this is not followed by a shear condition, the pilot could begin to disregard the necessity to respond to any alert provided by the system. Whether this is correct can only be established by human factors research aimed at determining the specific requirements of general aviation pilots in windshear situations. This study should also include an evaluation of the optimum form of warning message by determining the response time of pilots when the warning is provided in each of the two suggested forms.

7.6.2 Development and Verification using Measured Aircraft Parameters

The windshear detection system has been designed and verified using simulation techniques, and, in particular, the aircraft dynamics used in the simulations were derived using the linearised, small perturbation model. In practice, the small perturbation signals are extracted from the sensor signals using high-pass filtering as discussed in Chapter 5. In order to design the filtering and to test the resulting system performance a representation of the typical output from the sensors, when they are measuring the total aircraft dynamics, is required. This could be obtained using a flight simulator or as recorded data from an actual aircraft.

The data would also enable the operation of the detection system to be evaluated and verified over the whole flight envelope when the simulator or aircraft is flown though typical manoeuvres. For simulator testing, windshear and turbulence encounters could be simulated and, although an aircraft should not be flown through low altitude windshear at low airspeed, airborne windshear detection systems can be tested by recording the aircraft parameters as the aircraft passes through similar events at higher altitudes and speeds and examining the response of the system.

7.6.3 Prototype Development

An important stage in the of development of the system, after the concept has been proved, would be to build a prototype instrument. The system algorithm could be implemented either by using a dedicated processor as would be required by the final system, or by effecting the algorithms in real-time on a computer and interfacing this to the sensors and warning system. This would enable the integration of the various constituents of the system to be tested. Further evaluation of the system would be difficult without undergoing flight trials.

APPENDIX A: AIRCRAFT EQUATIONS OF MOTION

The motion of an aircraft results from the forces and moments acting upon it, and these arise from inertial, gravitational and aerodynamic effects. The equations in their most general form are non-linear and complex, but by considering specifically the motion of an aircraft under a typical range of flight conditions they can be greatly simplified. The derivation of the linearised equations of motion is well documented [6, 16, 83] but the following is a summary of the analysis and the implicit assumptions.

The form of the equations depends on the axis system on which they are based. A 'body-fixed' axis system, where the axes pass through the centre of gravity of the aircraft and remain fixed relative to the aircraft, is often used when considering aircraft-based observations because many sensor measurements are made with respect to a body-fixed axis system. The system is shown in Figure A1. The system most generally used for analysis of longitudinal aircraft control and dynamics is the 'stability axis system', a body-fixed axis system where the x-axis, in the equilibrium state, is pointed into the relative wind as shown in Figure A2.

The gravitational and inertial terms in the equations arise from the force due to the earth's gravity and from the motion of the aircraft in a moving reference frame respectively. The low speed of the aircraft and short duration of the dynamics under consideration allow both the mass of the aircraft to be considered to be constant and the inertial effects caused by the rotation of the earth and its movement relative to inertial space to be ignored. In addition, general aviation aircraft are usually of conventional aircraft design, and so for control and stability studies, the effects of structural flexibility on the dynamics of such aircraft are negligible: the aircraft can be assumed to be a rigid body.

This assumption allows earth fixed axes to be considered as an inertial reference frame, and Newton's Second Law can be applied to the aircraft. The inertial equations in the body-fixed axis system of a body in a rotating axis system relative to inertial space are given below. (These equations assume that the X-Z plane is a plane of symmetry. When considering a body-fixed axis system for a conventional aircraft this approximation is usually found to be valid.)

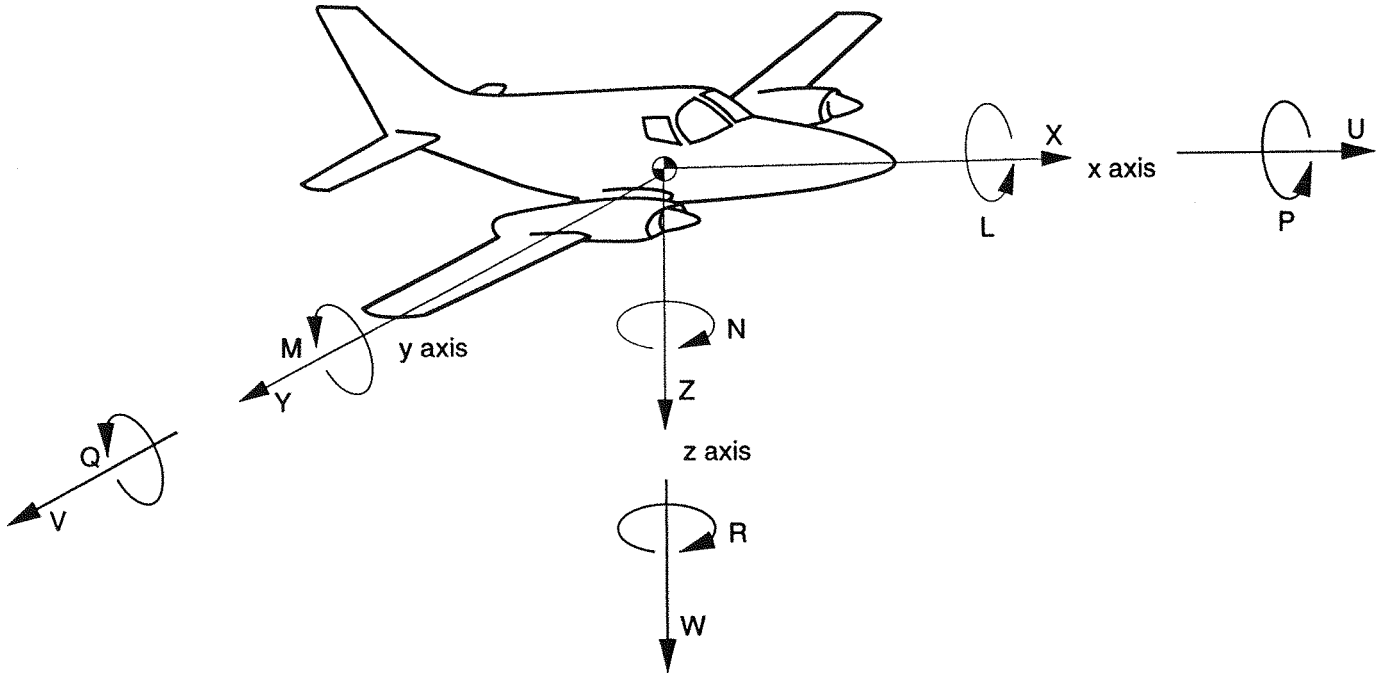

Figure A1: Body-Fixed Axis System

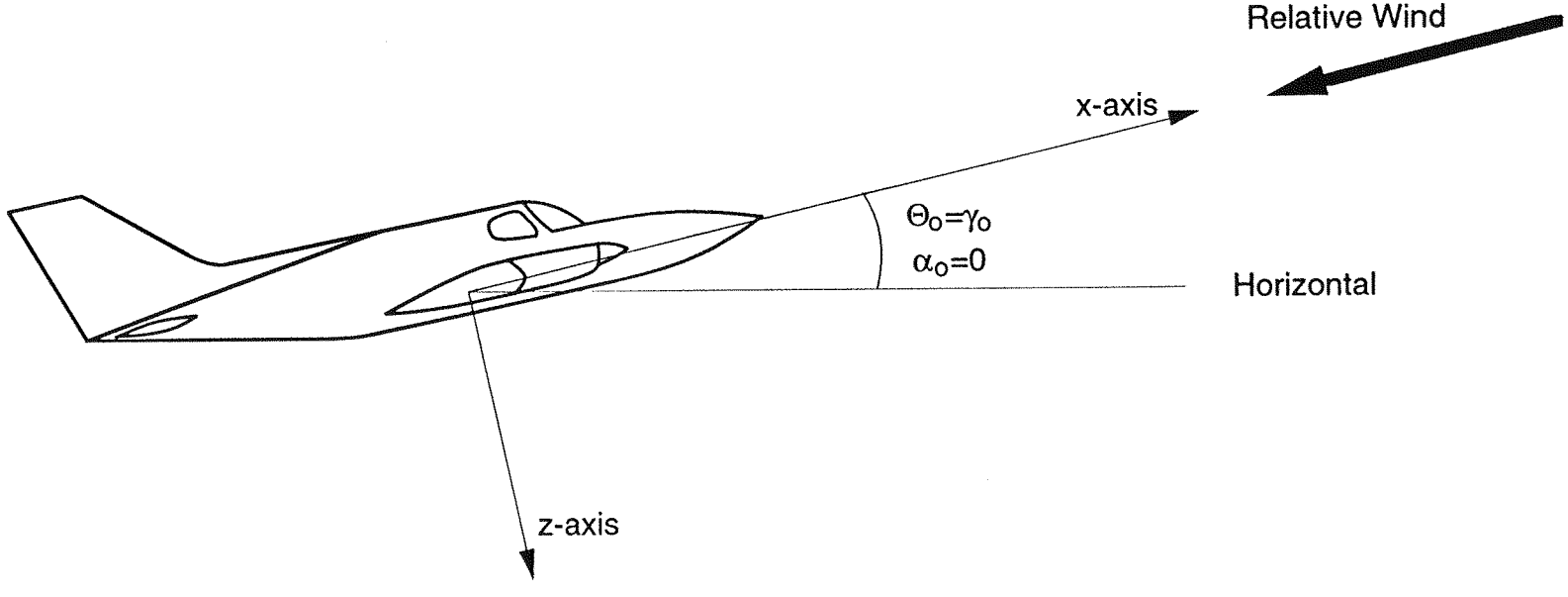

Figure A2: Stability Axis System

$$\sum X = m(\dot{U} + QW - RV) \quad \text{(A1)}$$

$$\sum Y = m(\dot{V} + RU - PW) \quad \text{(A2)}$$

$$\sum Z = m(\dot{W} + PV - QU) \quad \text{(A3)}$$

$$\sum L = \dot{P}I_{xx} - \dot{R}I_{xz} - QR(I_{zz} - I_{yy}) - PQI_{xz} \quad \text{(A4)}$$

$$\sum M = \dot{Q}I_{yy} + PR(I_{xx} - I_{zz}) - R^2 I_{xz} + P^2 I_{xz} \quad \text{(A5)}$$

$$\sum N = \dot{R}I_{zz} - \dot{P}I_{xz} + PQ(I_{yy} - I_{xx}) - QRI_{xz} \quad \text{(A6)}$$

where m is the mass of the body, X, Y and Z are the applied forces, and U, V and W the linear velocities, in the x, y and z-axis directions respectively. L, M and N are the applied moments and P, Q and R are the roll, pitch and yaw rates about the x, y and z axes respectively. The sense of these parameters is shown in Figure A1. I_{xx}, I_{yy} and I_{zz} are the moments of inertia and I_{xz} a product of inertia, which are defined in the conventional way.

The forces and moments include aerodynamic and propulsive terms, and the effects of gravity. The atmosphere exerts forces on the aircraft giving rise to the aerodynamic terms. It is known that the force, F, acting on a body moving through a fluid is given by equation A7. [84]

$$F = \tfrac{1}{2} C \rho V^2 s \quad \text{(A7)}$$

Where C is a dimensionless coefficient, ρ is the density of the fluid, V is the velocity of the body relative to the fluid and s is the characteristic area of the body.

The aerodynamic forces and moments acting on an aircraft can be expressed in these forms. The lift and drag of the aircraft are aerodynamic forces acting perpendicular to and parallel to the relative wind, as shown in Figure A3, and these can be resolved into the body-fixed axes.

Further simplifications can be made by considering the motion of the aircraft about a reference or 'trim' position. The deviation from this position is usually small, therefore, by making small angle approximations and neglecting higher order terms and other terms which are usually insignificant, the equations can be linearised about this point. Such analysis also allows the longitudinal and lateral motion to be decoupled. In the following analysis only longitudinal motion is considered.

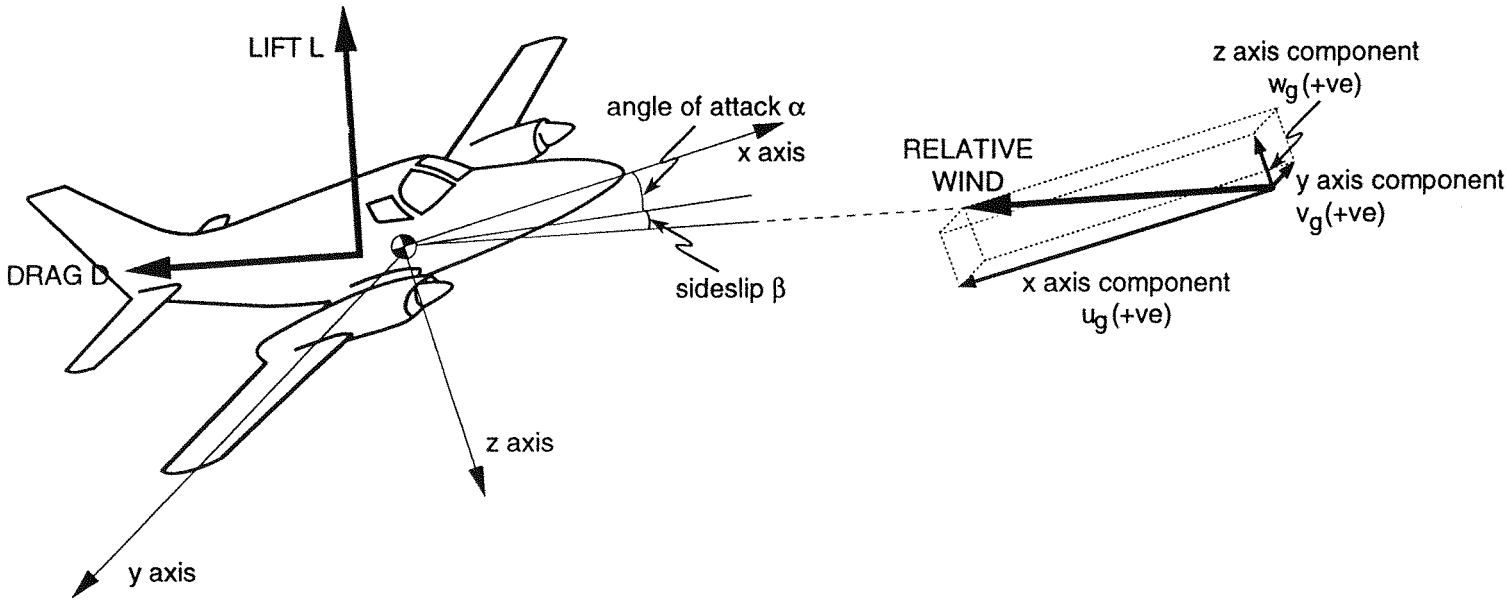

Figure A3: Axis System for Analysis of Forces

The steady state 'trim' parameters relate to the aircraft in equilibrium and are denoted with the subscript 0. For example

$$U = U_0 + u \tag{A8}$$

where U is the total aircraft velocity in the x direction, U_0 is the trim value of the aircraft velocity, and u is the small change in aircraft velocity from the trim value.

The linearised equations of aircraft motion for small perturbations from straight, symmetric equilibrium in this axis system are:

$$\dot{u} = X_u(u+u_g) + X_w(w+w_g) - g\cos\Theta_0\theta + \sum X_\delta\delta \tag{A9}$$

$$\dot{w} = Z_u(u+u_g) + Z_w(w+w_g) + Z_q(q+q_g) + U_0 q + g\sin\Theta_0\theta + \sum Z_\delta\delta \tag{A10}$$

$$\dot{q} = M_u(u+u_g) + M_w(w+w_g) + M_{\dot{w}}(\dot{w}+\dot{w}_g) + M_q(q+q_g) + \sum M_\delta\delta \tag{A11}$$

$$\dot{\theta} = q \tag{A12}$$

u_g and w_g are the velocities of the winds acting along the x-axis and z-axis respectively, q_g is the pitching gust and δ denotes a control input. Θ_0 and θ are the trim and perturbed pitch attitudes respectively, and g is the acceleration due to gravity. X_u is a dimensional stability derivative, which is a function of the partial derivative for the change in X with respect to the change in u viz.

$$X_u = \frac{1}{m}\frac{\partial X}{\partial u} \tag{A13}$$

The other stability derivatives in equations (A9) to (A12) are defined in a similar manner. [16]

The terms associated with the stability derivatives represent the motion of the aircraft relative to the atmosphere. If u_a and w_a are defined to be the air-relative forward and heave velocities respectively, then

$$u_a = u + u_g \tag{A14}$$

$$w_a = w + w_g \tag{A15}$$

The terms are additive because of the sense in which the wind components have been defined viz. a headwind and an updraft are both defined to be positive quantities although these act along the negative x-axis and the negative z-axis respectively. A positive pitching gust is also defined to be a nose-down pitching motion i.e. in the negative pitch direction. These can be seen in Figure A3.

For the case of level flight, the flight path angle, $\gamma_0 = 0$, and hence, for the stability axis system, $\Theta_0 = 0$. The gravitational terms in equations (A9) and (A10) could, therefore, be simplified.

The linearised equations can be further simplified by substituting for $\dot{w}$ from equation A10 into equation A11, the pitch rate equation.

$$\dot{q} = \tilde{M}_u(u+u_g) + \tilde{M}_w(w+w_g) + \tilde{M}_q q + (\tilde{M}_q - 2M_{\dot{w}}U_0)q_g + \sum \tilde{M}_\delta \delta \quad \text{(A16)}$$

where

$$\tilde{M}_u = M_u + M_{\dot{w}}Z_u \quad \text{(A17)}$$

$$\tilde{M}_w = M_w + M_{\dot{w}}Z_w \quad \text{(A18)}$$

$$\tilde{M}_\delta = M_\delta + M_{\dot{w}}Z_\delta \quad \text{(A19)}$$

$$\tilde{M}_q = M_q + M_{\dot{w}}Z_q + M_{\dot{w}}U_0 \quad \text{(A20)}$$

The latter relationship, equation A20, is a valid simplification of the terms because the variation in the distribution of a vertical gust along the aircraft can be considered to be equivalent to a pitching gust q_g i.e.

$$q_g = -\frac{\partial w_g}{\partial x} \quad \text{(A21)}$$

Expressing this distribution in terms of time dependence rather than spatial dependence gives

$$q_g = \frac{-\frac{\partial w_g}{\partial t}}{\frac{\partial x}{\partial t}} = -\frac{\dot{w}_g}{U_0} \quad \text{(A22)}$$

A pitching gust can therefore be represented by a time varying vertical gust component.

The longitudinal aerodynamics for an aircraft controlled in longitudinal motion by the deflection of the elevator, δ_e, and the change of thrust, δ_T, can now be expressed as a state equation viz.

$$\dot{\mathbf{x}} = \mathbf{A}\mathbf{x} + \mathbf{B}\mathbf{u} + \mathbf{E}\mathbf{w}_{ind} \tag{A23}$$

where

$$\mathbf{x} \equiv \begin{bmatrix} u \\ w \\ q \\ \theta \end{bmatrix} \tag{A24}$$

$$\mathbf{u} \equiv \begin{bmatrix} \delta_e \\ \delta_T \end{bmatrix} \tag{A25}$$

$$\mathbf{w}_{ind} \equiv \begin{bmatrix} u_g \\ w_g \\ q_g \end{bmatrix} \tag{A26}$$

$$\mathbf{A} = \begin{bmatrix} X_u & X_w & 0 & -g \\ Z_u & Z_w & U_0 + Z_q & 0 \\ \tilde{M}_u & \tilde{M}_w & \tilde{M}_q & 0 \\ 0 & 0 & 1 & 0 \end{bmatrix} \tag{A27}$$

$$\mathbf{B} = \begin{bmatrix} X_{\delta_e} & X_{\delta_T} \\ Z_{\delta_e} & Z_{\delta_T} \\ \tilde{M}_{\delta_e} & \tilde{M}_{d_T} \\ 0 & 0 \end{bmatrix} \tag{A28}$$

$$\mathbf{E} = \begin{bmatrix} X_u & X_w & 0 \\ Z_u & Z_w & Z_q \\ \tilde{M}_u & \tilde{M}_w & \tilde{M}_q - 2M_{\dot{w}}U_0 \\ 0 & 0 & 0 \end{bmatrix} \tag{A29}$$

APPENDIX B: CESSNA 402B LONGITUDINAL MATHEMATICAL MODEL

The linear model of the Cessna 402B have been derived from the longitudinal dynamics of the aircraft as part of a NASA research project. [17] The units used in this model are maintained, velocities are measured in feet per second and angular measurements in radians.

Sea Level Take-Off

Airspeed: 184 ft/s

$$\mathbf{A} = \begin{bmatrix} -0.0278 & 0.0525 & 0 & -31.7843 \\ -0.3128 & -1.1730 & 168.0472 & -4.5816 \\ 0.0007 & -0.0299 & -7.5327 & 0.0784 \\ 0 & 0 & 1 & 0 \end{bmatrix} \qquad \text{(B1)}$$

Table B1: Modal characteristics - take-off at sea-level

Eigenvalues	Phugoid Mode	
-2.1092		
-6.6174	frequency:	0.150 rad/s
-0.0035 + 0.1504i	damping:	0.023
-0.0035 - 0.1504i		

Sea Level Climb

Airspeed: 211 ft/s

$$\mathbf{A} = \begin{bmatrix} -0.0228 & 0.0606 & 0 & -32.0688 \\ -0.2954 & -1.3325 & 193.8879 & -2.5320 \\ 0.0023 & -0.0307 & -8.1525 & 0.0406 \\ 0 & 0 & 1 & 0 \end{bmatrix} \qquad \text{(B2)}$$

Table B2: Modal characteristics - climb at sea-level

Eigenvalues	Phugoid Mode	
-2.3646		
-7.1297	frequency:	0.151 rad/s
-0.0067 + 0.1511i	damping:	0.044
-0.0067 - 0.1511i		

Climb at 5 000 feet

Airspeed: 227 ft/s

$$\mathbf{A} = \begin{bmatrix} -0.0212 & 0.0554 & 0 & -32.075 \\ -0.2724 & -1.2413 & 211.2008 & -2.3835 \\ 0.0016 & -0.0315 & -7.5786 & 0.0330 \\ 0 & 0 & 1 & 0 \end{bmatrix} \quad \text{(B3)}$$

Table B3: Modal characteristics - climb at 5 000 feet

Eigenvalues	Phugoid Mode	
-2.5742		
-6.2554	frequency:	0.145 rad/s
-0.0058 + 0.1443i	damping:	0.040
-0.0058 - 0.1443i		

Cruise at 20 000 feet

Airspeed: 358 ft/s

$$\mathbf{A} = \begin{bmatrix} -0.0178 & 0.0512 & 0 & -32.1733 \\ -0.1790 & -1.2343 & 343.0714 & 0 \\ 0.0008 & -0.0327 & -7.1964 & 0 \\ 0 & 0 & 1 & 0 \end{bmatrix} \quad \text{(B4)}$$

Table B4: Modal characteristics - cruise at 20 000 feet

Eigenvalues	Phugoid Mode	
-4.2157 + 1.5298i		
-4.2157 - 1.5298i	frequency:	0.105 rad/s
-0.0085 + 0.1043i	damping:	0.082
-0.0085 - 0.1043i		

Sea Level Approach

Airspeed: 160 ft/s

$$\mathbf{A} = \begin{bmatrix} -0.0525 & 0.1315 & 0 & -32.1253 \\ -0.3840 & -1.0456 & 147.072 & 1.6320 \\ 0.0049 & -0.0234 & -6.2240 & -0.0264 \\ 0 & 0 & 1 & 0 \end{bmatrix} \quad \text{(B5)}$$

Table B5: Modal characteristics - approach at sea-level

Eigenvalues	Phugoid Mode	
-1.8211		
-5.4372	frequency:	0.215 rad/s
-0.0319 + 0.2125i	damping:	0.148
-0.0319 - 0.2125i		

Derivation of B Matrix

The input matrix, **B**, relates the change in the aircraft state vector to control input vector of elevator deflection and thrust change. This is not described explicitly in the reference, but the effect of the elevator can be derived. The input matrix elements of an elevator with a surface area of one fifth of the standard area are given, and so these values can be scaled by a factor of five to yield the matrix elements which relate, approximately, the changes in the state vector to the elevator deflection.

The effect of thrust is must be obtained independently. The maximum thrust can be estimated using the performance figure for the Cessna 402B [76]:

Maximum Rate of Climb at Sea Level 1450 ft min^{-1} (24.2 fts^{-1})

The energy of the aircraft is:

$$E = \tfrac{1}{2} m V_a^2 + mgh \quad \text{(B6)}$$

and the rate of change of energy is

$$\dot{E} = mV_a\dot{V}_a + mg\dot{h} \tag{B7}$$

In order to achieve the maximum rate of climb the airspeed is held approximately constant and the increase in the energy of the aircraft is in the form of potential energy. If, instead, the potential energy is held constant i.e. the aircraft maintains a constant altitude, and the kinetic energy is allowed to increase, the maximum acceleration of the aircraft can be estimated.

Trading the rate of climb for acceleration produces:

$$\dot{V}_a = \frac{g\dot{h}}{V_a} \tag{B8}$$

Substituting the values for the maximum rate of climb and the airspeed at take-off gives an estimate of the maximum acceleration potential of the aircraft at sea-level.

$$\dot{V}_{a\,\max} = 4.2\ \text{fts}^{-2} \tag{B9}$$

The quoted power, P, is 500 hp which is approximately equivalent to 275 500 lb.ft/s. Using this, and a representative velocity value, the maximum thrust can be derived:

$$T_{\max} = \frac{P}{V_a} = \frac{275500}{184} \approx 1500\,\text{lbf} \tag{B10}$$

Now

$$X_{\partial T} T_{\max} = \dot{V}_{a\,\max} \tag{B11}$$

and so $X_{\partial T}$ can be determined.

$$X_{\partial T} = \frac{V_{a\,\max}}{T_{\max}} = \frac{4.2}{1500} = 0.0028\,\text{ft / lbf.s}^2 \tag{B12}$$

An estimation of the input matrix for the sea-level take-off condition becomes:

$$\mathbf{B} = \begin{bmatrix} 0 & 0.0028 \\ 33.2120 & 0 \\ -18.8250 & 0 \\ 0 & 0 \end{bmatrix} \tag{B13}$$

Here the elevator deflection is expressed in radians and can vary over a range ± 0.21 radians ($\pm 12^{\circ}$).

APPENDIX C: DRYDEN TURBULENCE

The form and intensity of the Dryden turbulence to be used in testing windshear detection systems for transport aircraft is specified by the FAA. [31] The appropriate x, y and z-axis mathematical models are described by a set of transfer functions viz.

$$F_u(s) = \sigma_u \sqrt{\frac{\tau_u}{\pi}} \frac{1}{(1+\tau_u s)} \tag{C1}$$

$$F_v(s) = \sigma_v \sqrt{\frac{\tau_v}{2\pi}} \frac{(1+\sqrt{3}\tau_v s)}{(1+\tau_v s)(1+\tau_v s)} \tag{C2}$$

$$F_w(s) = \sigma_w \sqrt{\frac{\tau_w}{2\pi}} \frac{(1+\sqrt{3}\tau_w s)}{(1+\tau_w s)(1+\tau_w s)} \tag{C3}$$

where σ_u, σ_v and σ_w correspond to the required rms intensities of the turbulence being used.

The variable τ_i determines the bandwidth of the particular filter. It is defined as the ratio of scale length to the true airspeed i.e.

$$\tau_i = \frac{L_i}{U_a} \tag{C4}$$

The values of σ and L which should be used with the transfer functions are specified for a series of altitudes - see Tables C1 and C2.

Table C1: rms intensities for Dryden turbulence model

Altitude (ft)	rms intensities (ft/s)		
	σ_u	σ_v	σ_w
100	5.6	5.6	3.5
300	5.15	5.15	3.85
700	5.0	5.0	4.3
900	5.0	5.0	4.45
1500	4.85	4.85	4.7

Table C2: scale lengths for Dryden turbulence model

Altitude (ft)	scale lengths (ft)		
	L_u	L_v	L_w
100	260	260	100
300	540	540	300
700	950	950	700
900	1123	1123	900
1500	1579	1579	1500

These values were obtained from experimental evidence and were specified by the FAA; they differ from the values for Dryden turbulence parameters recommended in MIL-F-8785B. To use these models for testing a windshear detection system, suitable time-domain representations of turbulence can be generated by applying bandlimited white noise of unit spectral density to filters with the appropriate transfer functions. [6]

For a bandlimited white noise signal of unit spectral density:

$$S_n(jw) \equiv \begin{cases} 1 & \omega \le \omega_0 \\ 0 & \omega > \omega_0 \end{cases} \qquad \text{(C5)}$$

If white noise of insufficient bandwidth is applied to the filter the variance (mean square value) of the output will be reduced. The variance is given by [85]:

$$\sigma^2 = \int_{-\infty}^{\infty} |F(jw)|^2 \, S_n(jw) dw \qquad \text{(C6)}$$

or, for a single-sided power spectral density function

$$\sigma^2 = 2\int_{0}^{\infty} |F(jw)|^2 \, S_n(jw) dw \qquad \text{(C7)}$$

This integration can be performed analytically for the Dryden Gust filters. For example, the frequency response of the x-axis turbulence filter is:

$$|F_u(jw)|^2 = \sigma_u{}^2 \frac{\tau_u}{\pi} \frac{1}{(1+\tau_u{}^2 jw^2)} \qquad \text{(C8)}$$

Hence the rms intensity of the turbulence is

$$\sigma^2 = 2\sigma_u{}^2 \frac{\tau_u}{\pi} \int_0^{\omega_0} \frac{1}{(1+\tau_u{}^2 jw^2)} dw \qquad \text{(C9)}$$

$$\sigma^2 = \frac{2\sigma_u{}^2}{\pi} \tan^{-1}(\omega_0 \tau_u) \qquad \text{(C10)}$$

The variance of the output depends on the bandwidth of the white noise.

$$\lim_{\omega_0 \tau_u \to \infty} \tan^{-1}(\omega_0 \tau_u) = \frac{\pi}{2} \qquad \text{(C11)}$$

The corresponding variance of the x-axis turbulence with a white noise input of wide bandwidth is, therefore:

$$\sigma^2 = \frac{2\sigma_u{}^2}{\pi} \frac{\pi}{2} = \sigma_u{}^2 \qquad \text{(C12)}$$

The bandwidth of the white noise is selected such that the error in the variance of the output calculated using equation C10 is negligible.

APPENDIX D: THE LUENBERGER OBSERVER

A linear time-invariant system can be expressed in a standard form as

$$\dot{\mathbf{x}} = \mathbf{A}\mathbf{x} + \mathbf{B}\mathbf{u} \tag{D1}$$

$$\mathbf{y} = \mathbf{C}\mathbf{x} \tag{D2}$$

where $\mathbf{x}$ is the state vector of dimension n, $\mathbf{u}$ is the input vector of dimension m and $\mathbf{y}$ is the output vector of dimension p. The matrices $\mathbf{A}$, $\mathbf{B}$ and $\mathbf{C}$ are of order $[n \times n]$, $[n \times m]$ and $[p \times n]$ respectively.

If $\mathbf{C}$ is not singular the state vector may be derived from the output vector using simple matrix inversion:

$$\mathbf{x} = \mathbf{C}^{-1}\mathbf{y} \tag{D3}$$

However, the $\mathbf{C}$ matrix cannot be assumed to be non-singular, and $p \neq n$, in general.

There is an important class of linear control methods which uses state feedback to effect the control, and for these techniques a knowledge of the full state vector is required. However, in practice, it is uncommon for every state variable to be measurable. For this reason, techniques for calculating or estimating the state vector have been developed.

D1.1 Luenberger Observer Theory

Luenberger first proposed a method of estimating the state vector by means of another dynamic system, an observer, into which the input and output variables of the first system are fed. [86, 87] He approached the problem by requiring that the observer be designed so that its state vector, $\mathbf{x}_e$, was some linear transformation $\mathbf{T}$ of the state vector $\mathbf{x}$. The simpler problem of a free system, without any external inputs, is considered first.

For the free system the state equation is reduced to

$$\dot{\mathbf{x}} = \mathbf{A}\mathbf{x} \tag{D4}$$

The equation relating the output vector to the state vector remains unchanged viz.

$$\mathbf{y} = \mathbf{C}\mathbf{x} \tag{D5}$$

The observer is then defined as a time-invariant linear system with its input vector being the output of the system being observed.

$$\dot{\mathbf{x}}_e = \mathbf{F}\mathbf{x}_e + \mathbf{K}\mathbf{y} = \mathbf{F}\mathbf{x}_e + \mathbf{K}\mathbf{C}\mathbf{x} \tag{D6}$$

If the observer state vector is expressed as the transform of the system state vector,

$$\mathbf{x}_e = \mathbf{T}\mathbf{x} \tag{D7}$$

then, from equations D4 and D6,

$$\mathbf{T}\dot{\mathbf{x}} = \mathbf{T}\mathbf{A}\mathbf{x} \tag{D8}$$

$$\mathbf{T}\dot{\mathbf{x}} = \mathbf{F}\mathbf{T}\mathbf{x} + \mathbf{K}\mathbf{C}\mathbf{x} \tag{D9}$$

So **T** must satisfy the relationship

$$\mathbf{T}\mathbf{A} - \mathbf{F}\mathbf{T} = \mathbf{K}\mathbf{C} \tag{D10}$$

Provided that **A** and **F** have no common eigenvalues there is a solution for **T**. That the transformation provides a suitable design of observer can be shown by considering the errors in the system.

It is required that the observer state vector $\mathbf{x}_e$ be the transformation of the system state vector **Tx**. The difference between the two state vectors is

$$\dot{\mathbf{x}}_e - \mathbf{T}\dot{\mathbf{x}} = \mathbf{F}\mathbf{x}_e - \mathbf{T}\mathbf{A}\mathbf{x} + \mathbf{K}\mathbf{C}\mathbf{x} \tag{D11}$$

When D10 is substituted into this relationship it becomes

$$\dot{\mathbf{x}}_e - \mathbf{T}\dot{\mathbf{x}} = \mathbf{F}(\mathbf{x}_e - \mathbf{T}\mathbf{x}) \tag{D12}$$

which has as its solution

$$\mathbf{x}_e(t) - \mathbf{T}\mathbf{x}(t) = e^{\mathbf{F}t}(\mathbf{x}_e(0) - \mathbf{T}\mathbf{x}(0)) \qquad \text{(D13)}$$

The difference between the observer system state variables and the linear transformation of the system state variables are the errors in the observer. The error vector will decay asymptotically towards zero, whatever the initial conditions, provided that the matrix, **F**, is chosen so that its eigenvalues have negative real parts. The rate of decay will be also be determined by the nature of the **F** matrix, and for a practical observer it is generally required that the observer dynamics be significantly faster than the system dynamics, to allow effective observation of the system. This is achieved by suitable allocation of the eigenvalues.

This theorem can be extended to include the non-free system defined by the equations D1 and D2. The observer input now comprises some transformation of the system input vector as well as feedback from the system output vector.

$$\dot{\mathbf{x}}_e = \mathbf{F}\mathbf{x}_e + \mathbf{K}\mathbf{y} + \mathbf{G}\mathbf{u} \qquad \text{(D14)}$$

If as before **T** is chosen to satisfy the relationship in equation D10 then the difference between the observer state vector and the transformation of the system state vector can be found using equations D1 and D14 as

$$\dot{\mathbf{x}}_e - \mathbf{T}\dot{\mathbf{x}} = \mathbf{F}\mathbf{x}_e - \mathbf{T}\mathbf{A}\mathbf{x} + \mathbf{K}\mathbf{C}\mathbf{x} + (\mathbf{G} - \mathbf{T}\mathbf{B})\mathbf{u} \qquad \text{(D15)}$$

This can be reduced to a similar form to equation D12 by substituting equation D10

$$\dot{\mathbf{x}}_e - \mathbf{T}\dot{\mathbf{x}} = \mathbf{F}(\mathbf{x}_e - \mathbf{T}\mathbf{x}) + (\mathbf{G} - \mathbf{T}\mathbf{B})\mathbf{u} \qquad \text{(D16)}$$

By choosing the observer input matrix **G** so that $\mathbf{G} \equiv \mathbf{T}\mathbf{B}$, equation D16 becomes identical to the error equation, equation D12, and the observer will have the desired properties. The response of the observer will again be determined by the matrix **F**.

The transform matrix **T** must be invertible so that the state vector of the system can be derived from that of the observer. If **T** is chosen to be the identity matrix **I**, the estimate produced by observer state vector is the system state vector itself, rather than a transformation of the vector. When $\mathbf{T} \equiv \mathbf{I}$, then from equation D10

$$\mathbf{F} = \mathbf{A} - \mathbf{KC} \tag{D17}$$

The observer state equation then becomes

$$\dot{\mathbf{x}}_e = (\mathbf{A} - \mathbf{KC})\mathbf{x}_e + \mathbf{Ky} + \mathbf{Bu} \tag{D18}$$

The coefficient matrix, A, and the output matrix, C, are both known and it follows that the design of the observer is reduced to determining the matrix, **K**, which specifies the feedback from the system output vector to the observer. **K** may be considered as the gain matrix of the observer.

A block diagram of the system and the observer is shown in figure D1. The observer is implemented in the form given in equation D19 which is achieved by rearranging equation D18.

$$\dot{\mathbf{x}}_e = \mathbf{A}\mathbf{x}_e + \mathbf{K}(\mathbf{y} - \mathbf{C}\mathbf{x}_e) + \mathbf{Bu} \tag{D19}$$

D1.2 Observability

It is evident from the discussion above that, in order to be able to design an observer for a given system, it must be possible to place the eigenvalues of the observer arbitrarily. This is possible if, and only if, the system is 'observable'. This property is defined as follows:

A state variable model of a dynamic system is said to be completely state observable if, for any time t_0, *there exists a time* $t_1 > t_0$ *such that a knowledge of the output vector* $\mathbf{y}(t)$ *and the input vector* $\mathbf{u}(t)$ *in the time interval* $t_0 \le t \le t_1$ *is sufficient to determine the initial state* $\mathbf{x}(t_0)$ *uniquely.* [88]

Examination of the observer state equation D18 shows that such a condition is implicit in the observer design because it is the input and output vectors which are being used to estimate the state vector. A time invariant linear

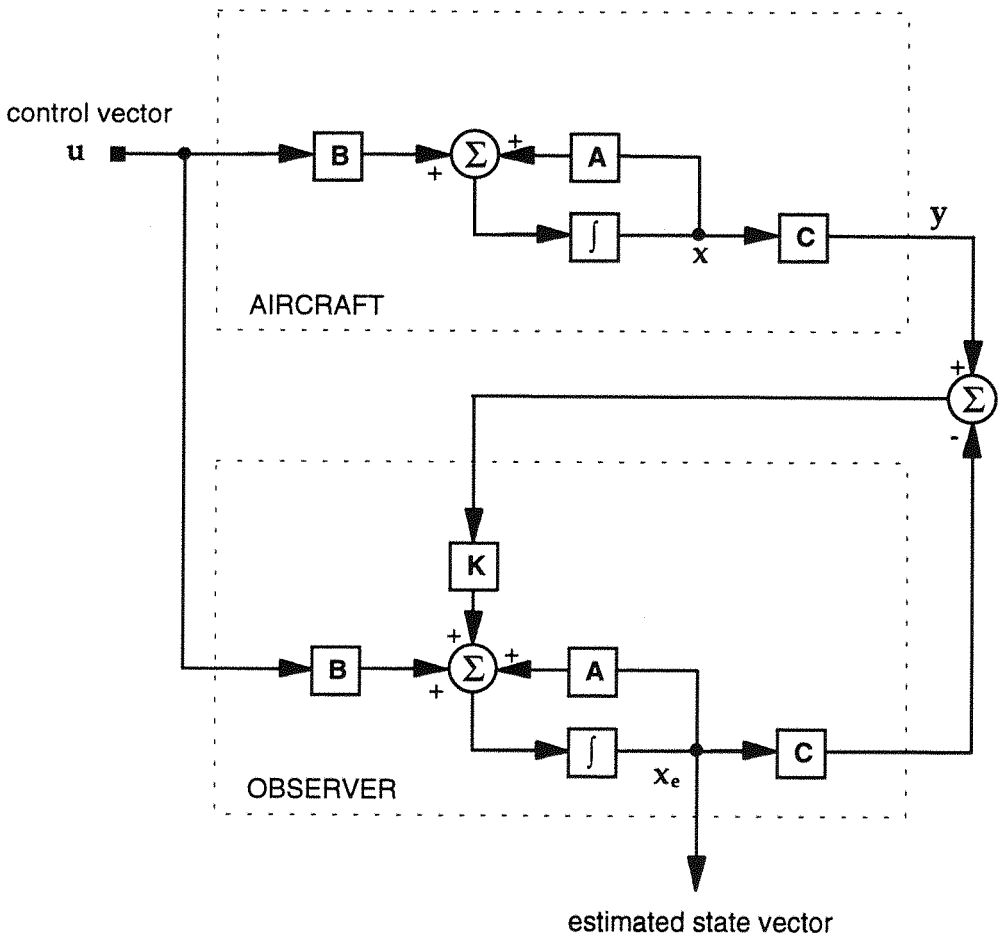

Figure D1: Block Diagram of a System and Observer

system can be tested to check whether it is observable using the method below.

A necessary and sufficient condition for a linear continuous time-invariant system to be completely state observable is that

$$\text{rank}\left[\mathbf{C}^{\mathrm{T}}, \mathbf{A}^{\mathrm{T}}\mathbf{C}^{\mathrm{T}}, \ldots, \left(\mathbf{A}^{\mathrm{T}}\right)^{n-1}\mathbf{C}^{\mathrm{T}}\right] = n \qquad \text{(D20)}$$

where n is the order of the system.

APPENDIX E: OPTIMAL DESIGN OF THE OBSERVER GAIN

The gain matrix, K, must be designed so that the observer has the following desired properties: it must be stable and the its dynamics should be faster than the system which it is observing. There are various methods which may be applied and two methods commonly used are pole-placement and optimal control.

Optimal control methods allow the system to be designed to give the best possible performance. There must be some means of evaluating the performance quantitatively and this is implemented by means of a performance index. A summary of the optimal control design theory is presented below and the subject is well documented elsewhere. [88, 89, 90]

We begin by defining a system

$$\dot{\mathbf{v}} = \mathbf{R}\mathbf{v} + \mathbf{S}\mathbf{w} \tag{E1}$$

where $\mathbf{v}$ is the state vector and $\mathbf{w}$ is the input vector to be controlled.

The most common form of performance index is the quadratic index. For an optimal regulator design the function to be minimised can be written as

$$J = \tfrac{1}{2}\int_0^\infty (\mathbf{v}^T\mathbf{M}\mathbf{v} + \mathbf{w}^T\mathbf{N}\mathbf{w})dt \tag{E2}$$

here $\mathbf{M}$ and $\mathbf{N}$ are symmetric positive semi-definite and positive definite matrices respectively i.e.

$$\mathbf{M} = \mathbf{M}^T \geq \mathbf{0} \tag{E3}$$

$$\mathbf{N} = \mathbf{N}^T > \mathbf{0} \tag{E4}$$

These represent the weighting matrices which define the relative importance of keeping the elements of the state vector close to zero, for which the coefficients of $\mathbf{M}$ should be large, while not requiring excessive feedback - reduced by making the coefficients of $\mathbf{N}$ large. The design of control systems using this form of index is known as the Linear Quadratic Problem (LQP).

This quadratic index has the advantage that it yields an optimal control design of linear state feedback form. If the optimal feedback for the system above is defined to be **L** then

$$\mathbf{w} = \mathbf{L}\mathbf{v} \tag{E5}$$

and the state equation for the controlled system can be reduced to

$$\dot{\mathbf{v}} = (\mathbf{R} + \mathbf{S}\mathbf{L})\mathbf{v} \tag{E6}$$

The optimal solution to the problem yields the feedback control law

$$\mathbf{w} = -\mathbf{N}^{-1}\mathbf{S}^{T}\mathbf{P}\mathbf{v} \tag{E7}$$

where **P** is the solution to the Algebraic Riccati Equation (A.R.E.)

$$\mathbf{P}\mathbf{R} + \mathbf{R}^{T}\mathbf{P} - \mathbf{P}\mathbf{S}\mathbf{N}^{-1}\mathbf{S}^{T}\mathbf{P} + \mathbf{M} = \mathbf{0} \tag{E8}$$

Consider now the design of an observer gain matrix. For a system defined in equations D1 and D2 the observer state equation is given by equation D18. If the error between the system state and the observer state is defined to be **e** where

$$\mathbf{e} = \mathbf{x} - \mathbf{x}_{e} \tag{E9}$$

then it can be seen that

$$\dot{\mathbf{e}} = (\mathbf{A} - \mathbf{K}\mathbf{C})\mathbf{e} \tag{E10}$$

Whereas for the control problem it was required to choose feedback, **L**, to optimise equation E6, the observer requires the selection of a suitable feedback matrix, K, to optimise equation E10. The solution can be derived by analogy.

The solution of equation E10 is

$$\mathbf{e}(t) = e^{(\mathbf{A}-\mathbf{K}\mathbf{C})t}\mathbf{e}(0) \tag{E11}$$

The eigenvalues can be evaluated from the determinant of the system. Now

$$\det[\mathbf{sI}-(\mathbf{A}-\mathbf{KC})] \equiv \det\left[\mathbf{sI}-(\mathbf{A}-\mathbf{KC})^{\mathrm{T}}\right] \tag{E12}$$

and

$$(\mathbf{A}-\mathbf{KC})^{\mathrm{T}} \equiv \mathbf{A}^{\mathrm{T}}-\mathbf{C}^{\mathrm{T}}\mathbf{K}^{\mathrm{T}} \tag{E13}$$

As a consequence the eigenvalues of $\mathbf{A}^{\mathrm{T}}-\mathbf{C}^{\mathrm{T}}\mathbf{K}^{\mathrm{T}}$ and $\mathbf{A}-\mathbf{KC}$ are identical and the feedback control law obtained from using $\mathbf{A}^{\mathrm{T}}$ and $\mathbf{C}^{\mathrm{T}}$ can be used to derive the observer gain matrix, $\mathbf{K}$.

If the LQP solution for equation E6 is compared with the matrix expression $\mathbf{A}^{\mathrm{T}}-\mathbf{C}^{\mathrm{T}}\mathbf{K}^{\mathrm{T}}$ it can be seen that both solutions are equivalent if

$$\mathbf{A} \equiv \mathbf{R}^{\mathrm{T}} \tag{E14}$$

$$\mathbf{C} \equiv \mathbf{S}^{\mathrm{T}} \tag{E15}$$

$$\mathbf{K} \equiv -\mathbf{L}^{\mathrm{T}} \tag{E16}$$

Therefore, by analogy, the feedback which optimises the observer equation

$$\dot{\mathbf{x}}_{\mathrm{e}} = (\mathbf{A}-\mathbf{KC})\mathbf{x}_{\mathrm{e}} + \mathbf{Ky} + \mathbf{Bu}$$

according to the performance index

$$J = \tfrac{1}{2}\int_0^{\infty} (\mathbf{e}^{\mathrm{T}}\mathbf{Qe} + \mathbf{y}^{\mathrm{T}}\mathbf{Ry})dt \tag{E17}$$

is

$$\mathbf{K} = \left(\mathbf{R}^{-1}\mathbf{CP}\right)^{\mathrm{T}} \tag{E18}$$

This entirely defines the optimal observer parameters.

REFERENCES

1. Federal Aviation Authority, USA *Windshear Training Aid* February 1987
2. National Research Council, USA *Low-altitude Wind Shear and Its Hazard to Aviation* National Academy Press 1983
3. *NTSB Determines Probable Causes of Delta Accident* Aviation Week & Space Technology 26th Jan 1986 pp. 95-99
4. Trevino G.T. and R. Laituri *Structure of Wind-Shear Turbulence* NASA CR 4213 January 1989
5. McCarthy J. and P.Clyne *A Strategy for avoidance of Hazardous Weather in the Airport Terminal Area* 40th International Air Safety Seminar, Flight Safety Foundation, October 1987, Tokyo Japan
6. McLean D. *Automatic Flight Control Systems* Prentice Hall 1990
7. Dunlop S. and F. Wilson *The Hamlyn Guide to Weather Forecasting* Hamlyn, London 1980
8. *Handbook of Aviation Meteorology* 3rd Edition 1994, HMSO, London
9. Fujita T.T. *The Downburst - Microburst and Macroburst* SMRP-RP 210 University of Chicago 1985
10. Scott W.B. *NTSB Urges Studies on Mountain Winds* Aviation Week & Space Technology 11th Jan 1993 pp. 34-35
11. Christie D.R. and K.J. Muirhead *Solitary Waves, A Low-Level Wind Shear Hazard to Aviation* Int. J. Aviation Safety 1983 pp. 169-191
12. Doviak R.J. and D.R. Christie *Thunderstorm Generated Solitary Waves: A Wind Shear Hazard* J. Aircraft **26**(5) May 1989 pp. 423-431
13. Swolinsky M. *Windshear Models for Aircraft Hazard Investigation* AGARD Flight Mechanics Symposium May 1989 Gol, Norway
14. Wiener E.L. and D. C. Nagel (Editors) *Human Factors in Aviation* Academic Press 1988
15. Roscoe S.N. (Editor) *Aviation Psychology* Iowa State University Press 1980
16. McRuer, D., I. Ashkenas and D. Graham *Aircraft Dynamics and Automatic Control* Princeton University Press 1973

17. Davis D.J., D.J. Linse, R. Suikat and D.P. Entz *Preliminary Control Law and Hardware Designs for a Ride Quality Augmentation System for Commuter Aircraft* NASA CR 4014 September 1986

18. *Federal Aviation Administration Terminal Doppler Weather Radar Operational Demonstration* Fact Sheet prepared by National Center for Atmospheric Research, Boulder, Colorado July 1988

19. Phillips E.H. *NASA will Study Heavy Rain Effects on Wing Aerodynamics* Aviation Week & Space Technology 13th Feb 1989 pp. 38-41

20. Hansen R. *Boeing Windshear Systems* AIAA Guidance, Navigation and Control Conference, August 1987 Paper No. AIAA-87-2342-C

21. Hinton D.A. *Flight-Management Strategies for Escape From Microburst Encounters* NASA TM-4057 August 1988

22. *Crew Techniques Reflect Need to Recognise, Avoid Wind Shear* Aviation Week & Space Technology 22nd Sept 1986 pp. 61-62

23. *Flight Path Control in Windshear* Airliner Jan-March 1985 pp. 1-12

24. Higgins P.R. and A. Roosme *Hazards of Landing Approaches and Take-offs in a Windshear Environment* Boeing Airliner January 1977 pp. 2-20

25. Stengel R.F. *Solving the Pilots' Windshear Problem* Aerospace America March 1985 pp. 82-85

26. Nordwall B.D. *ALPA Disputes FAA Recommendations for Wind Shear Recovery Method* Aviation Week & Space Technology 13th Oct 1986 pp. 133-135

27. Hinton D.A. *Piloted-Simulation Evaluation of Recovery Guidance for Microburst Wind Shear Encounters.* NASA TP 2886 March 1989

28. Hinton D.A. *Relative Merits of Reactive and forward-Look Detection for Wind-Shear Encounters During Landing Approach for Various Microburst Escape Strategies* NASA TM 4158 February 1990

29. Kessler E. *Low-Level Windshear Alert Systems and Doppler Radar in Aircraft Terminal Operations.* J. Aircraft **27**(5) 1990 pp. 423-428

30. IBIS Aerosystems *The Cockpit As a Workplace* course notes prepared for Meggitt Avionics March 1994

31. Federal Aviation Authority *TSO-C117 Airborne Windshear Warning and Escape Guidance Systems for Transport Aircraft* July 1990

32. Etkin B. *Turbulent Wind and its Effect on Flight* UTIAS Review no 44 August 1980

33. Shu S. and B. Etkin *Model of the Wind Field in a Downburst* J Aircraft **22**(7) July 1985 pp. 595-601

34. Wingrove R.C., R.E. Bach Jr. and T.A. Schultz *Analysis of Severe Atmospheric Disturbances from Airline Flight Records* AGARD Flight Mechanics Symposium May 1989 Gol, Norway

35. Bach R.E. and R.C. Wingrove *Analysis of Windshear from Airline Flight Data* J. Aircraft **26**(2) 1989 pp. 103-109

36. Wingrove R.C. and R.E. Bach Jr. *Severe Winds in the Dallas/Ft. Worth Microburst Measured from Two Aircraft.* J. Aircraft **26**(3) 1989 pp. 221-224

37. Bach R.E. and R.C. Wingrove *The Analysis of Airline Flight Records for Winds and Performance with Application to the Delta 191 Accident* AIAA-86-2227-CP August 1986

38. Schultz T.A. *Multiple Vortex Ring Model of the DFW Microburst* J. Aircraft **27**(2) 1990 pp. 163-168

39. Wilson F.W. Jnr and J.A.Fluek *A Study of The Methodology of Low Altitude Wind Shear Detection with a Special Emphasis on the LLWAS Concept* February 1986 Federal Aviation Administration Report No. DOT/FAA/PM-86/4

40. *Safety Board Cites Limitations of Airport Weather Surveillance* Aviation Week & Space Technology 12th Jan 1987 pp. 113-121

41. Ott J. *Inquiry Focuses on Wind Shear as Cause of Delta L-1011 Crash* Aviation Week & Space Technology 12th August 1985 pp. 16-19

42. *Windshear detection Technology Examined in 727 Accident* Aviation Week & Space Technology 7th Oct 1985 pp. 89-91

43. Bruggink G.M. *Convective Violence and Humility* Int. J. Aviation Safety 1983 pp. 133-137

44. Hughes F. *LLWAS Credited with Helping 737 Survive Major Microburst* Aviation Week & Space Technology 16th July 1990 pp. 91-93

45. Mahapatra P.R. and D.S. Zrnic *Sensors and Systems to Enhance Aviation Safety Against Weather Hazards* Proc. IEEE **79**(9) 1991 pp. 1234-1267

46. Evans J. and D. Turnbull *Development of an Automated Windshear Detection system using Doppler Weather Radar.* Proc. IEEE **77**(11) 1989 pp. 1661-1673

47. D. Turnbull D., J. McCarthy, J. Evans and D. Zrnic *The FAA Doppler Weather Radar (TDWR) Program* 3rd International Conference on the Aviation Weather System, Anaheim, February 1989

48. Lerner E.J. *Taming the Killer Windshear* Aerospace America May 1986 pp. 38-42

49. D. Turnbull D., J. McCarthy, J. Evans and D. Zrnic *The FAA Doppler Weather Radar (TDWR) Program* 3rd International Conference on the Aviation Weather System, Anaheim, February 1989

50. Phillips E.H. *New Sensors Reduce Windshear Risk* Aviation Week & Space Technology 18th October 1994 p53

51. Hughes D. *Predictive Wind Shear Nears Service Debut* Aviation Week & Space Technology 24th October 1994 pp.36-37

52. Merrifield J.T. *Boeing Developing Pilot Training Procedures in Windshear Training Program* Aviation Week & Space Technology 24th March 1986 pp. 50-57

53. *Airframe Manufacturers Combating Wind Shear with Common Training and Devices* Aviation Week & Space Technology 22nd Sept 1986 pp. 83-89

54. Stein K.J. Windshear *Provides a Timely Warning* Aviation Week & Space Technology 2nd March 1981 pp. 62-63

55. Lerner E. J. *Immediate Relief from Windshear* Aerospace America September 1986 pp. 20-22

56. Greene L.M. *Low-Altitude Windshear Protection can be Obtained* ICAO Bulletin April 1986 pp. 10-13

57. Johnson B.C. *Windshear Detection: A Report on the First Such Airborne Device to be Commercially Certified* ICAO Bulletin March 1986 pp. 14-17

58. Johnston B. *Sensing Windshear* Sensors March 1986

59. Honeywell *Standard Windshear Computer Pilot's Handbook* August 1989 unpublished, supplied by Honeywell Inc., Phoenix, Arizona

60. Stein K. J. *Forward-looking Windshear Radar Poised for Commercial Service* Avionics June 1993 pp. 22-26

61. Bracalente E.M., C.L. Britt and W.R. Jones *Airborne Doppler Radar Detection of Low-Altitude Wind Shear.* J. Aircraft **27**(2) 1990 pp. 151-157

62. Woodfield A.A., J.M. Vaughan *Airspeed and Wind Shear Measurements with an Airborne CO_2 CW Laser.* Int. J. Aviation Safety 1983 pp. 207-223

63. Robb D.W. *New Technologies Emerge for Airborne Windshear Sensors* Avionics April 1992 pp. 24-32

64. Targ R., M.J. Kavaya, R.M. Huffaker R.L.Bowles *Coherent Lidar Airborne Windshear Sensor: Performance Evaluation* Applied Optics **30**(15) May 1991 pp. 2013-2026

65. Bracalente E.M. and V.E. Delmore *Wind Shear Detection: Forward Looking Sensor Technology* NASA Conference Publication 10004 DOT/FAA/PS-87/2 October 1987

66. Scott W.B. *Researchers Developing Airborne Flir with Ability to Pinpoint Microbursts* Aviation Week & Space Technology 19th Feb 1990 pp. 69-71

67. Pallett E.H.J. *Aircraft Instruments and Integrated Systems* Longman 1992

68. *Tables relating to Altitudes, Airspeed and Mach Numbers for Use in Aeronautical Instrument Design and Calibration* British Standard 2G 199:1984

69. *MATLAB Reference Guide* The MathWorks, Inc. August 1992

70. *SIMULINK User's Guide* The MathWorks, Inc. April 1993

71. McCormick B.W. *Aerodynamics, Aeronautics and Flight Mechanics* Wiley 1979

72. Philips E.H. *Pilots, ATC Blamed for USAir Accident* Aviation Week & Space Technology 10th April 1995 pp. 32-33

73. Hughes D. *More Wind Shear Detail Might Have Aided DC-9* Aviation Week & Space Technology 11th July 1994 pp. 24-25

74. Frost W. *Flight in Low-Level Wind Shear* NASA CR-3678 March 1983

75. Wanke C. and R.J. Hansman *Alert Generation and Cockpit Presentation for an Integrated Microburst Alert System* AIAA Paper No. 91-0266 1991

76. *All the World's Aircraft 82-83* Janes pp. 348-350

77. Hawkins F.H. *Human Factors in Flight* Gower Technical Press 1987

78. Simpson C.A. and K. Marchionda-Frost *Synthesised Speech Rate and Pitch Effect on Intelligibility of Warning Messages for Pilots* Human Factors **26** 1984 pp. 506-517

79. Robinson C.P. and R.E. Eberts *Comparison of Speech and Pictorial Displays in a Cockpit Environment* Human Factors **29** 1987 pp. 31-44

80. Patterson R.D. *Guidelines for Auditory Warning systems on Civil Aircraft* CAA Paper 82017 1982

81. Byblow W.D. *Effects of Redundancy in the Comparison of Speech and Pictorial Displays in the Cockpit Environment* Applied Ergonomics **21** 1990 pp. 121-128

82. Kiernan V. *When Planes Fall Out of the Skies* New Scientist 29th April 1995 pp. 41-44

83. Etkin B. *Dynamics of Flight: Stability and Control* 2nd Ed. Wiley 1982

84. Massey *Mechanics of Fluids* 5th Ed. Van Nostrand Reinhold (UK) 1983

85. Newland D.E. *An Introduction to Random Vibration and Spectral Analysis* 2nd Ed. Longman 1984

86. Luenberger D. G. *Observing the State of a Linear System.* IEEE Trans. Military Electronics **8**(4) April 1964 pp. 74-80

87. Luenberger D. G. *Observers for Multivariable Systems.* IEEE Trans. Automatic Control **11**(2) 1966 pp. 190-197

88. Owens D.H. *Multivariable and Optimal Systems* Academic Press 1981

89. Bryson A.E. and Y-C. Ho *Applied Optimal Control* Hemisphere Publishing Corporation 1975

90. Stevens B.L. and F.L. Lewis *Aircraft Control and Simulation* Wiley 1992